Spring 2015

Studies of Arctic halogen chemistry from the snowpack to the gas phase

Kyle D Custard
Purdue University

Graduate School Form 30
(Updated 11/20/2014)

PURDUE UNIVERSITY
GRADUATE SCHOOL
Thesis/Dissertation Acceptance

This is to certify that the thesis/dissertation prepared

By Kyle D. Custard

Entitled STUDIES OF ARCTIC HALOGEN CHEMISTRY FROM THE SNOWPACK TO THE GAS PHASE

For the degree of Doctor of Philosophy

Is approved by the final examining committee:

Paul B. Shepson

Greg Michalski

Peter T. Kissinger

Scott A. McLuckey

To the best of my knowledge and as understood by the student in the Thesis/Dissertation Agreement, Publication Delay, and Certification/Disclaimer (Graduate School Form 32), this thesis/dissertation adheres to the provisions of Purdue University's "Policy on Integrity in Research" and the use of copyrighted material.

Paul B. Shepson

Approved by Major Professor(s): _____

_____

Approved by: R. E. Wild 04/13/2015

Head of the Department Graduate Program Date

STUDIES OF ARCTIC HALOGEN CHEMISTRY FROM THE SNOWPACK TO THE GAS PHASE

A Dissertation

Submitted to the Faculty

of

Purdue University

by

Kyle D. Custard

In Partial Fulfillment of the

Requirements of the Degree

of

Doctor of Philosophy

May 2015

Purdue University

West Lafayette, Indiana

ACKNOWLEDGEMENTS

A countless number of people were critical toward the completion of this work in which I am grateful for. I would like to thank my advisor, Paul Shepson, for providing the opportunity to conduct exciting research in a unique environment which has allowed me to grow as a critical thinker and problem solver. I also owe a tremendous amount of thanks to the Jonathon Amy Chemical Instrumentation Facility and the Chemistry Shop for all the help provided over the last several years. I would also like to thank past and current Shepson group members that assisted in the completion of this work along with companionship.

I also thank my family for the limitless amount of support and love provided over the years during my time away from home. My mom and dad have always been there for me and enabled me to pursue my dreams and goals. Without them this would not have been possible.

TABLE OF CONTENTS

Page

Page

Page

LIST OF TABLES

LIST OF FIGURES

Figure Page

Figure Page

Figure Page

Figure Page

ABSTRACT

Custard, Kyle David. PhD., Purdue University, May 2015. Studies of Arctic Halogen Chemistry from the Snowpack to the Gas Phase. Major Professor: Paul B. Shepson.

The temporary depletion of both tropospheric ozone and gaseous mercury during the Arctic springtime has been a focus of active research over the past several decades. Both of these phenomena have been linked to chemical reactions with halogen radicals. In particular, bromine atoms have been shown to act as the primary driver for these chemical depletions, although both chlorine and iodine atoms also contribute. Molecular bromine, along with its oxidation products, have been well studied in the Arctic, yet chlorine has not. Chlorine is known to impact the local oxidation capacity via its high reactivity with volatile organic compounds. Despite this understanding and the direct observations of atmospheric Cl_2, the source and release mechanism has not yet been determined.

This work describes experiments conducted during February 2014 in Barrow, Alaska, where in-snowpack production of BrCl and Cl_2 were observed. These measurements were accompanied by vertical profile experiments to determine flux emission rates of Br_2 and Cl_2 from the snowpack. Furthermore, ambient chemical ionization mass spectrometer measurements of ClO, a first of their kind, are reported from the Bromine, Mercury, and Ozone Experiment (BROMEX) 2012 field campaign.

This data was compared to model simulations representative of the sampling time period to investigate current understanding of the chlorine radical cycle. Finally, using data collected during the Ocean-Atmosphere-Sea Ice-Snowpack (OASIS) 2009 field campaign, we developed a model to study the impact that anthropogenic NO_x emissions has on the bromine radical cycle.

CHAPTER 1 INTRODUCTION

1.1 Atmospheric Chemistry

The earth's atmosphere extends to around 100 km above the planet's surface and consists of four distinct layers. These layers are held together by earth's gravity, and can be distinguished by unique temperature profiles that change with altitude (Figure 1.1).

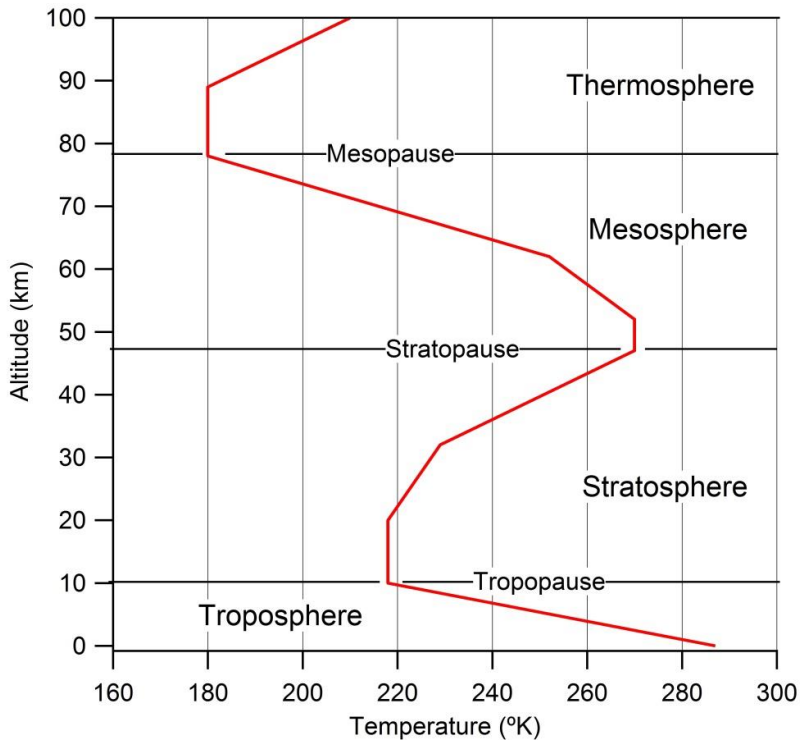

Figure 1.1 Plot of altitude as a function of temperature, showing the four distinct layers of the earth's atmosphere (Wallace and Hobbs, 1977).

Each layer serves a purpose towards sustaining human life, yet no layer has a more immediate impact on human life than the troposphere through its unique oxidation chemistry (see Section 1.2). Comprising the lowest ~10% by height, the troposphere encompasses more than 80% of the mass of the entire atmosphere. These gases mix and react because of turbulence, enabled in part by the buoyancy caused by decreases in temperature as altitude increases throughout the troposphere (Figure 1.1). Turbulent mixing is also caused by air flow over a rough surface, and shear forces. The lowest part of the troposphere directly influenced by the surface is known as the atmospheric/planetary boundary layer. The atmospheric/planetary boundary layer can extend anywhere from 200 m to 2 km above the surface. The boundary layer (BL) is impacted by surface emissions, both natural and anthropogenic, and these emissions, along with sunlight, lead to the complex chemical composition and chemistry of the troposphere.

1.1.1. Oxidation Chemistry

The troposphere cleanses itself of pollutants via oxidation chemistry, induced mostly by the hydroxyl radical (OH), which controls the oxidation capacity of the troposphere within the mid-latitudes (Thompson, 1992). Tropospheric OH is formed from the photolysis of O_3, followed by singlet oxygen reaction with a water molecule, as shown in reaction 1.1 and 1.2 (Michelsen et al., 1994).

$$O_3 + h\nu \rightarrow O(^1D) + O_2 \quad (1.1)$$

$$O(^1D) + H_2O \rightarrow 2OH \quad (1.2)$$

$$OH + VOC \rightarrow \text{Products} \quad (1.3)$$

This unique chemistry occurs mostly in the troposphere as it contains 99% of earth's water vapor. As a result of reactions 1.1 - 1.3, the average global OH concentration of OH is $1x10^{6}$ molecoles·cm^{-3}, although this can vary depending on local atmospheric composition, actinic flux, and relative humidity (Singh et al., 1995;Prinn et al., 1995).

OH oxidizes a wide variety of species in the atmosphere. Volatile organic compounds (VOC) emitted both from natural and anthropogenic sources influence atmospheric OH concentrations by acting as one of its main sinks. An example of this is its reaction with saturated hydrocarbons (Reactions 1.3-1.7). Methane chemistry is shown below in reactions (1.4-1.7), as an example VOC (Lelieveld et al., 1998).

$$CH_4 + OH \rightarrow CH_3 + H_2O \quad (1.4)$$

$$CH_3 + O_2 \rightarrow CH_3OO \quad (1.5)$$

$$CH_3OO + NO \rightarrow CH_3O + NO_2 \quad (1.6)$$

$$CH_3O + O_2 \rightarrow HCHO + HO_2 \quad (1.7)$$

The sequence begins by OH reacting via hydrogen atom abstraction to form an alkyl radical and a water molecule. Molecular oxygen will add to the alkyl radical forming a peroxy radical, which is then reduced to an alkoxy radical via reaction with nitric oxide. The alkoxy radical will react with molecular oxygen to form a stable product that can be removed from the atmosphere via dry or wet deposition.

Although OH is destroyed in the above reaction sequence, a normal byproduct of VOC oxidation is HO_2, which can act as an oxidizing agent to reform OH (Reaction 1.8).

$$HO_2 + NO \rightarrow OH + NO_2 \quad (1.8)$$

With the addition of reaction 1.8, VOC oxidation becomes a self-propelled chain reaction that leads to the formation of NO_2 and a carbonyl compound. In addition to the

reformation of OH, the NO_2 formed from the VOC oxidation can lead to ozone formation.

$$NO_2 + h\nu \rightarrow NO + O(^3P) \quad (1.9)$$

$$O_2 + O(^3P) \rightarrow O_3 \quad (1.10)$$

Note that reactions 1.9-1.11 lead to a null cycle; it is only reactions like 1.6 that oxidize NO to NO_2 that effectively produce a net gain in O_3.

$$O_3 + NO \rightarrow NO_2 + O_2 \quad (1.11)$$

In urban areas, large amounts of coal or motor fuel combustion cause high concentrations (1ppb) of NO_x ($NO_x = NO + NO_2$), leading to high levels of O_3 (Chameides et al., 1992). Tropospheric O_3 is known to have adverse effects on human health and high mixing ratios are correlated with an increase in local mortality rate (Bell et al., 2004). Mixing ratio in atmospheric chemistry refers to the ratio of the number of moles of a specific molecule per mole of air. Another byproduct of concentrated high volume combustion is smog. Smog refers to air pollution caused by side products from combustion such as soot particles and various gas-phase species such as hydrocarbons. However metropolitan areas are not the only place where smog can be experienced.

1.2. Arctic Tropospheric Chemistry

The Arctic is an isolated region of the world, free of major local anthropogenic sources. During the middle of the 20th century pilots traversing the Arctic during late winter and early spring experienced dramatic decreases in horizontal visibility (Schnell, 1984). The decrease in visibility was a result of high levels of aerosols ensuing to what is now known as Arctic haze (Schnell, 1984). At first it was believed that the long range

transport of windblown desert dust from Asia was the cause. However, chemical analysis of the haze revealed that the source was from anthropogenic combustion activity (Barrie et al., 1981).

With no major combustion sources located in the Arctic it was proposed that the pollution was transported from the mid-latitudes. Observations by Shaw and Rahn discovered the haze was originating from parts of Eurasia (Rahn et al., 1977;Shaw, 1982). The chemical composition of Arctic Haze primarily consists of sulfur (SO_2), originating from coal-burning plants. Oxidation of SO_2 leads to the production of sulfuric acid (H_2SO_4), as shown in reactions 1.12-1.14 (Langner and Rodhe, 1991).

$$SO_2 + OH + M \rightarrow HOSO_2 + M \quad (1.12)$$

$$HOSO_2 + O_2 \rightarrow HO_2 + SO_3 \quad (1.13)$$

$$SO_3 + H_2O \rightarrow H_2SO_4 \quad (1.14)$$

In the mid-latitudes aerosols that can cause haze have residence times of a few days before they are removed from the atmosphere by either wet or dry deposition. However, the unique atmospheric conditions of the Arctic extend the lifetime of anthropogenic aerosols. During the Arctic fall and winter, solar radiation is greatly reduced, allowing the atmosphere to enter a stagnant state with respect to scale turbulence. The cooled snow is a very good black body radiator of IR radiation and causes an inversion layer that stabilizes the BL and inhibits turbulent mixing that would help remove aerosols by deposition to the surface. Furthermore, the cold temperatures reduce the moisture flux in the atmosphere, limiting scavenging of aerosols by wet deposition. The decreased relative humidity also mitigates the ability of clouds to form which can remove aerosols

through precipitation (Shaw, 1995). The combination of these conditions is believed to lead to the buildup of Arctic haze.

The discovery of Arctic haze incited studies to analyze the Arctic atmosphere year-round. During this continuous year-round monitoring, the ground level mole ratio of O_3 dropped from background levels of ~40 ppb to less than 5 ppb over the course of several hours to a day during the spring time (Barrie et al., 1988;Bottenheim et al., 1986). These ozone depletion events (ODEs) were found to be unique to the springtime Arctic and Antarctic (Saiz-Lopez et al., 2007). In the mid-latitudes the average O_3 lifetime in the troposphere is approximately 10 days with the main loss being photolysis as shown in reactions 1.1-1.2. Eventually, Bottenheim et al. observed that ODEs can extend from the surface to 2 km altitude, as shown in Figure 1.2 (Bottenheim et al., 2002). This showed that ODEs originated close to the surface and extended upward, acknowledging the presence of a close to surface depletion mechanism.

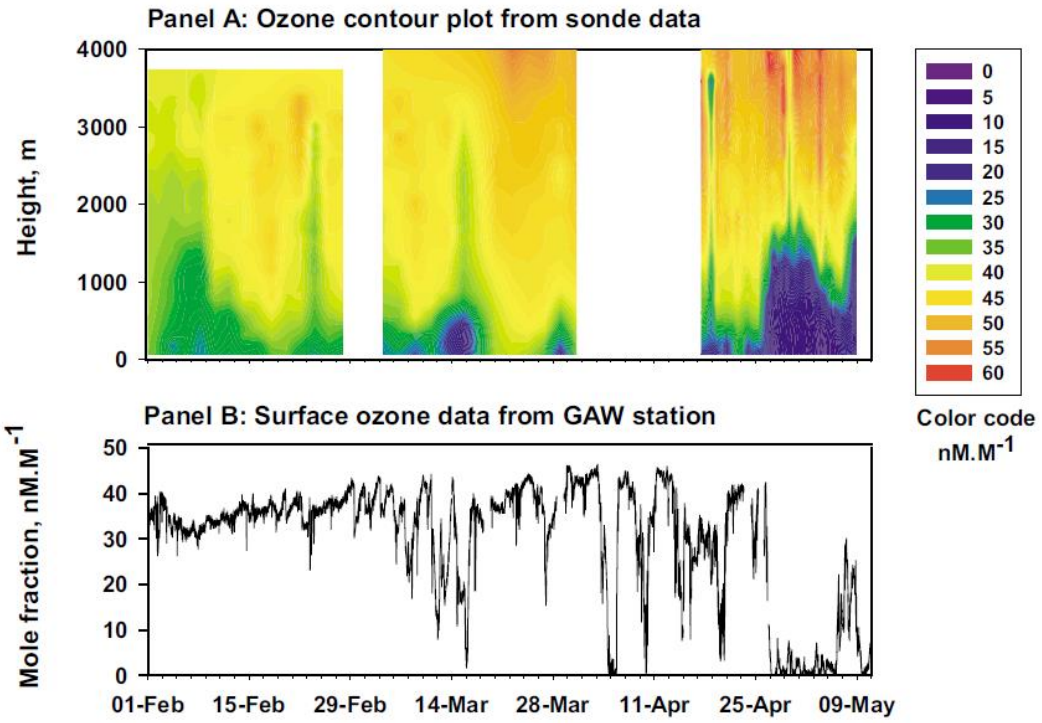

Figure 1.2 Ozone concentration data from a sonde (Panel A), showing the vertical extent of ODEs, and surface measurements (Panel B), (Bottenheim et al., 2002).

1.2.1 Arctic Tropospheric Halogen Chemistry

Barrie et al. observed several ODEs throughout the spring of 1986 at Alert, Nunavut and found an anti-correlation between ground level ozone and filterable bromine. Whatman 41 filters were used to collect particulate bromide and gaseous HBr, where the sum represents filterable bromine. As shown in Figure 1.3, when ozone concentrations drop filterable bromine levels rise; conversely, when ozone levels recover the filterable bromine returns to background levels (Barrie et al., 1988).

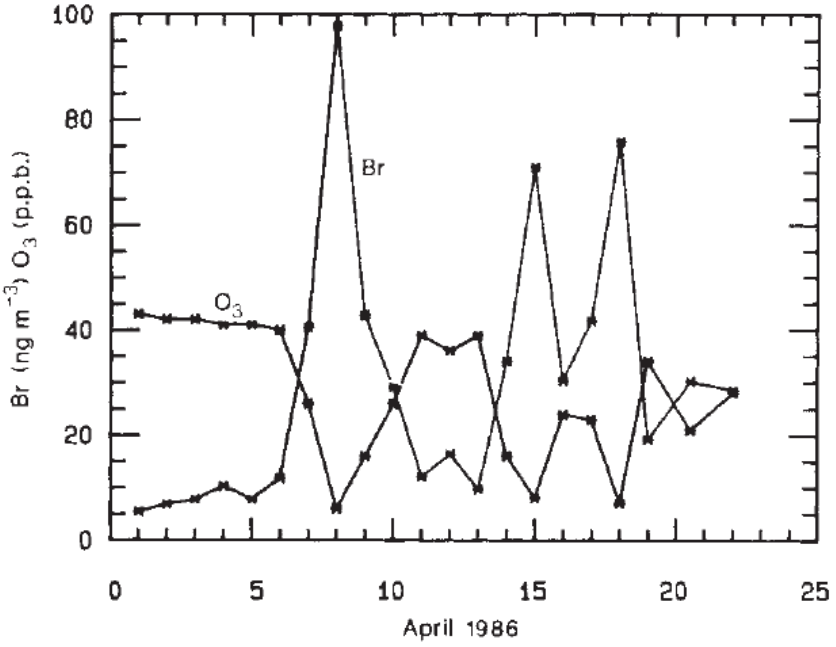

Figure 1.3 Ground level ozone concentrations and filterable bromine concentrations collected at Alert in 1986 (Barrie et al., 1988).

Barrie et al. proposed a mechanism that involved bromine initiated ozone depletion, as shown in reactions 1.15-1.17.

$$2 \times (Br + O_3 \rightarrow BrO + O_2) \quad (1.15)$$

$$BrO + BrO \rightarrow 2Br + O_2 \quad (1.16)$$

$$\text{Net: } 2\,O_3 \rightarrow 3\,O_2 \quad (1.17)$$

This reaction scheme of bromine-induced destruction of ozone is autocatalytic, where the bromine used to destroy ozone in reaction 1.15 is regenerated in reaction 1.16. McConnell et al. proposed that gas-phase regeneration of bromine would not be able to sustain ODEs due to conversion to chain terminating products as shown in reactions 1.18-1.20 (McConnell et al., 1992).

$$Br + RCHO \rightarrow HBr \quad (1.18)$$

$$BrO + NO_2 \rightarrow BrONO_2 \quad (1.19)$$

$$BrO + HO_2 \rightarrow HOBr + OH \quad (1.20)$$

They proposed that aerosols loaded with sea salt bromide will scavenge these bromine termination products and release Br_2 back in the atmosphere. Fan and Jacob (1992) proposed an aqueous phase mechanism to support an aerosol bromine release mechanism as shown in reactions 1.21-1.24.

$$HOBr_{(g)} + \text{aerosol} \rightarrow HOBr_{(aq)} \quad (1.21)$$

$$BrONO_{2(g)} + \text{aerosol} \rightarrow HOBr_{(aq)} + HNO_{3(aq)} \quad (1.22)$$

$$HOBr_{(aq)} + Br^- + H^+ \rightarrow Br_{2(aq)} + H_2O \quad (1.23)$$

$$Br_{2(aq)} \rightarrow Br_{2(g)} \quad (1.24)$$

In this mechanism, one bromine atom enters the aqueous phase and as a result two bromine atoms are produced. This exponential release is known as the "bromine explosion" and is the driver for ODEs (Vogt et al., 1996). The heterogeneous halogen chemistry proposed above has been shown by model simulations to occur either on the surface snowpack or aerosols to deplete ozone to the extent at which it has been observed in the Arctic (Tang and McConnell, 1996;Michalowski et al., 2000). It should be noted that this aerosol uptake of reactive bromine species accounts for the inverse correlation between aerosols and BrO via reaction 1.25 (Shepson et al., 2012).

$$HBr_{(g)} + \text{aerosols} \rightarrow Br^-_{(aq)} \quad (1.25)$$

Direct measurements of inorganic bromine species (Br_2, HOBr, and BrO) were conducted by (Liao et al., 2012) in Barrow, Alaska during the 2009 Ocean-Atmosphere-Sea Ice-Snowpack (OASIS) field study. As shown in Figure 1.4 spikes in BrO and HOBr

concentrations occur during the daytime when Br_2 is photolyzed and reacts with ozone. These observations support the proposed mechanisms for bromine-initiated ODEs.

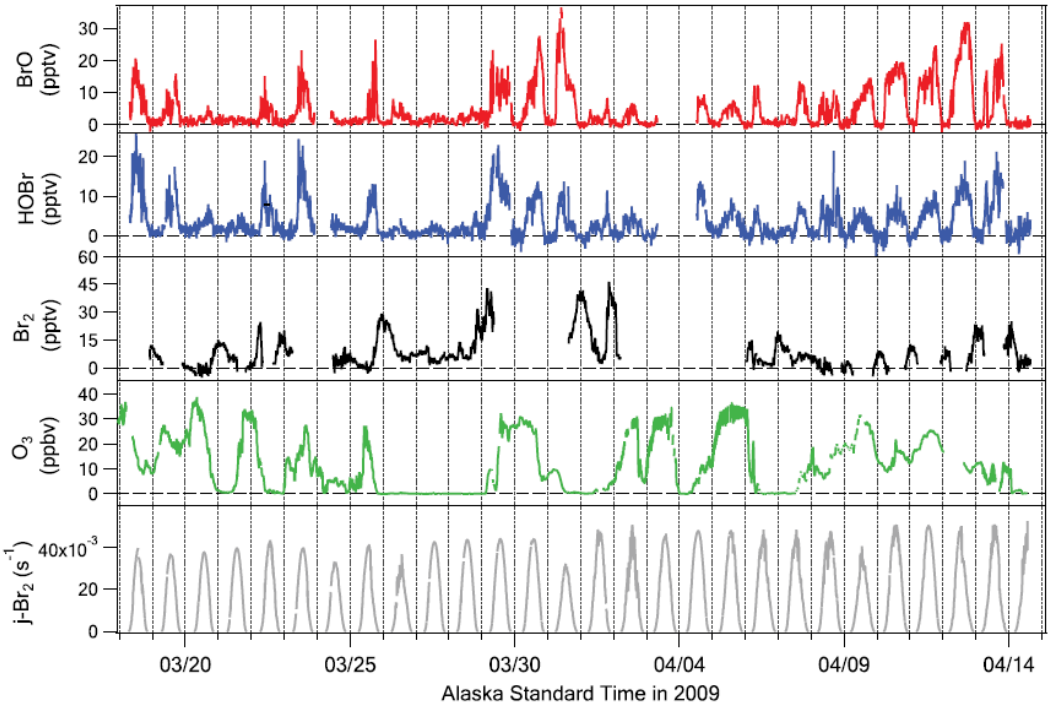

Figure 1.4 Ground based measurements of BrO, HOBr, Br_2, and O_3 during the OASIS field campaign (Liao et al., 2012).

Ozone is not the only chemical species to be affected by Arctic halogen chemistry. VOC concentrations have shown to significantly decrease during ODEs. Jobson (1994) collected ambient air samples in 3.2 L electropolished stainless steel canisters in Alert, NU, Canada, from January 21 to April 19 (during this time, Alert went from 24 hr darkness to 24 hr light). The canisters were analyzed for non-methane hydrocarbons (NMHC). Throughout the field study the average NMHC concentrations

decreased, consistent with OH kinetics. However, during ODEs a sudden decrease was observed followed by a recovery with ozone as shown in Figure 1.5.

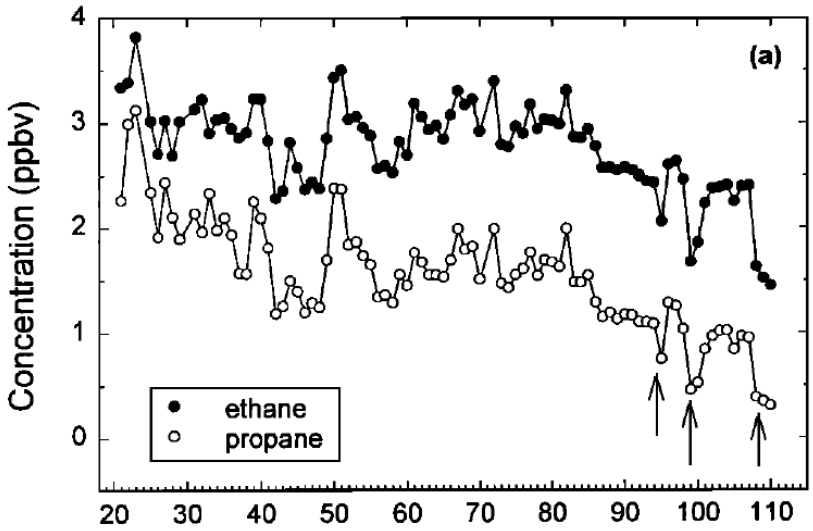

Figure 1.5 Ethane and propane concentrations from Alert in 1992, indicative of active halogen chemistry (Jobson et al., 1994).

Using the difference between the background concentrations and the concentrations observed during ODEs of the quantified hydrocarbons, along with their respective reaction rate constant with chlorine atoms, Jobson was able to calculate a chlorine atom concentration ranging from $3.9x10^3$ to $7.7x10^4$ molecules·cm^{-3}. They concluded that this amount of chlorine would compensate for the faster VOC concentration decrease rates. The presence of active chlorine chemistry in the Arctic was also evaluated by(Muthuramu et al., 1994) and by (Keil and Shepson, 2006), who quantified halogenated volatile organic hydrocarbons (HVOC) to estimate chlorine and bromine atom concentrations. Bromine and chlorine atoms react rapidly with small alkenes, such

as ethene and propene, to yield halogenated aldehydes and ketones, as shown in reactions 1.26-1.33 (Kleindienst et al., 1989).

$CH_2=CH_2 + X \rightarrow CH_2XCH_2$ (1.26)

$CH_2XCH_2 + O_2 \rightarrow CH_2XCH_2OO$ (1.27)

$CH_2XCH_2OO + NO \rightarrow CH_2XCH_2O + NO_2$ (1.28)

$CH_2XCH_2O + O_2 \rightarrow CH_2CHO + HO_2$ (1.29)

$CH_3CHCH_2 + X \rightarrow CH_3CHCH_2X$ (1.30)

$CH_3CHCH_2X + O_2 \rightarrow CH_3CH(OO)CH_2X$ (1.31)

$CH_3CH(OO)CH_2X + NO \rightarrow CH_3CH(O)CH_2X + NO_2$ (1.32)

$CH_3CH(O)CH_2X + O_2 \rightarrow CH_3C(O)CH_2X + HO_2$ (1.33)

The unique products formed along with their percent yield are known for both chlorine and bromine atoms reacting with ethene and propene (Keil and Shepson, 2006;Kleindienst et al., 1989). The percent yield values were used by Keil and Shepson to calculate bromine and chlorine atom steady state concentrations of ~$1.6x10^7$ and 0.5 to $1.7x10^5$ molecules·cm^{-3}, respectively. While these chlorine atom steady state concentration values are an order of magnitude larger than that determined by Jobson, it was hypothesized that chlorine's direct impact towards ODEs would be minimal relative to bromine.

While it was previously known that there was a large photolytic source of Cl atoms, the precursor was not proven. Impey et al. measured total photolyzable chlorine (Cl_2 + HOCl) at levels up to 100 ppt during the dark period at Alert, Nunavut(Impey et al., 1997). Photolyzable chlorine was not detected after the Polar Sunrise. However, for the first time in the Arctic, high concentrations of Cl_2 were directly observed in Barrow,

Alaska during the spring of 2009 (Liao et al., 2014). These observations were constrained in a 1-D box model to calculate a chlorine atom concentration for this time period. As shown in Figure 1.6 the chlorine atom concentration can reach levels as high as $6x10^5$ molecules·cm^{-3}, an order of magnitude higher than previous estimates. Based on these concentrations, Liao et al concluded that chlorine chemistry could more likely indirectly affect ODEs via the production of HO_2 from the oxidation of VOC, similar to the reaction mechanism shown previously (1.3-1.6). From reaction 1.15, this additional HO_2 could lead to enhanced HOBr production, which is a prime component of the bromine heterogeneous recycling. An increase in HOBr would result in a higher outward flux of Br_2, presumably leading to faster ODE developments.

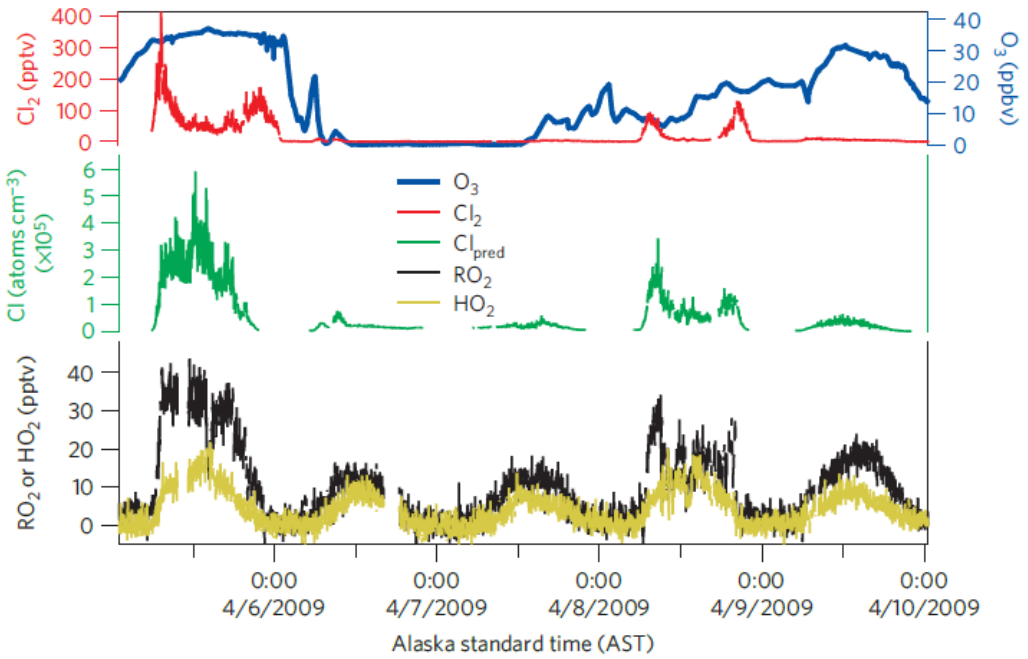

Figure 1.6 Model output chlorine atom concentrations based on observed Cl_2, O_3, and RO_2/HO_2 concentrations (Liao et al., 2014).

Along with ozone and VOCs, it has been shown that atmospheric mercury can also be depleted via halogen chemistry in the Arctic during the polar spring (Schroeder et al., 1998). Mercury is an anthropogenic atmospheric pollutant (from coal combustion) primarily found in its elemental form, Hg^0, within the atmosphere. The global average concentration of atmospheric Hg^0 is around 1.7 $ng \cdot m^{-3}$(Steffen et al., 2008), despite the major sources being located in the Northern mid-latitudes. The reason for this is Hg^0 has a typical tropospheric lifetime of 1 year, allowing for horizontal and vertical mixing throughout the atmosphere and long range transport which includes all the way to the Arctic.

Depletion of gaseous elemental mercury (GEM) has been found to correlate with ODEs, leading to the hypothesis that halogen chemistry is involved, as shown in Figure

1.7 (Moore et al., 2014). The following mechanisms (1.34 & 1.35) have been proposed for the oxidation of GEM to Hg^{2+} compounds that can be easily removed from the atmosphere via dry or wet deposition to the snowpack or sea ice surface (Lindberg et al., 2002).

$$BrO/ClO + Hg^0 \rightarrow HgO + Br/Cl \quad (1.34)$$

$$Hg^0 + 2\,Br/Cl \rightarrow HgBr_2/HgCl_2 \quad (1.35)$$

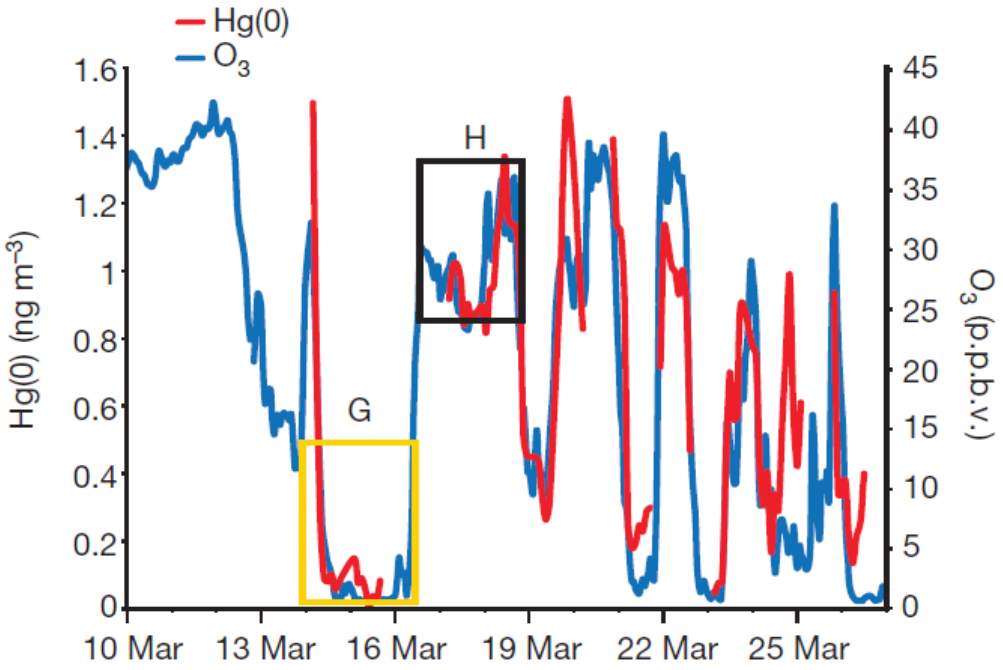

Figure 1.7 A comparison of GEM and O_3 in Barrow, Alaska during the BROMEX field campaign (Moore et al., 2014).

During the summer melt season the mercury can enter the Arctic ecosystem, where its fate is not well understood. Hammerschmidt et al. (2006) showed that an increase in monomethylmercury (CH_3Hg^+) was correlated with an increase of Hg sediment loading

from the atmosphere (Hammerschmidt et al., 2006). Methylmercury bioaccumulates in species found in the Arctic which can be passed onto humans, leading to health problems which includes birth defects (Ninomiya et al., 1995).

1.3 Halogen Sources

Extensive field studies along with countless laboratory experiments have been dedicated toward determining the source of atmospheric halogens along with their chemical release mechanism (Abbatt et al., 2010;Huff and Abbatt, 2002;Wren et al., 2013;Pratt et al., 2013;Foster et al., 2001). Potential sources include halogenated organic compounds, frost flowers, blowing snow, sea ice, snow, aerosols and open ocean (Simpson et al., 2007b;Kaleschke et al., 2004;Yang et al., 2010). Frost flowers are ice crystals that can form when sea ice freezes in the presence of moist air, the warmer sea ice compared to the overlying air can supersaturate the air leading to condensation and deposition (Douglas et al., 2012). Early observations of ODEs noted that wind directions at ODE onset correlated with air masses originating from over the sea ice (Bottenheim et al., 1990). The Global Ozone Monitoring Experiment (GOME) satellite has shown significant enhancements of BrO during the spring months over the Arctic sea ice as shown in Figure 1.8 (Richter et al., 1998), though the interpretation of the satellite data remains unclear. Satellite derived BrO concentrations represent the total column, and despite advances in interpretation it remains difficult to infer anything about the chemistry occurring at the surface (Salawitch et al., 2010;Peterson et al., 2014).

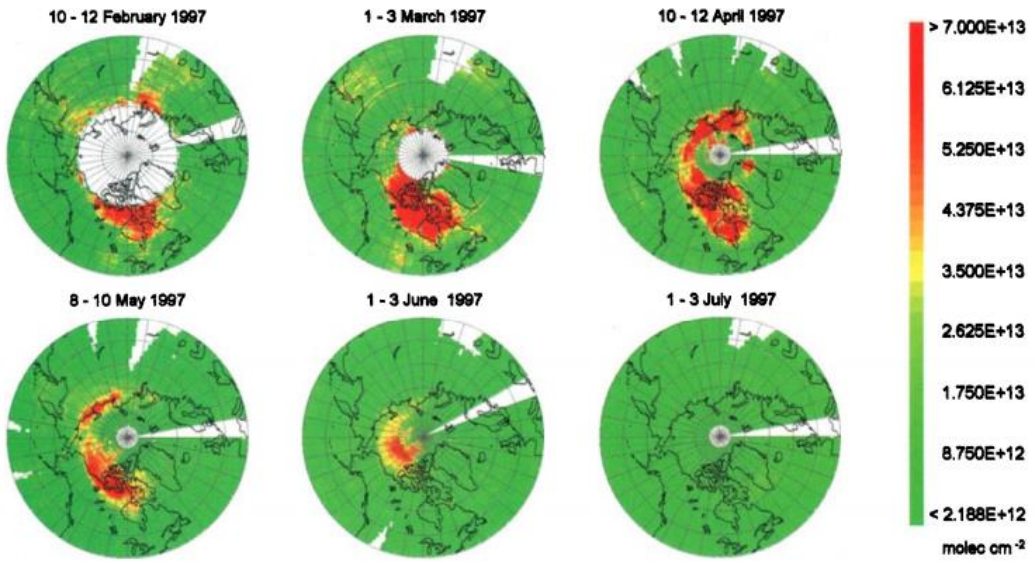

Figure 1.8 Satellite images of BrO from the GOME satellite, showing BrO column density changes throughout the year of 1997 (Richter et al., 1998).

Simpson et al. (2007a) observed a positive correlation between BrO levels in air parcels that had been in contact with first-year sea ice (FYI) (Simpson et al., 2007a). In that study BrO was used as an indicator for active halogen chemistry based on reactions 1.15 & 1.16 and was continuously monitored using multiple-axis differential optical absorption spectroscopy (MAX-DOAS). Coupled with back trajectory models, Simpson et al. were able to determine that BrO concentration increased when an air parcel had passed over a section of FYI.

The Arctic Ocean contains two types of sea ice, first-year sea ice and multi-year sea ice (MYI). FYI and MYI differ in that FYI forms during the most recent winter freeze up event while MYI formed during a previous winter freeze and survived the summer melt season(s) (Comiso, 2012). MYI can range anywhere in age from two years

old to over five years old (Maslanik et al., 2011). During the initial ice formation a thin brine layer forms on the surface of the sea ice and contains a high concentration of sea salts (Perovich and Richtermenge, 1994). It was found when salt solutions freeze, halide ions are forced to the surface by the nascent ice crystal lattice, creating a highly saline aqueous phase (Cho et al., 2002). However, this thin brine layer disappears as the ice ages via snow deposition. This brine layer results in FYI having a much higher salinity value than MYI. Breaking waves that occur in polynyas and leads, which are cracks in the sea ice that occur in FYI, yield sea water droplets that evaporate and form sea salt aerosols (Nilsson et al., 2001). Sea salt aerosols then can deposit onto the snowpack surface, influencing the chemical composition of the snow. Thus, it has been hypothesized that sea salt aerosols could be the source of atmospheric halogens.

Once sea salt halides were determined to be the origin of atmospheric reactive halogens, research became focused on determining the specific source along with the release mechanism. Laboratory studies have shown that sea ice surfaces can be a reactive media, not only absorbing species but also releasing them (Abbatt, 2003). Abbatt et al. (2010) observed the release of Br_2 release from frozen surfaces containing chloride, bromide, iodide and nitrate when the surface was irradiate by a xenon arc lamp (Abbatt et al., 2010). They noted that Br_2 production did not occur in the absence of NO_3^- or during higher pH ($\geq$7) conditions, leading to a proposed mechanism involving H^+ along with condensed phase OH that was photolytically produced. Snow chamber experiments conducted in Barrow, Alaska by Pratt et al. (2013) support this mechanism (Pratt et al., 2013). Pratt et al. exposed various types of ice and snow samples (FYI and different layers within the snowpack, including tundra surface snow) to solar radiation along with

O_3. Tundra and FYI surface snow were the only samples that produced molecular Br_2 when exposed to light and background concentrations of O_3 (30 ppb). The release was enhanced when the sample was exposed to O_3 as shown in Figure 1.9.

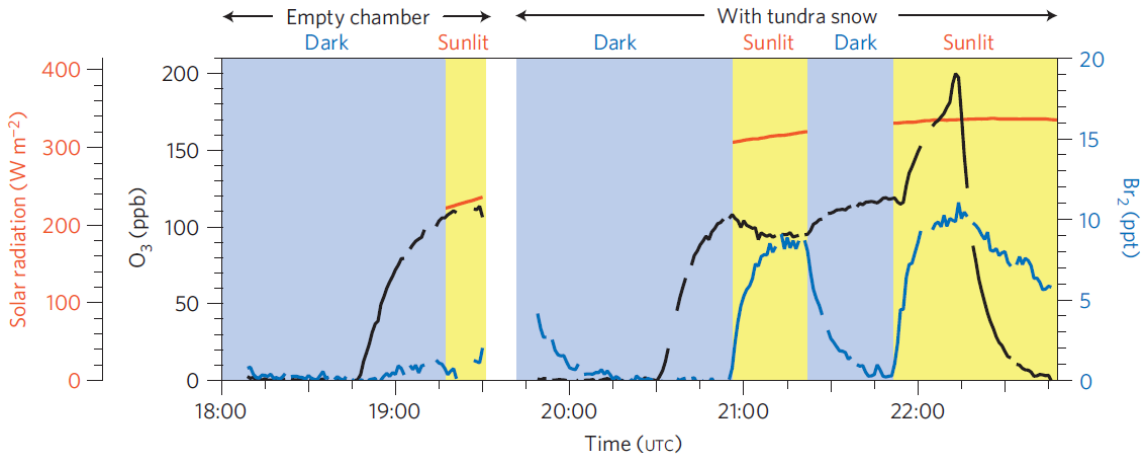

Figure 1.9 Results of a snowchamber experiment showing the production of Br_2 from irradiated tundra surface snow (Pratt et al., 2013).

Based on their observations, Pratt et al. developed a photochemical production mechanism for Br_2 within the surface snowpack based on the laboratory studies of Abbatt et al. (Abbatt et al., 2010;George and Anastasio, 2007).

$$NO_2^- + h\nu \rightarrow NO\cdot + O\cdot^- \quad (1.36)$$

$$O\cdot^- + H^+ \rightarrow \cdot OH \quad (1.37)$$

$$\cdot OH + Br^- \leftrightarrow HO\cdot Br^- \quad (1.38)$$

$$HO\cdot Br^- + H^+ \rightarrow Br\cdot + H_2O \quad (1.39)$$

$$Br\cdot + Br^- \leftrightarrow Br_2^- \quad (1.40)$$

$$2\ Br_2^- \rightarrow Br_3^- + Br^- \quad (1.41)$$

$$Br_3^- \leftrightarrow Br^- + Br_2 \quad (1.42)$$

Pratt et al. established that the initial release of Br_2 occurs in the surface-level snowpack where it is believed that deposition of acidic species (HNO_3 and H_2SO_4) provide the needed acidic conditions; H_2SO_4 is an important component of "Arctic Haze" aerosol. Solar radiation can penetrate into the snowpack to enable photolysis of various species (NO_3^-, NO_2^-, and H_2O_2) to produce condensed phase OH (King and Simpson, 2001;Chu and Anastasio, 2003;Mack and Bolton, 1999;Anastasio et al., 2007). Although lab studies have shown the potential for sea ice surfaces to release halogens, the higher surface area of surface snow compared to the sea ice surface make snow a better candidate for halogen activation in the Arctic (Aguzzi and Rossi, 2002;Wren et al., 2013). Lab studies have also shown that the buffering capacity of the sea ice surface prevents the production of a low pH environment which is crucial for halogen activation (Wren and Donaldson, 2012).

There is still much to be addressed in the field of Arctic halogen chemistry. Although we have an understanding of the source and release mechanism of molecular bromine these two components for molecular chlorine still remain unknown. This lack of understanding proposes the questions do we understand the chlorine chemistry occurring in the Arctic boundary layer. Despite the detection of both molecular Br_2 and Cl_2 in the Arctic surface boundary layer, their flux from their respective source has not been quantified.

1.4 Impact of a Warming Arctic

Over the past 130 years the earth's surface temperature has been increasing. However this increase has been most dramatic in the Arctic region and mostly over the past 30 to 40 years (Serreze and Barry, 2011). Figure 1.10 shows the average surface temperature increase for the time period of 1960 to 2009, as recorded by the National Aeronautics and Space Administration (NASA). The arctic warming is ~1.9 times greater than the global average increase.

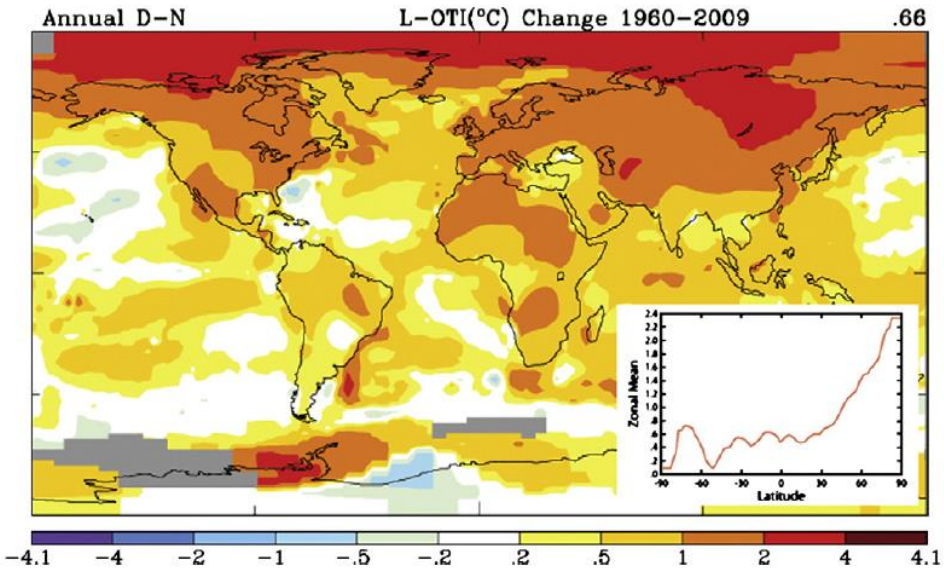

Figure 1.10 Average surface temperature increase from 1960 to 2009 (http://data.giss.nasa.gov/gistemp/).

This enhanced warming in the Arctic has been termed Arctic amplification and is a positive feedback system encompassing several factors (Screen and Simmonds, 2010).

The process begins with the initial increase in surface radiation from the elevated levels of greenhouse gases, resulting in the initial surface temperature increase (Forster and Ramaswamy, 2007). As a result of this temperature increase, sea ice melting is greater in intensity with regard to both area and volume (Stroeve et al., 2012). Not only has the total coverage area of the sea ice been declining over the past several decades (as shown in Figure 1.11), the overall distribution of Arctic sea ice has shifted from the majority being MYI to now mostly FYI (Maslanik et al., 2011). Maslanik et al used satellite images to determine that the percent coverage by MYI went from 75% in the mid 1980's to 45% in 2011.

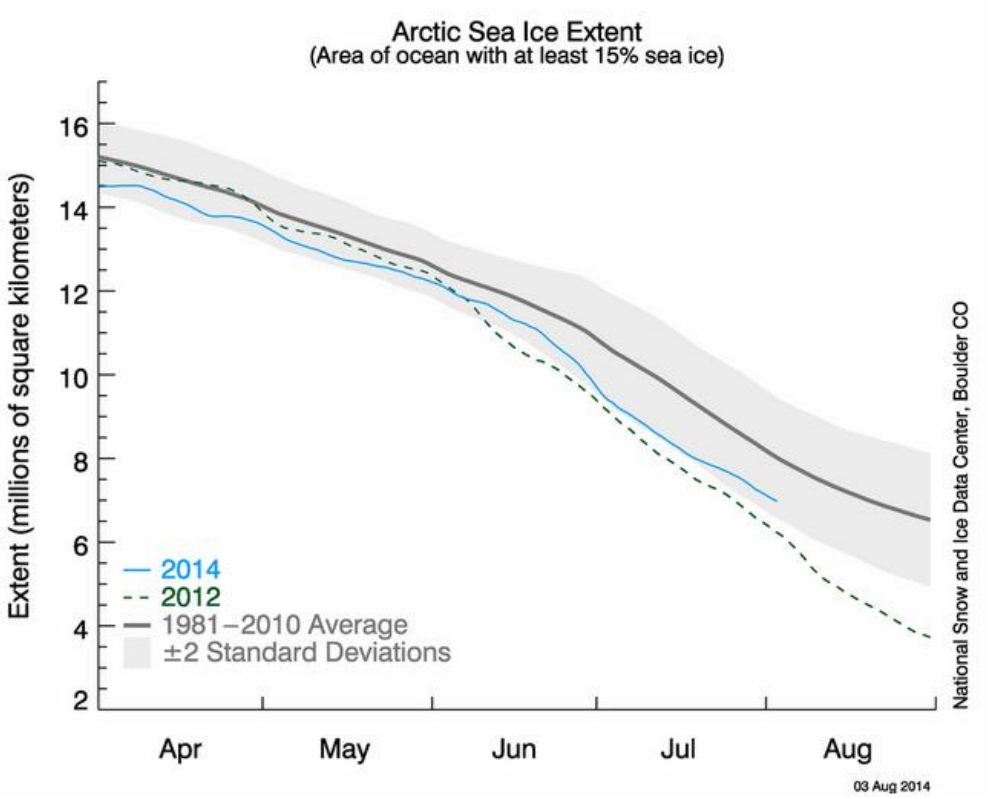

Figure 1.11 The arctic sea ice extent as of August 4, 2014 (blue trace) along with the daily ice extent for 2012 (green trace) and the average daily ice extent for the time span of 1981 to 2010 (grey trace). The shaded grey region represents the two standard deviation range of the measurements (http://nsidc.org/).

FYI is generally thinner than MYI and is thus more susceptible to melting during the summer melt season than MYI, leading to more open water during the summer. Open water absorbs solar radiation where sea ice reflects it away; this additional radiation input as sea ice retreats leads to more sea ice loss. As shown in Figure 1.12, this creates a positive feedback system, resulting in less sea ice and higher surface temperatures (Stroeve et al., 2012). Furthermore, the sea ice acts as a barrier between the warm ocean water and, in the winter, the much colder air above. When some of the sea ice is

removed there is a large increase in water vapor flux into the atmosphere, leading to greater relative humidity, and more cloud cover. Clouds along with water vapor are very reflective greenhouse agents, and thus this leads to warming for more sea ice loss, and more water vapor input.

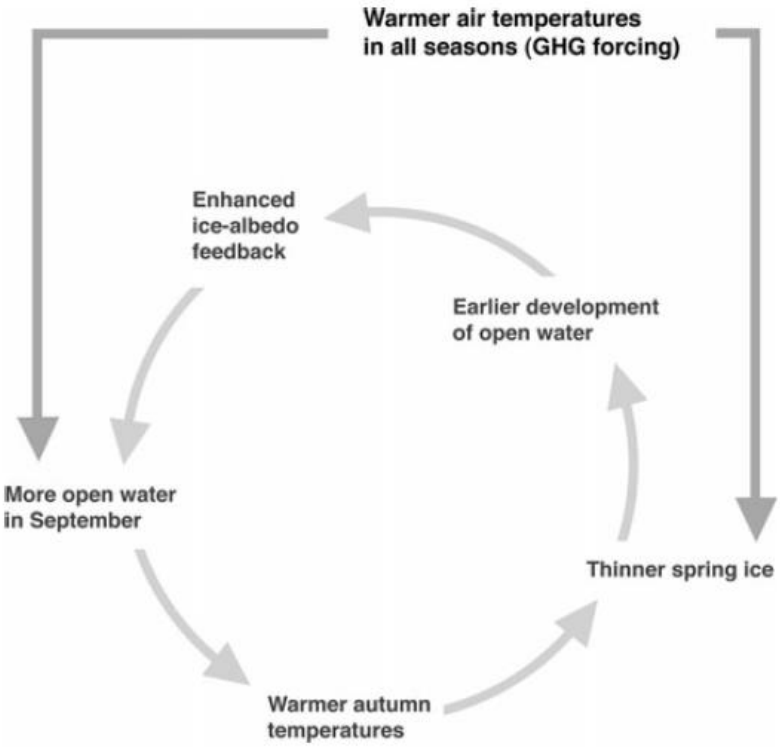

Figure 1.12 Graphic representation of the ice-albedo feedback system

As the percentage of sea ice coverage in the Arctic continues to shift towards FYI, this will lead to a more saline Arctic surface. As sea salt is the source of atmospheric

molecular halogens, ODEs could become prevalent throughout the Arctic during spring until it becomes ice-free.

1.5 Research Objectives and Statement of Purpose

This thesis addresses the unique halogen chemistry of the Arctic boundary layer that occurs during the polar sunrise. Aspects thoroughly investigated include molecular halogen sources, halogen radical cycling, and the effect of NO_x on halogen chemistry. The cycling of BrO_x and ClO_x was studied during the 2012 BROMEX field campaign in Barrow, Alaska via the deployment of the flowtube method as described in Chapter 2. Using a 0-D model the effect of NO_x on the halogen chemistry cycle was investigated. In Chapter 3, it will be discussed how observations from the 2009 field campaign OASIS were used to examine the impact that NO_x had on radical species concentrations during a 10 day period, along with the results of this investigation. The production of molecular halogens within the Arctic snowpack was studied using a chemical ionization mass spectrometer during in-snow experiments. These experiments along with flux measurements that were conducted in Barrow, Alaska during January and February of 2014 will be discussed in Chapter 4. In Chapter 5 I will discuss the future needs to expand our understating of halogen chemistry in the Arctic.

1.6 References

Abbatt, J., Oldridge, N., Symington, A., Chukalovskiy, V., McWhinney, R. D., Sjostedt, S., and Cox, R. A.: Release of Gas-Phase Halogens by Photolytic Generation of OH in Frozen Halide-Nitrate Solutions: An Active Halogen Formation Mechanism?, Journal of Physical Chemistry A, 114, 6527-6533, 10.1021/jp102072t, 2010.

Abbatt, J. P. D.: Interactions of atmospheric trace gases with ice surfaces: Adsorption and reaction, Chemical Reviews, 103, 4783-4800, 10.1021/cr0206418, 2003.
Aguzzi, A., and Rossi, M. J.: Heterogeneous hydrolysis and reaction of BrONO2 and Br2O on pure ice and ice doped with HBr, Journal of Physical Chemistry A, 106, 5891-5901, 10.1021/jp014383e, 2002.

Anastasio, C., Galbavy, E. S., Hutterli, M. A., Burkhart, J. F., and Friel, D. K.: Photoformation of hydroxyl radical on snow grains at Summit, Greenland, Atmospheric Environment, 41, 5110-5121, 10.1016/j.atmosenv.2006.12.011, 2007.

Barrie, L., Bottenheim, J., Schnell, R., Crutzen, P., and Rasmsssen, R.: Ozone Destruction and Photochemical-Reactions at Polar Sunrise in the Lower Arctic Atmosphere, Nature, 334, 138-141, 10.1038/334138a0, 1988.

Barrie, L. A., Hoff, R. M., and Daggupaty, S. M.: The influence of mid-latitudinal pollution sources on haze in the Canadian Arctic, Atmospheric Environment, 15, 1407-1419, 10.1016/0004-6981(81)90347-4, 1981.

Bell, M. L., McDermott, A., Zeger, S. L., Samet, J. M., and Dominici, F.: Ozone and short-term mortality in 95 US urban communities, 1987-2000, Jama-Journal of the American Medical Association, 292, 2372-2378, 10.1001/jama.292.19.2372, 2004.

Bottenheim, J., Barrie, L., Atlas, E., Heidt, L., Niki, H., Rasmussen, R., and Shepson, P.: Depletion of Lower Tropospheric Ozone During Arctic Spring - The Polar Sunrise Experiment 1988, Journal of Geophysical Research-Atmospheres, 95, 18555-18568, 10.1029/JD095iD11p18555, 1990.

Bottenheim, J., Fuentes, J., Tarasick, D., and Anlauf, K.: Ozone in the Arctic lower troposphere during winter and spring 2000 (ALERT2000), Atmospheric Environment, 36, 2535-2544, 10.1016/S1352-2310(02)00121-8, 2002.

Bottenheim, J. W., Gallant, A. G., and Brice, K. A.: Measurements of NO_y species and O_3 at 82^o N latitude, Geophysical Research Letters, 13, 113-116, 10.1029/GL013i002p00113, 1986.

Chameides, W. L., Fehsenfeld, F., Rodgers, M. O., Cardelino, C., Martinez, J., Parrish, D., Lonneman, W., Lawson, D. R., Rasmussen, R. A., Zimmerman, P., Greenberg, J., Middleton, P., and Wang, T.: Ozone precursor relationships in the ambient atmosphere, Journal of Geophysical Research-Atmospheres, 97, 6037-6055, 1992.

Cho, H., Shepson, P. B., Barrie, L. A., Cowin, J. P., and Zaveri, R.: NMR investigation of the quasi-brine layer in ice/brine mixtures, Journal of Physical Chemistry B, 106, 11226-11232, 10.1021/jp020449+, 2002.

Chu, L., and Anastasio, C.: Quantum yields of hydroxyl radical and nitrogen dioxide from the photolysis of nitrate on ice, Journal of Physical Chemistry A, 107, 9594-9602, 10.1021/jp0349132, 2003.

Comiso, J. C.: Large Decadal Decline of the Arctic Multiyear Ice Cover, Journal of Climate, 25, 1176-1193, 10.1175/jcli-d-11-00113.1, 2012.

Douglas, T., Domine, F., Barret, M., Anastasio, C., Beine, H., Bottenheim, J., Grannas, A., Houdier, S., Netcheva, S., Rowland, G., Staebler, R., and Steffen, A.: Frost flowers growing in the Arctic ocean-atmosphere-sea ice-snow interface: 1. Chemical composition, Journal of Geophysical Research-Atmospheres, 117, 10.1029/2011JD016460, 2012.

Fan, S., and Jacob, D.: Surface Ozone Depletion in Arctic Spring Sustained by Bromine Reactions on Aerosols, Nature, 359, 522-524, 10.1038/359522a0, 1992.

Forster, P., and Ramaswamy, V.: Changes in Atmospheric Constituents and in Radiative Forcing, in: Climate Change 2007: the Physical Science Basis, edited by: Solomon, S., Qin, D., Manning, M., Marquis, M., Averyt, K., Tignor, M. M. B., Miller, H. L., and Chen, Z. L., Cambridge Univ Press, New York, 129-234, 2007.

Foster, K., Plastridge, R., Bottenheim, J., Shepson, P., Finlayson-Pitts, B., and Spicer, C.: The role of Br-2 and BrCl in surface ozone destruction at polar sunrise, Science, 291, 471-474, 10.1126/science.291.5503.471, 2001.

George, I. J., and Anastasio, C.: Release of gaseous bromine from the photolysis of nitrate and hydrogen peroxide in simulated sea-salt solutions, Atmospheric Environment, 41, 543-553, 10.1016/j.atmosenv.2006.08.022, 2007.

Hammerschmidt, C. R., Fitzgerald, W. F., Lamborg, C. H., Balcom, P. H., and Tseng, C. M.: Biogeochemical cycling of methylmercury in lakes and tundra watersheds of Arctic Alaska, Environmental Science & Technology, 40, 1204-1211, 10.1021/es051322b, 2006.

Huff, A. K., and Abbatt, J. P. D.: Kinetics and product yields in the heterogeneous reactions of HOBr with ice surfaces containing NaBr and NaCl, Journal of Physical Chemistry A, 106, 5279-5287, 10.1021/jp014296m, 2002.

Impey, G., Shepson, P., Hastie, D., Barrie, L., and Anlauf, K.: Measurements of photolyzable chlorine and bromine during the Polar sunrise experiment 1995, Journal of Geophysical Research-Atmospheres, 102, 16005-16010, 10.1029/97JD00851, 1997.

Jobson, B. T., Niki, H., Yokouchi, Y., Bottenheim, J., Hopper, F., and Leaitch, R.: Measurements of C2–C6 hydrocarbons during the Polar Sunrise 1992 Experiment: Evidence for Cl atom and Br atom chemistry, Journal of Geophysical Research-Atmospheres, 99, 25355-25368, 10.1029/94jd01243, 1994.

Kaleschke, L., Richter, A., Burrows, J., Afe, O., Heygster, G., Notholt, J., Rankin, A. M., Roscoe, H. K., Hollwedel, J., Wagner, T., and Jacobi, H. W.: Frost flowers on sea ice as a source of sea salt and their influence on tropospheric halogen chemistry, Geophysical Research Letters, 31, 10.1029/2004gl020655, 2004.

Keil, A. D., and Shepson, P. B.: Chlorine and bromine atom ratios in the springtime Arctic troposphere as determined from measurements of halogenated volatile organic compounds, Journal of Geophysical Research-Atmospheres, 111, 11, 10.1029/2006jd007119, 2006.

King, M., and Simpson, W.: Extinction of UV radiation in Arctic snow at Alert, Canada (82 degrees N), Journal of Geophysical Research-Atmospheres, 106, 12499-12507, 10.1029/2001JD900006, 2001.

Kleindienst, T. E., Shepson, P. B., Nero, C. M., and Bufalini, J. J.: THE PRODUCTION OF CHLORINE ATOMS FROM THE REACTION OF OH WITH CHLORINATED HYDROCARBONS, International Journal of Chemical Kinetics, 21, 863-884, 10.1002/kin.550211002, 1989.

Langner, J., and Rodhe, H.: A GLOBAL 3-DIMENSIONAL MODEL OF THE TROPOSPHERIC SULFUR CYCLE, Journal of Atmospheric Chemistry, 13, 225-263, 10.1007/bf00058134, 1991.

Lelieveld, J., Crutzen, P. J., and Dentener, F. J.: Changing concentration, lifetime and climate forcing of atmospheric methane, Tellus Series B-Chemical and Physical Meteorology, 50, 128-150, 10.1034/j.1600-0889.1998.t01-1-00002.x, 1998.

Liao, J., Huey, L., Tanner, D., Flocke, F., Orlando, J., Neuman, J., Nowak, J., Weinheimer, A., Hall, S., Smith, J., Fried, A., Staebler, R., Wang, Y., Koo, J., Cantrell, C., Weibring, P., Walega, J., Knapp, D., Shepson, P., and Stephens, C.: Observations of inorganic bromine (HOBr, BrO, and Br-2) speciation at Barrow, Alaska, in spring 2009, Journal of Geophysical Research-Atmospheres, 117, 10.1029/2011JD016641, 2012.

Liao, J., Huey, L., Liu, Z., Tanner, D., Cantrell, C., Orlando, J., Flocke, F., Shepson, P., Weinheimer, A., Hall, S., Ullmann, K., Beine, H., Wang, Y., Ingall, E., Stephens, C., Hornbrook, R., Apel, E., Riemer, D., Fried, A., Mauldin, R., Smith, J., Staebler, R., Neuman, J., and Nowak, J.: High levels of molecular chlorine in the Arctic atmosphere, Nature Geoscience, 7, 91-94, 10.1038/NGEO2046, 2014.

Lindberg, S. E., Brooks, S., Lin, C. J., Scott, K. J., Landis, M. S., Stevens, R. K., Goodsite, M., and Richter, A.: Dynamic oxidation of gaseous mercury in the Arctic troposphere at polar sunrise, Environmental Science & Technology, 36, 1245-1256, 10.1021/es0111941, 2002.

Mack, J., and Bolton, J. R.: Photochemistry of nitrite and nitrate in aqueous solution: a review, Journal of Photochemistry and Photobiology a-Chemistry, 128, 1-13, 10.1016/s1010-6030(99)00155-0, 1999.

Maslanik, J., Stroeve, J., Fowler, C., and Emery, W.: Distribution and trends in Arctic sea ice age through spring 2011, Geophysical Research Letters, 38, 10.1029/2011gl047735, 2011.

McConnell, J., Henderson, G., Barrie, L., Bottenheim, J., Niki, H., Langford, C., and Templeton, E.: Photochemical Bromine Producation Implicated in Arctic Boundary-Layer Ozone Depletion, Nature, 355, 150-152, 10.1038/355150a0, 1992.

Michalowski, B., Francisco, J., Li, S., Barrie, L., Bottenheim, J., and Shepson, P.: A computer model study of multiphase chemistry in the Arctic boundary layer during polar sunrise, Journal of Geophysical Research-Atmospheres, 105, 15131-15145, 10.1029/2000JD900004, 2000.

Michelsen, H. A., Salawitch, R. J., Wennberg, P. O., and Anderson, J. G.: Production of $O(^1D)$ from photolysis of O_3, Geophysical Research Letters, 21, 2227-2230, 10.1029/94gl02052, 1994.

Moore, C. W., Obrist, D., Steffen, A., Staebler, R. M., Douglas, T. A., Richter, A., and Nghiem, S. V.: Convective forcing of mercury and ozone in the Arctic boundary layer induced by leads in sea ice, Nature, 506, 81-84, 10.1038/nature12924, 2014.

Muthuramu, K., Shepson, P. B., Bottenheim, J. W., Jobson, B. T., Niki, H., and Anlauf, K. G.: RELATIONSHIPS BETWEEN ORGANIC NITRATES AND SURFACE OZONE DESTRUCTION DURING POLAR SUNRISE EXPERIMENT 1992, Journal of Geophysical Research-Atmospheres, 99, 25369-25378, 10.1029/94jd01309, 1994.

Nilsson, E. D., Rannik, U., Swietlicki, E., Leck, C., Aalto, P. P., Zhou, J., and Norman, M.: Turbulent aerosol fluxes over the Arctic Ocean 2. Wind-driven sources from the sea, Journal of Geophysical Research-Atmospheres, 106, 32139-32154, 10.1029/2000jd900747, 2001.

Ninomiya, T., Ohmori, H., Hashimoto, K., Tsuruta, K., and Ekino, S.: Expansion of methylmercury poisoning outside of minamata: An epidemiological study on chronic methylmercury poisoning outside of minamata, Environmental Research, 70, 47-50, 10.1006/enrs.1995.1045, 1995.

Perovich, D. K., and Richtermenge, J. A.: SURFACE CHARACTERISTICS OF LEAD ICE, Journal of Geophysical Research-Oceans, 99, 16341-16350, 10.1029/94jc01194, 1994.

Peterson, P., Simpson, W., Pratt, K., Shepson, P., Frieb, U., Zielcke, J., Platt, U., Walsh, S., and Nghiem, S.: Meteorological controls on the vertical distribution of bromine monoxide in the lower troposphere, Atmos. Chem. Phys., 23949-23994, 2014.

Pratt, K., Custard, K., Shepson, P., Douglas, T., Pohler, D., General, S., Zielcke, J., Simpson, W., Platt, U., Tanner, D., Huey, L., Carlsen, M., and Stirm, B.: Photochemical production of molecular bromine in Arctic surface snowpacks, Nature Geoscience, 6, 351-356, 10.1038/NGEO1779, 2013.

Prinn, R. G., Weiss, R. F., Miller, B. R., Huang, J., Alyea, F. N., Cunnold, D. M., Fraser, P. J., Hartley, D. E., and Simmonds, P. G.: Atmospheric trends and lifetime of CH_3CCl_3 and global OH concentrations, Science, 269, 187-192, 10.1126/science.269.5221.187, 1995.

Rahn, K. A., Borys, R. D., and Shaw, G. E.: Asian source of Arctic haze bands, Nature, 268, 713-715, 10.1038/268713a0, 1977.

Richter, A., Wittrock, F., Eisinger, M., and Burrows, J. P.: GOME observations of tropospheric BrO in northern hemispheric spring and summer 1997, Geophysical Research Letters, 25, 2683-2686, 10.1029/98gl52016, 1998.

Saiz-Lopez, A., Mahajan, A. S., Salmon, R. A., Bauguitte, S. J. B., Jones, A. E., Roscoe, H. K., and Plane, J. M. C.: Boundary layer halogens in coastal Antarctica, Science, 317, 348-351, 10.1126/science.1141408, 2007.

Salawitch, R., Canty, T., Kurosu, T., Chance, K., Liang, Q., da Silva, A., Pawson, S., Nielsen, J., Rodriguez, J., Bhartia, P., Liu, X., Huey, L., Liao, J., Stickel, R., Tanner, D., Dibb, J., Simpson, W., Donohoue, D., Weinheimer, A., Flocke, F., Knapp, D., Montzka, D., Neuman, J., Nowak, J., Ryerson, T., Oltmans, S., Blake, D., Atlas, E., Kinnison, D., Tilmes, S., Pan, L., Hendrick, F., Van Roozendael, M., Kreher, K., Johnston, P., Gao, R., Johnson, B., Bui, T., Chen, G., Pierce, R., Crawford, J., and Jacob, D.: A new interpretation of total column BrO during Arctic spring, Geophysical Research Letters, 37, 10.1029/2010GL043798, 2010.

Schnell, R. C.: ARCTIC HAZE AND THE ARCTIC GAS AND AEROSOL SAMPLING PROGRAM (AGASP), Geophysical Research Letters, 11, 361-364, 10.1029/GL011i005p00361, 1984.

Schroeder, W. H., Anlauf, K. G., Barrie, L. A., Lu, J. Y., Steffen, A., Schneeberger, D. R., and Berg, T.: Arctic springtime depletion of mercury, Nature, 394, 331-332, 10.1038/28530, 1998.

Screen, J. A., and Simmonds, I.: The central role of diminishing sea ice in recent Arctic temperature amplification, Nature, 464, 1334-1337, 10.1038/nature09051, 2010.
Serreze, M. C., and Barry, R. G.: Processes and impacts of Arctic amplification: A research synthesis, Global and Planetary Change, 77, 85-96, 10.1016/j.gloplacha.2011.03.004, 2011.

Shaw, G. E.: Evidence for a central Eurasin source area of Arctic haze in Alaska, Nature, 299, 815-818, 10.1038/299815a0, 1982.

Shaw, G. E.: The Arctic haze phenomenon, Bulletin of the American Meteorological Society, 76, 2403-2413, 10.1175/1520-0477(1995)076<2403:tahp>2.0.co;2, 1995.

Shepson, P., Ariya, P., and Deal, C.: Ocean-Atmosphere-Sea Ice-Snowpack Interactions, Changes, and Feedbacks in Polar Regions: A Scientific Challenge for the 21st Century, 11, EOS, 117-118, 2012.

Simpson, W., Carlson, D., Honninger, G., Douglas, T., Sturm, M., Perovich, D., and Platt, U.: First-year sea-ice contact predicts bromine monoxide (BrO) levels at Barrow, Alaska better than potential frost flower contact, Atmospheric Chemistry and Physics, 7, 621-627, 2007a.

Simpson, W., von Glasow, R., Riedel, K., Anderson, P., Ariya, P., Bottenheim, J., Burrows, J., Carpenter, L., Friess, U., Goodsite, M., Heard, D., Hutterli, M., Jacobi, H., Kaleschke, L., Neff, B., Plane, J., Platt, U., Richter, A., Roscoe, H., Sander, R., Shepson, P., Sodeau, J., Steffen, A., Wagner, T., and Wolff, E.: Halogens and their role in polar boundary-layer ozone depletion, Atmospheric Chemistry and Physics, 7, 4375-4418, 2007b.

Singh, H. B., Kanakidou, M., Crutzen, P. J., and Jacob, D. J.: High concentrations and photochemical fate of oxygenated hydrocarbons in the global troposphere, Nature, 378, 50-54, 10.1038/378050a0, 1995.

Steffen, A., Douglas, T., Amyot, M., Ariya, P., Aspmo, K., Berg, T., Bottenheim, J., Brooks, S., Cobbett, F., Dastoor, A., Dommergue, A., Ebinghaus, R., Ferrari, C., Gardfeldt, K., Goodsite, M. E., Lean, D., Poulain, A. J., Scherz, C., Skov, H., Sommar, J., and Temme, C.: A synthesis of atmospheric mercury depletion event chemistry in the atmosphere and snow, Atmospheric Chemistry and Physics, 8, 1445-1482, 2008.

Stroeve, J. C., Serreze, M. C., Holland, M. M., Kay, J. E., Malanik, J., and Barrett, A. P.: The Arctic's rapidly shrinking sea ice cover: a research synthesis, Climatic Change, 110, 1005-1027, 10.1007/s10584-011-0101-1, 2012.

Tang, T., and McConnell, J.: Autocatalytic release of bromine from Arctic snow pack during polar sunrise, Geophysical Research Letters, 23, 2633-2636, 10.1029/96GL02572, 1996.

Thompson, A. M.: THE OXIDIZING CAPACITY OF THE EARTHS ATMOSPHERE - PROBABLE PAST AND FUTURE CHANGES, Science, 256, 1157-1165, 10.1126/science.256.5060.1157, 1992.

Vogt, R., Crutzen, P., and Sander, R.: A mechanism for halogen release from sea-salt aerosol in the remote marine boundary layer, Nature, 383, 327-330, 10.1038/383327a0, 1996.

Wallace, J. M., and Hobbs, P. V.: Atmospheric science : an introductory survey, Academic Press, New York, xvii, 467 p. pp., 1977.

Wren, S. N., and Donaldson, D. J.: How does deposition of gas phase species affect pH at frozen salty interfaces?, Atmospheric Chemistry and Physics, 12, 10065-10073, 10.5194/acp-12-10065-2012, 2012.

Wren, S. N., Donaldson, D. J., and Abbatt, J. P. D.: Photochemical chlorine and bromine activation from artificial saline snow, Atmospheric Chemistry and Physics, 13, 9789-9800, 10.5194/acp-13-9789-2013, 2013.

Yang, X., Pyle, J. A., Cox, R. A., Theys, N., and Van Roozendael, M.: Snow-sourced bromine and its implications for polar tropospheric ozone, Atmospheric Chemistry and Physics, 10, 7763-7773, 10.5194/acp-10-7763-2010, 2010.

CHAPTER 2 A FLOWING CHEMICAL REACTION METHOD FOR THE QUANTITATIVE DETECTION OF HALOGEN FREE RADICALS IN ARTIC AMBIENT AIR

2.1 Introduction

It has been observed that halogen radicals are the main cause of ozone depletion events (ODEs) and atmospheric mercury depletion events (AMDE) experienced during polar sunrise in the Arctic (Barrie et al., 1988;Bottenheim et al., 1986;Schroeder et al., 1998). To gain a proper understanding of the complex chemistry involved in ODEs and AMDEs, ambient halogen radical concentrations must be known. Early attempts at quantifying reactive halogen species involved indirect techniques, one being a kinetic analysis of NMHC decay during ODEs (Ariya et al., 1998;Jobson et al., 1994;Keil and Shepson, 2006;Cavender et al., 2008). Long path-differential optical absorption spectrometry (LP-DOAS) was used as an early direct measurement method for detecting halogen radical species and was deployed during the 1992 Polar Sunrise Experiment. *Hausmann and Platt* (1994) were able to measure ambient BrO concentrations up to 17 ppt at Alert, Canada, during April. Differential optical absorption spectrometry (DOAS) has been used extensively to measure halogen oxides concentrations at various locations around the world including the Arctic, Antarctica, for volcanic emissions in Europe, and coastal Europe (Carpenter et al., 1999;Tuckermann et al., 1997;Honninger and Platt, 2002;Peters et al., 2005;Kreher et al., 1997;Bobrowski et al., 2007). DOAS works by

analyzing the narrow band absorption in the UV and visible region that is unique for the desired specie. The concentration is derived by fitting the absorption in the spectral range appropriate of the species (Platt and Stutz, 2008).

Other halogen oxides that have been detected by DOAS include IO, which has been quantified at Mace Head on the coast of Ireland at levels up to 2.5 ppt and up to 21 ppt on the coast of Antarctica at the Halley Station (Saiz-Lopez et al., 2006;Saiz-Lopez et al., 2007). The only published ClO Arctic data occurred during two different field campaigns in Ny-Ålesund, Spitsbergen, in the spring of 1995 and 1996 by *Tuckermann* (1997). DOAS was used to detect near surface ClO, at levels up to 21 ppt (1995) and 10 ppt (1996), although measurements were close to the limit of detection of 18 and 8.5 ppt, respectively (Tuckermann et al., 1997). But, in the 18 years since the Tuckermann et al. paper, there have been no reports of ClO measurements, and no reported progress in analytical methodologies.

Chemical ionization mass spectrometry (CIMS) has the ability to directly detect halogen monoxide radicals (ClO, BrO, and IO). *Liao* et. al. reported ambient BrO concentrations of up to 35 ppt in Barrow, Alaska during April of 2012 (Liao et al., 2012). They reported an intercomparison of LP-DOAS and CIMS, and found that BrO concentrations during low NO_x and medium wind speeds were highly correlated (R^2=0.85) (Liao et al., 2011). The high correlation confirmed that both techniques are capable of detecting and accurately quantifying atmospheric BrO. However, both DOAS and CIMS techniques do not allow for the detection and quantification of halogen atoms. The flowing chemical reaction method was developed, to directly quantify BrO_x (BrO + Br) and ClO_x (ClO + Cl) via the conversion of halogen radicals to a stable and detectable

halogenated product, through the reaction of Br and Cl radicals with a reactant that will incorporate the halogen atom into a stable product analyte molecule.

2.2 Method Theory

The ability to directly quantify halogen radicals' (ClO_x and BrO_x) mole ratios in the Arctic ambient air is needed to further understand the chemistry that is the driving force behind ozone depletion events (ODEs) and atmospheric mercury depletion events (AMDEs). A flowing chemical reaction (flowtube) method was developed at Purdue University to measure ambient halogen radicals' mole ratios by converting the highly reactive halogen radicals into a stable and detectable halogenated ketone product through a series of reactions, utilizing a halogen atom scavenging reagent gas (Tackett, 2008). Dr. Phil Tackett designed the flowtube and a means to conduct sampling via gas chromatography. The reaction takes place on a time scale several orders of magnitude shorter than the residence time (~9.4 secs) inside of the flowtube. For the flowtube method to work properly, the halogen radical scavenger (reagent gas) was selected based on several criteria:

1. The reagent gas must not occur naturally in the Arctic atmosphere at mole ratios that would lead to interferences within blank and ambient measurements, to ensure that a low limit of detection can be achieved.
2. The time scale for the reaction of the reagent gas with Br and Cl atoms must allow for reaction completion within the first few centimeters of the flowtube to eliminate loss of the halogen radicals to the walls of the flowtube.

3. The reaction yield for the stable halogenated product must be high enough to allow for low concentration (low ppt) halogen radical quantification.
4. The halogenated products need to be separated (baseline resolved) and detected with high sensitivity using gas chromatography with electron capture detection (GC-ECD).

Previous deployments of the flowtube method used the reagent gases 1,1,1-trifluoropropene and allyl bromide with relative success (Tackett, 2008;Stephens, 2012). However, using 1,1,1-trifluoropropene leads to products that are relatively volatile and required a very low initial oven temperature (< -25°C) to properly separate the peaks using gas chromatography. In the lab this was done using liquid N_2, however the flowtube method was deployed in remote Arctic locations making the use of liquid nitrogen very expensive and impractical. Allyl bromide was able to detect BrO_x but the yield for the flowtube product of chlorine atoms reacting with allyl bromide was too low (0.3%). For these reasons a new reagent gas was selected, trans-2-butene.

The flowtube reaction scheme using trans-2-butene is as follows: First ambient air is pumped into the flowtube where it is immediately mixed with trans-2-butene and nitric oxide (NO). NO is needed to convert halogen monoxides to halogen radicals (2.1).

$$NO + XO\cdot \rightarrow NO_2 + \cdot X \qquad (2.1)$$

The halogen atoms attack the double bond in trans-2-butene and in the presence of molecular oxygen, a peroxy radical is formed. The NO added to the flowtube will then extract an oxygen atom from the peroxy radical to form NO_2 and yield an alkoxy radical. Molecular oxygen will then remove a hydrogen atom from the alpha carbon atom, forming HO_2 and the stable halogenated product.

$$\cdot X + CH_3CH{=}CHCH_3 \rightarrow CH_3CH(\cdot)CHXCH_3 \quad (2.2)$$

$$CH_3CH(\cdot)CHXCH_3 + O_2 \rightarrow CH_3CH(OO\cdot)CHXCH_3 \quad (2.3)$$

$$CH_3CH(OO\cdot)CHXCH_3 + NO \rightarrow CH_3CH(O\cdot)CHXCH_3 + NO_2 \quad (2.4)$$

$$CH_3CH(O\cdot)CHXCH_3 + O_2 \rightarrow CH_3C(=O)CHXCH_3 + HO_2 \quad (2.5)$$

The products that result from the above reaction scheme are 3-bromo-2-butanone (Br-butanone) and 3-chloro-2-butanone (Cl-butanone) for the addition by Br and Cl radicals, respectively.

2.3 Flowtube Design

The original development and deployment of the flowing chemical reaction chamber was performed and described in detail in Tackett (2008). Therefore, only a brief description of the flowing chemical reaction chamber will be given here.

The 750 cm long quartz flowtube (Figure 2.1) is equipped with a 20 mm ID opening at one end to serve as the inlet into the flowtube for sampling ambient air. Quartz was used to enable photochemical processes for method development. The opposite end of the flowtube has a ¼″ OD vacuum port that is attached to a diaphragm pump to draw the ambient air through the flowtube at a rate of 1.5 slpm. The flowtube has four ¼″ OD glass side ports for introducing the reagent gases into the flowtube along with sampling the final stable halogenated product. The two side ports (left side) located near the inlet each connect to a quartz gas dispersion frit for introducing the reagent gases into the flowtube. The frits were designed to disperse the reagents at the head of the flowtube in countercurrent fashion. Turbulence within the flowtube enhances mixing of

the ambient radicals with the reagent gases. An image of the flowtube is shown in Figure 2.1.

Figure 2.1 Photo of the quartz flowtube used in the flowing chemical reaction method. The reagent gas inlet frit is located on the far left and the sampling inlet is located on the far right side of the flowtube.

The dimensions and flow rate for the flowtube were based on minimizing wall loss of the sampled halogen radicals. Within the limit of laminar flow, molecular diffusion can be used to calculate the time scale (τ_{MD}) for which the radicals will diffuse to the walls of the flowtube and be irreversibly absorbed. The τ_{MD} is influenced by the size of the diffusing gases, the temperature and pressure within the vessel, along with the medium in which the molecule is traveling. First, laminar flow within the flowtube must be ensured so that the only cause of mass transfer to the walls will be from molecular diffusion. Laminar flow is defined as smooth, undistributed flow where the flow layers run parallel to one another. To determine if a flow is laminar the Reynolds number (R_e) can be calculated (Equation 2.I).

$$R_e = \frac{u \cdot d}{\nu} \qquad (2.I)$$

The Reynolds number characterizes the flow and is calculated using the fluid linear velocity (u) in $m \cdot s^{-1}$, the inner diameter of the flowtube (d), and the kinematic viscosity of the fluid (ν) in $m^2 \cdot s^{-1}$. Laminar flow is defined as a Reynolds number of <2300. The fluid linear velocity is calculated using Equation 2.II.

$$u = \frac{\text{flowrate}}{\pi \cdot r^2} \qquad (2.II)$$

For the flowtube method a volumetric flow rate of 1.5 slpm is used, that along with the flowtube's radius (r) of 1 cm, a linear velocity of 0.08 $m \cdot s^{-1}$ is achieved. At a temperature of 300K, air has a kinematic velocity of 1.6×10^{-5} $m^2 \cdot s^{-1}$, as calculated using the online Engineering Toolbox (http://www.engineeringtoolbox.com/). This yields a Reynolds number of 100 which is within the laminar flow regime.

The molecular diffusion time scale can be calculated using Equation 2.III, where r represents the radius of the flowtube in meters and D_g represents the gas-phase diffusion coefficient for the specie of interest (Roberts and Webster, 2002).

$$\tau_{MD} = \frac{r^2}{2 \cdot D_g} \qquad (2.III)$$

Of the four species of interest, (ClO, Cl, BrO and Br) Cl atoms have the largest diffusion coefficient of 0.183 $cm^2 \cdot s^{-1}$. The gas-phase diffusion coefficient was calculated using Equation (2.IV), where k is the boltzmann constant (1.38×10^{-23} $m^2 \cdot kg \cdot s^{-1} \cdot K^{-1}$), T is the temperature (273K), and *f* is the frictional velocity.

$$D_g = \frac{k \cdot T}{f} \qquad (2.IV)$$

Equation 2.III yields a time scale of ~2.7 seconds for Cl atoms to diffuse to the walls of the flowtube. Therefore, the flowtube reaction mechanism must occur within a time scale much less than 2.7 seconds to minimize the loss of halogen radicals to the flowtube walls. Based on the chlorine atom's timescale for molecular diffusion (2.7 secs), the entire flowtube reaction mechanism should occur within ~0.027 seconds. This is two orders of magnitude faster than the molecular diffusion timescale, which will minimize wall loss. The first step toward achieving the desired time scale of ~0.027 seconds is to determine the NO concentration needed to convert all the XO to X.

$$\frac{1}{\tau} = k_{ClO+NO} \cdot [NO] \qquad (2.V)$$

Given that k_{ClO+NO} is 2.04×10^{-11} $cm^3 \cdot molec^{-1} \cdot s^{-1}$, we calculate an NO concentration of 72 ppb using equation 2.V, which represents the necessary concentration needed to convert all the XO to X on the desired timescale for the entire flowtube mechanism. However, a higher concentration of NO (1 ppm) was used during deployment based on NO calibration standard availability. This would only decrease the time scale for the conversion of XO to X. Using Equation 2.V, XO will have a lifetime of < 0.002 seconds, one order of magnitude less than the target time frame for the flowtube reaction mechanism.

Following the conversion of all the XO to X, trans-2-butene must then scavenge all the available halogen atoms. Using Equation 2.VI, an initial concentration of 52ppb was calculated for trans-2-butene, to ensure that all the halogen radicals will react with trans-2-butene within our desired flowtube reaction time frame.

$$\frac{1}{\tau} = k_{Cl+T2B} \cdot [T2B] \qquad (2.VI)$$

However, halogen atoms are extremely reactive and within the flowtube can be scavenged by various compounds present in the ambient Arctic air. The two main sinks for bromine and chlorine atoms in ambient air are ozone and methane, respectively. To guarantee that trans-2-butene reacts with >99% of the halogen atoms Equation 2.VII and 2.VIII were used to determine the necessary trans-2-butene concentration. For the bromine atom calculation the typical Arctic ambient ozone concentration of 40 ppb ($1x10^{12}$ molec·cm^{-3}) was used and the BrO + O_3 rate constant was $7x10^{-13}$ cm^3·molec^{-1}·s^{-1}. The solution from Equation 2.VII produced a trans-2-butene concentration of 370 ppb.

$$\frac{k[Br][T2B]}{k[Br][O_3]} = 100 \qquad \text{(2.VII)}$$

A similar calculation for the competing reaction of Cl + CH_4 was performed, using a methane concentration of 1.98 ppm ($5x10^{13}$ molec·cm^{-3}) and rate constant of $4.33x10^{-14}$ cm^3·molec^{-1}·s^{-1}. This yielded a concentration of 26 ppb for trans-2-butene.

$$\frac{k[Cl][T2B]}{k[Cl][CH_4]} = 100 \qquad \text{(2.VIII)}$$

Based on the two calculations a concentration of 370 ppb of trans-2-butene will be sufficient to react with 99% of both chlorine and bromine atoms. During the field deployment a concentration of 1.5 ppm was used for both NO and trans-2-butene, as excess of both had no effect on the chromatography during laboratory studies. This assured a >99% efficiency for trans-2-butene to react with both bromine and chlorine atoms, while allowing the flowtube reactions to complete on a time scale that is orders of magnitude faster than the molecular diffusion rate of Cl or Br atoms to the walls of the flowtube.

2.4 Product Yield

To properly quantify ClO_x and BrO_x using the flowtube method, the percent yield of the stable halogenated products was determined.

To experimentally determine the percent yield for the flowtube products, a covered Teflon (FEP, American Durafilm) bag (60L) was filled with compressed air (Ultra High Purity 5.0, Praxair). During the filling process the experimental reactants (trans-2-butene, molecular halogen, NO, O_2 and an OH scavenger) were injected into a glass tee that connected the air flow to the Teflon bag. An OH scavenger was used during the experiments to ensure that the decrease in the trans-2-butene concentration was from the reaction with the halogen atom and not OH. For the chlorine experiments benzene was used as an OH scavenger because the rate constant for OH reaction ($1.28x10^{-12}$ $cm^3 \cdot molec^{-1} \cdot s^{-1}$) with benzene was much greater than Cl radicals ($1.3x10^{-15}$ $cm^3 \cdot molec^{-1} \cdot s^{-1}$) reacting with benzene. For the bromine experiments, cyclohexane was used because OH radicals, but not Br atoms, react with cyclohexane. During the experiment the bag was periodically exposed to UV radiation for a short time to photolyze the molecular halogens into halogen radicals to initiate the reaction. After each irradiation, a sample was acquired and analyzed using the GC-ECD and a gas chromatograph equipped with a flame ionization detector (GC-FID). The GC-ECD was used to monitor the increase in concentration of the halogenated product, while the GC-FID was used to determine the decrease in concentration of trans-2-butene. The product yield was determined by plotting the concentration of Cl-butanone or Br-butanone product vs the loss of trans-2-butene on the x-axis. The slope of the plot is equal to the

fractional value of the product yield. Figure 2.2 shows the results from each product yield experiment for both bromine and chlorine reaction with trans-2-butene.

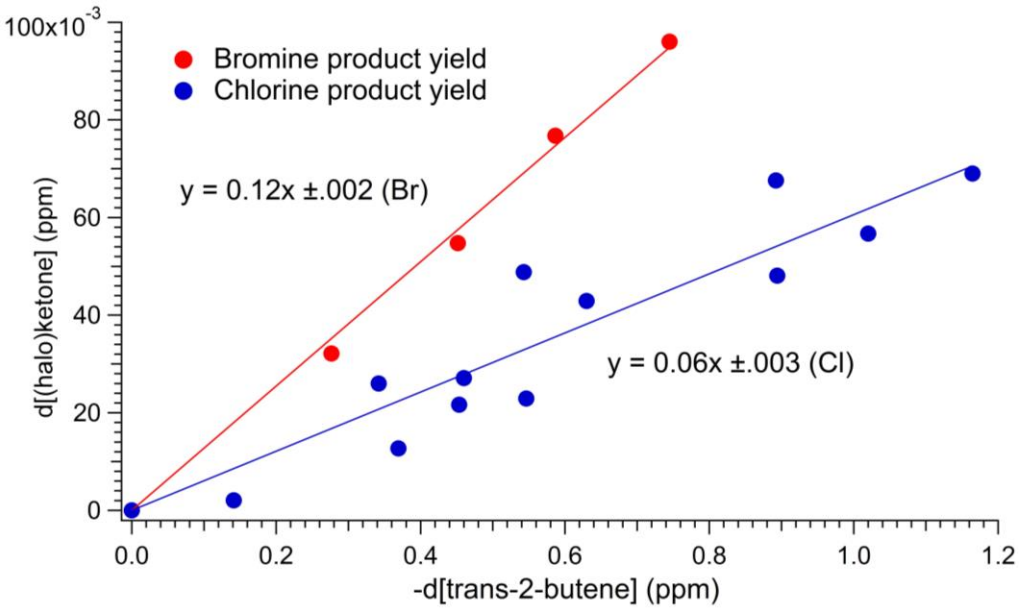

Figure 2.2 Plot of Cl-butanone and Br-butanone concentrations vs T2B loss during product yield experiments.

The percent yield for the desired product for the reaction of trans-2-butene with Br is 12(±.2) % while the percent yield is 6(±.3) % for the reaction with Cl. The best fit lines were forced through zero as the y-intercept was determined to be statistically insignificant.

2.5 Product Separation and Detection

The halogenated flowtube products were detected and quantified using a gas chromatograph with an electron capture detector (GC-ECD). The field deployment set-

up for the flowtube connected to the GC-ECD will be discussed in Section 2.7. The GC used was a HP 5890 Series II GC combined with an electron capture detector (ECD) that had a ^{63}Ni radioactive source. The ^{63}Ni source emits beta particles that collide with the ECD's makeup gas (5% methane in Argon), producing additional free electrons that establish an electrical current, which reduce the current within the ECD cell. This change in current is used to detect and quantify electronegative species in a sample. Separation of the halogenated ketone products was achieved using a Restek Rtx-624 (30m mid polarity 6% cyanopropylphenyl/94% dimethyl polysiloxane, .32mm ID, 1.8µm film thickness) column using He (UHP 5.0, Praxair) as a carrier gas with a column flow rate of 11mL·min^{-1}. Both the carrier gas and P5 were purified by flowing the gases through chemical traps that removed O_2, H_2O, and hydrocarbons from the flow. These species can lead to interferences and a larger background signal. This was done for both the lab studies and the field study. Samples were flushed through a heated (100°C) 180-mL stainless steel Siltek treated sample loop connected to a 6-port Valco switching valve which injects the sample onto the head of the column. Siltek is a Restek patented deposition process used to create inert surfaces for chromatography purposes. High purity He (UHP 5.0, Praxair) was used as the carrier gas to transfer the sample from the sample loop to the GC column for separation, then to the detector for quantification. The ECD detector used ECD grade P5 (5% methane in Argon, Praxair) make-up gas. A complete schematic of the laboratory GC set-up is shown in Figure 2.3.

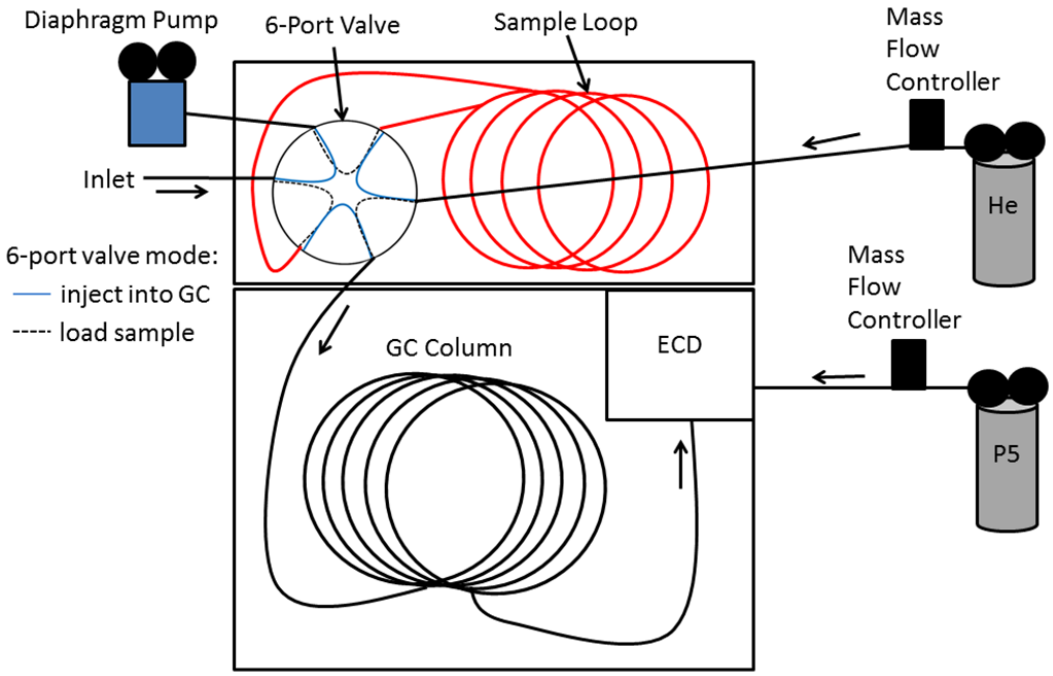

Figure 2.3 Schematic diagram of in-laboratory GC set-up to calibrate and optimize the GC conditions for Br-butanone and Cl-butanone before the field deployment.

The GC was calibrated for the flowtube products to ensure that the necessary limits of detection could be achieved so that ambient BrO_x and ClO_x in the Arctic could be quantified. The GC oven had a custom temperature program to allow for the flowtube products to be baseline resolved along with attaining Gaussian shaped peaks. The GC oven was cryocooled using liquid N_2 to -20°C for 9.5 minutes. This allowed for the flowtube products to collect at the head of the column while the entire sample air was passed through the column. The GC oven temperature was then increased to 150°C at a rate of 5°C·min^{-1}, and then increased to 230°C at 25°C·min^{-1} where it was held for 3 minutes to ensure that all the compounds injected into the column were eluted from the

GC column. An example chromatogram of the resolved product peaks, 3-chloro-2-butanone and 3-bromo-2-butanone, is shown in Figure 2.4.

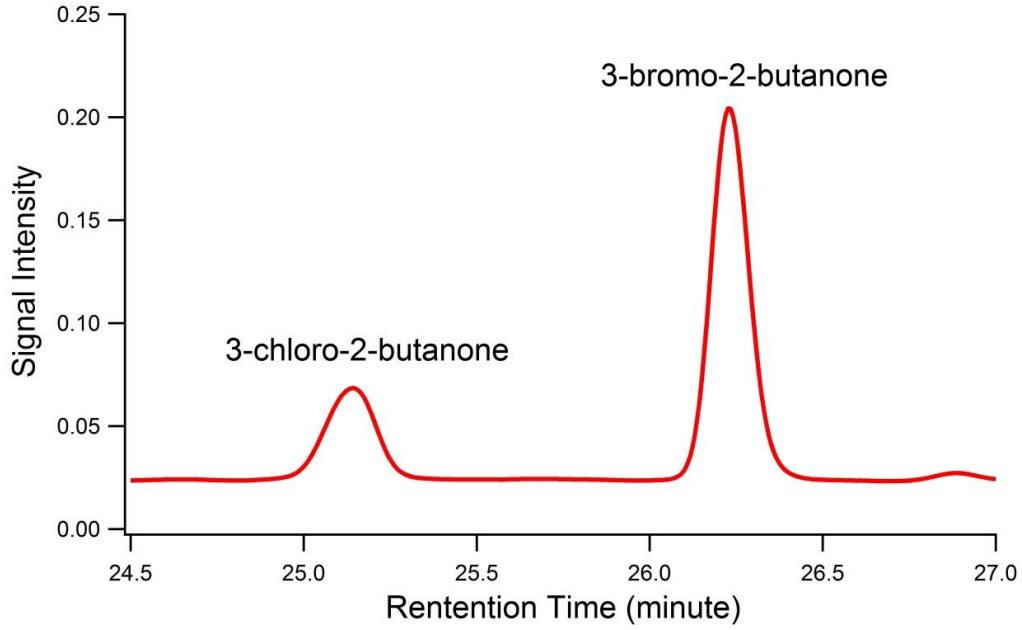

Figure 2.4 In-lab chromatogram of gas-phase calibration standards for Cl-butanone (45 ppt) and Br-butanone (32 ppt).

Instrument calibrations were performed in the laboratory using the field study deployment set-up (Fig. 2.5) prior to the field campaign. A calibration curve was made to ensure that the ECD response was linear with a zero intercept, and that it would be able to detect Cl-butanone and Br-butanone at low ppt levels (1-30 ppt) when connected to the flowtube field study set-up. A schematic of the in-lab set-up is shown in Figure 2.5. The only difference between the in-lab set-up versus the field study set-up was that the reagent gases were not connected to the flowtube for the in-lab field study set-up. Gas phase calibration standards were made in Teflon (FEP, American Durafilm) bags by

injecting known volumes (~10 μL) of a liquid phase standard containing 3-bromo-2-butanone (Sigma Aldrich) and 3-chloro-2-butanone (Alfa Aesar) dissolved in HPLC grade cyclohexane (Sigma Aldrich) into a known flow of compress air (UHP 5.0, Praxair). The Teflon bags, containing the flowtube products, were connected to the end of the flowtube via a heated ¼″ stainless steel Siltek treated calibration line that attached to a Teflon adapter (Figure 2.6). Teflon adapters were custom built by Randy Repogle of JAFCI. The Teflon adapter was secured to the inlet end of the flowtube, to allow the gas-phase standards to enter the flowtube system. In this way, the system was calibrated as used in the field.

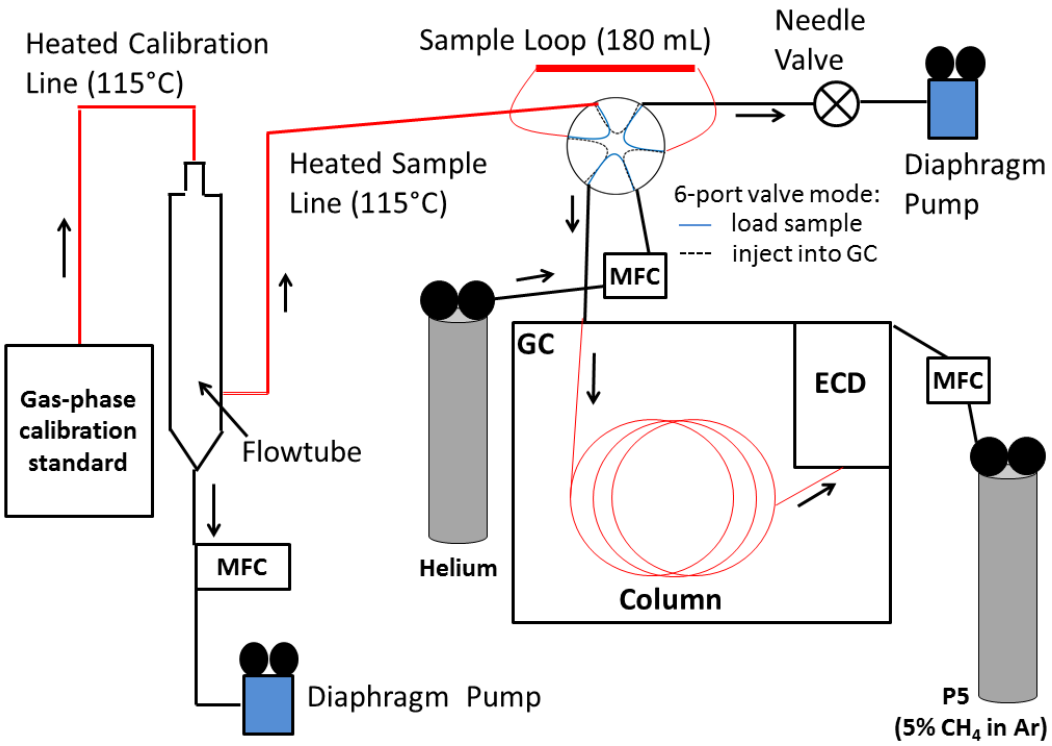

Figure 2.5 Schematic diagram of the in lab set-up of the flowtube field deployment system.

The flowtube's lower sampling port was connected to a heated (115°C) sample line (1/4″ OD stainless steel Siltek treated) that was attached to the GC-ECD via a 6-port switching valve (heated to 100°C). A 180 mL heated (100°C) sample loop (stainless steel Siltek treated) was used to allow for a lower detection limit. A larger sample loop allows for more analyte to be injected, in proportion to the sample volume. Blanks were collected by directly connecting UHP air (Praxair) to the inlet of the flowtube using the Teflon adaptor. The calibration curves for both products detected during the 2012 Barrow field deployment are shown in Figure 2.7. The sample line and calibration line used during the laboratory tests were used during the 2012 field deployment.

Figure 2.6 Teflon adaptor used in the field for connecting heated sample line to the end of the flowtube, for calibration curves.

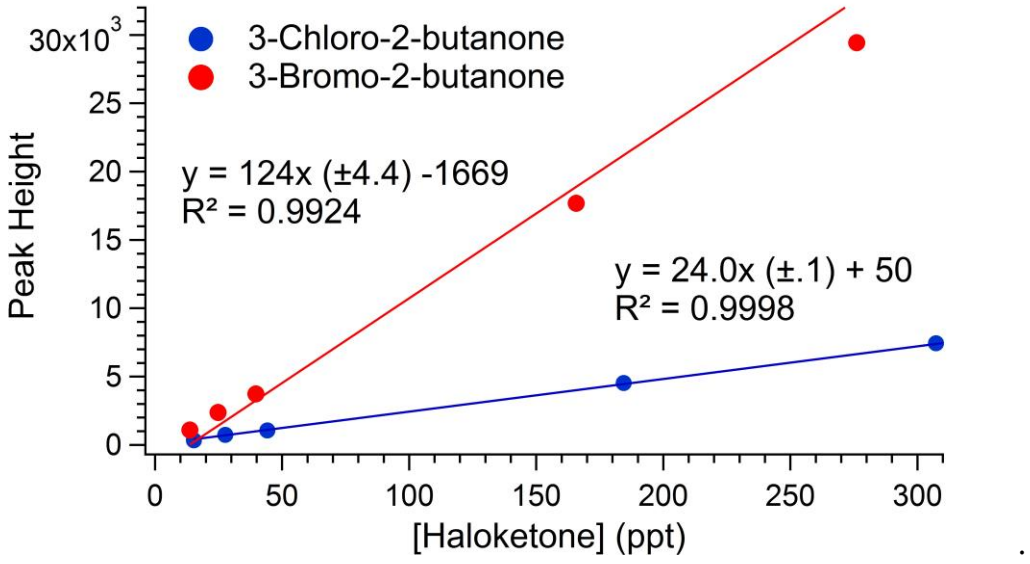

Figure 2.7 Calibration curve for Cl-butanone and Br-butanone during the 2012 BROMEX field campaign.

From the linear regression of the calibration curves the limits of detection (LOD) were calculated using Equation 2.IX.

$$\mathrm{LOD} = \frac{3\sigma_{blank}}{m} \quad (2.IX)$$

The standard deviation of the blank samples was calculated by determining the peak height and area within the retention time for both flowtube products for every blank sample taken. This was done using a Labview peak integration software routine. Retention times were determined based on the calibration samples. The LODs for 3-bromo-2-butanone and 3-chloro-2-butanone were found to be 0.26 ppt and 0.74 ppt, respectively. These were determined to be sufficient to detect and quantify ambient BrO_x and ClO_x, since previous measurements indicated concentrations in the 5 to 35 ppt and 3 to 21 ppt range, respectively.

2.6 Bromine, Mercury, and Ozone Experiment (BROMEX) 2012

The Bromine, Ozone, and Mercury Experiment (BROMEX) field campaign was an international multi-disciplinary collaborative effort that took place in Barrow, Alaska during March and April of 2012. Barrow is located on the northernmost tip of Alaska enclosed by the Chukchi Sea on the west and the Beaufort Sea on the east and north (Figure 2.8). During BROMEX a range of gas phase chemical species were quantified including several inorganic halogen species (Br_2, Cl_2, BrO, ClO, and HOBr), O_3, and gaseous elemental mercury (GEM). Meteorological stations recorded wind speed and direction along with the ambient temperature at various heights above the snowpack. Downward radiation was measured using a radiometer.

Figure 2.8 Map of the Arctic Circle, highlighting the location of Barrow, Alaska.

The motivation behind BROMEX was to study the impact that Arctic sea ice reduction is having on boundary layer chemistry that involves bromine, ozone, and mercury (http://seaice.apl.washington.edu/AirChemistry/index.html).

2.7 Field Deployment Set-up and Location

During the 2012 BROMEX field campaign, the flowtube method was setup in a sampling trailer located on the tundra (71.27513° N, 156.64031° W), 3.5 km southeast of the Chukchi Sea and 4 km east of the town of Barrow, as shown in Figure 2.9.

Figure 2.9 Map showing the location of the sampling trailer used during BROMEX in relation to the town of Barrow, Chukchi Sea and the Beaufort Sea.

In the spring (Feb 17 to April 10) of 2012 the flowtube method was used during a field study in Barrow, AK as a part of NASA's BROMEX (Bromine, Ozone, and Mercury Experiment) field campaign. The flowtube was housed in a heated (30°C) insulated aluminum box (Ned Gangwer, Purdue Chemistry Shop) that was mounted to the roof of the previously mentioned sampling trailer. The inlet of the flowtube was 4.8 meters above the snowpack surface that surrounded the sampling trailer. Figure 2.10 shows the flowtube housing box mounted on the roof of the sampling trailer.

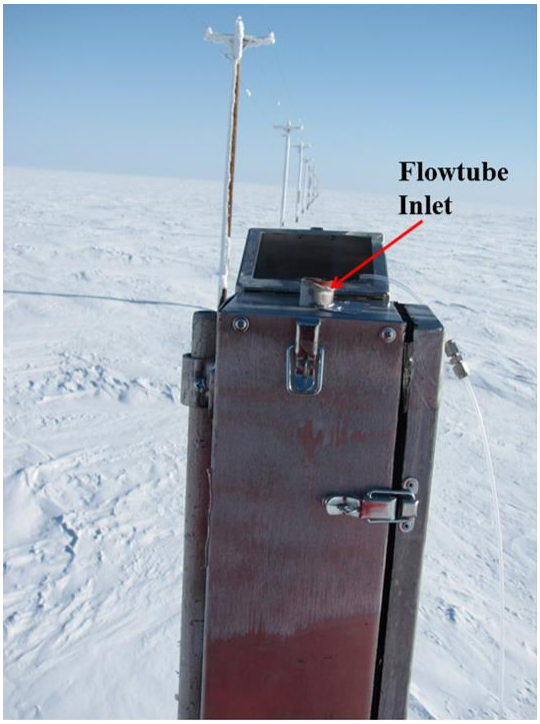

Figure 2.10 Image of flowtube in heated aluminum housing box from BROMEX field campaign.

The GC used for analysis along with the flowtube reagent gas cylinders and GC gas cylinders were stored inside the sampling trailer to which the flowtube was mounted. A schematic of the experimental set-up for the BROMEX field deployment is shown in Figure 2.11.

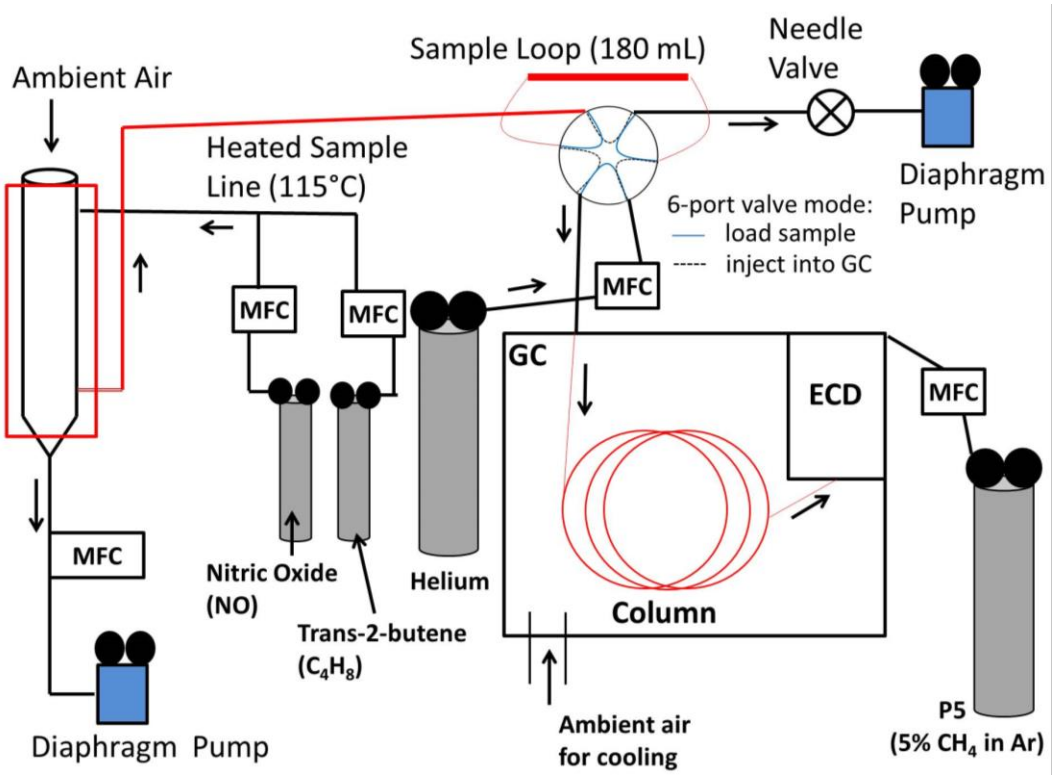

Figure 2.11 Schematic of the field deployment GC flowtube set-up for the BROMEX field campaign.

The flowtube was heated to 30°C using Omega heat wraps connected to a temperature controller. The aluminum housing was also insulated to help with the heating and to protect the fragile quartz flowtube. A heated (115°C) 3 meter ¼″ OD stainless steel Siltek treated sample line was used to connect the sampling port at the bottom of the flowtube to the GC's six-port valve via a sample line that connected the flowtube through a hole in the sampling trailer to the six-port valve. The reagent gases were connected to the flowtube's frit port via a 1/8″ OD Teflon line that was connected to a switching valve that controlled the release of the reagent gases into the flowtube. This

was controlled automatically within the data acquisition software used during the field deployment. Finally, a ¼″ OD Teflon line attached to a diaphragm pump was connected to the bottom of the flowtube. This provided a flow of 1.5 slpm ambient sample air through the flowtube.

2.8 Ambient Sampling

To initiate the collection of an ambient sample, three functions would occur automatically and simultaneously. First, the switching valve that controlled the reagent gases release to the flowtube opened. Second, the pump that pumped the ambient sample through the sample line and through the sample loop was turned on. Finally, the GC six-port valve was switched to load mode. Load mode diverts the flow of the six port valve so that an ambient sample can fill the sample loop. The sample loop was flushed for 2.5 minutes (> 5 times) to ensure a fresh sample was loaded in the sample loop before the six-port valve switched back to inject mode. While in inject mode the GC carrier gas (UHP 5.0 He) flushes the sample out of the sample loop and onto the head of the column. When the six port valve switches to inject mode the GC's temperature program automatically starts, as described earlier in Section 2.5. In the interest of economy, after the temperature program was completed the GC oven was cooled by pulling cold ambient air through the wall of the building into the GC oven via a blower. The blower was controlled by a relay switch connected to the GC and was turned on automatically when the oven needed to be cooled or held at a temperature below 25°C. The entire process resulted in hourly data points. A portion of a sample chromatogram for an ambient sample taken March 16 at 21:53 (UTC) during the BROMEX field campaign is shown in

Figure 2.12. Ambient samples were also collected only when trans-2-butene, but not NO, was released into the flowtube. This allowed for the quantification of only the halogen atom's concentration and not the total ClO_x or BrO_x concentration (reactions 2.2-2.5).

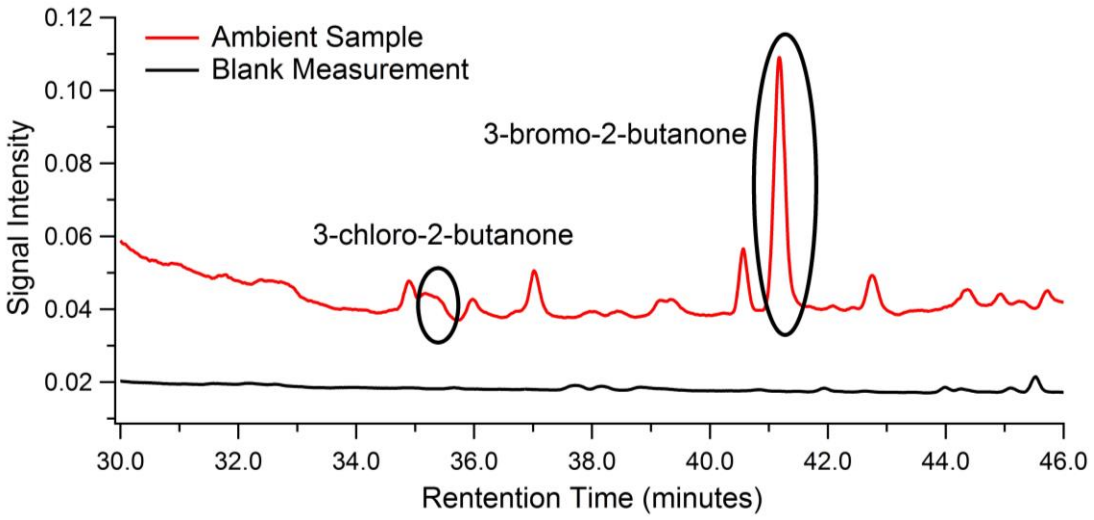

Figure 2.12 Ambient sample (red) and ambient blank (black) measurement showing bromobutanone and chlorobutanone product peaks during BROMEX 2012.

2.9 Blank Measurements and Calibrations

A different procedure was implemented during calibrations and blank measurements to ensure we were not producing any Br-butanone and Cl-butanone during those measurements, and to investigate the possibility of any carry-over between samples or cooling ambient compounds. A heated (115°C) 3.2 meter long ¼″ OD stainless steel Siltek treated calibration line was connected to the inlet of the flowtube via a Teflon adapter, as previously described in Section 2.5. A Teflon bag containing a gas-phase calibration standard was connected to the end of the calibration line that was inside the

sampling trailer. Once the Teflon bag was connected, the sampling procedure was started, as described previously. After the sample was injected into to the head of the column the Teflon adapter was removed from the flow tube's inlet to allow for ambient air to be pulled through the flowtube and, if planned, another gas-phase calibration standard was prepared in the Teflon bag.

A week after the GC-ECD was setup and the baseline was allowed to stabilize, an extensive calibration curve was produced for the flowtube products, ranging from 1 to 120 ppt. After that, one or two calibration points were obtained daily and added to the initial calibration curve to monitor the GC-ECD sensitivity throughout the field campaign. During the field campaign the LOD for bromobutanone and chlorobutanone were 1.5 and 7.5 ppt, respectively. The higher LOD during the field campaign could be due to a higher baseline signal compared to the lab studies.

To properly quantify ClO_x and BrO_x concentrations based on our measurements, blank measurements needed to be obtained to subtract from the ambient signal. Several blank samples were acquired daily to ensure the baseline was steady and to track interference peaks. Six different types of blanks were collected, four for ambient measurements and two for calibration measurements, as follows:

- Ambient air without reagent gases present
- Ambient air with only NO present
- UHP air directly connected to flowtube
- UHP air directly connected to the flowtube with trans-2-butene
- UHP air sampled through calibration line that was connected to flowtube
- Teflon bag filled with UHP directly connected to GC

Sampling ambient air in the absence of the reagent gases would show any ambient compounds that have a similar retention time as our flowtube products. Sampling ambient air with just NO would show if the NO mixture had any impurities that were causing interfering peaks. The same test was done when UHP air and trans-2-butene were sampled. UHP air directly connected to the flowtube was used to show the baseline of our field measurement without any interference from species in the ambient air. UHP air sampled through the calibration line was used to check for contamination from the calibration line that would interfere with the calibration curve. Finally, Teflon bags were filled with UHP and directly connected to the GC to measure any contamination from the Teflon bags. The most common blanks performed were only sampling ambient air and sampling UHP air through the calibration line. A sample chromatogram for an ambient air blank is shown in Figure 2.12 (black line).

2.10 Results

BrO_x and ClO_x measurements were performed from March 13th to April 3rd 2012. However, data collection was not continuous due to instrumentation malfunctions that occurred from March 25-29. A time series of BrO_x, ClO_x, O_3 and radiation from March 17 to 23 is shown in Figure 2.13.

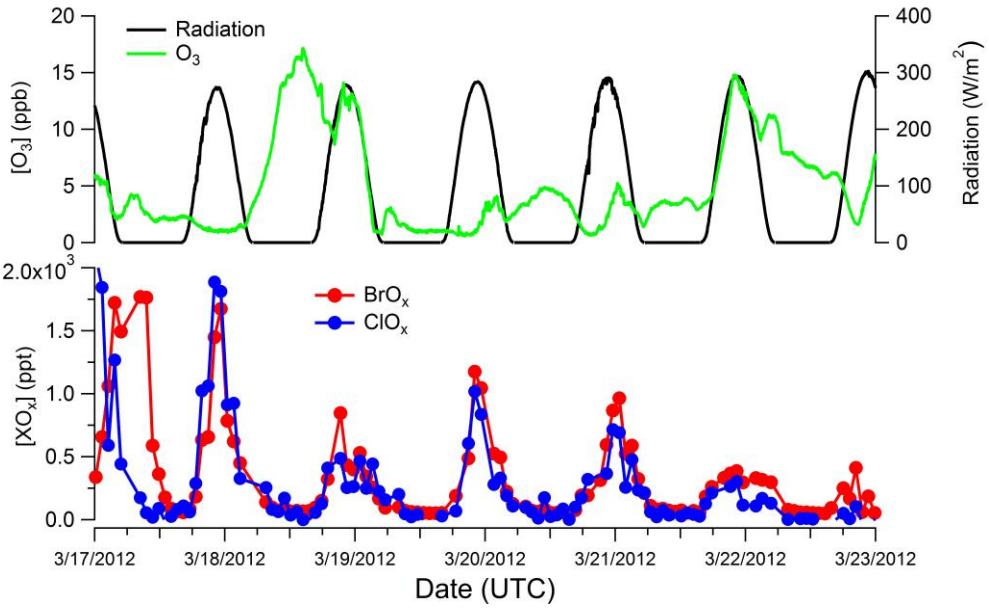

Figure 2.13 Time series measurements of BrO_x, ClO_x, O_3 and radiation from BROMEX 2012.

Ground level O_3 concentration measurements along with downwelling radiation measurements were provided by the National Oceanic and Atmospheric Administration (NOAA) base located in Barrow, Alaska. Shown in Figure 2.13, ClO_x and BrO_x were found to positively correlate to radiation, as expected due to the generation of bromine and chlorine radicals from photolysis of their respective molecular halogens precursors. Furthermore, retention times between the calibration standards and ambient measurements peaks prove that our ambient signals were genuine and truly were the desired flowtube products, bromobutanone and chlorobutanone. The principle of separation in gas chromatography involves the interaction between the stationary phase coating the internal walls of the GC column and the chemicals entering the column. Everything that enters the column will have a unique interaction with the stationary phase

based on its size, polarity, and functional groups. Those factors along with the specie's volatility lead to its retention time. Therefore, when the ambient peak matches our calibration standard's retention time we are confident in the identity of the peak.

In Figure 2.13 the daytime BrO_x and ClO_x peaks range from 500 to 2000 ppt which are 32 and 83 times greater than the average observed and modeled concentrations of BrO and ClO, respectively (Liao et al., 2012;Piot and von Glasow, 2008;Stutz et al., 2011;Honninger and Platt, 2002;Tuckermann et al., 1997). Inside the same sampling trailer where the flowtube method was deployed we also had a CIMS there to detect ambient BrO and ClO. A times series plot of the CIMS BrO and ClO data that overlap with the flowtube's BrO_x and ClO_x is shown in Figure 2.14. A comparison of concentrations reveals that the flowtube's concentrations are ~ 80x greater than those of the CIMS method.

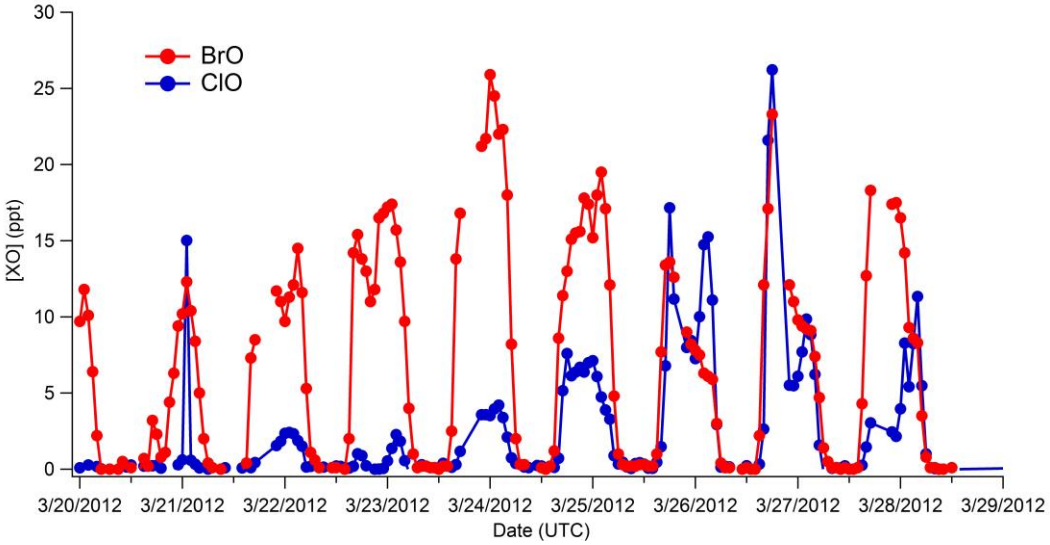

Figure 2.14 Time series measurements of BrO and ClO from BROMEX 2012.

The huge difference between the CIMS and flowtube method's XO concentrations lead us to believe that an inference led to the high concentrations obtained using the flowtube method. One possible source for the very high calculated BrO_x and ClO_x concentrations could be blank interferences. This would cause higher reported peak heights resulting in fluctuated calculated concentrations. However, both bromobutanone and chlorobutanone peaks for all the different types of blanks were very small and had no significant interference with the flowtube measurements. Also when quantifying the ambient measurements the average blank sample's signal was subtracted from the ambient signal to account for any background inference. Another possible source would be that the percent yield for both flowtube products was too low. As an upper limit, we calculated the concentrations using a yield of 100% for both products, yields BrO_x and ClO_x concentrations that were still too high, ranging from 50 ppt to 200 ppt. As to this date we are still unsure of what caused the error in the flowtube method measurements.

2.11 Future Directions

Although the flowtube method did not produce comprehensible data during the BROMEX field campaign, the method still has the potential to capture the BrO_x and ClO_x profiles. However, during the course of this work we were able to develop a CIMS method to detect BrO and ClO in real time. The CIMS instrument will be discussed in detail in Chapter 3. Here the ion chemistry that occurs within the CIMS that allows us to detect ClO and BrO will be described. The CIMS uses CH_3I to produce the reagent ion, I^-, which ionizes the halogen species, as shown in reaction 2.6-2.7

$$I^- + BrO \rightarrow IBrO^- \quad (2.6)$$

$$I^- + ClO \rightarrow IClO^- \quad (2.7)$$

ClO and BrO measurements conducted during BROMEX 2012 are shown in Figure 2.14. The CIMS method has several advantages over the flowtube method such as real time measurements and ease of deployment.

2.12 References

Ariya, P. A., Jobson, B. T., Sander, R., Niki, H., Harris, G. W., Hopper, J. F., and Anlauf, K. G.: Measurements of C-2-C-7 hydrocarbons during the Polar Sunrise Experiment 1994: Further evidence for halogen chemistry in the troposphere, Journal of Geophysical Research-Atmospheres, 103, 13169-13180, 10.1029/98jd00284, 1998.

Barrie, L., Bottenheim, J., Schnell, R., Crutzen, P., and Rasmsssen, R.: Ozone Destruction and Photochemical-Reactions at Polar Sunrise in the Lower Arctic Atmosphere, Nature, 334, 138-141, 10.1038/334138a0, 1988.

Bobrowski, N., von Glasow, R., Aiuppa, A., Inguaggiato, S., Louban, I., Ibrahim, O. W., and Platt, U.: Reactive halogen chemistry in volcanic plumes, Journal of Geophysical Research-Atmospheres, 112, 10.1029/2006jd007206, 2007.

Bottenheim, J. W., Gallant, A. G., and Brice, K. A.: Measurements of NO_y species and O_3 at 82^o N latitude, Geophysical Research Letters, 13, 113-116, 10.1029/GL013i002p00113, 1986.

Carpenter, L. J., Sturges, W. T., Penkett, S. A., Liss, P. S., Alicke, B., Hebestreit, K., and Platt, U.: Short-lived alkyl iodides and bromides at Mace Head, Ireland: Links to biogenic sources and halogen oxide production, Journal of Geophysical Research-Atmospheres, 104, 1679-1689, 10.1029/98jd02746, 1999.

Cavender, A., Biesenthal, T., Bottenheim, J., and Shepson, P.: Volatile organic compound ratios as probes of halogen atom chemistry in the Arctic, Atmospheric Chemistry and Physics, 8, 1737-1750, 2008.

Hausmann, M., and Platt, U.: Spectroscopic measurement of bromine oxide and ozone in the high arctic during Polar Sunrise Experiment 1992, Journal of Geophysical Research-Atmospheres, 99, 25399-25413, 10.1029/94jd01314, 1994.

Honninger, G., and Platt, U.: Observations of BrO and its vertical distribution during surface ozone depletion at Alert, Atmospheric Environment, 36, 2481-2489, 10.1016/s1352-2310(02)00104-8, 2002.

Jobson, B. T., Niki, H., Yokouchi, Y., Bottenheim, J., Hopper, F., and Leaitch, R.: Measurements of C2–C6 hydrocarbons during the Polar Sunrise 1992 Experiment: Evidence for Cl atom and Br atom chemistry, Journal of Geophysical Research-Atmospheres, 99, 25355-25368, 10.1029/94jd01243, 1994.

Keil, A. D., and Shepson, P. B.: Chlorine and bromine atom ratios in the springtime Arctic troposphere as determined from measurements of halogenated volatile organic compounds, Journal of Geophysical Research-Atmospheres, 111, 11, 10.1029/2006jd007119, 2006.

Kreher, K., Johnston, P. V., Wood, S. W., Nardi, B., and Platt, U.: Ground-based measurements of tropospheric and stratospheric BrO at Arrival Heights, Antarctica, Geophysical Research Letters, 24, 3021-3024, 10.1029/97gl02997, 1997.

Liao, J., Sihler, H., Huey, L., Neuman, J., Tanner, D., Friess, U., Platt, U., Flocke, F., Orlando, J., Shepson, P., Beine, H., Weinheimer, A., Sjostedt, S., Nowak, J., Knapp, D., Staebler, R., Zheng, W., Sander, R., Hall, S., and Ullmann, K.: A comparison of Arctic BrO measurements by chemical ionization mass spectrometry and long path-differential optical absorption spectroscopy, Journal of Geophysical Research-Atmospheres, 116, 10.1029/2010JD014788, 2011.

Liao, J., Huey, L., Tanner, D., Flocke, F., Orlando, J., Neuman, J., Nowak, J., Weinheimer, A., Hall, S., Smith, J., Fried, A., Staebler, R., Wang, Y., Koo, J., Cantrell, C., Weibring, P., Walega, J., Knapp, D., Shepson, P., and Stephens, C.: Observations of inorganic bromine (HOBr, BrO, and Br-2) speciation at Barrow, Alaska, in spring 2009, Journal of Geophysical Research-Atmospheres, 117, 10.1029/2011JD016641, 2012.

Peters, C., Pechtl, S., Stutz, J., Hebestreit, K., Honninger, G., Heumann, K. G., Schwarz, A., Winterlik, J., and Platt, U.: Reactive and organic halogen species in three different European coastal environments, Atmospheric Chemistry and Physics, 5, 3357-3375, 2005.

Piot, M., and von Glasow, R.: The potential importance of frost flowers, recycling on snow, and open leads for ozone depletion events, Atmospheric Chemistry and Physics, 8, 2437-2467, 2008.

Platt, U., and Stutz, J.: Differential Optical Absorption Spectroscopy Principles and Applications Introduction, in: Differential Optical Absorption Spectroscopy: Principles and Applications, Physics of Earth and Space Environments, Springer-Verlag Berlin, Berlin, 1-+, 2008.

Roberts, P. J. W., and Webster, D. R.: Environmental fluid mechanics: theories and applications, Amer Society of Civil Engineers, 2002.

Saiz-Lopez, A., Shillito, J. A., Coe, H., and Plane, J. M. C.: Measurements and modelling of I-2, IO, OIO, BrO and NO3 in the mid-latitude marine boundary layer, Atmospheric Chemistry and Physics, 6, 1513-1528, 2006.

Saiz-Lopez, A., Mahajan, A. S., Salmon, R. A., Bauguitte, S. J. B., Jones, A. E., Roscoe, H. K., and Plane, J. M. C.: Boundary layer halogens in coastal Antarctica, Science, 317, 348-351, 10.1126/science.1141408, 2007.

Schroeder, W. H., Anlauf, K. G., Barrie, L. A., Lu, J. Y., Steffen, A., Schneeberger, D. R., and Berg, T.: Arctic springtime depletion of mercury, Nature, 394, 331-332, 10.1038/28530, 1998.

Stephens, C.: Studies of Tropospheric Halogen Radical Chemistry During Ozone and Mercury Depletion Events in the Arctic Purdue University, 383 pp., 2012.

Stutz, J., Thomas, J., Hurlock, S., Schneider, M., von Glasow, R., Piot, M., Gorham, K., Burkhart, J., Ziemba, L., Dibb, J., and Lefer, B.: Longpath DOAS observations of surface BrO at Summit, Greenland, Atmospheric Chemistry and Physics, 11, 9899-9910, 10.5194/acp-11-9899-2011, 2011.

Tackett, P. J.: Investigation of the multiple roles of tropospheric halogen chemistry during Arctic ozone depletion events, Purdue University, 194 p. pp., 2008.

Tuckermann, M., Ackermann, R., Golz, C., LorenzenSchmidt, H., Senne, T., Stutz, J., Trost, B., Unold, W., and Platt, U.: DOAS-observation of halogen radical-catalysed arctic boundary layer ozone destruction during the ARCTOC-campaigns 1995 and 1996 in Ny-Alesund, Spitsbergen, Tellus Series B-Chemical and Physical Meteorology, 49, 533-555, 10.1034/j.1600-0889.49.issue5.9.x, 1997.

CHAPTER 3 IN-SNOWPACK AND VERTICAL PROFILE EXPERIMENTS CONDUCTED IN BARROW, ALASKA DURING THE WINTER OF 2014

3.1 Introduction

Halogen chemistry has been widely studied throughout the Arctic over the past several decades (Domine et al., 2008;Grannas et al., 2007;Simpson et al., 2007). Bromine, in particular, has been linked with ozone depletion events (ODEs), where ozone drops from background levels of 40 ppb to below 5 ppb (Barrie et al., 1988;Oltmans et al., 1989). This has been shown to occur sporadically during the Arctic springtime (Oltmans et al., 2012). As most of these measurements took place at coastal locations, sea salt was proposed as one of the first sources of atmospheric molecular halogens (McConnell et al., 1992). It has been hypothesized that aerosols provided the initial release and a surface for heterogeneous recycling of atmospheric Br_2 to occur during ODEs (Fan and Jacob, 1992;McConnell et al., 1992). The acidic environment of sulphuric aerosols provide the low pH conditions that are necessary to produce Br_2 in the aqueous phase, which can later be released into the gas-phase (Fan and Jacob, 1992). However, heterogeneous recycling of HOBr on the surface snowpack was shown in a modeling study to be necessary in order to match simulated O_3 depletion rates to observations (Michalowski et al., 2000). This provided evidence that heterogeneous recycling of halogens in the Arctic occurred on multiple ice surfaces. This furthered the

idea that not only is the snowpack needed for heterogeneous recycling but that it could be a direct source of molecular halogens. It was later discovered that the snowpack surface is open to deposition of sea salt, acidic aerosols, and stable bromine species (HOBr and $BrONO_2$) which can lead to the production of molecular halogens (Pratt et al., 2013;Wren et al., 2013;Cao et al., 2014). Pratt et al. conducted snow chamber experiments that showed the surface snowpack can produce molecular bromine in the presence of UV radiation and this production is enhanced by an increase in O_3 concentration due to heterogeneous chemistry as shown in reactions 3.1-3.6.

$$X_2 + h\nu \rightarrow 2X \quad (3.1)$$

$$X + O_3 \rightarrow XO + O_2 \quad (3.2)$$

$$XO + HO_2 \rightarrow HOX + O_2 \quad (3.3)$$

$$HOX_{(g)} \rightarrow HOX_{(aq)} \quad (3.4)$$

$$HOX_{(aq)} + H^+ + X/Y^- \rightarrow X_{2(aq)}/XY_{(aq)} + H_2O \quad (3.5)$$

$$X_{2(aq)}/XY_{(aq)} \rightarrow X_{2(g)}/XY_{(g)} \quad (3.6)$$

However, Cl_2 production was not observed during those snow chamber experiments, although concentrations up to 400 ppt have been observed in the Artic boundary layer during the spring time (Liao et al., 2014). Current Arctic models are inhibited by the lack of understanding of the source of and emission rates of atmospheric molecular halogens, especially for Cl_2. This information is crucial towards properly simulating future Arctic atmospheric composition, especially as the surrounding sea ice changes. To further investigate the source of Cl_2 and BrCl, we deployed a CIMS in Barrow, Alaska during January and February of 2014 to perform real time measurements of gas-phase inorganic halogens within the interstitial snowpack air. We attempted to determine if the tundra

snowpack could produce Cl_2 and BrCl. Additionally, vertical profile experiments were conducted above the surface snowpack in order to determine the flux rate of Br_2 and Cl_2 from the snowpack.

3.2 Experimental

3.2.1 Chemical Ionization Mass Spectrometer (CIMS)

Inorganic halogens (Br_2, Cl_2, and BrCl) were detected using a chemical ionization mass spectrometer (CIMS). Br_2 was monitored at mass $I^{79}Br^{79}Br^-$ (285 amu) and mass $I^{81}Br^{81}Br^-$ (289 amu), Cl_2 was monitored at mass $I^{35}Cl^{35}Cl^-$ (197 amu) and mass $I^{37}Cl^{35}Cl^-$ (199 amu), and BrCl was monitored at mass $I^{79}Br^{35}Cl^-$ (241amu) and mass $I^{79}Br^{37}Cl^-$ (243 amu). Each mass was monitored for 500 ms with a total integration period of 7.8s, giving a 6.4% duty cycle. The CIMS has been described previously in *Liao* et. al. [2012] and *Pratt* et. al. [2013] so only a brief description will be given here. The CIMS samples at atmospheric pressure, pulling 8.2 slpm of ambient air through a 25 cm long, 0.65 cm ID PFA tube that was housed in a custom three-way inlet valve, which will be described below. After the sampled ambient air passes through the inlet valve, a portion of the flow (2 slpm) enters the CIMS flow reactor through a 0.51 mm diameter orifice. The flow reactor is a 18 cm length of stainless tube coated with PTFE. Inside the flow reactor the analytes of interest (Cl_2, Br_2, and BrCl) were ionized by $I\cdot(H_2O)_n^-$ via reaction 3.7-3.9.

$$Br_2 + I(H_2O)_n^- \rightarrow Br_2I^- + (H_2O)_n \quad (3.7)$$

$$Cl_2 + I(H_2O)_n^- \rightarrow Cl_2I^- + (H_2O)_n \quad (3.8)$$

$$BrCl + I(H_2O)_n^- \rightarrow BrClI^- + (H_2O)_n \quad (3.9)$$

Hydrated I^- clusters, $(H_2O)_nI^-$, were produced inside the flow reactor using a 2.0 slpm flow of CH_3I (5 ppm) in N_2 passed through a ^{210}Po ionizing source and mixed with a flow of humidified N_2 inside the flow reactor. Humidified N_2 was made by flowing N_2 through 28°C deionized water housed in a glass bubbler. The addition of water into the flow reactor was needed to increase the sensitivity of the inorganic halogens to the CIMS, as lab studies have shown the sensitivity towards halogens can be water dependent (Neuman et al., 2010).

To dissociate the weakly bound water clusters, via energetic collisions, to yield the detectable ion, a portion of the flow from the flow reactor was passed through a 0.81 mm diameter orifice and into the collisional dissociation chamber (CDC). The CDC is an ocotopole held at 0.67 hPa that uses a 4 $V \cdot cm^{-1}$ electric field. The ions that departed from the CDC were then guided, by a separate octopole, to a quadropole mass analyzer. The ions are separated and then detected by an electron multiplier detector (Exelis) where the ion counts are reported in Hz. A schematic diagram of the CIMS is shown in Figure 3.1.

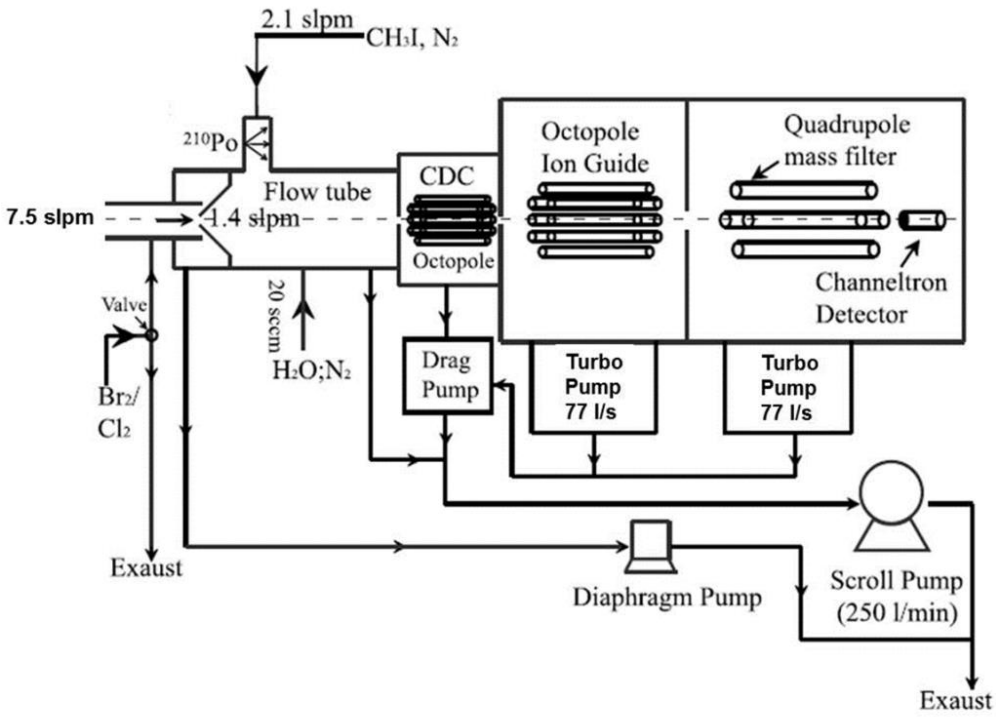

Figure 3.1 Schematic diagram of CIMS (Liao et al. 2012).

Ion peaks are resolved at 1 amu resolution, allowing for each different halogen isotope to be detected as a unique mass that was used to check the identity of each pair of halogenated detected species.

To confirm the identity of the detected masses isotopic ratio plots were used. An isotopic ratio plot is when two isotopes of the same specie (i.e. Br_2, Cl_2, and BrCl) are plotted against each other to enable comparison of the linear regression with their known isotopic ratio (Liao et al., 2011). Confirmation of the presence of a specific molecular halogen was achieved when the two masses best fit line had a slope value within ±5% of the isotopic ratio value for that specific molecular halogen. An example of mass $I^{81}Br^{81}Br^-$ (289amu) vs mass $I^{79}Br^{79}Br^-$ (285amu) is shown in Figure 3.2. The plot of

mass $I^{81}Br^{81}Br^-$ (289amu) vs mass $I^{79}Br^{79}Br^-$ (285amu) had a best fit line $R^2 = 0.997$ with a slope of .93, where the isotopic ratio is 0.97, confirming the presence of two bromine atoms. The isotopic ratio represents the ratio of the natural abundances for that specie. Masses $I^{35}Cl^{35}Cl^-$ (197 amu) and mass $I^{37}Cl^{35}Cl^-$ (199 amu) were plotted (not shown) against each other and had a $R^2 = 0.935$ with a slope of .63, confirming the presence of two chlorine atoms. Mass $I^{79}Br^{37}Cl^-$ (243 amu) and mass $I^{79}Br^{35}Cl^-$ (241amu) were plotted (not shown) against each other and had a $R^2 = 0.991$ with a slope of 1.2, confirming the presence of one Cl and one Br atom. This shows that the CIMS was not detecting any major interference at the masses we were monitoring during our experiments.

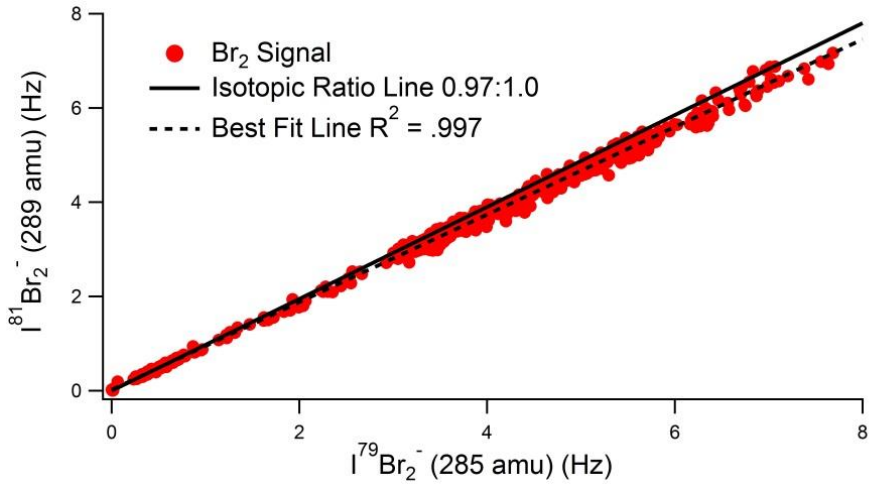

Figure 3.2 Isotopic ratio graph for Br_2 from an in-snow experiment in Barrow, Alaska on February 11, 2014.

3.2.1.1 Background and Calibration Measurements

To perform regular calibration and background measurements a three-way valve was used. A schematic of the three-way valve showing the difference between measurement and background mode is shown in Figure 3.3. Backgrounds were conducted every 20 minutes by diverting the sample flow entering the CIMS through a scrubber containing glass wool. Glass wool has been shown to efficiently remove gas-phase inorganic halogens from air flows (Neuman et al., 2010). We also tested this during the field study by mixing a stream of Br_2 (1.5 ppb) and Cl_2 (2.5 ppb) into a flow of breathing air and passing it through the glass wool scrubber. During the glass wool scrubber test the Br_2 and Cl_2 ion signals did not increase, indicating the glass wool removed 100% of the Cl_2 and Br_2.

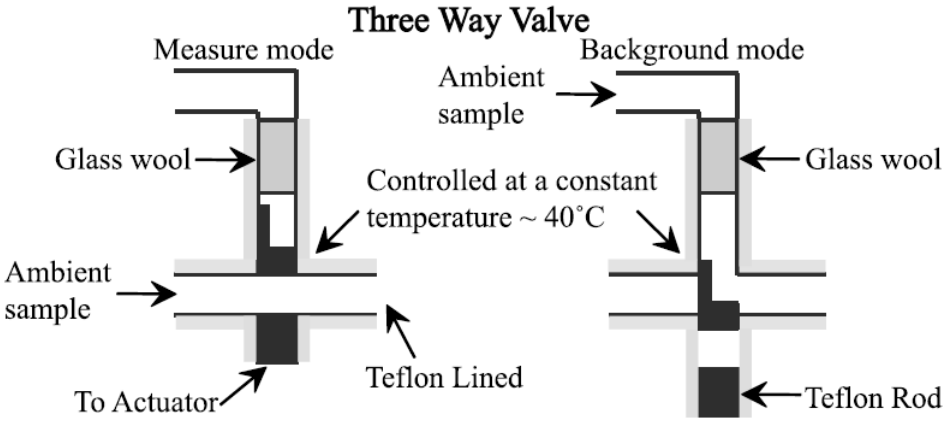

Figure 3.3 Schematic of the three way inlet valve showing the air flow during measurement and background mode courtesy of (Liao et al., 2011).

Calibrations were performed around every .5 hr by adding a 100 sccm flow of air containing a known concentration of Br_2 (1.5 ppb) and Cl_2 (2.5 ppb) into the ambient sample as it was entering the CIMS. Br_2 and Cl_2 sensitivities were calculated throughout the field campaign using Equations 3.I-3.III. First an ambient subtracted calibration signal was calculated by subtracting the interpolated ambient signal from the calibration signal (Eqn 3.I). The interpolated ambient signal represents the ambient X_2 signal before and after the calibration measurement.

$$\text{Calibration Signal} - \text{Interpolated Ambient Signal} = \text{Ambient Subtracted Calibration Signal} \quad \text{(3.I)}$$

The ambient subtracted calibration signal was then divided by the concentration of the molecular halogen added to the ambient flow to yield a Hz/ppt sensitivity (Eqn. 3.II).

$$\frac{\text{Ambient Subtracted Calibration Signal}}{X_2 \text{Concentration}} = \text{Calibration Sensitivity} \quad \text{(3.II)}$$

However, laboratory studies have shown that the CIMS sensitivity toward molecular halogens is influenced by the concentration of reagent ion. To correct for this the calibration sensitivity was normalized to the reagent ion at mass 147 Hz ($I\cdot(H_2{}^{18}O)^-$) to yield a calibration factor with units of Hz/Hz/ppt (Eqn 3.III).

$$\frac{\text{Calibration Sensitivity}}{\text{Reagent Ion Signal}} = \text{Calibration Factor} \quad \text{(3.III)}$$

To quantify the BrCl signal an average sensitivity of the Br_2 and Cl_2 sensitivities was assumed based on discussion with Greg Huey (personal discussion). During the in-snowpack experiments the Br_2 (285 amu), Cl_2 (197 amu), and BrCl (243 amu) 3σ 1

minute averaged limits of detection were 3.6 ppt, 1.0 ppt, and 3.2 ppt, respectively. Their respective uncertainties were calculated to be ±18%, ±21%, and ±19%, based on Equations 3.IV-3.VII. First, the absolute uncertainty in the X_2 calibration signal was calculated Eqn. 3.IV.

$$\text{cal signal } \sigma_{unc} = \sqrt{(\text{cal signal } \sigma)^2 + (\text{amb signal } \sigma)^2} \tag{3.IV}$$

The relative uncertainty for the CIMS sensitivity toward X_2 was calculated using Eqn. 3.V.

$$\frac{\text{sensitivity } \sigma}{\text{sensitivity}} = \sqrt{\left(\frac{\text{cal signal } \sigma_{unc}}{\text{cal} - \text{amb signal}}\right)^2 + \left(\frac{\text{perm source } [X_2]\sigma}{\text{perm source } [X_2]}\right)^2 + \left(\frac{147 \text{ signal } \sigma}{147 \text{ signal}}\right)^2} \tag{3.V}$$

Next the uncertainty in the ambient signal was calculated using Eqn. 3.VI.

$$\text{ambient signal } \sigma_{unc} = \sqrt{(\text{amb signal } \sigma)^2 + (\text{bck grd signal } \sigma)^2} \tag{3.VI}$$

Finally, the relative uncertainty for the concentration of X_2 was calculated using Eqn. 3.VII.

$$[X_2] \text{ relative uncertainty} = \sqrt{\left(\frac{\text{amb signal } \boldsymbol{\sigma}_{unc}}{\text{amb} - \text{bck grd signal}}\right)^2 + \left(\frac{\text{sensitivity } \sigma}{\text{sensitivity}}\right)^2 + \left(\frac{I(H_2O)_n^- \sigma}{I(H_2O)_n^-}\right)^2} \tag{3.VII}$$

During the flux experiments the Br_2 (285 amu) and Cl_2 (197 amu) 3σ 1 minute averaged limits of detection were .95 ppt and .70 ppt, with estimated uncertainties of ±30% and

±33%, respectively. The flux uncertainty was calculated using Equation 3.VIII, where z_0 represents the roughness length and U is the average wind speed at 10 m above the surface (Sec 3.3.2.1).

$$X_2 \text{ flux value relative uncertainty} = \sqrt{\left(\frac{[X_2]\,\sigma}{[X_2]}\right)^2 + \left(\frac{z_0\,\sigma}{z_0}\right)^2 + \left(\frac{U\,\sigma}{U}\right)^2} \qquad \text{(3.VIII)}$$

It should be noted that snowpack fluxes of BrCl are not reported because the measured masses, 241amu and 243 amu ratio, during ambient measurements did not fall on the linear regression for isotopic ratio of $I^{79}Br^{35}Cl^-$ (241amu) vs $I^{79}Br^{37}Cl^-$ (243 amu) during the gradient measurements, suggesting an interfering mass.

Permeation tubes containing Br_2 (VICI Metronics) and Cl_2 (VICI Metronics) were used to provide a constant emission of each molecular halogen for calibration purposes. Each permeation tube was stored in an oven held at 30°C that had a constant 100 sccm flow of N_2 passing through it to carry the molecular halogen to the CIMS. Both permeation ovens were connected to opposite sides of the switching valve via a 1/8″ OD Teflon line. The Teflon line was also connected to an exterior PTFE tee where one end lead through the switching valve to the PFA tube inside while the other end was connected to a needle valve joined to a diaphragm pump. The diaphragm pump was used to divert the permeation tube outlet flow away from CIMS inlet during ambient sampling. This flow was automatically closed during calibrations so that 100% of the permeation tube output was flowing into the CIMS inlet. For this calibration method to work

properly the molecular halogen permeation tube emission output must be known and constant.

The emission rates of Cl_2 and Br_2 permeation tubes are monitored by the conversion of I^- to I_3^- in a KI solution (5% KI). This was done by bubbling the permeation oven output through a glass impinger filled with a known volume of the KI solution, for a measured amount of time. The conversion reaction (3.10) shows a 1:1 conversion of each molecular halogen to I_3^-(Wu et al., 1963;Kazantseva et al., 2002). A 5% KI solution is used so that I^- is in kinetic excess, pushing the reaction toward the I_3^- side to ensure that all the X_2 is quantified.

$$X_2 + 3I^- \leftrightarrow 2X^- + I_3^- \quad (3.10)$$

The I_3^- concentration was quantified using a UV-Vis (Genesys, Spectronic 20) at 352 nm (Finley and Saltzman, 2008). The concentration was determined using Beer's law (Equation 3.IX) where A is the absorbance, Ɛ is the molar absorptivity ($L \cdot mol^{-1} \cdot cm^{-1}$), c is the concentration ($mol \cdot L^{-1}$), and b is the path length (cm) (Wei et al., 2005;Liao et al., 2011).

$$c = \frac{A}{\varepsilon \cdot b} \quad (3.IX)$$

The concentration is then converted to $ng \cdot min^{-1}$ using Equ 3.X where v is the volume of the liquid inside the bubbler, MW is the molecular weight of the molecular halogen, and t is the amount of time the permeation source was bubbled through the KI solution.

$$\text{Output}\,(ng \cdot min^{-1}) = \frac{c\left(mol \cdot L^{-1}\right) \cdot v(L) \cdot MW(g \cdot mol^{-1}) \cdot 1x10^{9} ng \cdot g^{-1}}{t\,(min)} \quad (3.X)$$

The stability of the permeation tubes emission rate during the 2014 Barrow Field Study is shown in Figure 3.4.

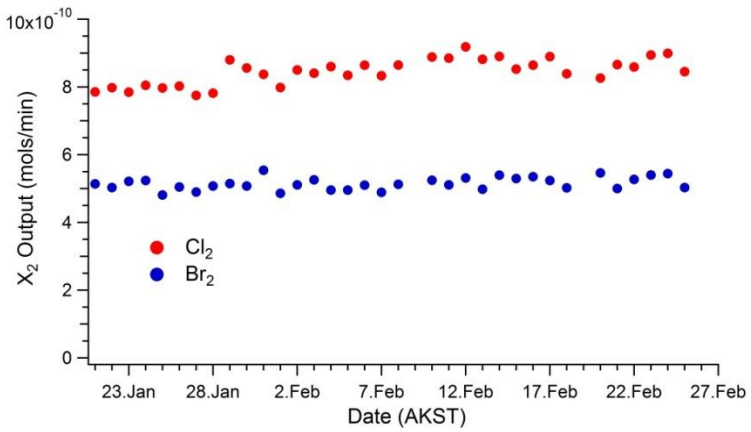

Figure 3.4 Emission rate for Cl_2 and Br_2 permeation tubes during Barrow Field Study in January and February 2014.

3.2.2 In-Snow Measurement Methods

The CIMS was deployed in the same sampling trailer used previously during the BROMEX 2012 field campaign (Chapter 2, Section 2). The production of molecular halogens (Br_2, Cl_2, and BrCl) in the interstitial snowpack air was studied by sampling the interstitial snowpack air in the presence of artificial illumination and externally generated O_3. A schematic of the experiment is shown in Figure 3.5 and the details of the experiment will be described in the following paragraphs.

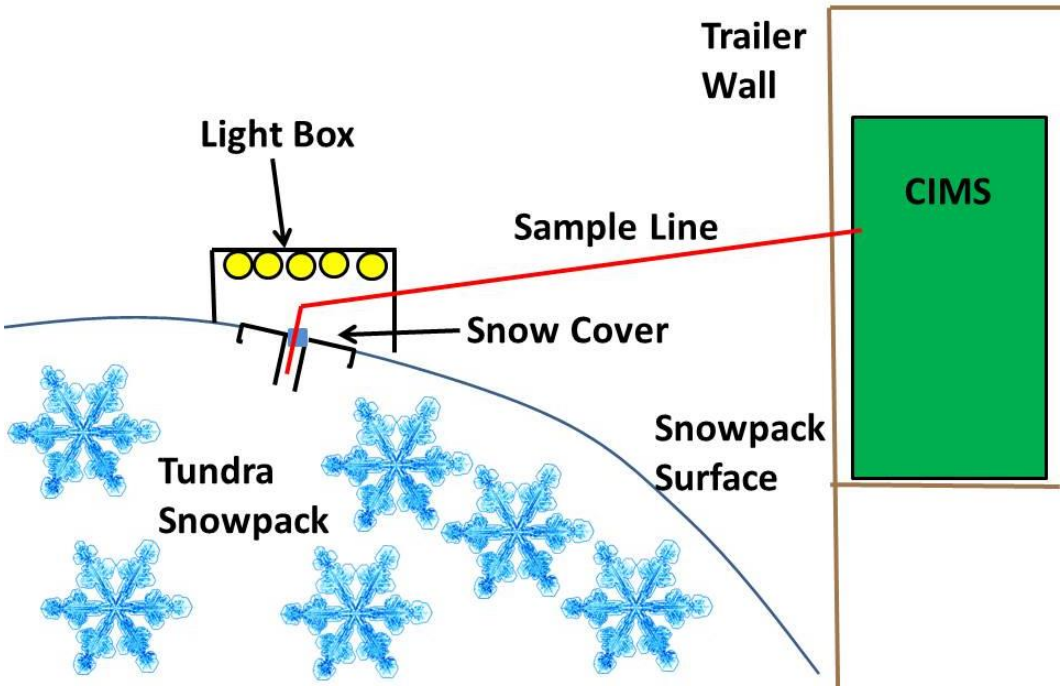

Figure 3.5 Schematic of the in-snowpack experiments conducted in Barrow, Alaska during January and February of 2014.

A heated (30°C) 380 cm FEP (1.27 cm ID) sample line was attached to the inlet of the CIMS three-way valve to allow us to sample within the snowpack. HOBr has been shown in lab studies to convert to Br_2 when absorbed onto Teflon surfaces coated with Br^-, via reaction 3.11(Neuman et al., 2010).

$$HOBr + Br^- + H^+ \rightarrow Br_2 + H_2O \quad (3.11)$$

To minimize this conversion from occurring during our experiments our sample line was cleaned before and after each experiment by rinsing it with mili-Q water and drying it with N_2. In-snowpack experiments were performed during early morning or late evening in the absence of natural UV radiation to allow us to control when and how long the snowpack was irradiated. To properly sample the interstitial snowpack air, a snow cover

was used to ensure that ambient air was not drawn into the snowpack directly via the sample line hole. The snow cover was custom built, using a 61cm x 61cm piece of 0.6 cm thick Acrylite OP-4 (CRYO Industries) mounted to a 61cm x 61cm aluminum frame with a 7.6 cm edge to press into the snowpack. The Acrylite OP-4 allows for ~ 60% transmission of 280nm radiation and ~92% of 395 nm radiation (Technical Data, CRYO Industries). A 5.4 cm inner diameter circle was cut out for the sample line in the center of the cover. Before the in-snow experiments were started the snow cover was pushed into the snowpack until the Acrylite sheet contacted the snowpack surface. A sampling hole of a desired depth was then bored into the snowpack using a clean (water and acetone rinsed) stainless steel ice auger drill bit, leaving a 5.4cm ID hole into which the sample line was inserted, then sealed to the cover. A custom built heated light housing unit containing 6 solar simulating lights (UVA-340, Q-Labs) was placed 15 cm directly above the snowpack being sampled, as shown in Figure 3.6.

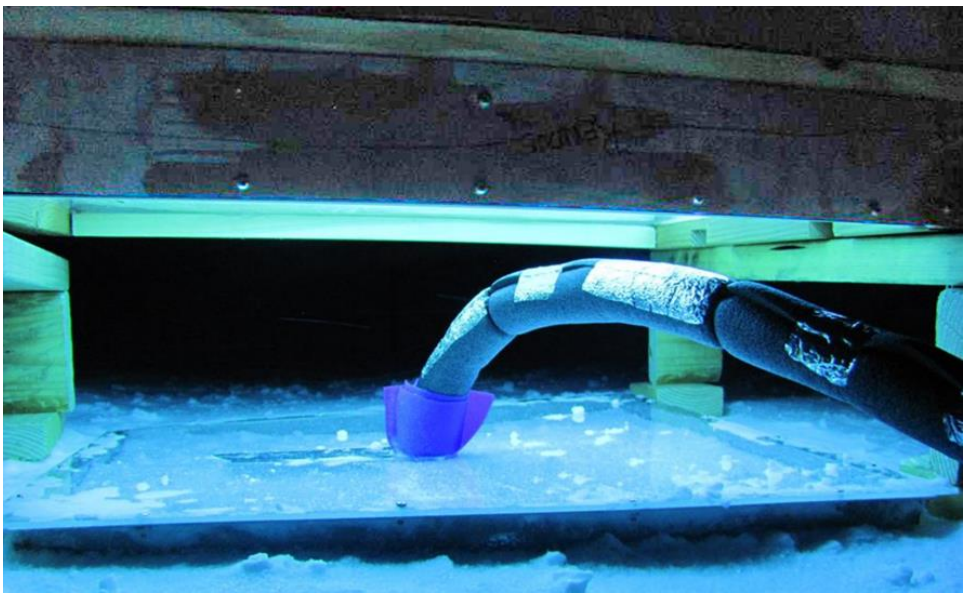

Figure 3.6 Image of in-snowpack experiment conducted on February 11, 2014.

The solar simulating lights were used to test for the possibility of photochemical generation of oxidants that produce the molecular halogens, e.g. OH (Pratt et al., 2013;Abbatt et al., 2010). The photochemical production of aqueous phase OH was observed when nitrate doped ice was exposed to UV radiation via reaction 3.12(Chu and Anastasio, 2003).

$$NO_3^- + h\nu \xrightarrow{H^+} OH + NO_2^- \quad (3.12)$$

Based on the UVA-340 spectrum (Figure 3.7) the photolysis of aqeuous phase NO_3^- should be possible despite its peak in molar absorptivity occurring at 305 nm (Figure 3.8).

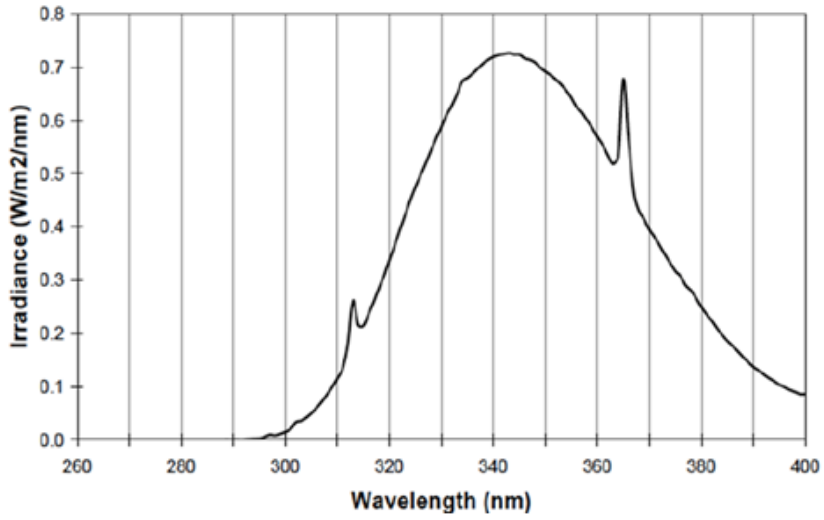

Figure 3.7 Spectral power distributions for the Q-Lab UVA-340 lamps used during the in-snowpack experiments (Q-labs Specification Sheet).

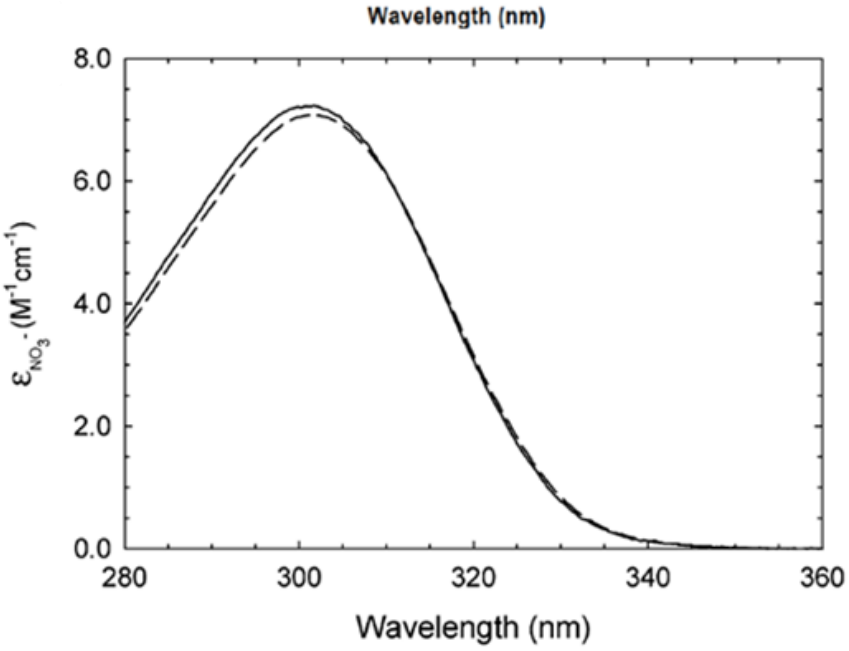

Figure 3.8 Base-10 molar absorptivities of aqueous NO_3^- at 278 K (solid line) and 293 K (dashed line) (Chu and Anastasio, 2003).

Upon completion of the set-up, the experiment was started by sampling the snowpack interstitial air in the absence of UV light. After several minutes of montoring constant signals of Br_2, Cl_2, and BrCl in the dark, background and calibration measurements were conducted, then the lights were turned on to illuminate the snowpack. The lights were left on for a set amount of time to examine the gas-phase production of the molecular halogens. At the end of the experiment the lights were turned off for around 5 minutes and then back on to confirm the intial response of the snowpack to the UV raidation. During the experiment on February 11, externally generated O_3 was produced by passing a flow of breathing quality compressed air (1.5 lpm) through an O_3 generator (model 97-0067-01, UVP). A PFA (1/4″ ID) line was attached to the outlet end of the O_3 generator and placed in the snowpack next to the sample line to increase the O_3 snowpack concentration of interistial air that we were sampling.

3.2.3 Vertical Profile Methods

Vertical profile measurements of inorganic halogens (Br_2 and Cl_2) were achieved by sampling ambient air at various heights (0-100 cm) above the tundra snowpack outside of the sampling trailer. Vertical profile experiments were conducted in the same locations as the in-snowpack experiments. The 380 cm FEP line (1.27cm ID) sample line heated to 30°C was attached to the inlet of the CIMS to allow for height varying sampling (Figure 3.9). Outside the sampling trailer the sample line was attached to an adjustable bipod that allowed for consistent height variations above the snowpack.

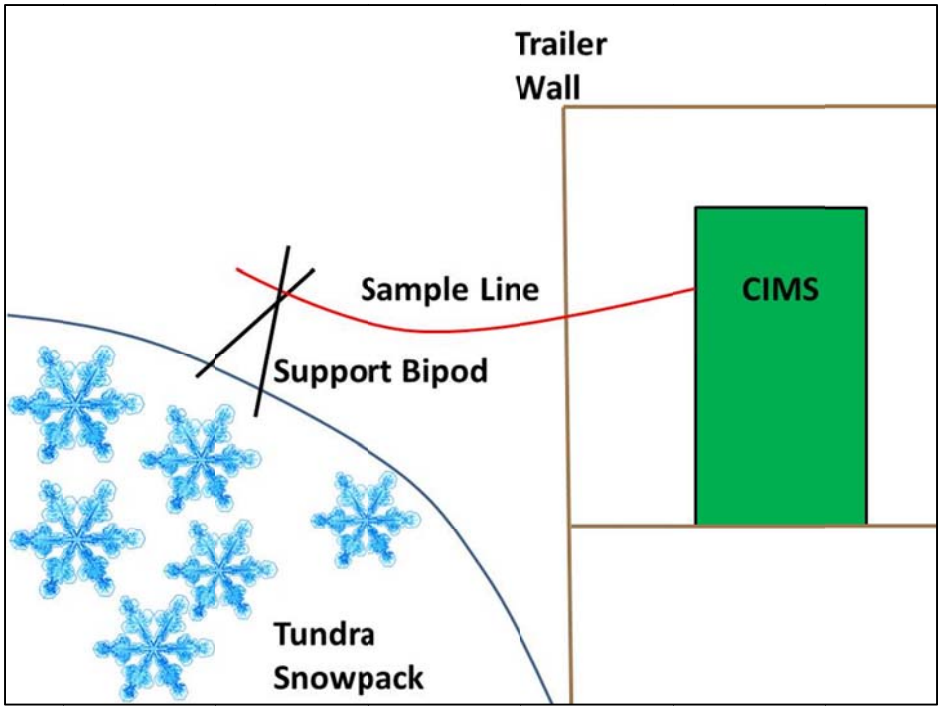

Figure 3.9 Image of vertical profile experiment conducted in Barrow, Alaska.

3.3 Results and Discussion

3.3.1 In-snowpack Experiments

Two in-snowpack experiments were conducted during the month of Febuary 2014, during early morning/late evening, as this allowed us to control the exposure of UV radiation to the snowpack. The experiment conducted on February 8 was started at 6:30 pm (AKST), well after the sun had set for the day. In the absence of light the Br_2, Cl_2, and BrCl measured concentrations, within the interstial snowapck air, were below the CIMS LOD. This indicated the lack of a dark production mechanism. For this experiment the lights were turned on from 7:30 pm (AKST) on Feb. 8 to 8:30 am (AKST) of Feb. 9. Upon artifically illuminating the snowpack, production of Br_2, Cl_2,

and BrCl was observed, as shown in Figure 3.10a. The gaps in the data throughout the experiment are times when the CIMS was performing background measurements and calibrations. During this experiment BrCl mimics the production of Br_2 in that both increase quickly once the lights were turned on and remain constant until ~ 4:00 (AKST) of Feb 9. Around 4:00 (AKST) on Feb. 9 an increase in wind speed caused wind pumping of the snowpack that raised the snowpack O_3 concnetration from 5 to 15 ppb. Wind motion on the windward side of surface features (e.g. sastrugi) cause a pressure increase/decrease on the windward/leeward side of the bumps. This forces ambient air into the snowpack mixing with and pushing interstitial air out of the snowpack (Colbeck, 1997). This increase in snowpack O_3 concentration resulted in an enhanced production of gas-phase Br_2 and BrCl, but not Cl_2. During this experiment Cl_2 production follows a very different pattern compared to Br_2 and BrCl. All three molecular halogens showed immediate production upon snowapck illumination but the Cl_2 concentration slowly rose for ~5 hours while Br_2 and BrCl reached a constant concentration after 30 mins. Furthermore, once Cl_2 reached its maximum concentration it slowly decreased until ~4:00 (AKST), when the concentration levels off coinciding with the increase in snowpack O_3 concentration. From this experiment it was clear that the increased snowpack O_3 concentration enhanced the production of both Br_2 and BrCl, however the impact on Cl_2 production remained unclear. For this reason another in-snowpack experiment was conducted the morning of Febuary 11 during which externally generated O_3 was pumped into the snowpack to examine its influence on molecular halogen production.

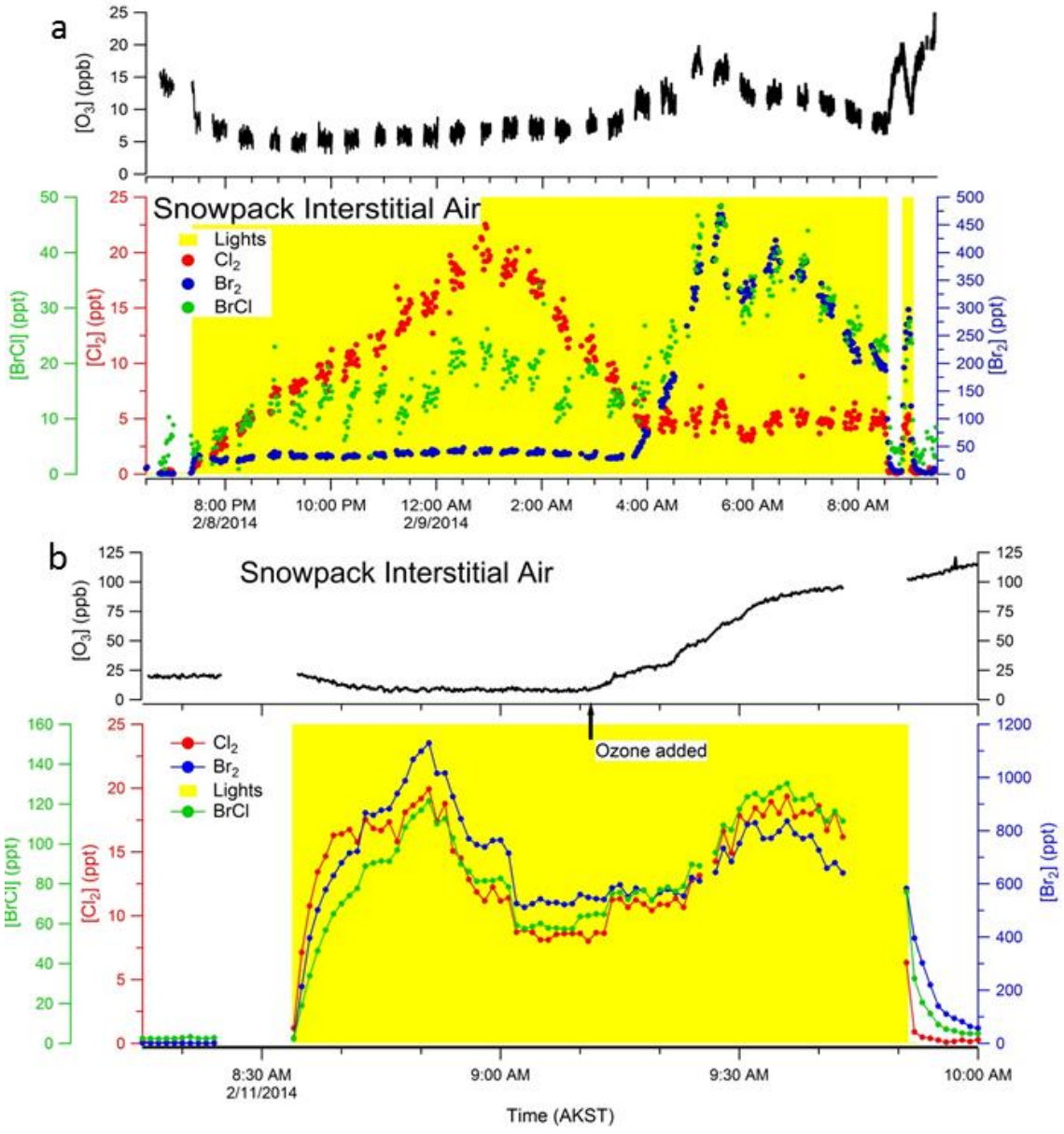

Figure 3.10 In-snowpack molecular halogen production for Feb 8 (a) and Feb 11(b) experiments.

The February 11 experiment was started at 8:15 am (AKST) and the snowpack was sampled in the dark for around 20 mins. Once again all three molecular halogens were below the LOD. The lights were then turned on and molecular halogen (Br_2, Cl_2,

and BrCl) production instantly occurred, as it did on February 8. However, during this experiment the production of all three molecular halogens reached a maximum after ~ 15 minutes, after which they decreased and leveled off after ~30 minutes of the lights being turned on. The constant production was monitored for ~ 10 minutes before externally generated O_3 was added. As shown in Figure 3.10b the concentration of all three molecular halogens (Br_2, Cl_2, and BrCl) is enhanced upon the increase of snowpack O_3 from 8 to 100 ppb.

These experiments represent the first time, that we know of, that Cl_2 production was observed within the snowpack. Similar to the snowchamber experiments conducted by *Pratt* et al. (2013), halogen production was light dependent, support the OH-mediated production mechanism proposed based on previous lab observations for Br_2 (Pratt et al., 2013;Abbatt et al., 2010). *Knipping* et al. (2000) observed Cl_2 production from irradiated aquaeous NaCl aerosols and proposed a condensed phase OH production mechanism. The following mechanism (reactions 3.13-3.15) was proposed for the observed Cl_2 production from the *Knipping* et al. laboratory study which could be applied to Br_2 for the sunlight snowpack (Knipping and Dabdub, 2002) .

$$OH\cdot + Cl^- \leftrightarrow HOCl\cdot^- \quad (3.13)$$

$$HOCl\cdot^- + Cl^- \rightarrow OH^- + Cl_2\cdot^- \quad (3.14)$$

$$Cl_2^- + Cl_2^- \rightarrow Cl_2 + 2Cl^- \quad (3.15)$$

Similar to the Br_2 explosion mechanism, as described in Section 1.2.2., O_3 can increase the Cl_2 release via the following catalytic cycle:

$$Cl_2 + h\nu \rightarrow 2Cl \quad (3.16)$$

$$Cl + O_3 \rightarrow ClO + O_2 \quad (3.17)$$

$$ClO + HO_2 \rightarrow HOCl + OH \quad (3.18)$$

$$HOCl_{(g)} + H^+_{(aq)} + Cl^-_{(aq)} \rightarrow Cl_{2(g)} + H_2O_{(l)} \quad (3.19)$$

Here reaction 3.19 occurs in the condensed phase.

Recently Cl_2 was observed, during a lab study, to be produced from illuminated artifical snow doped with NaCl in the presence of O_3 (Wren et al., 2013). This follows our observations of the need for light to activate molecular halogen production. However, Wren et al. (2013) observed that the initial Cl_2 production depended on the presence of gas-phase Br_2 and concluded the intial release mechanism for Cl_2 involved the formation of HOCl via Reaction 3.16-18, where the initial Cl atom source was BrCl photolysis. This differs from our observations of all three molecular halogens being produced simulatenously once the snowpack was illuminated. A possible reason for the discrepancy between observations could be due to a difference in aqueous OH concentrations. During their experiments Wren *et al*. did not directly add a potential OH source to their artificial snow, potenially limiting the aqueous OH concentration. This could lead to concentrations that are much less than what is typical for the Arctic coastal snowpack, leading to a difference in observations.

The observation of in-snowpack BrCl production was also a first of its kind. Although BrCl has been detected in the Arctic at levels up to 35 ppt in Alert, Nunavut, Canada, the source was unknown (Spicer et al., 2002;Foster et al., 2001). Previous observations cited reaction 3.20 as a potential aquesous phase reaction that could occur at an acidic ice surface that would yield gas-phase BrCl (Foster et al., 2001).

$$HOBr + H^+ + Cl^- \rightarrow BrCl + H_2O \quad (3.20)$$

From reaction 3.20, a Br_2 dependence might be expected to be associated with BrCl production as HOBr is produced when Br_2 is photolyzed in a O_3 rich environment. Reaction 3.20 could explain the BrCl concentration increase when the snowpack O_3 concentration was increased in the presence of snowpack Br_2. BrCl in the snowpack intersital air mimics the Br_2 release, notable during the February 8th in-snowpack experiment when the spike in the O_3 snowpack concentration casued an enhancment in the Br_2 and BrCl production.

However, all three molecular halogens (Br_2, Cl_2, and BrCl) are produced simultanesouly when the lights are turned on. This infers that all three could be produced by a similar, or a coupled photochemical mechanism. Based on our results we know that the production mechanism is photochemically activated and that O_3 is involved with a gas-phase phase mechanism that enhances this production. We believe the proposed initiation mechanism shown below (reaction 3.21-3.26), that is based on previous laboratory studies testing the production of molecular halogens from synthetic ice and snow surfaces, is consistent with our findings (Abbatt et al., 2010;Wren et al., 2013).

$$OH + X^- \rightarrow HOX^- \quad (3.21)$$

$$OH + Y^- \rightarrow HOY^- \quad (3.22)$$

$$HOX^- + X^- + H^+ \rightarrow X_2^- + H_2O \quad (3.23)$$

$$HOY^- + X^- + H^+ \rightarrow XY^- + H_2O \quad (3.24)$$

$$X_2^- + X_2^- \rightarrow X_2 + 2X^- \quad (3.25)$$

$$XY^- + XY^- \rightarrow XY + X^- + Y^- \quad (3.26)$$

3.3.2 Vertical Profile Experiments

Vertical profile experiments were conducted on February 14th and 16th during which ambient air at various heights (0-100 cm) above the snowpack was sampled repetitively so that a concentration gradient could be determined. For both experiments ambient air was sampled from ~9:00 am until ~4:00 pm (AKST) to allow for a complete diurnal measurement that included varying radiation strength. As shown from our in-snowpack experiments, molecular halogen production within the snowpack is photochemically induced. Therefore, measuring the concentration gradient over a range of radiation coniditions will allow us to better understand the flux from the snowpack. Both experiements yielded a negative concentration gradient above the snow surface, signifying an in-snowpack production, and emission of the products to the overlying atmosphere.

Shown in Figure 3.11 is the concentration gradients observed for the Februaury 16th experiment for both Br_2 and Cl_2. The figure clearly illustrates the concentration gradient, above the snowpack. Another point of interest is the influence that the time of day has on halogen production. During peak sunlight hours ~13:00 we observed the greatest surface concentration compared to hours of reduced sunlight (9:30 and 15:46).

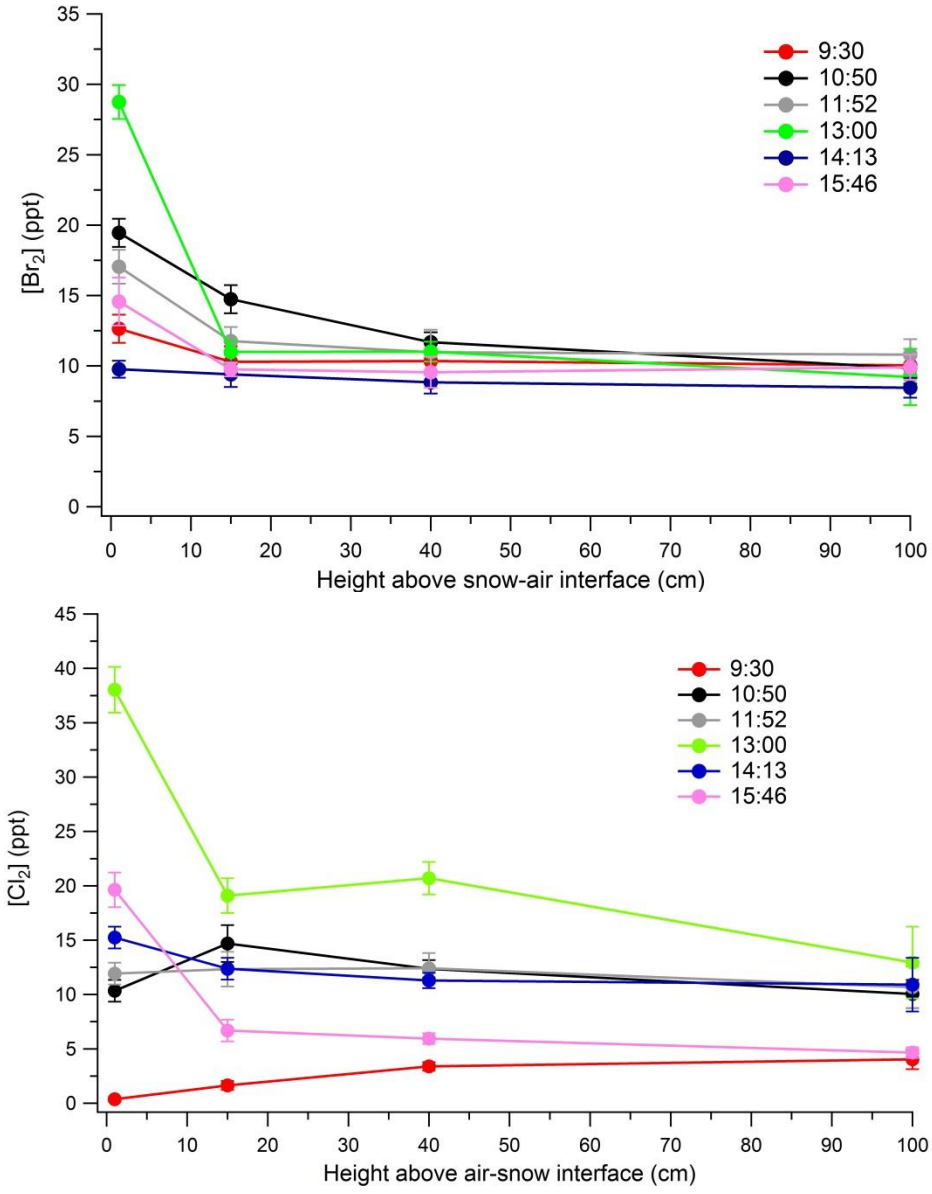

Figure 3.11 Br_2 and Cl_2 vertical profile measurements for February 16, 2014, separated based on sampling time. Errors bars represent 1σ of the mean for each indidvidual height measurement.

The concentration gradients observed for each sampling cycle were combined with calculated eddy diffusivity values, representative of that sampling time, to determine time varying flux values for Br_2 and Cl_2.

3.3.2.1 Flux calculations

Flux values were calculated using the gradient method equation (Equ. 3.XI) described in Guimbaud et al. (Guimbaud et al., 2002).

$$Flux = -K\frac{dC}{dz} \quad \text{(3.XI)}$$

Generally, the eddy diffusivity (K) is calcluated using on-site high frequency wind speed measurements. However, these were not available during our measurements so a modified equation (Equ. 3.XII) was used to calculate the eddy diffusivity. Ralf Staebler of Environment Canada assisted with the eddy diffusisivty calculations.

$$K = \kappa z_s u^* \quad \text{(3.XII)}$$

The friction velocity (u^*) was calculated, using Equ. 3.XIII, where κ is the van Karman constant (0.4), U is the mean wind speed at 10m (m/s), z is the height of the wind speed measurement (m), and z_o is the roughness length (m).

$$u^* = \frac{\kappa U(10m)}{ln\left(\frac{10m}{z_0}\right)} \quad \text{(3.XIII)}$$

The roughness length at various locations on the tundra near Barrow was previously determined through direct momentum flux measurements using sonic anenometers at various heights above the snowpack (Boylan et al., 2014). Wind speed measurements

were carried out at the NOAA Barrow Observatory (http://www.esrl.noaa.gov/gmd/obop/brw/), located 5 km north of the sampling trailer.

$$z_s = \frac{z_2 - z_1}{ln\left(\frac{z_2}{z_1}\right)} \quad \text{(3.XIV)}$$

The logarithmic mean for the two sampling heights (z_s), was calculated using Eqn. 3.XIV, where z_1 represents the lower and z_2 the upper sampling height. The logarithmic mean of the two sampling heights, the friction velocity, and the van Karman constant were combined to calculate the eddy diffusivity values for each sampling segment. The u^* is the only changing component of the eddy diffusivity, as it depends on the wind speed, which is generally changing throughout the experiments. For the flux calculation from Eqn. 3.III, dC/dz is the change in concentration as a function of height above the surface, approximated by $C(z_2)$-$C(z_1)/(z_2$-$z_1)$. Time-resolved fluxes and corresponding down welling radiation are shown in Figure 3.12. Maximum values for Br_2 and Cl_2 fluxes occurred near mid-day when radiation was at a maximum, however this is heavily dependent on the wind speed as this leads to wind pumping of the snowpack (Albert et al., 2002).

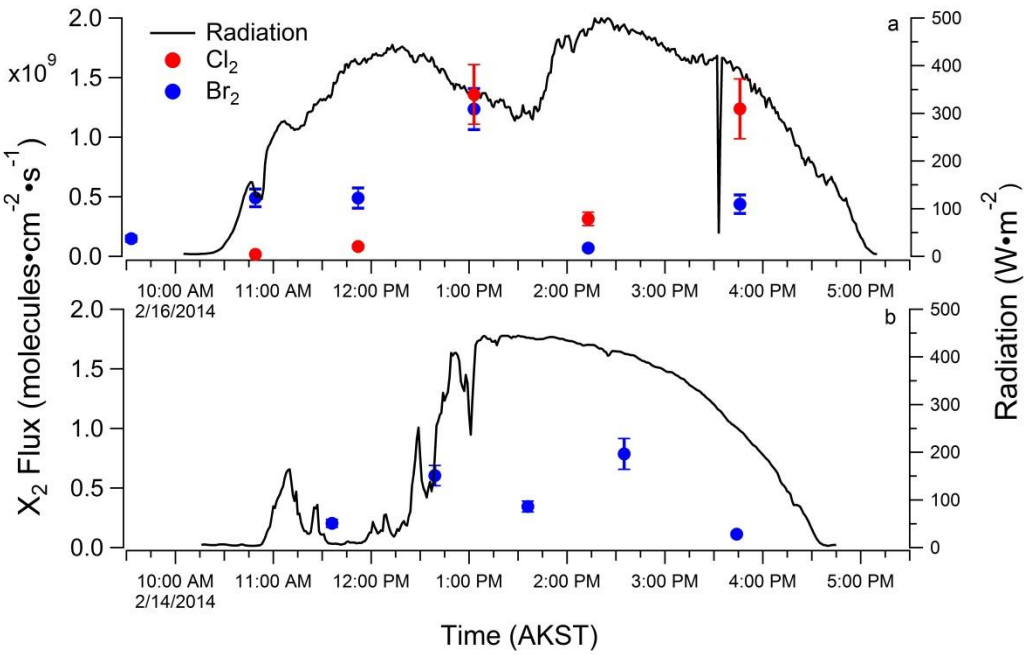

Figure 3.12 Br_2 and Cl_2 flux values at z = 1cm with corresponding radiation: 16 February 2014 (**a**) and 14 February 2014 (**b**). The error bars denote relative uncertainty (Sec 3.2.1.1) in the flux calculation.

Table 3.1: Calculated flux rates for Br_2 and Cl_2 from Feb 14 and 16 experiments

Date & Time	Br_2 Flux (molecules·cm^{-2}·s^{-1})	Cl_2 Flux (molecules·cm^{-2}·s^{-1})
Feb 14 11:36	2.0×10^{8} ($\pm0.6\times10^{8}$)	N/A
Feb 14 12:39	6.0×10^{8} ($\pm1.8\times10^{8}$)	N/A
Feb 14 13:36	3.5×10^{8} ($\pm1.1\times10^{8}$)	N/A
Feb 14 14:35	7.9×10^{8} ($\pm2.4\times10^{8}$)	N/A
Feb 14 15:44	1.1×10^{8} ($\pm0.36\times10^{8}$)	N/A
Feb 16 09:33	1.5×10^{8} ($\pm0.5\times10^{8}$)	N/A
Feb 16 10:49	4.9×10^{8} ($\pm1.5\times10^{8}$)	0.16×10^{8} ($\pm0.05\times10^{8}$)
Feb 16 11:52	4.9×10^{8} ($\pm1.5\times10^{8}$)	0.83×10^{8} ($\pm0.27\times10^{8}$)
Feb 16 13:03	12×10^{8} ($\pm3.6\times10^{8}$)	14×10^{8} ($\pm4.6\times10^{8}$)
Feb 16 14:13	0.69×10^{8} ($\pm0.2\times10^{8}$)	3.1×10^{8} ($\pm1.0\times10^{8}$)
Feb 16 15:46	4.4×10^{8} ($\pm1.3\times10^{8}$)	12×10^{8} ($\pm4.0\times10^{8}$)

As these are the first reported Br_2 and Cl_2 fluxes, the only previously reported flux values were from model simulations studying Arctic halogen chemistry based on previous observations (Lehrer et al., 2004;Toyota et al., 2014;Piot and von Glasow, 2008, 2009), e.g. those needed to simulate BrO observations. Only Br_2 fluxes have been reported in the literature as the majority of the Arctic based observations have been with respect to BrO, for which measurements have existed for a couple decades (Hausmann and Platt, 1994). Br_2 fluxes of 9.0 $x10^7$to 2.7 $x10^9$ molecules$\cdot cm^{-2}\cdot s^{-1}$, have been produced or used within modeling studies examining the springtime Arctic halogen chemistry (Lehrer et al., 2004;Toyota et al., 2014;Piot and von Glasow, 2008, 2009). Our observed Br_2 fluxes presented here lie close to the upper range of modeling studies reported for Br_2. One difference between our flux values and those reported from modeling studies is that our flux values are based on observations from early February when no ODEs occurred, whereas the modeling studies are based on observations from later in the spring when ODEs are a common occurrence and more intense, with greater solar irradiance. ODEs lead to the production of gas-phase HOBr and HOCl which can deposit onto the surface snowpack, altering its [Br^-] and [Cl^-] amd providing oxidizing agents to the snowpack. The transition from late winter (~Feb) to early spring (March/April) in the Arctic leads to an increase in both the magnitude and duration of solar radiation that reaches the snow surface, stimulating additional photolysis within the snowpack. The heightened photolysis of NO_3^-/H_2O_2 within the snowpack leads to more condensed phase OH production which can lead to more halogen production via reaction 3.20-25. Based on this we can assume that our flux values represent a less active snowpack compared to later in the spring when the additional radiation prompts ozone

depletions that promote chemistry which can lead to a higher flux rate of molecular halogens from the snowpack. This is also supported when comparing our observed Br_2 and Cl_2 ambient concentration to those observed during March/April. Our February Br_2 and Cl_2 daytime concentrations range from 5 to 25 and 5 to 20 ppt, respectively. Whereas previous observation record Br_2 ranging from 15 to 45 ppt and Cl_2 from 10 to 400 ppt during the day, much higher than what we observed. However, it should be noted that the measured atmospheric concentrations of molecular halogens depend on several variables including emission rates, atmospheric mixing, and photochemical loss. During the spring months of April and March both atmospheric mixing and photochemical loss of molecular halogens will be greater compared to February. This further supports that the emission rates of molecular halogen from the snowpack will be much greater in the spring compared to our winter time observations.

3.3.2.2 Potential Source

Based on our observations we have determined that the snowpack has the ability to produce molecular halogens that can transport into the overlaying atmosphere. To determine the significance of the snowpack as a source for molecular halogens to the boundary layer we calculated the surface-layer concentration corresponding to each flux value and compared it to the average atmospheric concentration measured at that time. This will also allow us to evaluate whether there are sources other than the snowpack contributing to the atmospheric molecular halogen concentration, e.g. sea salt aerosols. First the volumetric flux was calculated by dividing the flux value by the effective mixing height (Z^*) for that point in time (Equ. 3. XV), yielding an effective volumetric flux. The

effective mixing height, Z^*, represents the height at which the molecules of a specific specie emitted from a surface have decayed by 1/e of the starting surface concentration.

$$Z^* = \sqrt{K\tau} \quad \text{(3.XV)}$$

The volumetric flux signifies the production rate of the snowpack for Cl_2 or Br_2 at that time.

$$\text{Volumetric Flux} = \frac{\text{Flux}}{Z^*} \quad \text{(3.XVI)}$$

Using Equation 3.XV the effective mixing height was calculated using the eddy diffusivity (K) and the respective photochemical lifetime (τ) of Cl_2 or Br_2 for that time of day. The time-varying values for τ for Cl_2 and Br_2 were calculated during the measurement periods using Equ. 3.XVII, where J_{X_2} is the time-dependent photolysis rate of either Br_2 or Cl_2.

$$\tau = \frac{1}{J_{X_2}} \quad \text{(3.XVII)}$$

The photolysis rates used in our calculation were determined by scaling previously measured photolysis rates from Barrow to their respective radiation to yield a photolysis scaling factor with units $m^2 \cdot W^{-1} \cdot s^{-1}$ (Shetter and Muller, 1999). The radiation value corresponding to each flux measurement time was multiplied by the photolysis scaling factor, to yield the photolysis rate at that time. The calculated photolysis values were compared to photolysis values calculated using the TUV model and were found to be with 5% of each other. Down welling short wave radiation data during our measurements were obtained from the ARM facility in Barrow and used to determine the photolysis rates of Cl_2 and Br_2 (http://www.arm.gov/sites/nsa/operations). Based on the

effective mixing height calculation loses of ~11.5% for Cl_2 and ~30% for Br_2 were occurring at our highest measurement height of 100cm. The atmospheric concentration of Br_2 and Cl_2 is calculated by dividing the volumetric flux rate by its respective photolysis rate (Equ. 3.XVIII). Photochemical loss represents the most significant (greater than 95%) loss of Cl_2 and Br_2 in the Arctic boundary layer.

$$[X_2] = \frac{\text{Volumetric Flux}}{\text{Photolysis Rate}} \qquad \text{(3.XVIII)}$$

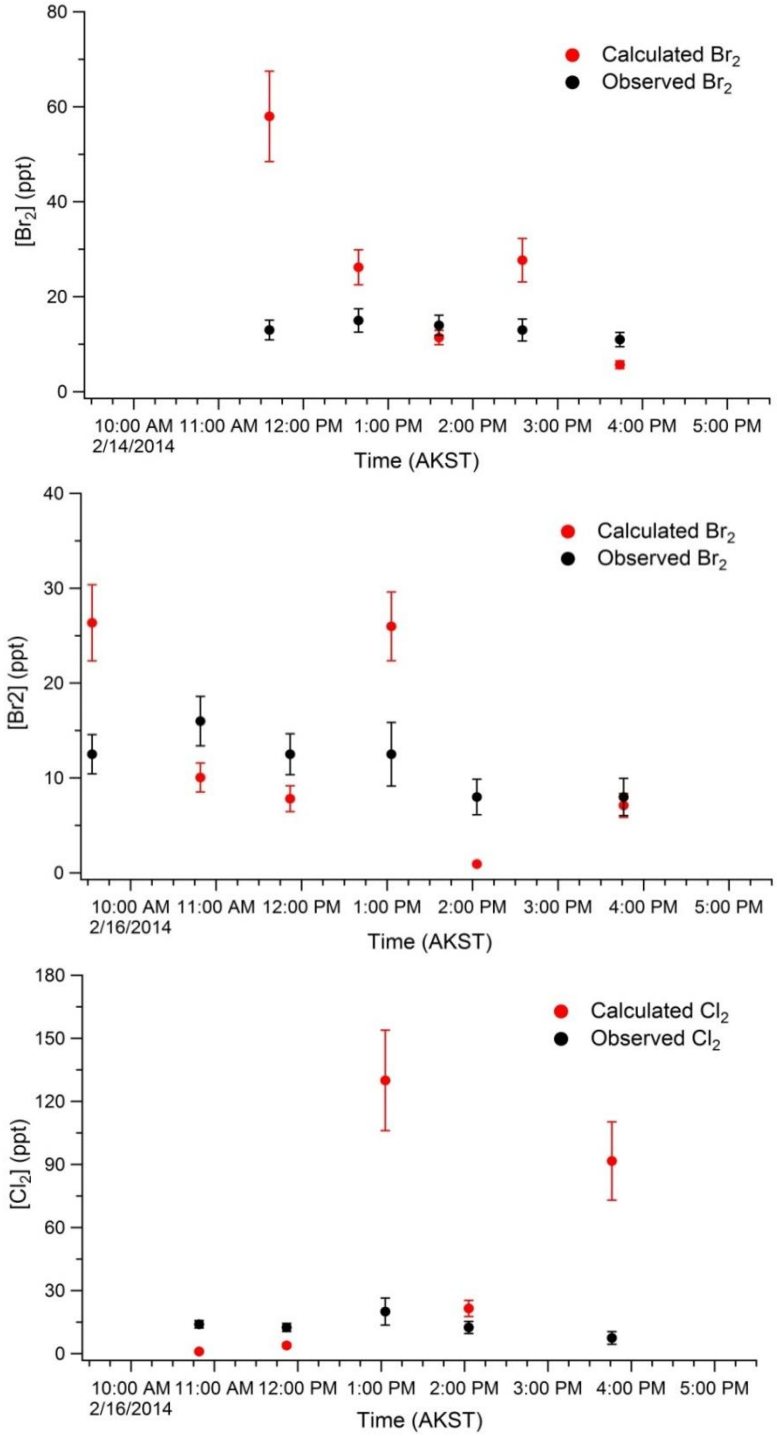

Figure 3.13 Observed and calculated Br_2 and Cl_2 concentrations during Feb 14 and 16 flux experiments (error bars are based on relative error from Br_2 and Cl_2 mole ratio calculations).

We would expect that the calculated Br_2 and Cl_2 mole ratio would be identical if the snowpack was the only source, while if an additional source exists (i.e. sea salt aerosols) the calculated mole ratio would be lower than observed. However, for Cl_2 the high calculated mole ratios came at a time when the surface (1 cm) Cl_2 mole ratio spiked (Figure 3.11). The elevated mole ratios yielded flux values 1-2 orders of magnitude larger than the other flux measurements for that day (Table 3.1). We note that during that time the winds temporally decreased from around 8 to 6 m/s (Figure 3.14). This drop in wind speed would decrease the mixing occurring at the surface and could lead to greater surface level concentrations.

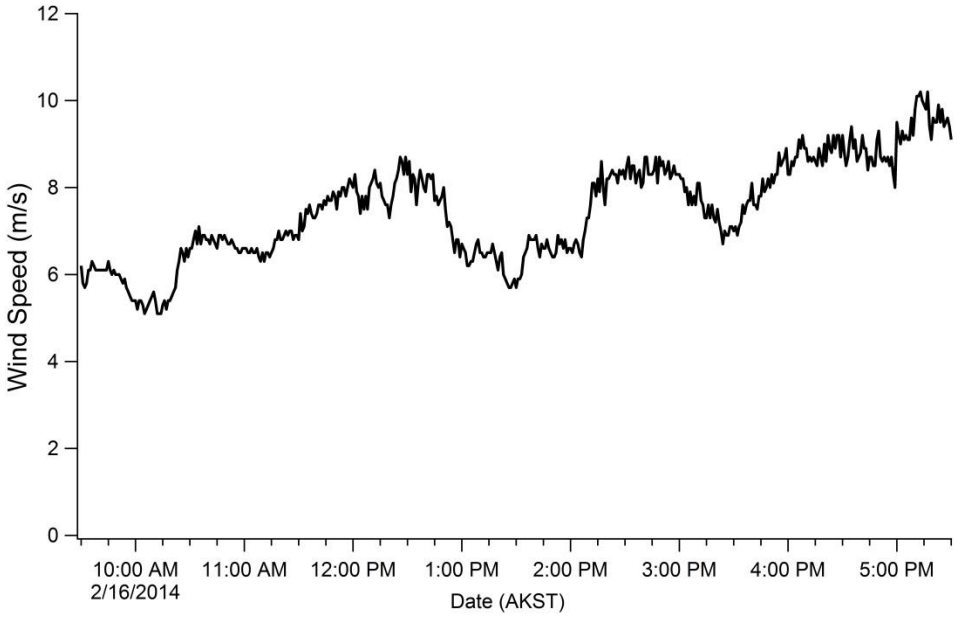

Figure 3.14 Wind speed data from Feb 16th flux experiment.

Differences between the observed vs calculated concentrations ranged from 12 to 158% (1 to 40 ppt) and 52 to 173% (9 to 100 ppt) for Br_2 and Cl_2, respectively. This results in a calculated to observed Br_2 and Cl_2 concentration ratios of 1.66 (±2.4) and 3.5 (±5.7), respectively. The uncertainty here represents the standard deviation of the data. Based on these results we cannot say for certain the significance of snowpack based molecular halogen emissions are to the overall atmospheric concentration.

3.4 Conclusions

From the two in-snowpack experiments conducted in Barrow, Alaska in February 2014 we found that the snowpack is a potential source for atmospheric Br_2, Cl_2, and BrCl. The production of molecular halogens was the result of photochemical reactions occuring at the surface of snow grains (flakes) and the production was enhanced in the presence of O_3. Prior to this work the source of atmospheric Cl_2 and BrCl was unknown. From the vertical profile experiments we were able to derive flux values for both Cl_2 and Br_2 from the tundra snowpack. Using the calcualted flux values we were able to evaluate the snow as an overall source of atmospheric molecular halogens and found it to have the potential to be a dominant source. Although further flux measurements are needed to confirm these findings, our calculated flux rates provide base values that can be used in future modeling studies of Arctic halogen chemistry. Based on our observations, if the Arctic salinity continues to increase, as dicussed in Section 1.4, it is possible that halogen production could be strengthened in the future. As first year sea ice is also more susceptible to cracks compared to multi-year sea ice, exposing open water which can replenish surface ozone by inducing vertical mixing (Moore et al., 2014). If surface

ozone is being replenished more often this could also lead to an enhancment in halogen production, based on the results from our experiments.

3.5 References

Abbatt, J., Oldridge, N., Symington, A., Chukalovskiy, V., McWhinney, R. D., Sjostedt, S., and Cox, R. A.: Release of Gas-Phase Halogens by Photolytic Generation of OH in Frozen Halide-Nitrate Solutions: An Active Halogen Formation Mechanism?, Journal of Physical Chemistry A, 114, 6527-6533, 10.1021/jp102072t, 2010.

Albert, M. R., Grannas, A. M., Bottenheim, J., Shepson, P. B., and Perron, F. E.: Processes and properties of snow-air transfer in the high Arctic with application to interstitial ozone at Alert, Canada, Atmospheric Environment, 36, 2779-2787, 10.1016/s1352-2310(02)00118-8, 2002.

Barrie, L., Bottenheim, J., Schnell, R., Crutzen, P., and Rasmsssen, R.: Ozone Destruction and Photochemical-Reactions at Polar Sunrise in the Lower Arctic Atmosphere, Nature, 334, 138-141, 10.1038/334138a0, 1988.

Boylan, P., Helmig, D., Staebler, R., Turnipseed, A., Fairall, C., and Neff, W.: Boundary layer dynamics during the Ocean-Atmosphere-Sea-Ice-Snow (OASIS) 2009 experiment at Barrow, AK, Journal of Geophysical Research-Atmospheres, 119, 2261-2278, 10.1002/2013jd020299, 2014.

Cao, L., Sihler, H., Platt, U., and Gutheil, E.: Numerical analysis of the chemical kinetic mechanisms of ozone depletion and halogen release in the polar troposphere, Atmospheric Chemistry and Physics, 14, 3771-3787, 10.5194/acp-14-3771-2014, 2014.

Chu, L., and Anastasio, C.: Quantum yields of hydroxyl radical and nitrogen dioxide from the photolysis of nitrate on ice, Journal of Physical Chemistry A, 107, 9594-9602, 10.1021/jp0349132, 2003.

Colbeck, S. C.: Model of wind pumping for layered snow, Journal of Glaciology, 43, 60-65, 1997.

Domine, F., Albert, M., Huthwelker, T., Jacobi, H., Kokhanovsky, A., Lehning, M., Picard, G., and Simpson, W.: Snow physics as relevant to snow photochemistry, Atmospheric Chemistry and Physics, 8, 171-208, 2008.

Fan, S., and Jacob, D.: Surface Ozone Depletion in Arctic Spring Sustained by Bromine Reactions on Aerosols, Nature, 359, 522-524, 10.1038/359522a0, 1992.

Finley, B. D., and Saltzman, E. S.: Observations of Cl_2, Br_2, and I_2 in coastal marine air, Journal of Geophysical Research-Atmospheres, 113, 10.1029/2008jd010269, 2008.

Foster, K., Plastridge, R., Bottenheim, J., Shepson, P., Finlayson-Pitts, B., and Spicer, C.: The role of Br_2 and BrCl in surface ozone destruction at polar sunrise, Science, 291, 471-474, 10.1126/science.291.5503.471, 2001.

Grannas, A. M., Jones, A. E., Dibb, J., Ammann, M., Anastasio, C., Beine, H. J., Bergin, M., Bottenheim, J., Boxe, C. S., Carver, G., Chen, G., Crawford, J. H., Domine, F., Frey, M. M., Guzman, M. I., Heard, D. E., Helmig, D., Hoffmann, M. R., Honrath, R. E., Huey, L. G., Hutterli, M., Jacobi, H. W., Klan, P., Lefer, B., McConnell, J., Plane, J., Sander, R., Savarino, J., Shepson, P. B., Simpson, W. R., Sodeau, J. R., von Glasow, R., Weller, R., Wolff, E. W., and Zhu, T.: An overview of snow photochemistry: evidence, mechanisms and impacts, Atmospheric Chemistry and Physics, 7, 4329-4373, 2007.

Guimbaud, C., Grannas, A. M., Shepson, P. B., Fuentes, J. D., Boudries, H., Bottenheim, J. W., Domine, F., Houdier, S., Perrier, S., Biesenthal, T. B., and Splawn, B. G.: Snowpack processing of acetaldehyde and acetone in the Arctic atmospheric boundary layer, Atmospheric Environment, 36, 2743-2752, 10.1016/s1352-2310(02)00107-3, 2002.

Hausmann, M., and Platt, U.: Spectroscopic measurement of bromine oxide and ozone in the high arctic during Polar Sunrise Experiment 1992, Journal of Geophysical Research-Atmospheres, 99, 25399-25413, 10.1029/94jd01314, 1994.

Kazantseva, N. N., Ernepesova, A., Khodjamamedov, A., Geldyev, O. A., and Krumgalz, B. S.: Spectrophotometric analysis of iodide oxidation by chlorine in highly mineralized solutions, Analytica Chimica Acta, 456, 105-119, 10.1016/s0003-2670(01)01625-7, 2002.

Knipping, E. M., Lakin, M. J., Foster, K. L., Jungwirth, P., Tobias, D. J., Gerber, R. B., Dabdub, D., and Finlayson-Pitts, B. J.: Experiments and simulations of ion-enhanced interfacial chemistry on aqueous NaCl aerosols, Science, 288, 301-306, 10.1126/science.288.5464.301, 2000.

Knipping, E. M., and Dabdub, D.: Modeling Cl_2 formation from aqueous NaCl particles: Evidence for interfacial reactions and importance of Cl_2 decomposition in alkaline solution, Journal of Geophysical Research-Atmospheres, 107, 30, 10.1029/2001jd000867, 2002.

Lehrer, E., Honninger, G., and Platt, U.: A one dimensional model study of the mechanism of halogen liberation and vertical transport in the polar troposphere, Atmospheric Chemistry and Physics, 4, 2427-2440, 2004.

Liao, J., Sihler, H., Huey, L., Neuman, J., Tanner, D., Friess, U., Platt, U., Flocke, F., Orlando, J., Shepson, P., Beine, H., Weinheimer, A., Sjostedt, S., Nowak, J., Knapp, D., Staebler, R., Zheng, W., Sander, R., Hall, S., and Ullmann, K.: A comparison of Arctic BrO measurements by chemical ionization mass spectrometry and long path-differential optical absorption spectroscopy, Journal of Geophysical Research-Atmospheres, 116, 10.1029/2010JD014788, 2011.

Liao, J., Huey, L., Liu, Z., Tanner, D., Cantrell, C., Orlando, J., Flocke, F., Shepson, P., Weinheimer, A., Hall, S., Ullmann, K., Beine, H., Wang, Y., Ingall, E., Stephens, C., Hornbrook, R., Apel, E., Riemer, D., Fried, A., Mauldin, R., Smith, J., Staebler, R., Neuman, J., and Nowak, J.: High levels of molecular chlorine in the Arctic atmosphere, Nature Geoscience, 7, 91-94, 10.1038/NGEO2046, 2014.

McConnell, J., Henderson, G., Barrie, L., Bottenheim, J., Niki, H., Langford, C., and Templeton, E.: Photochemical Bromine Production Implicated in Arctic Boundary-Layer Ozone Depletion, Nature, 355, 150-152, 10.1038/355150a0, 1992.

Michalowski, B., Francisco, J., Li, S., Barrie, L., Bottenheim, J., and Shepson, P.: A computer model study of multiphase chemistry in the Arctic boundary layer during polar sunrise, Journal of Geophysical Research-Atmospheres, 105, 15131-15145, 10.1029/2000JD900004, 2000.

Moore, C. W., Obrist, D., Steffen, A., Staebler, R. M., Douglas, T. A., Richter, A., and Nghiem, S. V.: Convective forcing of mercury and ozone in the Arctic boundary layer induced by leads in sea ice, Nature, 506, 81-84, 10.1038/nature12924, 2014.

Neuman, J., Nowak, J., Huey, L., Burkholder, J., Dibb, J., Holloway, J., Liao, J., Peischl, J., Roberts, J., Ryerson, T., Scheuer, E., Stark, H., Stickel, R., Tanner, D., and Weinheimer, A.: Bromine measurements in ozone depleted air over the Arctic Ocean, Atmospheric Chemistry and Physics, 10, 6503-6514, 10.5194/acp-10-6503-2010, 2010.

Oltmans, S., Schnell, R., Sheridan, P., Peterson, R., Li, S., Winchester, J., Tans, P., Sturges, W., Kahl, J., and Barrie, L.: Seasonal Surface Ozone and Filterable Bromine Relationship in the High Arctic, Atmospheric Environment, 23, 2431-2441, 10.1016/0004-6981(89)90254-0, 1989.

Oltmans, S. J., Johnson, B. J., and Harris, J. M.: Springtime boundary layer ozone depletion at Barrow, Alaska: Meteorological influence, year-to-year variation, and long-term change, Journal of Geophysical Research-Atmospheres, 117, 18, 10.1029/2011jd016889, 2012.

Piot, M., and von Glasow, R.: The potential importance of frost flowers, recycling on snow, and open leads for ozone depletion events, Atmospheric Chemistry and Physics, 8, 2437-2467, 2008.

Piot, M., and von Glasow, R.: Modelling the multiphase near-surface chemistry related to ozone depletions in polar spring, Journal of Atmospheric Chemistry, 64, 77-105, 10.1007/s10874-010-9170-1, 2009.

Pratt, K., Custard, K., Shepson, P., Douglas, T., Pohler, D., General, S., Zielcke, J., Simpson, W., Platt, U., Tanner, D., Huey, L., Carlsen, M., and Stirm, B.: Photochemical production of molecular bromine in Arctic surface snowpacks, Nature Geoscience, 6, 351-356, 10.1038/NGEO1779, 2013.

Shetter, R. E., and Muller, M.: Photolysis frequency measurements using actinic flux spectroradiometry during the PEM-Tropics mission: Instrumentation description and some results, Journal of Geophysical Research-Atmospheres, 104, 5647-5661, 10.1029/98jd01381, 1999.

Simpson, W., von Glasow, R., Riedel, K., Anderson, P., Ariya, P., Bottenheim, J., Burrows, J., Carpenter, L., Friess, U., Goodsite, M., Heard, D., Hutterli, M., Jacobi, H., Kaleschke, L., Neff, B., Plane, J., Platt, U., Richter, A., Roscoe, H., Sander, R., Shepson, P., Sodeau, J., Steffen, A., Wagner, T., and Wolff, E.: Halogens and their role in polar boundary-layer ozone depletion, Atmospheric Chemistry and Physics, 7, 4375-4418, 2007.

Spicer, C., Plastridge, R., Foster, K., Finlayson-Pitts, B., Bottenheim, J., Grannas, A., and Shepson, P.: Molecular halogens before and during ozone depletion events in the Arctic at polar sunrise: concentrations and sources, Atmospheric Environment, 36, 2721-2731, 10.1016/S1352-2310(02)00125-5, 2002.

Toyota, K., McConnell, J. C., Staebler, R. M., and Dastoor, A. P.: Air-snowpack exchange of bromine, ozone and mercury in the springtime Arctic simulated by the 1-D model PHANTAS - Part 1: In-snow bromine activation and its impact on ozone, Atmospheric Chemistry and Physics, 14, 4101-4133, 10.5194/acp-14-4101-2014, 2014.

Wei, Y. J., Liu, C. G., and Mo, L. P.: Ultraviolet absorption spectra of iodine, iodide ion and triiodide ion, Spectroscopy and Spectral Analysis, 25, 86-88, 2005.

Wren, S. N., Donaldson, D. J., and Abbatt, J. P. D.: Photochemical chlorine and bromine activation from artificial saline snow, Atmospheric Chemistry and Physics, 13, 9789-9800, 10.5194/acp-13-9789-2013, 2013.

Wu, C., Birky, M. M., and Hepler, L. G.: THERMOCHEMISTRY OF SOME BROMINE AND IODINE SPECIES IN AQUEOUS SOLUTION, Journal of Physical Chemistry, 67, 1202-&, 10.1021/j100800a009, 1963.

CHAPTER 4 THE NO_X DEPENDENCE OF BROMINE CHEMISTRY IN THE ARCTIC BOUNDARY LAYER

4.1 Introduction

Over the past several decades, Arctic sea ice has been undergoing a transition in its overall area coverage, as well as the overlying ice type. According to the National Snow and Ice Data Center (NSIDC), Arctic sea ice extent over the past 5 years has been ~20% less compared to the values from 1981-2010 (www.nsidc.org). This difference for July through November is shown in Figure 4.1.

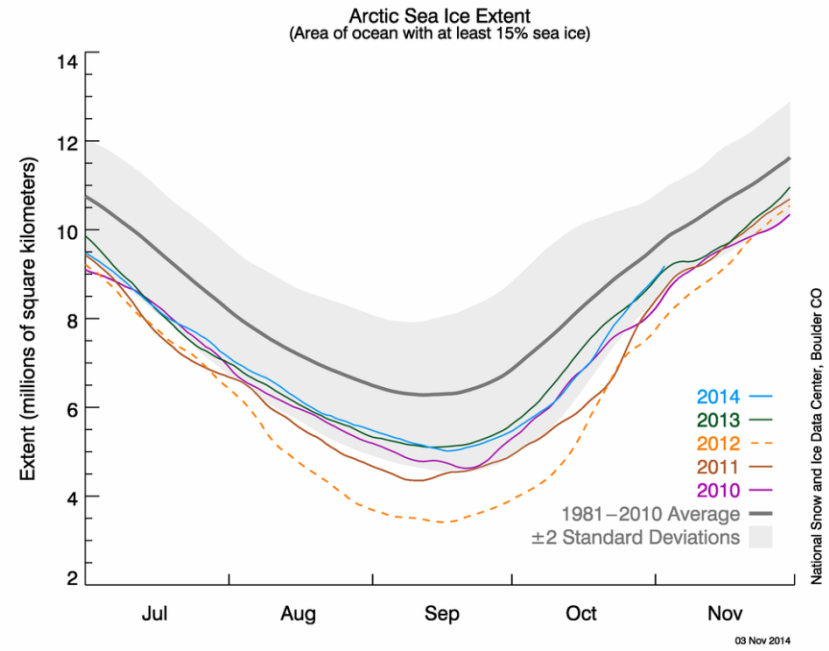

Figure 4.1 July to November sea ice extent for 2010-2014 along with the average sea ice extent from 1981-2010 (www.nsidc.org).

Additionally, the sea ice has been transitioning from mostly multi-year sea ice (MYI) to now first-year sea ice (FYI) (Maslanik et al., 2011). Maslanik et al. reported that the March sea ice coverage was ~75% MYI in the mid 1980's and has since dropped to 45% by 2011. FYI is sea ice that formed during the fall freeze up that has not survived a melt season, whereas MYI has survived at least one melt season (May-Sept). FYI is also generally thinner than MYI, making it more susceptible to melting and easier to traverse through with icebreakers (Maslanik et al., 2007). With less sea ice coverage it is believed that coastal development, shipping, and oil and gas exploration will increase throughout the Arctic (Peters et al., 2011;Corbett et al., 2010), which could lead to an increase in anthropogenic emissions, particularly NO_x ($NO_x = NO_2 + NO$).

Laboratory studies have shown that gas-phase NO_x can lead to the formation of $ClNO_2$ from Cl^- doped substrates, via reaction 4.1-4.3 (Roberts et al., 2008;Roberts et al., 2009;Finlaysonpitts et al., 1989).

$$NO_2 + O_3 + M \rightarrow NO_3 + O_2 \quad (4.1)$$

$$NO_2 + NO_3 \rightarrow N_2O_5 \quad (4.2)$$

$$N_2O_5 + Cl^- \rightarrow ClNO_2 + NO_3^- \quad (4.3)$$

Reactions 4.1-4.3 are believed to have an impact on the available atmospheric chlorine at coastal sites where potential anthropogenic NO_x sources are closely located. Riedel et al. conducted measurements of Cl_2 and $ClNO_2$ along the Los Angeles basin where maximum concentrations of 200 and 2100 pptv were observed, respectively. Although Cl_2 can be formed by reaction 4.4, Riedel et al. observed varying amounts of

correlation between Cl_2 and $ClNO_2$, indicating a potentially different source (Roberts et al., 2008;Riedel et al., 2012).

$$ClNO_2 + H^+_{(aq)} + Cl^-_{(aq)} \rightarrow Cl_2 + HONO \quad (4.4)$$

The above reactions are examples of how NO_x can impact halogen chemistry at the mid-latitudes but may not be representative of the less-polluted Arctic. Laboratory studies have shown that NO_x can play a role in halogen oxidation from frozen surfaces. $ClNO_2$ can be produced by flowing N_2O_5 over ice doped with Br^- and Cl^- (Lopez-Hilfiker et al., 2012). Lopez-Hilfiker et al. coated the inner walls of a flowtube, held at ~ 240 K, in ice consisting of varying ratios of $[Cl^-]$:$[Br^-]$. For ratios typical of the Arctic snow surface they observed a 1:1 release of Br_2:$ClNO_2$.

Complimenting these lab studies, modeling studies have also similarly shown that NO_x can react with halogen radicals to also produce reactive halogen species. Inorganic halogen nitrates or nitryl halides are formed when NO_x reacts with halogen radicals (R4.5-4.9) which can further react to yield reactive halogen species through aqueous phase chemistry (Cao et al., 2014;Toyota et al., 2014;Thomas et al., 2012;Morin et al., 2007;Morin et al., 2012;Evans et al., 2003;Aguzzi and Rossi, 1999, 2002;von Glasow et al., 2002;Thorn et al., 1993), and thereby alter the gas phase halogen reaction pathways.

$$XO + NO_2 \rightarrow XONO_2 \quad (4.5)$$

$$XO + NO \rightarrow X + NO_2 \quad (4.6)$$

$$X + NO_2 \rightarrow XNO_2 \quad (4.7)$$

$$XONO_2 \rightarrow XONO_{2(aq)} \quad (4.8)$$

$$XONO_{2(aq)} + H_2O \rightarrow HOX + HNO_3 \quad (4.9)$$

Lab studies have confirmed the potential that $BrONO_2$ could have on the bromine explosion during ODEs via reaction 4.9, where its hydrolysis on acidic ice surface yields HOBr (Hanson et al., 1996;Hanson, 2003;Aguzzi and Rossi, 2002). A summary of the halogen reaction pathways with and without the influence of anthropogenic NO_x is shown in Figure 4.2 (Grannas et al., 2002;Simpson et al., 2007).

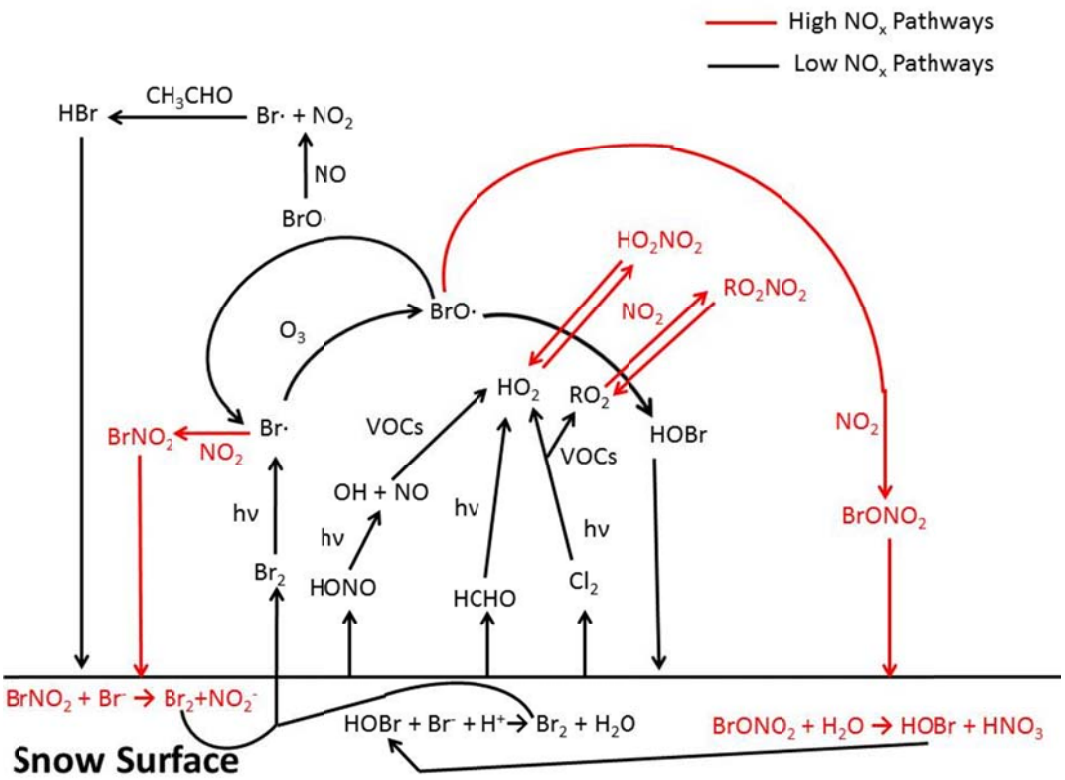

Figure 4.2 Halogen cycle in the Arctic boundary layer with (red trace) and without (black trace) the influence of anthropogenic NO_x (Abbatt et al., 2012;Simpson et al., 2007;Grannas et al., 2007).

Based on Figure 4.2, the impact that elevated NO_x concentrations will have on the halogen radical cycle is not straightforward as termination products ($BrNO_2$ and

$BrONO_2$) can lead to halogen production. Despite the potential for NO_x to impact the halogen chemistry that occurs in the Arctic, the increase in Arctic NO_x concentrations has not been studied until now.

The Arctic ambient air has been shown to have low background levels of NO_x, ranging from 10 to 100 pptv, as major anthropogenic sources are scarce within the pristine Arctic environment (Honrath et al., 2002). The primary source of atmospheric NO_x are photolabile precursors within the snowpack (Villena et al., 2011;Ridley et al., 2000;Honrath et al., 1999;Honrath et al., 2000) and long-range transport of organic nitrates and other photolabile species (Muthuramu et al., 1994). Observations of NO_x fluxes from the sunlit snowpack during Arctic based field studies (Grannas et al., 2007;Ridley and Orlando, 2003;Honrath et al., 1999;Honrath et al., 2002;Beine et al., 2002), coupled with lab studies, confirmed the ability of frozen surfaces doped with nitrite and nitrate to produce gas-phase NO_x when irradiated by UV light (reactions 4.10 – 4.11) (Dubowski et al., 2001;Dubowski et al., 2002;Honrath et al., 2000).

$$NO_3^- + h\nu \rightarrow NO_2 + O^- \quad (4.10)$$

$$NO_2^- + h\nu \rightarrow NO + O^- \quad (4.11)$$

To properly investigate the impact that high NO_x concentrations in the Arctic will have on Arctic halogen chemistry, we developed a multi-phase, zero-dimensional model to simulate the chemistry with varying concentrations of NO_x. During the 2009 Ocean-Atmosphere-Sea Ice- Snowpack (OASIS) field campaign, a suite of high-frequency, time resolved measurements of various gas-phase species occurred in Barrow, Alaska. These measurements provide the platform for our model by allowing us to constrain many chemical species (C_2H_2, C_2H_4, C_2H_6, C_3H_8, C_3H_6, *n*-C_4H_{10}, *i*-C_4H_{10}, HCHO, CH_3OCHO,

CH_3OCH_3, methyl ethyl ketone, CO, Hg, Br_2, and Cl_2) within our model to observations. Using our model we wanted to answer two basic questions surrounding the impact that elevated concentrations of NO_x would have on halogen chemistry:

- How is the rate of O_3 depletion affected by the presence of high NO_x concentrations?
- How will high NO_x concentrations impact the concentration of BrO_x (Br+BrO) along with its chain length?

4.2 Model Description

A multiphase, zero-dimensional model was originally developed by Dr. Chelsea Thompson using the FACSIMILE software (Stephens et al., 2012). The model has been described in detail in Stephens et al., so a brief description will be provided. The model consists of 176 known Arctic gas-phase reactions along with 29 photolysis reactions (Appendix, Table 1 and 2). It also takes into account dry deposition for 19 gas-phase species to the snow/aerosol surface (Appendix, Table 3), along with 16 aqueous-phase reactions (Appendix, Table 4).

The model represents the time period from March 24 through April 2, 2009, during which a 3 day ODE occurred with O_3 concentrations < 1ppb, followed by a complete O_3 recovery. A large NO_x plume (~16 ppb) was observed during the first two days of the simulation, allowing us to look at a wide variety of boundary layer chemical conditions during our simulation. To investigate the impact that NO_x has on radical halogen chemistry inorganic precursors (Br_2 and Cl_2) along with a series of prevalent hydrocarbons (C_2H_2, C_2H_4, C_2H_6, C_3H_8, C_3H_6, *n*-C_4H_{10}, *i*-C_4H_{10}, HCHO, CH_3CHO,

CH_3OCH_3, methyl ethyl ketone, and CO) were constrained to the observations for the ten day period, shown in Figure 4.3a-d. Mole ratios of constrained gas-phase species along with the photolysis rates were called into the model every 10 minutes within the simulation. It should be noted that the constrained mole ratio for Br_2 on March 30th and 31st in the model is based on the observed diurnal average of March 29th and April 1st. As discussed in Liao et al. (2012) atmospheric observations for Br_2 on March 30th and 31st were not available.

Measurement methods for all the constrained species used in the model are listed in Appendix, Table 5. Time varying photolysis frequencies (J) were also calculated throughout the field campaign.

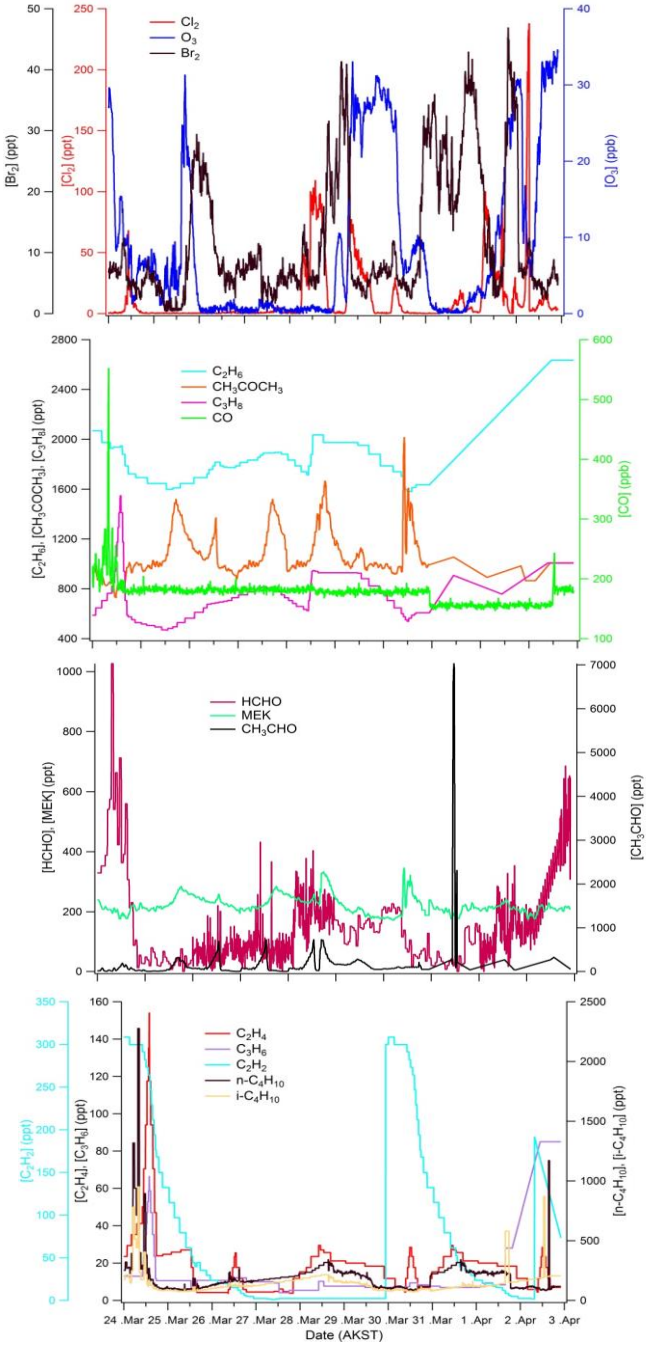

Figure 4.3 Species constrained within the model based on their observations during the 10 day period of March 24 through April 2.

Both CH_4 and water vapor concentration were held constant for the entire 10 day simulation. The water vapor concentration was calculated based on the observed meteorological conditions for March 25. On this day the relative humidity was 78% and the ambient temperature was -19.5°C, yielding a water vapor concentration of $2.23x10^{16}$ molecules·cm^{-3} (NOAA; Barrow airport data). A CH_4 concentration of 1.89 ppm was used for the entire simulation, as it represented the average CH_4 concentration for that time period as reported by the NOAA-ESRL Barrow Observatory.

To investigate how NO_x mole ratios impact the halogen chemistry in the Arctic, two NO_x scenarios were developed based on the NO_x observations from the OASIS field campaign. NO and NO_2 concentration measurements were conducted using a $NO+O_3$ chemiluminescence technique, where NO_2 was measured as NO via a photolytic converter (Ridley et al., 1994). The observed NO_x concentration during the 10 day period being simulated is shown in Figure 4.4. A "Low NO_x" case and a "High NO_x" case were used to create the two different scenarios, isolating a single parameter to vary between the two scenarios. It should be noted that we don't take into account other chemical species, such as VOCs, whose atmospheric concentrations are impacted by anthropogenic emissions. The two diurnal-cycle NO_x profiles were derived from the actual observed NO_x over the time period being simulated. The diurnal averages used in the model are shown in Figure 4.4. Using the criteria from Villena et al. (2011), clean and polluted days were separated for the time period of March 24 to April 2. Ambient CO concentrations were monitored for elevated concentrations to determine if the air mass was influenced by emissions from the town of Barrow (Villena et al., 2011). The non-influenced/background days were averaged together to calculate a "low NO_x" diurnal

average that ranged between 50 to 100 pptv. The same was done for the days influenced by local anthropogenic emissions, to create the "high NO_x" diurnal average characterized by NO_x mole ratios from 700 to 1600 pptv. Each diurnal average was fit to a curve to generate temporally smoothed profiles. Either the Low NO_x or High NO_x diurnal average was used for each day of the model simulation, depending on what scenario was being simulated. As the NO_x mole ratio was the only parameter being altered between simulations it allowed us to evaluate the NO_x-dependence of the chemistry.

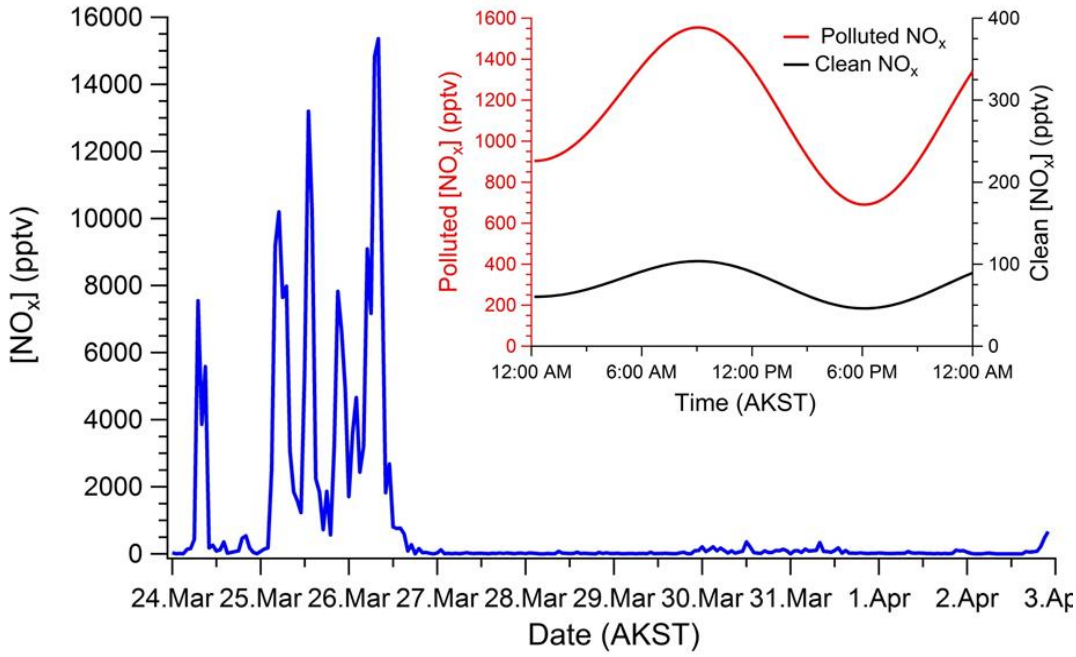

Figure 4.4 Observed ambient NO_x mole ratios from 2009 OASIS field campaign (blue), along with the diurnal averages used in for the two different scenarios.

4.3 Chemical Mechanisms

A complete list of all of the gas-phase reactions along with their respective rate constant values used in the model are listed in the Appendix Table 1. Rate constant values were calculated for 248K (average temperature during the simulated time period), unless specified otherwise. Chemical mechanisms for BrO_x, ClO_x, HO_x, NO_x, and VOCs prevalent during Arctic ODEs were used. Aqueous-phase mechanisms for halogen activation and their respective rate constants are listed in Appendix, Table 4. Reactions that take place on the snow grain surface are assumed to occur in the quasi-liquid-layer (QLL). Photochemical dissociation reactions used in this model are listed in Appendix, Table A.2. The photolysis frequencies (J) for both NO_2 and O_3 were calculated using 0.1 Hz measurements of downwelling actinic flux throughout the OASIS field campaign. All other species time varying photolysis rates were scaled to $J(NO_2)$ based on calculations using a modified version of the Tropospheric Ultraviolet and Visible Radiation (TUVR) model (Madronich, 2002).

4.4 Results and Discussion

4.4.1 Bromine Chain Length

Chain length calculations are used to evaluate the number of times a radical is propagated before it is terminated. A chain length value ≥ 1 indicates that the radical specie was regenerated at least once before the radical was destroyed. Using Equation 4.I (Thompson et al., 2014) the bromine radical chain length (Φ) for the 10 day simulation

was calculated for each NO_x scenario. As bromine chemistry is heavily linked with ozone depletion in the Arctic boundary layer (Barrie et al., 1988;Fan and Jacob, 1992), the bromine radical chain length represents the interconversion of Br and BrO, which consequently depletes ozone.

$$\phi = \frac{\left(\begin{array}{c} 2k[BrO]^2+k[BrO][ClO]+k[BrO][CH_3OO]+k[BrO][OH]+ \\ k[BrO]\left[O(^3P)\right]+k[BrO][CH_3OOO]+k[BrO][NO]+J[BrO] \end{array}\right)}{\left(\begin{array}{c} k[Br][HO_2]+k[Br][C_2H_2]+k[Br][C_2H_4]+k[Br][C_3H_6]+ \\ k[Br][HCHO]+k[Br][NO_2](0.15)+k[Br][CH_3CHO]+ \\ k[Br][C_3H_6O]+k[Br][C_4H_8O]+k[Br][CH_3OOH]+ \\ k[BrO][HO_2]+k[BrO][CH_3OO]+k[BrO][C_3H_6)]+ \\ k[BrO][NO_2] \end{array}\right)} \qquad (4.I)$$

The denominator for Equation 1 represents the reactions that form stable brominated species that end the Br propagation chain reaction. However, several of the termination reactions yield brominated species (HOBr and $BrONO_2$) that can regenerate Br radicals either through photolysis or heterogeneous reactions. This highlights the complexity of the halogen chemistry that occurs in the Arctic. Concerning pathways involving NO_x, *Orlando and Burkholder* (2000) used a Fourier transform- infrared spectrometer to study the Br + NO_2 reaction, where they determined at Arctic relevant temperatures (248K), the branching ratio was 85:15 for BrONO:$BrNO_2$ (Orlando and Burkholder, 2000). However, they noted that BrONO was very unstable and could thermally decompose back to Br + NO_2, isomerize to $BrNO_2$, or react with Br (R4.12).

$$Br + BrONO \rightarrow Br_2 + NO_2 \qquad (4.12)$$

To evaluate if BrONO was a true BrO_x sink, we calculated its atmospheric lifetime using Equ. 4.II.

$$\tau_{BrONO} = \frac{[BrONO]}{k_{TD}[BrONO]+k_{iso}[BrONO]+k[Br][BrONO]} \quad (4.II)$$

Using a thermal decomposition rate constant of $0.02s^{-1}$, a isomerization rate constant of $0.014s^{-1}$,a Br+BrONO rate constant of $1x10^{-12}$ $cm^3 \cdot molecules^{-1} \cdot s^{-1}$, and a [Br] of $5x10^7 molecules \cdot cm^{-3}$, the calculated BrONO atmospheric lifetime was 29 seconds. This was determined to be too short to qualify as a BrO_x termination product. Therefore, when calculating the bromine chain length the $Br+NO_2$ value was multiplied by the branching ratio for the reaction that yields $BrNO_2$. For our study the bromine chain length was only calculated during the daylight hours (10:00 to 18:00 AKST), as the BrO_x chain is photochemically propagated by the photolysis of Br_2. The bromine chain length was calculated for both NO_x scenarios for each day of the simulation.

The chain lengths in each scenario (Low and High NO_x) show a dependence on ambient O_3 concentration, where high chain lengths are observed when ozone is > 5ppb (Figure 4.5). From Figure 4.5, the effects of ozone on the bromine chain length are shown on March 26, 27, 28 and 31, where O_3 mole ratio is <5ppb and the bromine chain length is <1. Intuitively one would hypothesize that the bromine chain length should be longer for the Low NO_x case, as the ability for NO_x to act as a potential Br sink is less likely in this scenario. However, the average bromine chain length for the Low and High NO_x scenarios when O_3 mole ratio is > 5ppb was 1.72 (±0.70) and 1.81 (±0.35), respectively.

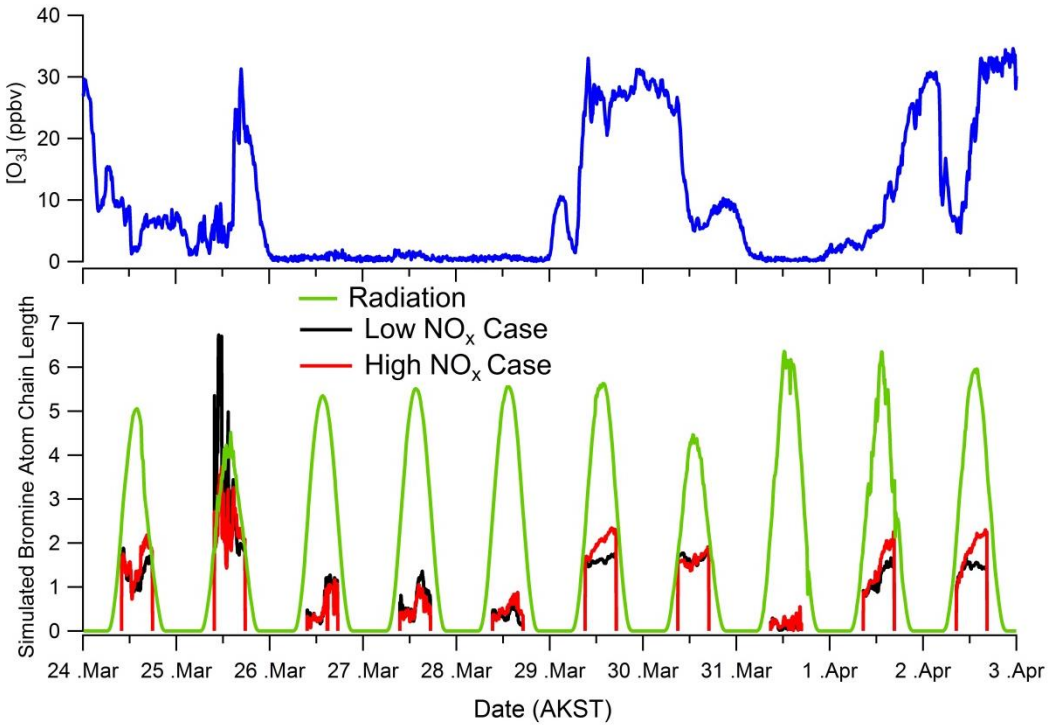

Figure 4.5 Simulated bromine chain length for the Low and High NO_x cases along with downwelling radiation and observed O_3 concentrations.

Indeed, NO_x, on a percentage basis, acts as a more dominant sink for BrO_x during the High NO_x compared to the Low NO_x case (Figure 4.6). The $Br+NO_2$ reaction occurs more often in the High NO_x case by a factor of 5, while the $BrO+NO_2$ reaction occurs 7% more often in the Low NO_x condition. The reason the $BrO+NO_2$ occurred more in the low NO_x case is that BrO mole ratio was much higher in the Low NO_x case (discussed later), providing available BrO to react with NO_2.

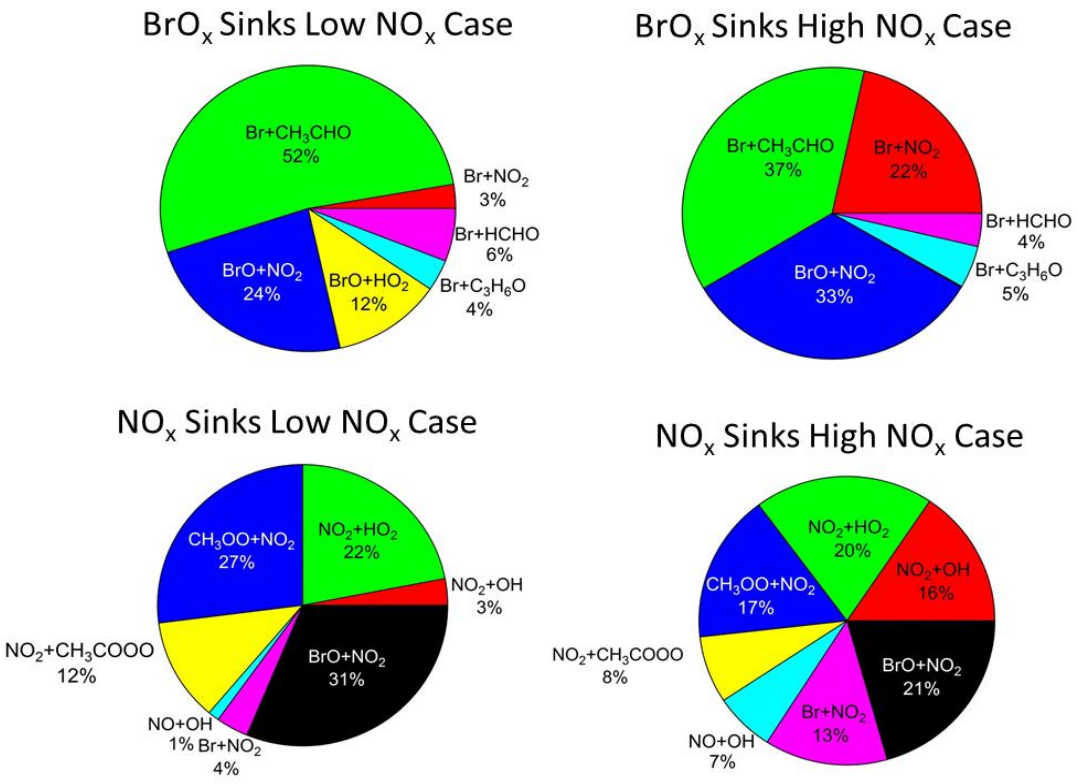

Figure 4.6 Fractional contributions of BrO_x and NO_x sink reactions from the low and high NO_x simulation cases.

The main reason the low NO_x case has a smaller average bromine chain length is that the reaction of Br + HO_2 occurs more frequently, by a factor of 170, during the low NO_x simulation. It should be noted that this reaction yields HOBr, which is known to participate in the aqueous phase chemistry that produces gas-phase Br_2 (Reaction 4.13).

$$HOBr + Br^- + H^+ \rightarrow Br_2 + H_2O \qquad (4.13)$$

The outcome of reaction 4.13 complicates the interpretation of the bromine chain length values because the regeneration of Br_2 is not taken into account within the calculation.

We calculated the net ozone loss rate to further investigate the effect that NO_x has on the principal reactions in which the atmospheric halogens participate.

4.4.2 Net O_3 Loss Rate

The net ozone loss rate was calculated using Equation 4.III, based on the work by *Thompson* et al. The net O_3 loss rate represents the sum of all the rates of reactions that destroy ozone subtracted by the sum of the rates that produce ozone. For the production term, the included reactions are ones for which the reactants BrO and ClO are a product of O_3 destruction. This is to act as an offset for the ozone destruction rate as NO_2 and XO can photolyze to form O_3, as shown in reactions 4.14-4.17.

$$\text{Net } O_3 \text{ Loss Rate} = \begin{pmatrix} k[Br][O_3] + k[Cl][O_3] + k\left[O(^1D)\right][H_2O] \\ + k[OH][O_3] + k[HO_2][O_3] - k[BrO][NO] \\ -J[BrO] - k[ClO][NO] - J[ClO] \end{pmatrix} \quad \text{(4.III)}$$

$$XO + h\nu \rightarrow X\cdot + O^1(D) \quad \text{(4.14)}$$

$$XO + NO \rightarrow X\cdot + NO_2 \quad \text{(4.15)}$$

$$NO_2 + h\nu \rightarrow NO + O^1(D) \quad \text{(4.16)}$$

$$O^1(D) + O_2 \rightarrow O_3 \quad \text{(4.17)}$$

The calculated net ozone loss rate for both scenarios for the 10 day simulation period is shown in Figure 4.7, along with the constrained O_3 mole ratio used in the model. Although the High NO_x case yielded, on average, a greater simulated bromine chain length, the Low NO_x case produced on average a net ozone loss rate that was a factor of 2 times faster compared to the High NO_x case.

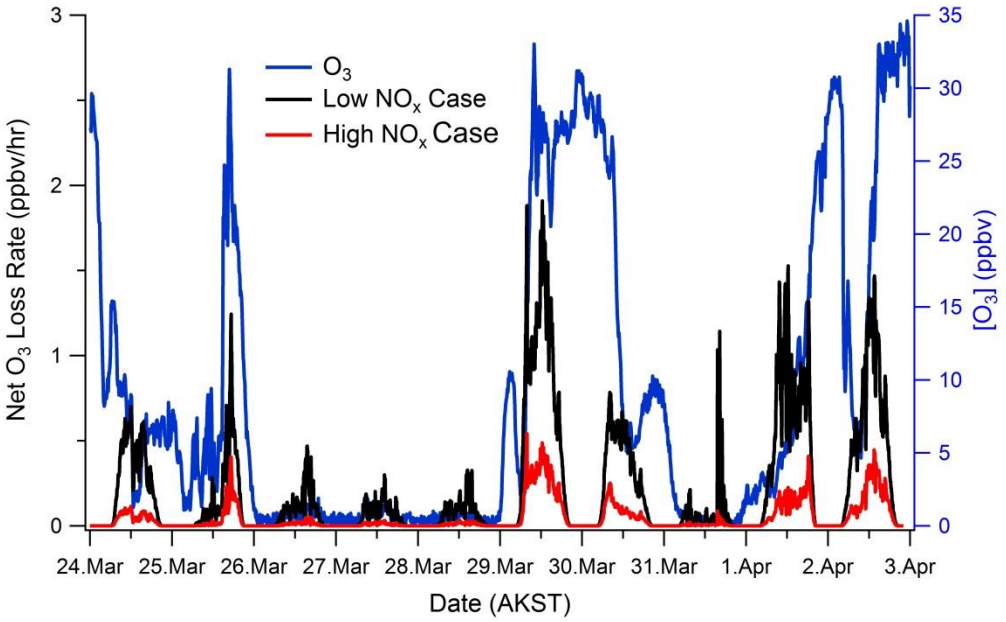

Figure 4.7 Calculated net O_3 loss rate for the low NO_x and high NO_x simulations, along with the observed O_3 mole ratios.

To study this further, we calculated the net ozone loss rate over the 10 day simulation with varying constrained NO_x mole ratios. Multiple NO_x diurnal profiles were developed by starting with the low NO_x conditions and step-wise increasing the NO_x by 250 pptv until a maximum peak of 2000 pptv was achieved. This equated to 9 different NO_x scenarios that are plotted in Figure 4.8 for the time period of 11:00-13:00 for March 30. March 30 was chosen as it fell into the "clean day" category during the OASIS field campaign. It was observed that ambient ozone was depleted on March 30 from 30 ppb to 5 ppb. Based on Figure 4.8, the net O_3 loss rate has a dramatic decrease by a factor of one and a half (from 0.80 to 0.52 ppbv/hr) over the increase of NO_x mole ratio of ~100 – 500 pptv, followed by a constant decrease to 0.40 ppb/hr at 2000 pptv of NO_x. This

clearly expresses the strong NO_x-dependence of the halogen chain reaction, especially for ambient conditions and slight changes in NO_x.

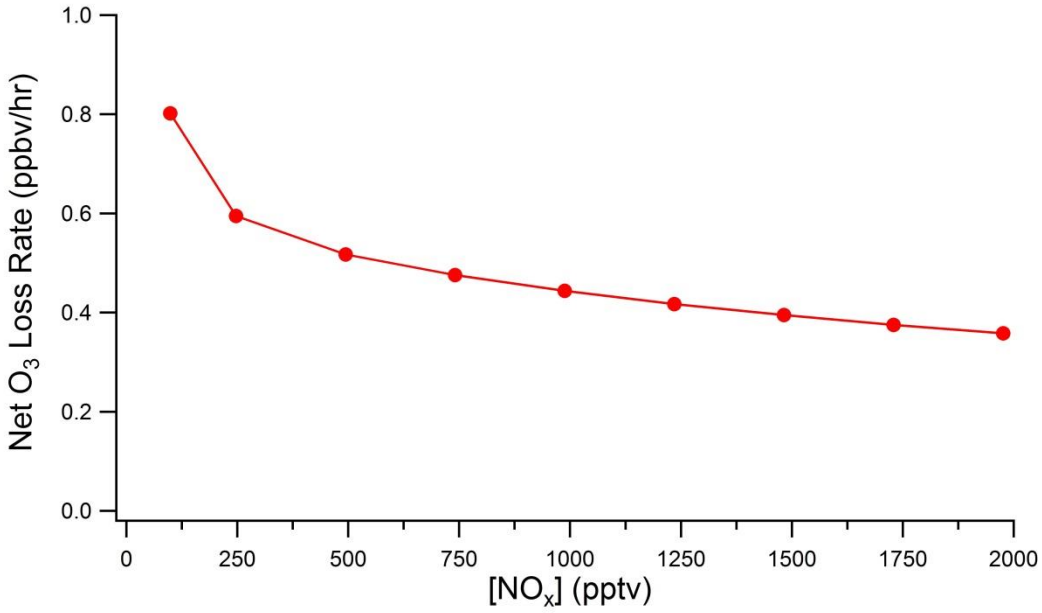

Figure 4.8 Net O_3 loss rate as a function of the NO_x mole ratio, for March 30th mid-day (11:00 to 13:00 AKST) conditions.

Based on the conditions of the model, the net O_3 loss rate only represents the sensitivity of the gas-phase O_3 loss-reactions towards NO_x, but does not consider the impact of $BrONO_2$ deposition (discussed below in Sect 4.4.3.). A regression of the observed [Br_2] vs observed [NO_x] reveals that the high NO_x conditions (>300 pptv) clearly hinder Br_2 production (Figure 4.9).

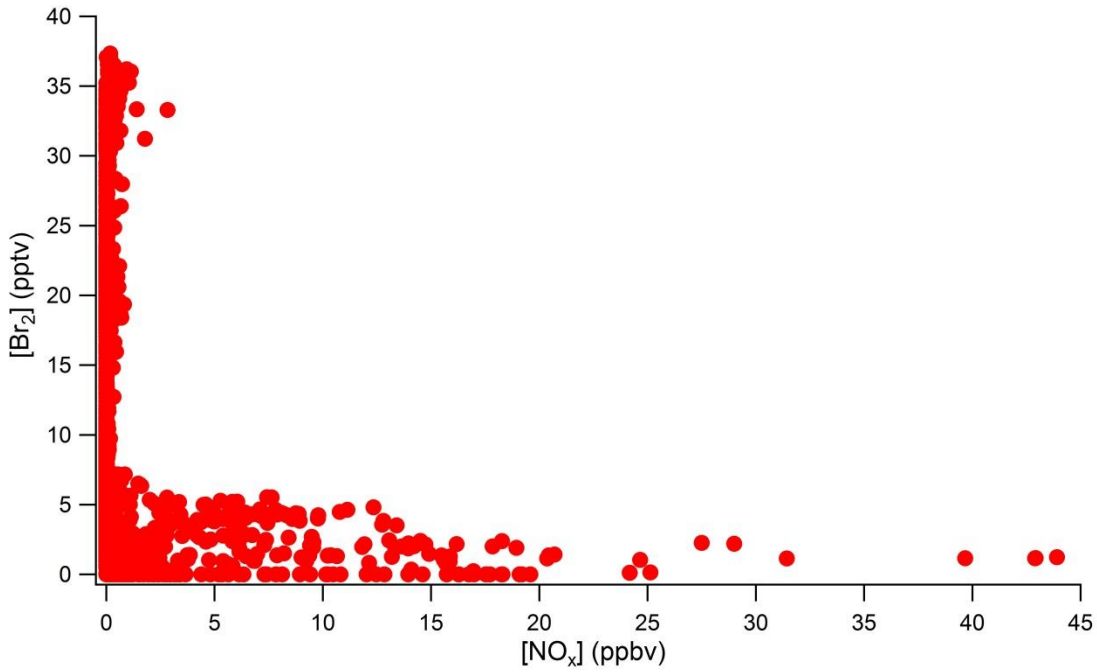

Figure 4.9 5 minute averages of observed concentrations of Br_2 and NO_x from OASIS 2009.

Since Br_2 is the main known precursor for ozone depletion it is expected that the O_3 loss rate will decrease as NO_x mole ratios are elevated, since Br atom production will be slower. For days when the ozone levels are close to zero (< 5 ppb), the net O_3 loss rate, as expected, is very low since the rate of ozone destruction will approach zero as O_3 is nearly completely removed (Fig 4.7). Based on these results, as the Arctic changes and point sources become more common, the influence of elevated NO_x levels on ozone loss rate could be more prominent.

The O_3 loss rate for March 30 from 11:00 to 13:00, based on the observations, was ~3.4 ppbv/hr. This is much faster than the calculated net O_3 loss rate for the Low NO_x case of 0.80 ppbv/hr. This low net O_3 loss rate for the Low NO_x simulation could be a

result of the constrained model Br_2 mole ratio not being representative of the ambient air in Barrow at that time; (discussed in Sect. 4.2). If the Br_2 mole ratio was actually higher at that time than what was prescribed in the model then the ozone destruction rate would increase. However, this apparent dramatic ozone loss rate could be the result of an ozone depleted air mass being transported to the measurement sight (Halfacre et al., 2014). Back trajectory calculations show that the sampled air mass of March 30 spent the previous 30 hours over the Beaufort Sea which during March is covered with sea ice. It is possible then that as the air mass travelled over the sea ice, active halogen chemistry depleted it of O_3 and that contributed to the observation depletion rate being greater than what the model simulated.

4.4.3 Model Simulated Species vs OASIS Observations

To further investigate how NO_x influences the net ozone loss rate and the bromine chain length, several relevant species crucial in the bromine cycle were examined. Br_2 along with its precursors (HOBr and $BrONO_2$) are produced in the gas-phase during ozone depletion (reactions 4.19-4.24).

$$Br_2 + h\nu \rightarrow 2Br \quad (4.19)$$

$$Br + O_3 \rightarrow BrO + O_2 \quad (4.20)$$

$$BrO + HO_2 \rightarrow HOBr + O_2 \quad (4.21)$$

$$BrO + NO_2 \rightarrow BrONO_2 \quad (4.22)$$

$$BrONO_2 + H_2O \rightarrow HOBr + HNO_3 \quad (4.23)$$

$$BrO + BrO \rightarrow Br_2/2Br + O_2 \quad (4.24)$$

The BrO self-reaction (Reaction 4.12) represents the primary gas-phase recycling reaction, whereas heterogeneous reactions of HOBr and $BrONO_2$ (4.13 & 4.23) at ice surfaces lead to the formation of gas-phase Br_2. We now compare how artificially elevated NO_x mole ratios influence HOBr, BrO, and $BrONO_2$ as compared to the observations from the OASIS field campaign. We find that simulated BrO during the Low NO_x case is similar (± 5pptv) to what was observed during OASIS for the majority of the 10 day simulation, as expected since most of the simulated days were observed as low NO_x days (Figure 4.10).

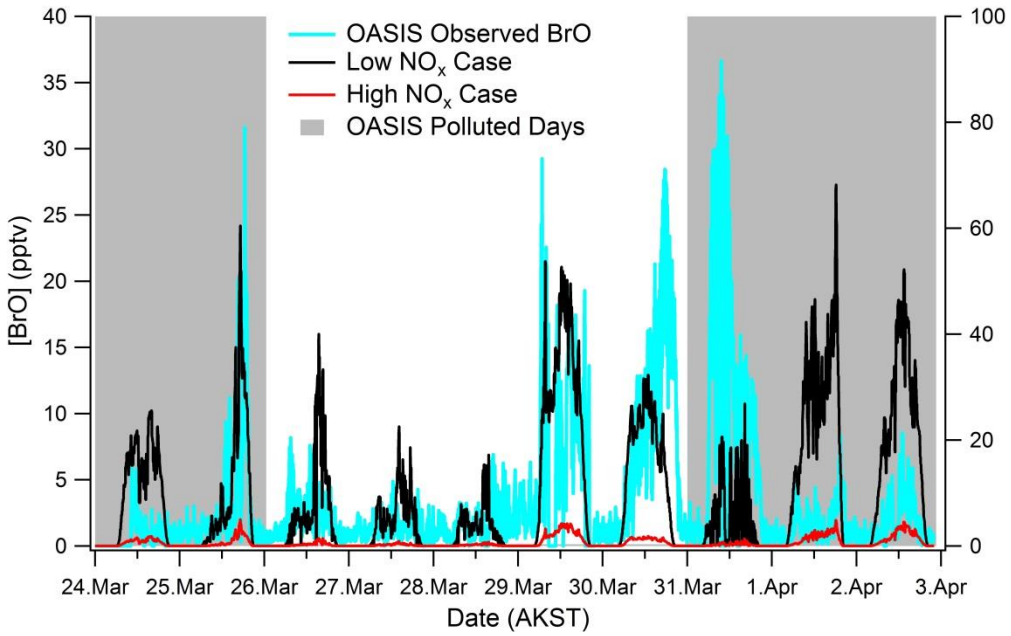

Figure 4.10 Simulated BrO mole ratio (low NO_x & high NO_x cases) and the observations during the study period.

However, on March 30th and 31st the low NO_x simulated BrO mole ratio is less than half of that observed during OASIS. As discussed earlier, Br_2 mole ratios were not available for March 30th and 31st and could have led to the under simulated BrO mole ratios. The simulated BrO mole ratio for the high NO_x case was highly suppressed, by an order of magnitude, compared to the low NO_x case. The high NO_x case daytime BrO mole ratio never exceeds 3pptv throughout the 10 day simulation, where the low NO_x case BrO mole ratio ranges from 2.5 to 25 pptv.

The simulated HOBr, for both NO_x scenarios, follow the same trend as BrO. The Low NO_x case HOBr is within ±5pptv of the observation whereas the HOBr mole ratio for the High NO_x case is much lower and never exceeds 2.5 pptv (Figure 4.11).

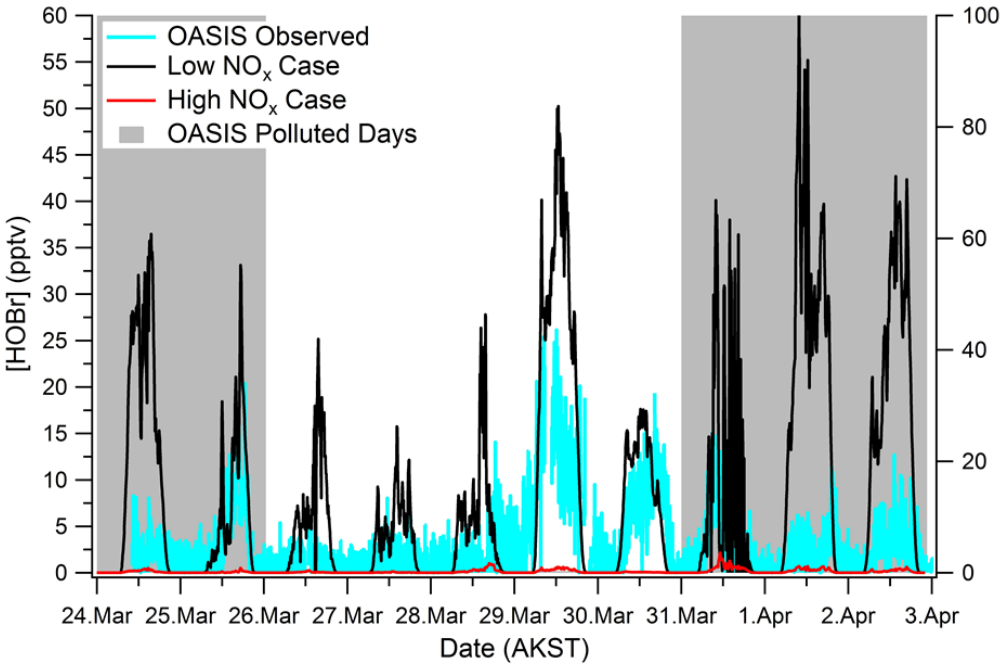

Figure 4.11 HOBr levels from the model simulations (low NO_x & high NO_x cases) and the observations during the simulation dates.

For the days of March 26th and March 29th the low NO_x simulated HOBr exceeds the observation by 2-3 times. This is due to the higher HO_2 mole ratio produced in the model compared to observations.

Based on Figures 4.10 and 4.11 it can be concluded that High NO_x mole ratios suppress both HOBr and BrO, and that is what is observed during OASIS on a high NO_x mole ratios day, March 24th. However, unlike BrO and HOBr, $BrONO_2$ is unaffected by the atmospheric NO_x mole ratios (Figure 4.12). This is due to the fact that while increased NO_x suppresses BrO, the rate of reaction 4.5 is compensated by the increase in NO_2 mole ratios.

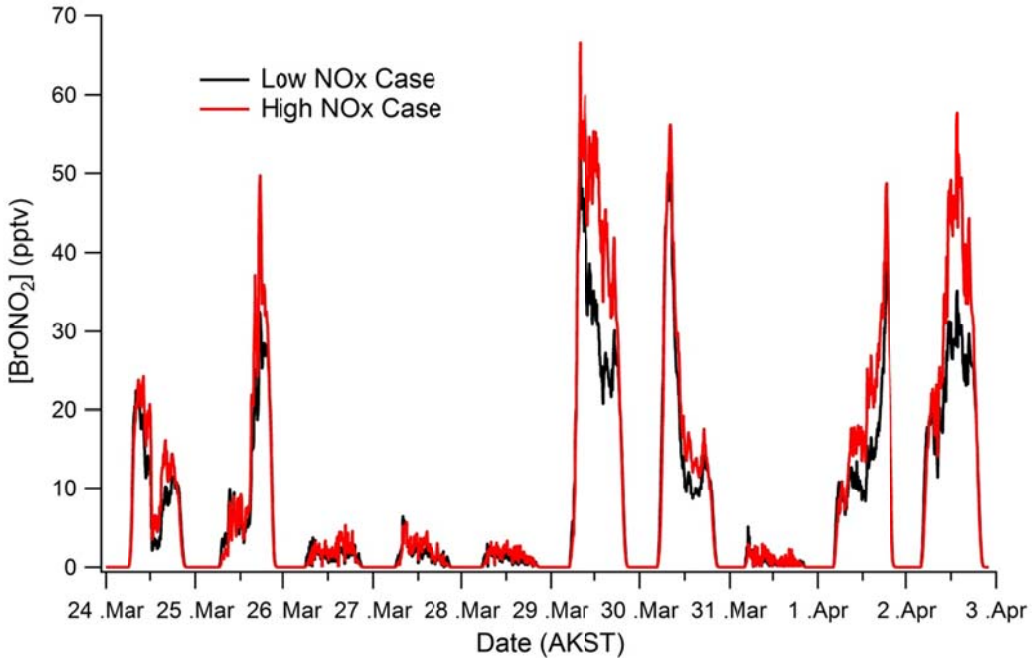

Figure 4.12 $BrONO_2$ mole ratio from the two simulation cases.

This is shown in Figure 4.12 where the simulated $BrONO_2$ does not change between the two different NO_x simulations. Additionally, when the model simulated $BrONO_2$ mole ratio for both NO_x simulations is plotted against the $BrONO_2$ production rate ($k_{BrO+NO2}[BrO][NO_2]$), it affirms that the $BrONO_2$ mole ratios follow $k_{BrO+NO2}[BrO][NO_2]$ (Figure 4.13).

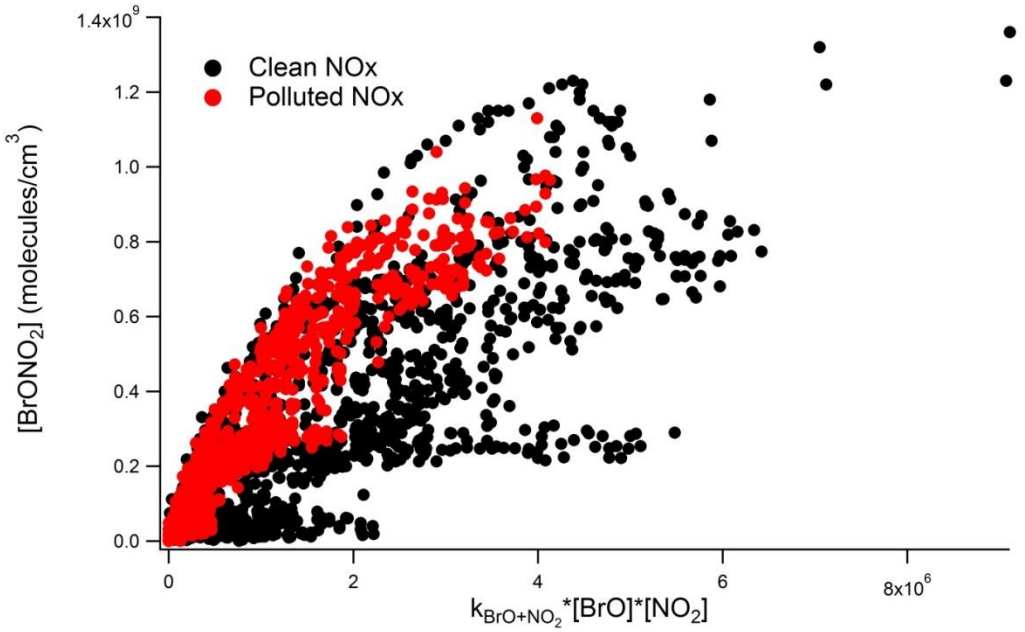

Figure 4.13 Simulated $BrONO_2$ mole ratio (low NO_x & high NO_x cases) plotted against the production rate of $BrONO_2$.

4.4.4 BrO_x and NO_x Sinks

Based on the results of our simulated BrO and HOBr, we concluded that NO_x influences the partitioning of BrO_x. To further understand the details of this influence we quantified the NO_x and BrO_x sinks by using counters to determine the main reactions

which convert NO_x and BrO_x to reservoir species. Counters tallying the number of times a reaction occur within the model through the 10 day simulation. When evaluating the entire 10 day simulation period NO_x plays a crucial role in the sink of BrO_x radicals, accounting for > 27% of the loss in the low NO_x case and for >50% in the high NO_x case (Figure 4.6). However, the reservoir species, $BrONO_2$ and $BrNO_2$, can both lead to Br_2 production through heterogeneous reactions. The other major contributor towards the termination of BrO_x is CH_3CHO, as it yields more than 35% of the total sink in both simulations. This is expected as field observations have shown CH_3CHO to be a major sink of Br radicals during ODEs (Shepson et al., 1996). However, in contrast to anthropogenic emissions generally acting as a source of CH_3CHO, during the 10 day simulation period the CH_3CHO mole ratios were not influenced by emissions from Barrow. This supports the belief that the snowpack as acting as the major source of CH_3CHO in the Arctic (Grannas et al., 2002). In terms of NO_x sinks, HO_2 plays an important role (~20%), but the reaction of NO_2 with Br and BrO act as a significant sink accounting for ~34% of the loss NO_x in both scenarios.

4.5 BROMEX Observations

To further investigate how anthropogenic NO_x influences Arctic halogen chemistry, focusing on the BrO_x cycle, both NO_2 and BrO were simultaneously measured in and around a large combustion plume in the coastal Arctic atmosphere. During the previously mentioned BROMEX 2012 field campaign, atmospheric measurements of inorganic halogens, O_3, and gaseous elemental mercury were obtained in Barrow, Alaska during the springtime (Feb. 26 – April 4, 2012). Purdue's Atmospheric Laboratory

Atmospheric Research (ALAR) was utilized during the BROMEX field campaign to collect BrO and NO_2 column densities (surface to ~700m) using an aircraft-mounted MAX-DOAS (General et al., 2014). ALAR is a Beechcraft Duchess Light Twin Engine airplane equipped with a Best Air Turbulence (BAT) probe for wind measurements, GPS, a micro-bead temperature probe and a 2B Technologies model 205 dual-beam O_3 monitor.

Prudhoe Bay is the largest oil field on the North Slope, located ~330 km southeast of Barrow, AK, and emits significant amounts of CO_2, NO_x, and CH_4 (Brooks et al., 1997;Jaffe et al., 1995). On March 30th, 2012 ALAR conducted flights near Purdue Bay, Alaska, to investigate the impact of anthropogenic emissions on local halogen chemistry. A section of the March 30th flight, presented in Figure 4.14, shows the BrO and NO_2 differential slant column density (DSCD) from that flight.

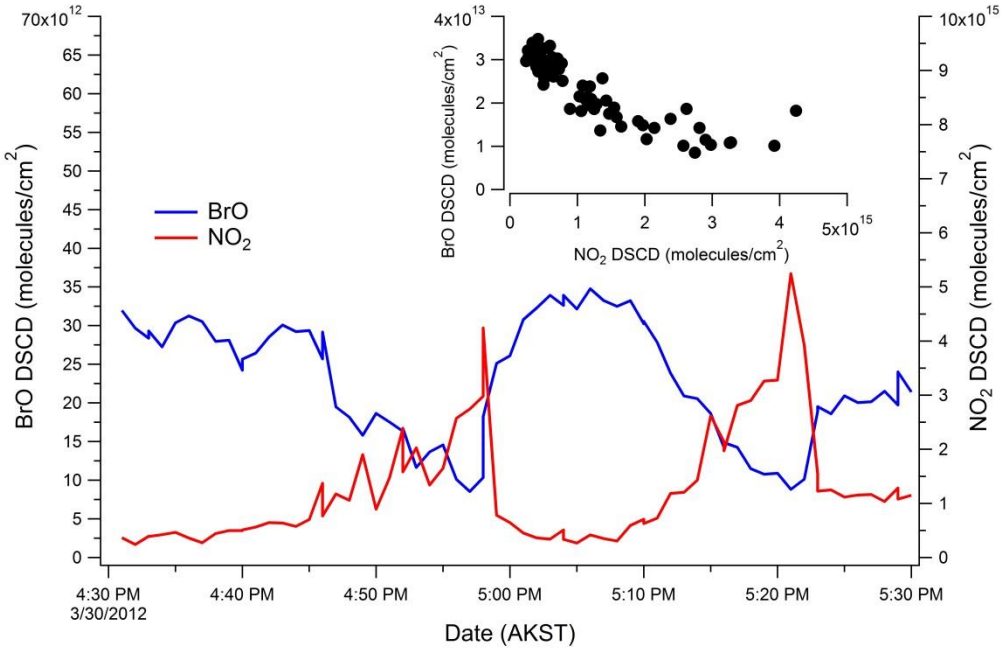

Figure 4.14 BrO and NO_2 measured mole ratios via MAX-DOAS during the BROMEX field campaign, near Prudhoe Bay (70°N,149°W), AK at 700m above the surface on March 30, 2012. The insert of the NO_2 versus BrO shows the anti-correlation between the two species.

ALAR intercepted an anthropogenic plume, exhibited by the spikes in the NO_2 DSCD. From Figure 4.14 a temporary depletion in BrO DSCD correlates with the spikes in NO_2 DSCD. This is furthered expressed by the insert inside Figure 4.14 that shows the BrO DSCD plotted against the NO_2 DSCD, where it shows that as NO_2 DSCD increases BrO DSCD decreases. Although the BrO_x sink products, $BrNO_2$ and $BrONO_2$, can interact with ice surfaces to re-emit Br_2, the overall net-effect of elevated NO_x levels is to hinder halogen recycling as observed in Figure 4.8 and 4.14. However, it is known that very large NO_x plumes have the ability to remove O_3 through the reaction with NO (4.25),

although a photosteady state will be established from NO_2 photolysis during sunlight hours.

$$NO + O_3 \rightarrow NO_2 + O_2 \quad (4.25)$$

If ozone is titrated out, via reaction 4.25, the BrO_x partitioning will shift from BrO towards Br, as BrO production will cease and then be lost through photolysis.

The source of the NO_x plumes in Prudhoe Bay are most likely combustion sources related to oil drilling, and pipeline management, via tall stacks. The latter would place the emissions aloft, where natural aerosol extinction is low compared to the surface (Breider et al., 2014). This would impact the efficiency of $BrONO_2$ to be recycled on an ice surface to re-emit Br_2. However, the point sources in Prudhoe Bay, which produce the anthropogenic emissions that contain the elevated levels of NO_x also yield a significant amount of aerosols (data not shown) (Peters et al., 2011). Therefore, the aerosol extinction is expected to increase if these point sources continue to grow in number throughout the Arctic, thereby providing additional airborne surfaces for $BrONO_2$ to react on.

4.6 Conclusions

From our modeling study, we found that elevated NO_x levels will have an influence on Arctic halogen chemistry. When comparing both simulated HOBr and BrO between the two NO_x scenarios, the high NO_x case completely suppresses both the HOBr and BrO to less than 3 pptv throughout the entire 10 day simulation period. On the other hand, on average the low NO_x case simulated both HOBr and BrO within ±5pptv of the mole ratios observed during OASIS. The high NO_x suppression is due to reaction 4.5 and

4.7, in which BrO_x is lost and not available to produce BrO or HOBr. The effects of the HOBr and BrO suppression could be seen when we compared the net ozone loss rate between the two NO_x scenarios. Without the production of HOBr and BrO the high NO_x case yields a lower net ozone loss rate compared to that of the low NO_x case. Arctic field based observations from both the OASIS 2009 and BROMEX 2012 field campaigns show the effect that NO_x has on the halogen cycle through the suppression of atmospheric BrO and Br_2 levels.

The findings of this work will become more important if anthropogenic emissions continue to increase in the Arctic from additional gas and oil exploration and shipping activity, as sea ice cover and thickness continue to decrease. Both of these transitions could impact the oxidation capacity of the Arctic atmosphere, along with the chemical pathways that occur there. Currently, the dominant oxidizing species in the Arctic surface layer are halogens. However, OH could become a factor, via O_3 photolysis (4.26), which would impact the oxidation capacity of the boundary layer. Especially with the recent transition in sea ice coverage from MYI to FYI, as FYI is more prone to cracks, exposing open water to air, which has been shown to produce convective mixing, bringing O_3 from aloft down to the surface (Moore et al., 2014). Yet, it must be considered that the impacts of climate change on the Arctic atmosphere are not straightforward, as the chemistry involved is very complex. FYI may be thinner and yield more exposed open water but its surface is also much more saline compared to that of MYI. These saline surfaces, particularly surface snow, are needed to produce atmospheric molecular halogens, yet the chemistry requires that the surface is acidified (Pratt et al., 2013). Acid levels within the surface snowpack depend on the depth of the

pack and its susceptibility to atmospheric deposition of acidic aerosol, which is dependent on the timing and rate of the snowfall, along with presence of sea ice. Recent observations by Webster et al. revealed that over the past 5 years (2009-2013) the snowpack depth covering the sea ice of the Beaufort and Chukchi seas has been decreasing at a significant rate (Webster et al., 2014). Long range transport of acidic species, for instance SO_2 and HNO_3, are needed to acidify the snow surface (Worthy et al., 1994). As more open water occurs during the Arctic springtime, latent heat fluxes will increase, resulting in an enhanced OH production based on the humidity dependence for the photolysis of ozone (4.26-48).

$$O_3 + h\nu \rightarrow O(^1D) + O_2 \quad (4.26)$$

$$O(^1D) + H_2O \rightarrow 2OH \quad (4.27)$$

$$O(^1D) + M \rightarrow O(^3P) + M^* \quad (4.28)$$

Based on this information one can see the complexity of all the competing factors that influence the chemistry that occurs in the Arctic atmosphere. To properly evaluate the physical and chemical processes that will be occurring in a changing Arctic, simultaneous field based observations along with simulations must be conducted. Finally, a lack of understanding exists for the products that result from the reactions of NO_x and halogen radicals. As we expect these products' mole ratios to increase as the Arctic changes, efforts should be made to expand on our understanding of their deposition rates along with aqueous phase chemistry that would follow. This is necessary to gain a greater understanding of these chemical processes to improve models.

4.7 References

Abbatt, J. P. D., Thomas, J. L., Abrahamsson, K., Boxe, C., Granfors, A., Jones, A. E., King, M. D., Saiz-Lopez, A., Shepson, P. B., Sodeau, J., Toohey, D. W., Toubin, C., von Glasow, R., Wren, S. N., and Yang, X.: Halogen activation via interactions with environmental ice and snow in the polar lower troposphere and other regions, Atmospheric Chemistry and Physics, 12, 6237-6271, 10.5194/acp-12-6237-2012, 2012.

Aguzzi, A., and Rossi, M. J.: The kinetics of the heterogeneous reaction of BrONO2 with solid alkali halides at ambient temperature. A comparison with the interaction of ClONO2 on NaCl and KBr, Physical Chemistry Chemical Physics, 1, 4337-4346, 10.1039/a904611i, 1999.

Aguzzi, A., and Rossi, M. J.: Heterogeneous hydrolysis and reaction of BrONO2 and Br2O on pure ice and ice doped with HBr, Journal of Physical Chemistry A, 106, 5891-5901, 10.1021/jp014383e, 2002.

Barrie, L., Bottenheim, J., Schnell, R., Crutzen, P., and Rasmsssen, R.: Ozone Destruction and Photochemical-Reactions at Polar Sunrise in the Lower Arctic Atmosphere, Nature, 334, 138-141, 10.1038/334138a0, 1988.

Beine, H., Honrath, R., Domine, F., Simpson, W., and Fuentes, J.: NOx during background and ozone depletion periods at Alert: Fluxes above the snow surface, Journal of Geophysical Research-Atmospheres, 107, 10.1029/2002JD002082, 2002.

Breider, T. J., Mickley, L. J., Jacob, D. J., Wang, Q. Q., Fisher, J. A., Chang, R. Y. W., and Alexander, B.: Annual distributions and sources of Arctic aerosol components, aerosol optical depth, and aerosol absorption, Journal of Geophysical Research-Atmospheres, 119, 4107-4124, 2014.

Brooks, S. B., Crawford, T. L., and Oechel, W. C.: Measurement of carbon dioxide emissions plumes from Prudhoe Bay, Alaska oil fields, Journal of Atmospheric Chemistry, 27, 197-207, 10.1023/a:1005890318796, 1997.

Cao, L., Sihler, H., Platt, U., and Gutheil, E.: Numerical analysis of the chemical kinetic mechanisms of ozone depletion and halogen release in the polar troposphere, Atmospheric Chemistry and Physics, 14, 3771-3787, 10.5194/acp-14-3771-2014, 2014.

Corbett, J. J., Lack, D. A., Winebrake, J. J., Harder, S., Silberman, J. A., and Gold, M.: Arctic shipping emissions inventories and future scenarios, Atmospheric Chemistry and Physics, 10, 9689-9704, 10.5194/acp-10-9689-2010, 2010.

Dubowski, Y., Colussi, A. J., and Hoffmann, M. R.: Nitrogen dioxide release in the 302 nm band photolysis of spray-frozen aqueous nitrate solutions. Atmospheric implications, Journal of Physical Chemistry A, 105, 4928-4932, 10.1021/jp0042009, 2001.

Dubowski, Y., Colussi, A. J., Boxe, C., and Hoffmann, M. R.: Monotonic increase of nitrite yields in the photolysis of nitrate in ice and water between 238 and 294 K, Journal of Physical Chemistry A, 106, 6967-6971, 10.1021/jp0142942, 2002.

Evans, M. J., Jacob, D. J., Atlas, E., Cantrell, C. A., Eisele, F., Flocke, F., Fried, A., Mauldin, R. L., Ridley, B. A., Wert, B., Talbot, R., Blake, D., Heikes, B., Snow, J., Walega, J., Weinheimer, A. J., and Dibb, J.: Coupled evolution of BrOx-ClOx-HOx-NOx chemistry during bromine-catalyzed ozone depletion events in the arctic boundary layer, Journal of Geophysical Research-Atmospheres, 108, 12, 10.1029/2002jd002732, 2003.

Fan, S., and Jacob, D.: Surface Ozone Depletion in Arctic Spring Sustained by Bromine Reactions on Aerosols, Nature, 359, 522-524, 10.1038/359522a0, 1992.

Finlaysonpitts, B. J., Ezell, M. J., and Pitts, J. N.: Formation of chemically active chlorine compounds by reactions of atmospheric NaCl particles with gaseous N_2O_5 and $ClONO_2$, Nature, 337, 241-244, 10.1038/337241a0, 1989.

General, S., Pöhler, D., Sihler, H., Bobrowski, N., Frieß, U., Zielcke, J., Horbanski, M., Shepson, P. B., Stirm, B. H., Simpson, W. R., Weber, K., Fischer, C., and Platt, U.: The Heidelberg Airborne Imaging DOAS Instrument (HAIDI) – a novel Imaging DOAS device for 2-D and 3-D imaging of trace gases and aerosols, Atmos. Meas. Tech. Discuss., 7, 2187-2257, 10.5194/amtd-7-2187-2014, 2014.

Grannas, A., Shepson, P., Guimbaud, C., Sumner, A., Albert, M., Simpson, W., Domine, F., Boudries, H., Bottenheim, J., Beine, H., Honrath, R., and Zhou, X.: A study of photochemical and physical processes affecting carbonyl compounds in the Arctic atmospheric boundary layer, Atmospheric Environment, 36, 2733-2742, 10.1016/S1352-2310(02)00134-6, 2002.

Grannas, A. M., Jones, A. E., Dibb, J., Ammann, M., Anastasio, C., Beine, H. J., Bergin, M., Bottenheim, J., Boxe, C. S., Carver, G., Chen, G., Crawford, J. H., Domine, F., Frey, M. M., Guzman, M. I., Heard, D. E., Helmig, D., Hoffmann, M. R., Honrath, R. E., Huey, L. G., Hutterli, M., Jacobi, H. W., Klan, P., Lefer, B., McConnell, J., Plane, J., Sander, R., Savarino, J., Shepson, P. B., Simpson, W. R., Sodeau, J. R., von Glasow, R., Weller, R., Wolff, E. W., and Zhu, T.: An overview of snow photochemistry: evidence, mechanisms and impacts, Atmospheric Chemistry and Physics, 7, 4329-4373, 2007.

Halfacre, J. W., Knepp, T. N., Shepson, P. B., Thompson, C. R., Pratt, K. A., Li, B., Peterson, P. K., Walsh, S. J., Simpson, W. R., Matrai, P. A., Bottenheim, J. W., Netcheva, S., Perovich, D. K., and Richter, A.: Temporal and spatial characteristics of ozone depletion events from measurements in the Arctic, Atmospheric Chemistry and Physics, 14, 4875-4894, 10.5194/acp-14-4875-2014, 2014.

Hanson, D., Ravishankara, A., and Lovejoy, E.: Reaction of BrONO2 with H2O on submicron sulfuric acid aerosol and the implications for the lower stratosphere, Journal of Geophysical Research-Atmospheres, 101, 9063-9069, 10.1029/96JD00347, 1996.

Hanson, D.: Reactivity of BrONO2 and HOBr on sulfuric acid solutions at low temperatures, Journal of Geophysical Research-Atmospheres, 108, 10.1029/2002JD002519, 2003.

Honrath, R. E., Peterson, M. C., Guo, S., Dibb, J. E., Shepson, P. B., and Campbell, B.: Evidence of NOx production within or upon ice particles in the Greenland snowpack, Geophysical Research Letters, 26, 695-698, 10.1029/1999gl900077, 1999.

Honrath, R. E., Guo, S., Peterson, M. C., Dziobak, M. P., Dibb, J. E., and Arsenault, M. A.: Photochemical production of gas phase NOx from ice crystal NO3, Journal of Geophysical Research-Atmospheres, 105, 24183-24190, 10.1029/2000jd900361, 2000.

Honrath, R. E., Lu, Y., Peterson, M. C., Dibb, J. E., Arsenault, M. A., Cullen, N. J., and Steffen, K.: Vertical fluxes of NOx, HONO, and HNO3 above the snowpack at Summit, Greenland, Atmospheric Environment, 36, 2629-2640, 10.1016/s1352-2310(02)00132-2, 2002.

Jaffe, D. A., Honrath, R. E., Furness, D., Conway, T. J., Dlugokencky, E., and Steele, L. P.: A determination of the CH_4, NO_x, and CO_2 emissions from the Prudhoe Bay, Alaska oil development, Journal of Atmospheric Chemistry, 20, 213-227, 10.1007/bf00694494, 1995.

Lopez-Hilfiker, F. D., Constantin, K., Kercher, J. P., and Thornton, J. A.: Temperature dependent halogen activation by N2O5 reactions on halide-doped ice surfaces, Atmospheric Chemistry and Physics, 12, 5237-5247, 10.5194/acp-12-5237-2012, 2012.

Madronich, S.: The Tropospheric visible Ultra-violet (TUV) model web page, National Center for Atmospheric Research, Boulder, CO, http://www. acd. ucar.edu/TUV 2002.

Maslanik, J., Stroeve, J., Fowler, C., and Emery, W.: Distribution and trends in Arctic sea ice age through spring 2011, Geophysical Research Letters, 38, 10.1029/2011gl047735, 2011.

Maslanik, J. A., Fowler, C., Stroeve, J., Drobot, S., Zwally, J., Yi, D., and Emery, W.: A younger, thinner Arctic ice cover: Increased potential for rapid, extensive sea-ice loss, Geophysical Research Letters, 34, 5, 10.1029/2007gl032043, 2007.

Moore, C. W., Obrist, D., Steffen, A., Staebler, R. M., Douglas, T. A., Richter, A., and Nghiem, S. V.: Convective forcing of mercury and ozone in the Arctic boundary layer induced by leads in sea ice, Nature, 506, 81-84, 10.1038/nature12924, 2014.

Morin, S., Savarino, J., Bekki, S., Gong, S., and Bottenheim, J.: Signature of Arctic surface ozone depletion events in the isotope anomaly (Delta O-17) of atmospheric nitrate, Atmospheric Chemistry and Physics, 7, 1451-1469, 2007.

Morin, S., Erbland, J., Savarino, J., Domine, F., Bock, J., Friess, U., Jacobi, H. W., Sihler, H., and Martins, J. M. F.: An isotopic view on the connection between photolytic emissions of NOx from the Arctic snowpack and its oxidation by reactive halogens, Journal of Geophysical Research-Atmospheres, 117, 15, 10.1029/2011jd016618, 2012.

Muthuramu, K., Shepson, P. B., Bottenheim, J. W., Jobson, B. T., Niki, H., and Anlauf, K. G.: Relationships Between Organic Nitrates and Surface Ozone Destruction During Polar Sunrise Experiment 1992, Journal of Geophysical Research-Atmospheres, 99, 25369-25378, 10.1029/94jd01309, 1994.

Orlando, J. J., and Burkholder, J. B.: Identification of BrONO as the major product in the gas-phase reaction of Br with NO2, Journal of Physical Chemistry A, 104, 2048-2053, 10.1021/jp993713g, 2000.

Peters, G. P., Nilssen, T. B., Lindholt, L., Eide, M. S., Glomsrod, S., Eide, L. I., and Fuglestvedt, J. S.: Future emissions from shipping and petroleum activities in the Arctic, Atmospheric Chemistry and Physics, 11, 5305-5320, 10.5194/acp-11-5305-2011, 2011.

Ridley, B., Walega, J., Montzka, D., Grahek, F., Atlas, E., Flocke, F., Stroud, V., Deary, J., Gallant, A., Boudries, H., Bottenheim, J., Anlauf, K., Worthy, D., Sumner, A., Splawn, B., and Shepson, P.: Is the Arctic surface layer a source and sink of NOx in winter/spring?, Journal of Atmospheric Chemistry, 36, 1-22, 10.1023/A:1006301029874, 2000.

Ridley, B. A., Walega, J. G., Dye, J. E., and Grahek, F. E.: DISTRIBUTIONS OF NO, NOX, NOY, AND O-3 TO 12-KM ALTITUDE DURING THE SUMMER MONSOON SEASON OVER NEW-MEXICO, Journal of Geophysical Research-Atmospheres, 99, 25519-25534, 10.1029/94jd02210, 1994.

Ridley, B. A., and Orlando, J. J.: Active nitrogen in surface ozone depletion events at alert during spring 1998, Journal of Atmospheric Chemistry, 44, 1-22, 10.1023/a:1022188822920, 2003.

Riedel, T. P., Bertram, T. H., Crisp, T. A., Williams, E. J., Lerner, B. M., Vlasenko, A., Li, S. M., Gilman, J., de Gouw, J., Bon, D. M., Wagner, N. L., Brown, S. S., and Thornton, J. A.: Nitryl Chloride and Molecular Chlorine in the Coastal Marine Boundary Layer, Environmental Science & Technology, 46, 10463-10470, 10.1021/es204632r, 2012.

Roberts, J. M., Osthoff, H. D., Brown, S. S., and Ravishankara, A. R.: N2O5 oxidizes chloride to Cl-2 in acidic atmospheric aerosol, Science, 321, 1059-1059, 10.1126/science.1158777, 2008.

Roberts, J. M., Osthoff, H. D., Brown, S. S., Ravishankara, A. R., Coffman, D., Quinn, P., and Bates, T.: Laboratory studies of products of N2O5 uptake on Cl- containing substrates, Geophysical Research Letters, 36, 5, 10.1029/2009gl040448, 2009.

Shepson, P. B., Sirju, A. P., Hopper, J. F., Barrie, L. A., Young, V., Niki, H., and Dryfhout, H.: Sources and sinks of carbonyl compounds in the arctic ocean boundary layer: Polar ice floe experiment, Journal of Geophysical Research-Atmospheres, 101, 21081-21089, 10.1029/96jd02032, 1996.

Simpson, W., von Glasow, R., Riedel, K., Anderson, P., Ariya, P., Bottenheim, J., Burrows, J., Carpenter, L., Friess, U., Goodsite, M., Heard, D., Hutterli, M., Jacobi, H., Kaleschke, L., Neff, B., Plane, J., Platt, U., Richter, A., Roscoe, H., Sander, R., Shepson, P., Sodeau, J., Steffen, A., Wagner, T., and Wolff, E.: Halogens and their role in polar boundary-layer ozone depletion, Atmospheric Chemistry and Physics, 7, 4375-4418, 2007.

Stephens, C., Shepson, P., Steffen, A., Bottenheim, J., Liao, J., Huey, L., Apel, E., Weinheimer, A., Hall, S., Cantrell, C., Sive, B., Knapp, D., Montzka, D., and Hornbrook, R.: The relative importance of chlorine and bromine radicals in the oxidation of atmospheric mercury at Barrow, Alaska, Journal of Geophysical Research-Atmospheres, 117, 10.1029/2011JD016649, 2012.

Thomas, J., Dibb, J., Huey, L., Liao, J., Tanner, D., Lefer, B., von Glasow, R., and Stutz, J.: Modeling chemistry in and above snow at Summit, Greenland - Part 2: Impact of snowpack chemistry on the oxidation capacity of the boundary layer, Atmospheric Chemistry and Physics, 12, 6537-6554, 10.5194/acp-12-6537-2012, 2012.

Thompson, C., Shepson, P., Liao, J., Huey, G., Apel, E., Cantrell, C., Flocke, F., Fried, A., Hall, S., Hornbrook, R., Knapp, D. J., Mauldin III, R., Montzka, D., Sive, B., Ullman, K., Weibring, P., and Weinheimer, A.: Interactions of bromine, chlorine, and iodine photochemistry during ozone depletions in Barrow, Alaska, Atmospheric Chemistry and Physics, *Submitted*, 2014.

Thorn, R. P., Daykin, E. P., and Wine, P. H.: Kinetics of the BrO+NO2 association reaction. Temperature and pressure dependence in the falloff regime, International Journal of Chemical Kinetics, 25, 521-537, 10.1002/kin.550250703, 1993.

Toyota, K., McConnell, J. C., Staebler, R. M., and Dastoor, A. P.: Air-snowpack exchange of bromine, ozone and mercury in the springtime Arctic simulated by the 1-D model PHANTAS - Part 1: In-snow bromine activation and its impact on ozone, Atmospheric Chemistry and Physics, 14, 4101-4133, 10.5194/acp-14-4101-2014, 2014.

Villena, G., Wiesen, P., Cantrell, C., Flocke, F., Fried, A., Hall, S., Hornbrook, R., Knapp, D., Kosciuch, E., Mauldin, R., McGrath, J., Montzka, D., Richter, D., Ullmann, K., Walega, J., Weibring, P., Weinheimer, A., Staebler, R., Liao, J., Huey, L., and Kleffmann, J.: Nitrous acid (HONO) during polar spring in Barrow, Alaska: A net source of OH radicals?, Journal of Geophysical Research-Atmospheres, 116, 10.1029/2011JD016643, 2011.

von Glasow, R., Sander, R., Bott, A., and Crutzen, P.: Modeling halogen chemistry in the marine boundary layer - 2. Interactions with sulfur and the cloud-covered MBL, Journal of Geophysical Research-Atmospheres, 107, 10.1029/2001JD000943, 2002.

Webster, M. A., Rigor, I. G., Nghiem, S. V., Kurtz, N. T., Farrell, S. L., Perovich, D. K., and Sturm, M.: Interdecadal changes in snow depth on Arctic sea ice, Journal of Geophysical Research-Oceans, 119, 5395-5406, 10.1002/2014jc009985, 2014.

CHAPTER 5 DIRECT ClO OBSERVATION IN BARROW, ALASKA

5.1 Introduction

The observation of episodic depletions of surface ozone from background levels of 40 ppb to less than 5 ppb has been well studied in the Arctic during the polar sunrise in spring (Bottenheim et al., 1990;Oltmans et al., 2012). Bromine chemistry has been connected with ozone depletion events (ODEs) based on the increase in filterable bromine along with the observation of BrO during ODEs (Barrie et al., 1988;Liao et al., 2012;Simpson et al., 2007;Honninger and Platt, 2002). Based on field observations molecular bromine can be produced within the snowpack where it can transport into the boundary layer (Pratt et al., 2013). As Br_2 mixes in the surface layer it will photodissociate into Br radicals and react with ozone forming BrO which initiates an auto catalytic bromine release that can deplete ozone, as shown in Reactions 5.1-5.5 (Fan and Jacob, 1992;Michalowski et al., 2000), where reaction 5.5 is a condensed phase process.

$$Br_2 + h\nu \rightarrow 2\,Br \quad (5.1)$$

$$Br + O_3 \rightarrow BrO + O_2 \quad (5.2)$$

$$BrO + BrO \rightarrow 2\,Br + O_2 \quad (5.3)$$

$$BrO + HO_2 \rightarrow HOBr + O_2 \quad (5.4)$$

$$HOBr + Br^- + H^+ \rightarrow Br_2 + H_2O \quad (5.5)$$

However, this is not the only mechanism for destroying ozone, and regenerating bromine radicals. As shown in reactions 5.6-5.8, the cross reaction of ClO with BrO can regenerate the bromine radical.

$$Cl_2 + h\nu \rightarrow 2\,Cl\cdot \quad (5.6)$$

$$Cl + O_3 \rightarrow ClO \quad (5.7)$$

$$ClO + BrO \rightarrow Br + Cl + O_2 \quad (5.8)$$

The significance of chlorine chemistry in the Arctic was first recognized by the rapid drop in concentration of certain non-methane hydrocarbons (NMHC) during low ozone events, which could not be explained via OH oxidation alone (Jobson et al., 1994). The observation prompted additional field studies to employ this hydrocarbon decay technique to evaluate chlorine chemistry (Ariya et al., 1998;Boudries and Bottenheim, 2000). High levels of molecular chlorine, up to 400 ppt, have been observed in the Arctic during the springtime, leading to the hypothesis that reaction 5.8 could be important toward bromine radical formation (Liao et al., 2014). Unfortunately, Arctic observations of ClO are very limited. Only one direct observation of ClO in the Arctic has previously been published, reporting ClO concentrations up to 30 ppt at Ny-Ålesund, Spitsbergen, using Differential Optical Absorption Spectroscopy (Tuckermann et al., 1997). However, this technique suffers from interferences at the ClO absorption wavelengths yielding high uncertainty and high limits of detection.

Here, for the first time, we report direct observations of ClO using a chemical ionization mass spectrometer (CIMS), while at the same time quantifying Cl_2 as well. The observations of Cl_2 enabled us to develop a 0-D model to further analyze our observations and examine our understanding of the chlorine cycle, e.g. the extent to

which the Cl radical chemistry is consistent with Cl_2 being the dominant source of those radicals.

5.2 Ambient Sampling Experimental

A chemical ionization mass spectrometer (CIMS) was deployed in Barrow, Alaska during the spring (March/April) of 2012 to measure ambient concentrations of Br_2, Cl_2, BrO, and ClO. This was a part of the previously described BROMEX field campaign (Section 2.6). The CIMS instrument was described earlier in Section 3.2.1., so only the sampling component will be described, as that is the only parameter that differs. The ambient sampling inlet deployed has previously been used to quantify ambient Br_2, BrO, and HOBr by *Liao et al*. [2012] and will briefly be described. Ambient air was sampled through a stainless steel ring torus attached to a 4.6 cm ID stainless steel tube extending 9 cm out of the sampling trailer wall. The stainless steel inlet was attached to the CIMS three way valve to allow for sampling of ambient air by the CIMS, while minimizing wall loss. Using an external blower, a flow of 900 slpm was pulled through the sampling inlet, and 2 slpm from this flow was sampled by the CIMS. The remaining flow was directed away as exhaust. Background and calibration measurements for Br_2 and Cl_2 were conducted using the same procedure described in Section 3.2.1.1. During the field campaign the limit of detections for Br_2, Cl_2, and ClO were 0.2 ppt, 0.5 ppt, and 0.3 ppt, respectively. The associated uncertainty for Br_2, Cl_2, and ClO were 21%, 25%, and 55%, respectively. Uncertainties for Cl_2 and Br_2 were calculated using the same procedure as used in Section 3.2.1.1, while the ClO uncertainty was calculated using Equation 5.I.

$$[\mathrm{ClO}]\ \text{relative uncertainty} = \sqrt{\left(\frac{\mathrm{ClO\ signal}\ \sigma}{\mathrm{ClO\ amb-bck\ grd\ signal}}\right)^2 + \left(\frac{\mathrm{ClO\ relative\ sensitivity}\ \sigma}{\mathrm{ClO\ relative\ sensitivity}}\right)^2 + \left(\frac{I(H_2O)_n\ \sigma}{I(H_2O)_n}\right)^2} \quad (5.I)$$

However, the instrument sensitivity factor (i.e. calibration factor) for ClO did not exist at the time of the measurements. Following the BROMEX field campaign this was determined through a series of laboratory experiments and will be described here.

5.3 ClO Calibration

5.3.1 Experimental Set-up

To properly quantify the ambient ClO concentrations from the signal measured during the BROMEX 2012 field campaign a relative sensitivity calibration factor needed to be determined. This factor is based on the CIMS sensitivity to the analytes relative to that for Cl_2, for which we had an absolute calibration method. Relative sensitivities were previously used to quantify BrO and HOBr signals measured during the OASIS 2009 field campaign, as described by *Liao* et al. [2012]. In the lab, Liao determined the sensitivity of the CIMS toward BrO and HOBr, through the production of gas-phase standards. The Br_2 sensitivity was also determined during these experiments, to yield a relative sensitivity of .47 ±25% and .50 ±25% for BrO and HOBr relative to Br_2, respectively. Relative sensitivities were necessary because calibration gas-phase standards for various halogen species (i.e. BrO, ClO, and HOBr) are not commercially valuable and difficult to synthesize. With relative sensitivity values, and our careful

monitoring of the CIMS sensitivity for Br_2 (or Cl_2) throughout the field campaign (using permeation devices), we can accurately quantify these other species using the determined instrument sensitivity, relative to that for Br_2.

As shown in reactions 5.6 and 5.7, ClO is produced when Cl_2 is photolyzed in the presence of O_3. To determine the CIMS sensitivity for ClO, we generated steady state ClO gas-phase standards within a continuous flowing halogen atom generator (flowtube), when all the sources and sinks of ClO are quantitatively. The approach we used is shown in reactions 5.9-5.11, below.

$$Cl_2 + h\nu \rightarrow 2\,Cl\cdot \qquad (5.9)$$

$$Cl\cdot + O_3 \rightarrow ClO\cdot + O_2 \qquad (5.10)$$

$$ClO\cdot + NO_2 \rightarrow ClONO_2 \qquad (5.11)$$

We calculate the steady state [ClO] by assuming that all Cl atoms react with O_3 (and not a volatile organic compound (VOC)). Cl atoms have a high reactivity toward VOCs and represent the main interfering sink for Cl atoms in our experiment. Cl atoms will only react with O_3 if the O_3 is kinetically in excess compared to any of the VOCs that may be present in our air flow. This was calculated using Equation 5.II, where the reaction rate constant for Cl + O_3 is $1.02\text{x}10^{-11}$ $cm^3\cdot molecules^{-1}\cdot s^{-1}$ and for Cl + VOC is $1\text{x}10^{-10}$ $cm^3\cdot molecules^{-1}\cdot s^{-1}$ (Atkinson et al., 2004). The Cl + VOC reaction rate coefficient is based on the assumption that the majority of the VOCs present our compressed tanks of N_2 and O_2 will be smaller chained (C_2-C_4) alkanes and alkenes, as they are the major non-methane hydrocarbon in ambient air. According to the specification sheets for the N_2 and O_2 used during our experiments the VOC concentration should be less than 0.1ppm.

$$\frac{k[\mathrm{Cl}][\mathrm{O_3}]}{k[\mathrm{Cl}][\mathrm{VOC}]} = 100 \qquad (5.\mathrm{II})$$

Using equation 5.II we determined a concentration of 98 ppm of O_3 was needed to ensure that over 99% of the Cl atoms reacted with O_3 during the experiment. This was determined experimentally to be correct (data not shown). Then if we equate the ClO production rate with the ClO loss rate, for conditions in which the only ClO loss process is the reaction with NO_2 (reaction 5.11), we get equation 5.III.

$$[\mathrm{ClO}]_{\mathrm{SS}} = \frac{2\mathrm{J}[\mathrm{Cl_2}]_{\mathrm{ss}}}{k[\mathrm{NO_2}]} \qquad (5.\mathrm{III})$$

In Equation 5.III, J represents the photolysis rate for Cl_2 within the flowtube, $[Cl_2]_{ss}$ is the steady state Cl_2 mole ratio, $[NO_2]$ is the NO_2 mole ratio, and the reaction rate constant for ClO with NO_2 used was $2.4\text{x}10^{-12}$ $cm^3 \cdot molecules^{-1} \cdot s^{-1}$(Atkinson et al., 2004). The photolysis rate was determined during previous ClO calibration experiments to be 0.0078 (±.002) s^{-1}. In Figure 5.1 $[Cl_2]_0$ represents the initial concentration of Cl_2 and $[Cl_2]_t$ corresponds to the Cl_2 concentration after the lights were turned on, which initiated the photodissociation of Cl_2. The schematic diagram of the experiment set-up is shown in Figure 5.2

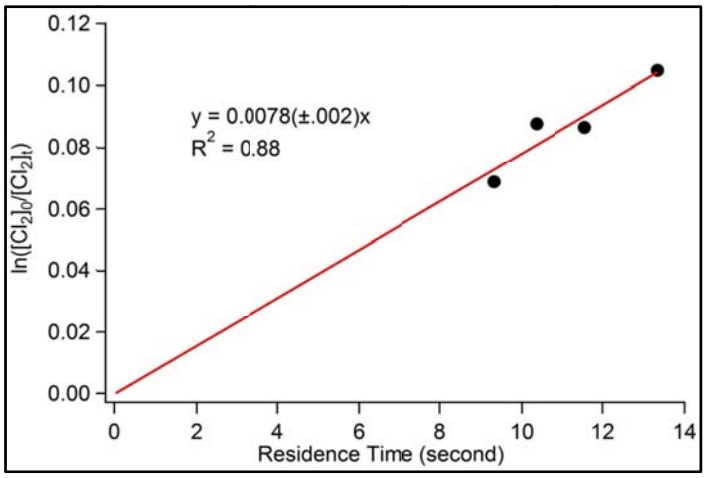

Figure 5.1 Experimental measurements from the Cl_2 photolysis experiments. The uncertainty represents 1σ of the slope of the data points.

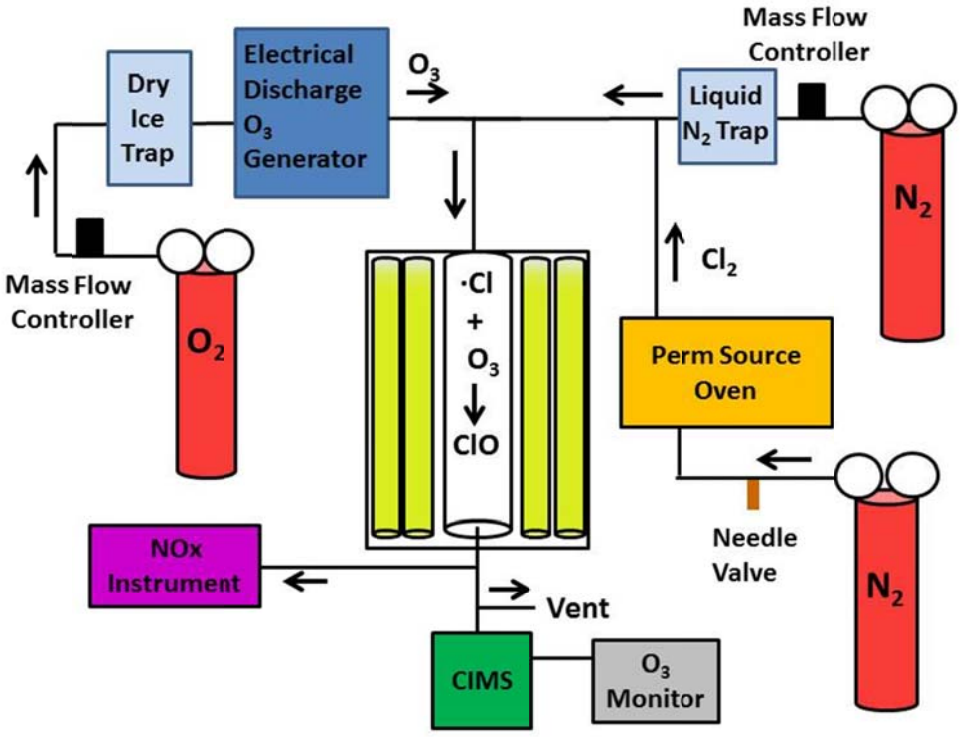

Figure 5.2 Schematic diagram for steady state gas-phase ClO calibration experiment.

The quartz flowtube used in this study was 122 cm long with an internal diameter of 6 cm that had tapered ends to fit ¼″ Swagelok fittings, shown in Figure 5.3. The flowtube was housed in a wooden photolysis box which contained 6 UV bulbs (UVA 340, Q-labs). The UV lights were controlled using a switch on the outside of the box to allow us to control Cl_2 photolysis during an experiment. High purity N_2 (UHP 5.0, Praxair) was used as the carrier gas and passed through the flowtube and into the CIMS. The N_2 was passed through a liquid N_2 trap, used to further purify the gas by condensing out possible impurities, mainly VOCs and NO_x. The liquid N_2 trap consisted of a coil of stainless steel tubing submerged in liquid N_2. The tubing on the outlet end of the trap was heated using heat wrap to increase the N_2 temperature back to room temperature (22°C). The flow rate of the N_2 carrier gas, within the flowtube, was controlled by a mass flow controller (20 LPM, MKS). Controlling the N_2 flow rate allowed us to alter the amount of Cl atoms produced within the flowtube.

Figure 5.3 Flowing halogen atom generator inside photolysis box

O_3 was generated by passing O_2 (UHP 5.0, Praxair) through a dry ice trap and then into a corona discharge ozone generator. The dry ice trap was set-up the same way as the liquid N_2 trap expect dry ice was used to cool the stainless steel tubing. The dry ice was used to cool the stainless steel coil instead of liquid N_2, as the latter is too cold and will condense out O_2. The corona discharge ozone generator works by electrically splitting the molecular O_2 into two singlet ground state (^3P) oxygen atoms (5.12). The singlet oxygen atom then reacts with an O_2 to yield O_3 (5.13).

$$O_2 + e^- \rightarrow 2O(^3P) \quad (5.12)$$

$$O(^3P) + O_2 + M \rightarrow O_3 \quad (5.13)$$

During experiments the O_3 mole ratio was measured using a dual-beam O_3 monitor (Model 205, 2B Technologies). The O_3 was quantified by measuring the light intensity

from a 254 nm mercury lamp after it passes through two different absorption cells. Both cells have the sampled air flowing through them but one of the absorption cell's air flow has been passed through an ozone scrubber. Within the ozone monitor instrument activated charcoal is used to remove O_3 from the air flow. The light intensity from the scrubbed air (I_0) acts as background for the sample, where the light intensity from the non-scrubbed air represents the sample (I). Within the instrument the O_3 mole ratio is calculated using Equation 5.IV, where C_{O3} is the concentration of O_3, L is the path length and σ is the absorption cross section of O_3, for λ=254nm.

$$C_{O3} = \frac{1}{L \cdot \sigma} \ln\left(\frac{I_O}{I}\right) \qquad (5.IV)$$

The reaction of ClO with NO_2 represents the main sink for gas-phase ClO and needs to be taken into consideration when calculating the ClO mole ratio. The NO_2 mole ratio was measured using a NO-NO_2-NO_x Analyzer (Thermo Environmental Instruments, Inc). The NO-NO_2-NO_x Analyzer can only quantify NO via reaction 5.14-5.15.

$$NO + O_3 \rightarrow NO_2^* + O_2 \qquad (5.14)$$

$$NO_2^* \rightarrow NO_2 + h\nu \qquad (5.15)$$

From reaction 5.14, an electronically excited NO_2 is produced and as it drops to the ground state (5.15) it releases the excess energy in the form of a photon. The photon is then detected and the light intensity is directly proportional to the NO mole ratio. To quantify the NO_x mole ratio the air sample is passed over a heated (315°C) molybdenum converter that reduces any NO_x to NO (5.16).

$$3NO_x + Mo \rightarrow 3NO + MoO_3 \qquad (5.16)$$

The NO mole ratio is then subtracted from the NO_x mole ratio to calculate the NO_2 mole ratio. However, it should be noted that other oxidized forms of NO_2 will be reduced on the molybdenum converter, including HNO_3, $ClONO_2$, $ClNO_2$, etc. This could lead to artificially high calculated NO_2 concentrations. To correct for this we used the NO_2 concentration recorded during the dark periods of the experiment.

5.3.2 Calibration Procedure

During the ClO calibration experiment the flowtube was connected to the inlet of the CIMS via a PFA Teflon tee. The carrier gas was then turned on and passed through the flowtube for the entire experiment. The O_3 generator outlet was then connected to the inlet of the flowtube and the O_2 flow rate was adjusted until the desired O_3 mole ratio was achieved. The NO_x instrument was then connected to the outlet of the flowtube so that the NO_2 mole ratio could be measured. For the experiment four different samples were taken. First, the carrier gas and O_3 was passed through the flowtube, in the dark, to act as a background measurement for the Cl_2 calibration measurement. After a stable signal was collected for at least 5 minutes, the Cl_2 perm source oven outlet was connected to the CIMS inlet, so that the CIMS could be calibrated for Cl_2 to allow for the CIMS Cl_2 sensitivity to be calculated during each ClO calibration point. Once the calibration measurement was completed the permeation source outlet was disconnected from the CIMS inlet and attached to the inlet end of the flowtube. During this time the lights were off so that no photolysis could occur. This represented the blank signal for ClO and also the measurement for the initial Cl_2 mole ratio, used in Equation 5.III. The measurement was made for approximately 10 minutes before the lights were turned on and reaction

5.6-5.7 was initiated. Upon turning on the lights the ClO signal (mass 178 amu) increased, then leveled off, and simultaneously the Cl_2 signal (mass 197 amu) decreased then leveled off. Data with the lights on were collected for several minutes, after which the process was started again, except the carrier gas flow rate was increased. Increasing the carrier gas flow rate decreased the steady state ClO mole ratio, allowing us to calibrate over a range of ClO mole ratios. The results from our experiment are shown in Table 5.1.

Table 5.1 Experimental relative sensitivity values for ClO to Cl_2 for a CIMS using CH_3I as the reagent ion.

Calibration Point #	ClO:Cl_2 Relative Sensitivity
1	0.31
2	0.25
3	0.23
4	0.31
5	0.12
6	0.18
7	0.09

Based on our experiments we were able to calculate a ClO:Cl_2 relative sensitivity of 0.21 ±.10, where the uncertainty represents 1 standard deviation of the average value. The average relative sensitivity was applied to our ClO data from the 2012 BROMEX field campaign to quantify the measured ClO signal.

5.4 BROMEX ClO Measurements Results and Discussion

From the BROMEX field campaign (discussed Sec 2.6) ClO measurements using the CIMS were conducted from March 3-29. However, the most significant ClO measurements took place from March 21-29, where air masses originated from the Beaufort and Chukchi and were not influenced by local emissions. A time series graph for O_3, Cl_2, ClO, and radiation from March 21-29 is shown in Figure 5.4.

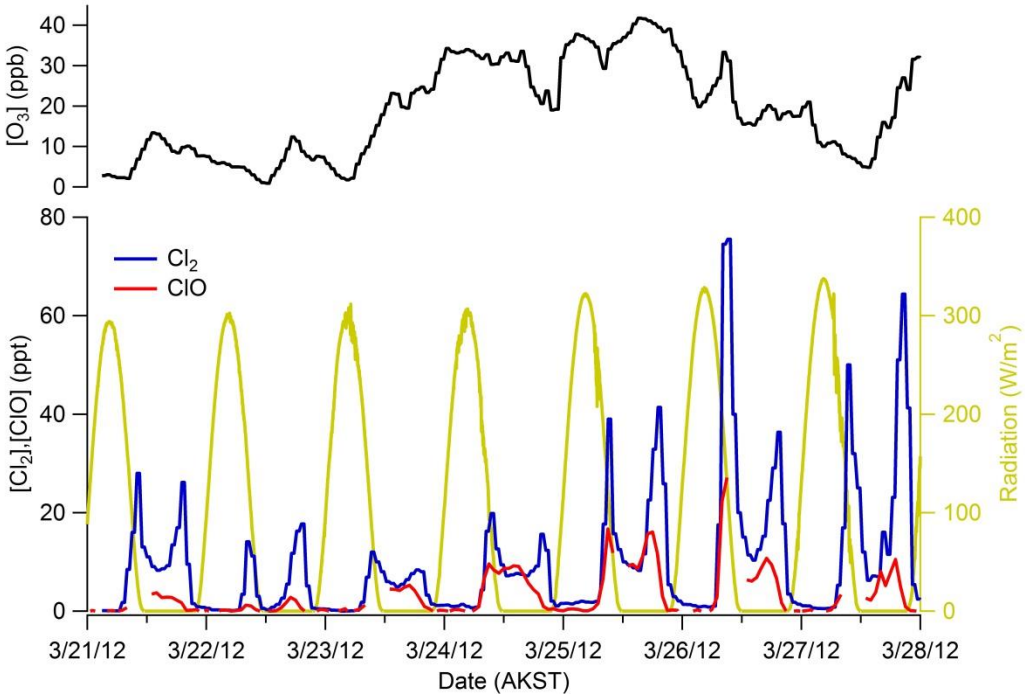

Figure 5.4 Ambient ClO and Cl_2 data collected using a CIMS during the 2012 BROMEX field campaign along with O_3 from that time. Error bars on the ClO data represents 55% calculated uncertainty.

During BROMEX, ClO ranged from 5-32 ppt, with mole ratios increasing in the morning and then dropping once the sun sets, as shown in Figure 5.5. This is expected as ClO is produced from a photochemically generated chlorine atom reacting with O_3.

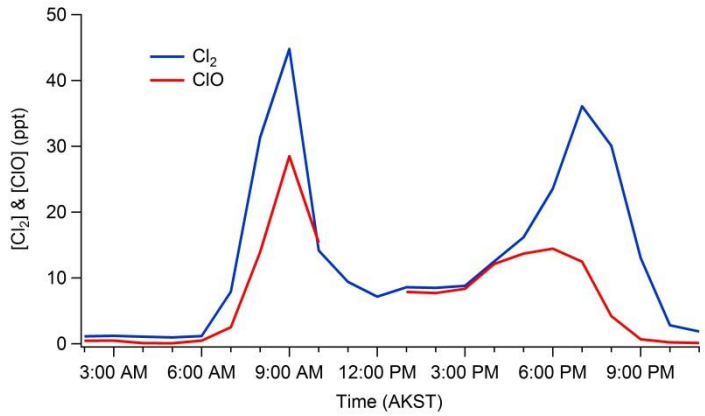

Figure 5.5 Cl_2 and ClO diurnal average for the data from March 24-27, 2012.

The early morning peak in Cl_2 and ClO likely results from a burst of production at sunrise after the overnight accumulation of precursors (HOCl, HNO_3, H_2O_2) onto the snowpack surface. This is followed by an increase in vertical mixing and downward transport of Cl_2-deficient air from aloft as the day continues, resulting in the decrease in concentration. As sun set approaches, the surface layer again becomes stable, and the remaining surface Cl_2 emissions from the snowpack accumulate in this shallow layer, resulting in an evening peak increase in concentration. The positive correlation between ClO and radiation, along with the isotopic graph (Figure 5.6), support that the detected masses at 178 and 181 amu were truly ClO.

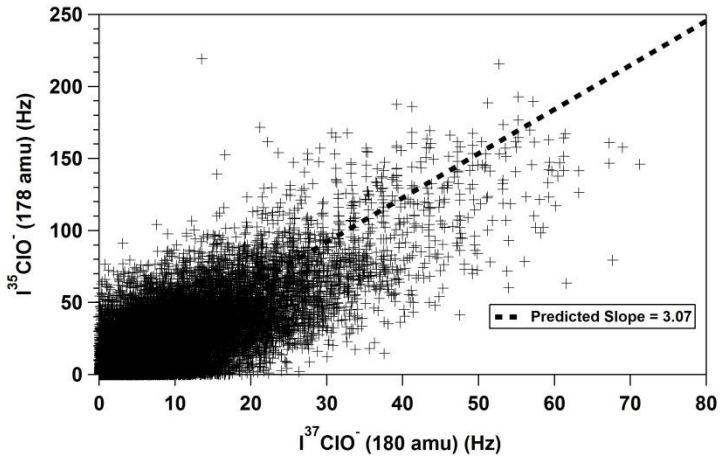

Figure 5.6 Isotopic plot of $I^{35}ClO^-$ (178 amu) vs $I^{37}ClO^-$ (180 amu) during the measurement time period of March 21-28, 2012.

It should be noted that the lack of mid-day ClO and Cl_2 observations that occurred during March 26, 27 and 28 are due to the CIMS being used for snow chamber experiments, therefore ambient data was not available during that time (Pratt et al., 2013). Our ClO observations fall in the range of the only previous Arctic ClO observations, by *Tuckermann et al.*, where ClO was detected at concentrations up to 30 ppt at Ny-Ålesund, Spitsbergen (Tuckermann et al., 1997).

Generally, the larger early morning spikes in Cl_2 correspond to large day time ClO mole ratios, such as on the 26 and 27. However, this is not the case on the 28th where Cl_2 is around 50 ppt but ClO only reaches ~12ppt. The significant differences between the 26th and 27th vs the 28th is that during the 26th and 27th the O_3 mole ratio is going through depletion, indicating active halogen chemistry. However, on the 28th the O_3 mole ratio was increasing from a depletion (<5ppb) back to background

concentrations (40 ppb), indicating a lack of halogen activity. As with previous observations for BrO and O_3, we do not observe an apparent correlation between ClO and O_3 mole ratio (Pohler et al., 2010;Liao et al., 2012). This observation can be explained by looking at the ClO steady state equation (Eqn 5.V).

$$[\mathrm{ClO}]_{SS} = \left(\frac{2\mathrm{J}[\mathrm{Cl_2}]}{\left(\begin{array}{c} 2k[\mathrm{ClO}] + k[\mathrm{NO_2}] + k[\mathrm{NO}] + \\ k[\mathrm{OH}] + k[\mathrm{HO_2}] + \mathrm{J} + k[\mathrm{CH_3OO}] + \\ k[\mathrm{CH_3COOO}] + k[\mathrm{BrO}] \end{array} \right)} \right) \mathrm{x} \frac{k[\mathrm{Cl}][\mathrm{O_3}]}{\sum k[\mathrm{Cl}][\mathrm{Cl\ sinks}]} \qquad (5.V)$$

Although the $[ClO]_{ss}$ depends on the Cl_2 concentration along with O_3, it is also influenced by the concentration of several species that act as ClO sinks. Sinks such as NO and NO_2 can have varying concentrations in the Arctic ambient air, depending on local emissions, which can impact the $[ClO]_{ss}$ (Section 4.2). The sinks shown in 5.V could be the reason why ambient ClO concentrations do not follow a simple pattern with ozone concentrations.

5.5 Model Description

A modified version of the 0-D model used in Sec 4.2 was used to investigate the ClO observations from March 21 to 29, 2012 that were obtained during this study. As this model has been described in detail previously (Section 4.2), only the differences will be described herein. For our simulations we constrained Br_2, Cl_2, O_3, and photolysis rates to the observations during that time. Br_2 and Cl_2 ambient measurements were acquired using the CIMS, and O_3 measurements were made using a dual-beam O_3 monitor (Model 205, 2B Technologies). Time varying photolysis rates were scaled to the local observed

radiation (NOAA/ESRL/GMD Solar Radiation group) based on previously calculated photolysis rates from the 2009 OASIS field campaign (Shetter and Muller, 1999). To check this method we compared our photolysis rate values to photolysis rate values calculated using a modified version of the Tropospheric Ultraviolet and Visible (TUV) radiation model (Madronich, 2002). Both values were within 5% of each other, confirming the accuracy of our method.

NO_2 and NO were constrained to "background" concentrations (Sec 4.2, Figure 4.3), as the wind direction indicated that the air masses being sampled were not influenced by the town of Barrow (not shown). Both CH_3COCH_3 and CH_3CHO were constrained within the model to observations from the OASIS 2009 field campaign (Sec 4.2, Figure 4.1) (Grannas et al., 2002). The constrained diurnal average of NO, NO_2, CH_3COCH_3, and CH_3CHO used in the model are shown in Figure 5.3a. The 7 day constrained mole ratios of Br_2 and Cl_2 used in the model are shown Figure 5.3b. The remaining VOCs were held to constant mole ratios based on previous average observations, shown in Table 5.2. This version of the model will be referred to as the "Base Model" herein.

Table 5.2 Constrained species and their respective constant concentrations used in the model for the BROMEX ClO simulations.

Species	Concentration (molecules·cm^3)
C_2H_2	7.98×10^9
C_2H_4	6.15×10^8
C_2H_6	4.53×10^{10}
C_3H_8	1.51×10^{10}
C_3H_6	3.37×10^8
n-CH_4H_{10}	3.78×10^9
i-CH_4H_{10}	2.52×10^9
HCHO	3.07×10^8
Methyl Ethyl Ketone (MEK)	6.30×10^9
HONO	5.11×10^9

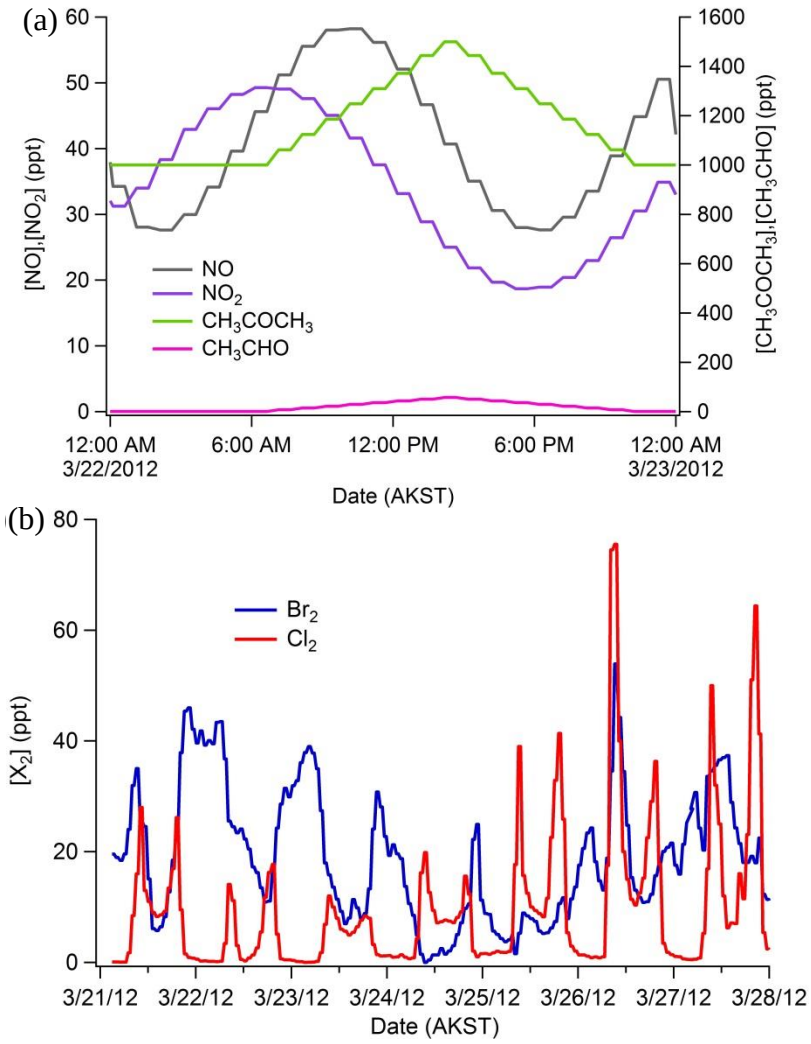

Figure 5.7 (a) Diurnal average of constrained NO, NO_2, CH_3COCH_3, and CH_3CHO. (b) Observed Br_2 and Cl_2 for the time period March 21-29, 2012 used in the model.

5.6 ClO Model Results and Discussion

A plot of the simulated ClO from the base model run along with the observed ClO is shown in Figure 5.8.

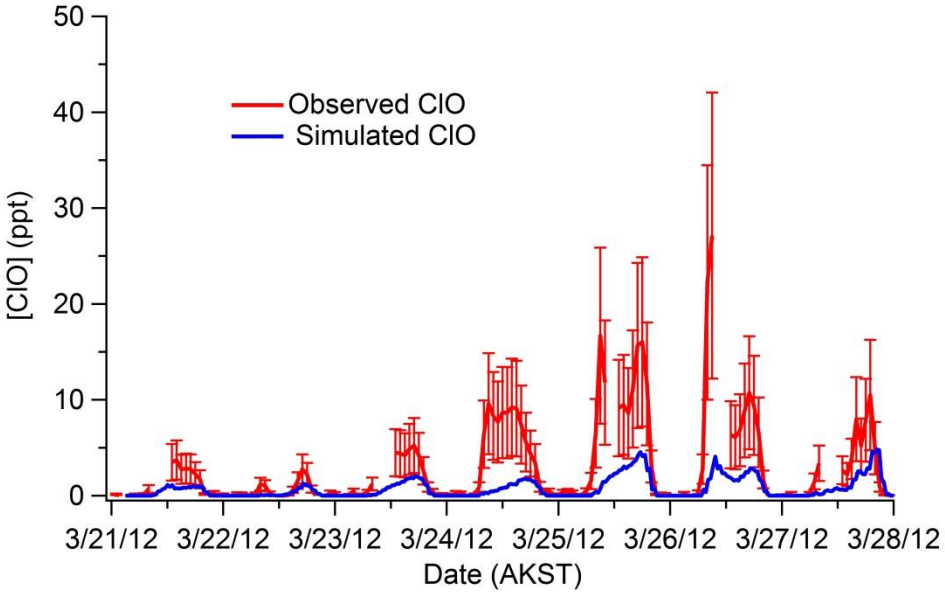

Figure 5.8 Simulated ClO and BROMEX observed ClO along with observed O_3.

The Base Model does a poor job accurately replicating ClO mole ratios, other than on March 22 when the observed ClO mole ratio is quite small (less than 5 ppt). When observed ClO concentrations were greater than 5 ppt the model under simulated ClO by 3 to 5.5 times the observed concentration.

Based on our comparison of the Base Model simulated ClO vs observed ClO we believe that the model under predicts ClO because within the model the major source of Cl radials is Cl_2. As discussed in Section 4.2, the tundra snowpack has the ability to photochemically produce BrCl, which can then be photolyzed to yield Cl radicals. In the model, the majority of BrCl was produced within the aqueous phase via reaction 5.17 but

its contribution towards chlorine radical's gas-phase concentration is insignificant, because the simulated BrCl concentration is very low.

$$HOBr + Cl^- + H^+ \rightarrow BrCl + H_2O \quad (5.17)$$

To address this we added a source of BrCl within the model to determine if the model was missing a potential chlorine radical source. Using previous BrCl and Cl_2 ambient data (unpublished), we determined a daytime [BrCl]/[Cl_2] ratio. Based on the observations the [BrCl]/[Cl_2] ratio ranged from 0.1 to 0.4. We fixed BrCl to the Cl_2 observations but scaled by .4[Cl_2]. However, the model still under simulated ClO during the 0.4[Cl_2] constrained simulation (not shown). Thus we conducted additional simulations with varying scales of the [BrCl]/[Cl_2] ratio, ranging from 1 to 10.

We found that when BrCl was constrained to 6[Cl_2], the simulated ClO was within the uncertainty of the observed ClO, shown in Figure 5.7.

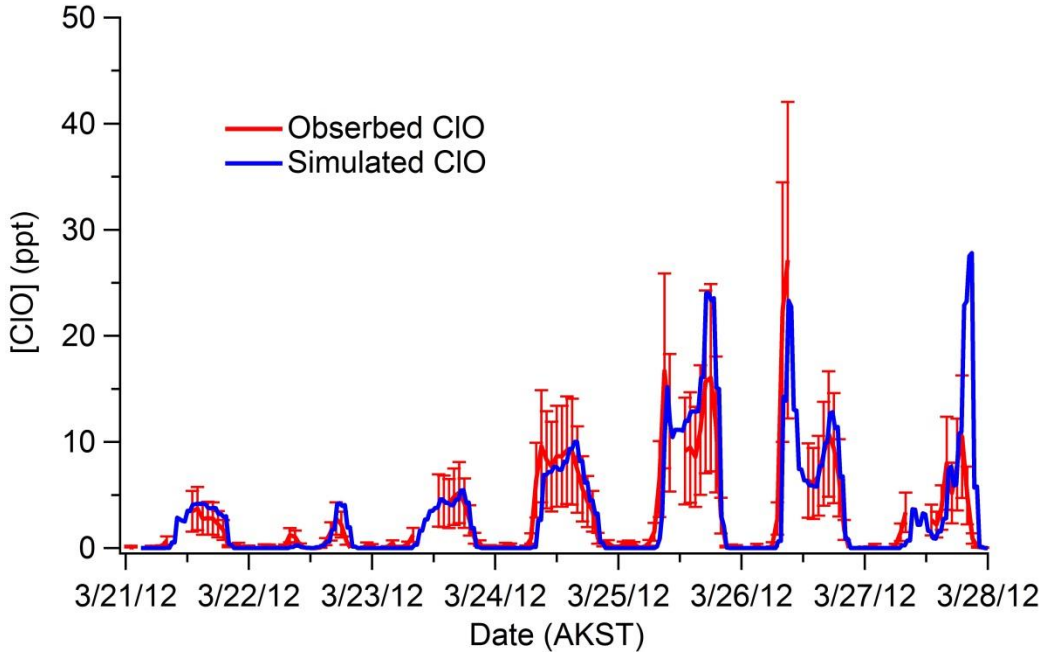

Figure 5.9 Simulated and observed ClO for the 6x BrCl constrained simulation.

Figure 5.9 shows that the simulated ClO, when [BrCl] equals 6[Cl_2], overlaps within the observed ClO uncertainty throughout the entire simulation period. Based on our modeling results a non Cl_2 and likely non-BrCl chlorine radical source is most likely missing within our observations, and thus our model. Even though the increase in the BrCl mole ratio was able to enhance the simulated ClO enough so that it better fit the observations, we don't believe that it alone is the missing factor. The daytime BrCl concentration when constrained to 6[Cl_2] ranged from 70 to 400 ppt, much larger than previous ambient observations (Foster et al., 2001;Spicer et al., 2002). Both *Foster et al.* and *Spicer et al*. recorded springtime ambient BrCl concentrations up to 35 ppt, which are 2-11 times lower than what was prescribed in our model. Although these measurements were obtained in Alert, Nunavat, Canada, they fall into the same range as unpublished ambient BrCl observations from Barrow, Alaska (Foster et al., 2001;Spicer et al., 2002).

BrCl could be a source for additional Cl radicals, although as described previously it is doubtful that it exists in the Arctic ambient air at the prescribed mole ratios. However, with the addition of several chlorinated photolabile species (i.e. HOCl, $ClNO_2$, $ClONO_2$) they could add up to a significant Cl atom contribution. All three additional proposed sources (HOCl, $ClNO_2$, and $ClONO_2$) have photochemical lifetimes (2-9 hours) that would allow for long range transport of these species. If a larger ambient ClO concentration was present upwind of a sampling site, then significant concentrations of HOCl, $ClNO_2$, and $ClONO_2$ could be produced upwind. Following transport to the sampling site, photolysis could occur, generating additional chlorine atoms. However, at this time none of the discussed species have been detected in the Arctic, although mid-latitude measurements exist.

HOCl was detected at the Cape Verde Atmospheric Observatory using a chemical ionization tandem mass spectrometer at concentrations up to 150 ppt (Lawler et al., 2011). Lawler et al. proposed that HOCl was produced from reaction 5.6-7 and 5.18, as gas-phase Cl_2 was produced from the oxidation of chloride in marine aerosols.

$$ClO + HO_2 \rightarrow HOCl + OH \quad (5.18)$$

Riedel et al. detected $ClNO_2$ during the night at concentrations up to 1800 ppt off the coast of California near Los Angeles (Riedel et al., 2012). They proposed that night time production of $ClNO_2$ was due to the reaction of anthropogenic NO_x with chloride containing marine aerosols. Lab studies have shown that N_2O_5 can react with Cl^- doped aerosols to yield $ClNO_2$, as shown in reactions 5.19-5.20 (Roberts et al., 2009;Finlaysonpitts et al., 1989).

$$N_2O_5 \rightarrow NO_2^+ + NO_3^- \quad (5.19)$$

$$NO_2^+ + Cl^- \rightarrow ClNO_2 \quad (5.20)$$

This could be very important in the Arctic where the snowpack is a known source of NO_x (Honrath et al., 1999;Honrath et al., 2002;Honrath et al., 2000). Field based measurements have shown that the NO_x concentration in the interstial snowpack can range from 3-10 times greater than ambient concentrations (Honrath et al., 1999). Reactions 5.19-5.20 could occur within the snowpack and release $ClNO_2$ into the surface layer above. Although both the HOCl and $ClNO_2$ measurements took place outside the Arctic, they do represent the significance that HOCl and $ClNO_2$ can partake in the chlorine cycle. They also prove that we have the ability to detect and quantify these species.

5.7 Conclusions

Using an in-lab setup we were able to determine the CIMS sensitivity to ClO, using $I(H_2O)^-$ as our reagent ion. This was needed to quantify ClO signals acquired during the spring of 2012 as a part of the BROMEX field campaign in Barrow, Alaska. Using our sensitivity factor we determined that our observed ClO measurements ranged from 5 to 28 ppt, similar to previous ClO observations of 3 to 30 ppt (Tuckermann et al., 1997). To further study the chlorine chemistry that is unique to the Arctic we developed a model to simulate the time period of our ClO observations. From our initial simulations we found that our model was undersimulating ClO. This made us believe that we were missing a Cl atom source, as our model's main Cl atom source was Cl_2 which was constrained to observations. Based on our findings from Section 4.2 the surface snowpack has the ability to produce BrCl, and possibility $ClNO_2$, which could transport into the surface layer. Although this is taken into account in our model, we decided to constrain BrCl, as a proxy Cl atom precursor to determine what concentration of an additional photolabile chlorinated source was needed to replicate the ClO observations.

We found that a concentration of six times the Cl_2 observation was needed to properly simulate ClO within the uncertainty of the observation. Based on the findings from our modeling study we believe that a potential Cl atom source in the Arctic is not being accounted for within our model. We proposed that several chlorinated photolabile species (HOCl, $ClNO_2$, and $ClONO_2$) could account for the missing chlorine atoms. All three have photochemical lifetimes ranging from 2-9 hours, allowing for long range (~30 km) transport in which their contribution toward to chlorine atom source would be unknown. Although both HOCl and $ClNO_2$ have been detected in the mid-latitudes, none

of the proposed species have been detected in the Arctic, despite the capability being available. From this work we reveal a knowledge gap in our understanding of the chlorine chemistry occurring in the Arctic. To properly understand the full impact that chlorine has on the Arctic atmosphere all possible chlorine atom sources must be known. Future field campaigns should focus on understanding and detecting HOCl, $ClNO_2$, and $ClONO_2$ and their impact on the chlorine cycle.

5.8 References

Ariya, P. A., Jobson, B. T., Sander, R., Niki, H., Harris, G. W., Hopper, J. F., and Anlauf, K. G.: Measurements of C-2-C-7 hydrocarbons during the Polar Sunrise Experiment 1994: Further evidence for halogen chemistry in the troposphere, Journal of Geophysical Research-Atmospheres, 103, 13169-13180, 10.1029/98jd00284, 1998.

Atkinson, R., Baulch, D. L., Cox, R. A., Crowley, J. N., Hampson, R. F., Hynes, R. G., Jenkin, M. E., Rossi, M. J., and Troe, J.: Evaluated kinetic and photochemical data for atmospheric chemistry: Volume I - gas phase reactions of O-x, HOx, NOx and SOx species, Atmospheric Chemistry and Physics, 4, 1461-1738, 2004.

Barrie, L., Bottenheim, J., Schnell, R., Crutzen, P., and Rasmsssen, R.: Ozone Destruction and Photochemical-Reactions at Polar Sunrise in the Lower Arctic Atmosphere, Nature, 334, 138-141, 10.1038/334138a0, 1988.

Bottenheim, J., Barrie, L., Atlas, E., Heidt, L., Niki, H., Rasmussen, R., and Shepson, P.: Depletion of Lower Tropospheric Ozone During Arctic Spring - The Polar Sunrise Experiment 1988, Journal of Geophysical Research-Atmospheres, 95, 18555-18568, 10.1029/JD095iD11p18555, 1990.

Boudries, H., and Bottenheim, J. W.: Cl and Br atom concentrations during a surface boundary layer ozone depletion event in the Canadian high Arctic, Geophysical Research Letters, 27, 517-520, 10.1029/1999gl011025, 2000.

Fan, S., and Jacob, D.: Surface Ozone Depletion in Arctic Spring Sustained by Bromine Reactions on Aerosols, Nature, 359, 522-524, 10.1038/359522a0, 1992.

Finlaysonpitts, B. J., Ezell, M. J., and Pitts, J. N.: Formation of chemically active chlorine compounds by reactions of atmospheric NaCl particles with gaseous N_2O_5 and $ClONO_2$, Nature, 337, 241-244, 10.1038/337241a0, 1989.

Foster, K., Plastridge, R., Bottenheim, J., Shepson, P., Finlayson-Pitts, B., and Spicer, C.: The role of Br-2 and BrCl in surface ozone destruction at polar sunrise, Science, 291, 471-474, 10.1126/science.291.5503.471, 2001.

Grannas, A., Shepson, P., Guimbaud, C., Sumner, A., Albert, M., Simpson, W., Domine, F., Boudries, H., Bottenheim, J., Beine, H., Honrath, R., and Zhou, X.: A study of photochemical and physical processes affecting carbonyl compounds in the Arctic atmospheric boundary layer, Atmospheric Environment, 36, 2733-2742, 10.1016/S1352-2310(02)00134-6, 2002.

Honninger, G., and Platt, U.: Observations of BrO and its vertical distribution during surface ozone depletion at Alert, Atmospheric Environment, 36, 2481-2489, 10.1016/s1352-2310(02)00104-8, 2002.

Honrath, R. E., Peterson, M. C., Guo, S., Dibb, J. E., Shepson, P. B., and Campbell, B.: Evidence of NOx production within or upon ice particles in the Greenland snowpack, Geophysical Research Letters, 26, 695-698, 10.1029/1999gl900077, 1999.

Honrath, R. E., Peterson, M. C., Dziobak, M. P., Dibb, J. E., Arsenault, M. A., and Green, S. A.: Release of NOx from sunlight-irradiated midlatitude snow, Geophysical Research Letters, 27, 2237-2240, 10.1029/1999gl011286, 2000.

Honrath, R. E., Lu, Y., Peterson, M. C., Dibb, J. E., Arsenault, M. A., Cullen, N. J., and Steffen, K.: Vertical fluxes of NOx, HONO, and HNO3 above the snowpack at Summit, Greenland, Atmospheric Environment, 36, 2629-2640, 10.1016/s1352-2310(02)00132-2, 2002.

Jobson, B. T., Niki, H., Yokouchi, Y., Bottenheim, J., Hopper, F., and Leaitch, R.: Measurements of C2–C6 hydrocarbons during the Polar Sunrise 1992 Experiment: Evidence for Cl atom and Br atom chemistry, Journal of Geophysical Research-Atmospheres, 99, 25355-25368, 10.1029/94jd01243, 1994.

Lawler, M. J., Sander, R., Carpenter, L. J., Lee, J. D., von Glasow, R., Sommariva, R., and Saltzman, E. S.: HOCl and Cl-2 observations in marine air, Atmospheric Chemistry and Physics, 11, 7617-7628, 10.5194/acp-11-7617-2011, 2011.

Liao, J., Huey, L., Tanner, D., Flocke, F., Orlando, J., Neuman, J., Nowak, J., Weinheimer, A., Hall, S., Smith, J., Fried, A., Staebler, R., Wang, Y., Koo, J., Cantrell, C., Weibring, P., Walega, J., Knapp, D., Shepson, P., and Stephens, C.: Observations of inorganic bromine (HOBr, BrO, and Br-2) speciation at Barrow, Alaska, in spring 2009, Journal of Geophysical Research-Atmospheres, 117, 10.1029/2011JD016641, 2012.

Liao, J., Huey, L., Liu, Z., Tanner, D., Cantrell, C., Orlando, J., Flocke, F., Shepson, P., Weinheimer, A., Hall, S., Ullmann, K., Beine, H., Wang, Y., Ingall, E., Stephens, C., Hornbrook, R., Apel, E., Riemer, D., Fried, A., Mauldin, R., Smith, J., Staebler, R., Neuman, J., and Nowak, J.: High levels of molecular chlorine in the Arctic atmosphere, Nature Geoscience, 7, 91-94, 10.1038/NGEO2046, 2014.

Madronich, S.: The Tropospheric visible Ultra-violet (TUV) model web page, National Center for Atmospheric Research, Boulder, CO. http://www.acd.ucar.edu/TUV 2002.

Michalowski, B., Francisco, J., Li, S., Barrie, L., Bottenheim, J., and Shepson, P.: A computer model study of multiphase chemistry in the Arctic boundary layer during polar sunrise, Journal of Geophysical Research-Atmospheres, 105, 15131-15145, 10.1029/2000JD900004, 2000.

Oltmans, S. J., Johnson, B. J., and Harris, J. M.: Springtime boundary layer ozone depletion at Barrow, Alaska: Meteorological influence, year-to-year variation, and long-term change, Journal of Geophysical Research-Atmospheres, 117, 18, 10.1029/2011jd016889, 2012.

Pohler, D., Vogel, L., Friess, U., and Platt, U.: Observation of halogen species in the Amundsen Gulf, Arctic, by active long-path differential optical absorption spectroscopy, Proceedings of the National Academy of Sciences of the United States of America, 107, 6582-6587, 10.1073/pnas.0912231107, 2010.

Pratt, K., Custard, K., Shepson, P., Douglas, T., Pohler, D., General, S., Zielcke, J., Simpson, W., Platt, U., Tanner, D., Huey, L., Carlsen, M., and Stirm, B.: Photochemical production of molecular bromine in Arctic surface snowpacks, Nature Geoscience, 6, 351-356, 10.1038/NGEO1779, 2013.

Riedel, T. P., Bertram, T. H., Crisp, T. A., Williams, E. J., Lerner, B. M., Vlasenko, A., Li, S. M., Gilman, J., de Gouw, J., Bon, D. M., Wagner, N. L., Brown, S. S., and Thornton, J. A.: Nitryl Chloride and Molecular Chlorine in the Coastal Marine Boundary Layer, Environmental Science & Technology, 46, 10463-10470, 10.1021/es204632r, 2012.

Roberts, J. M., Osthoff, H. D., Brown, S. S., Ravishankara, A. R., Coffman, D., Quinn, P., and Bates, T.: Laboratory studies of products of N2O5 uptake on Cl- containing substrates, Geophysical Research Letters, 36, 5, 10.1029/2009gl040448, 2009.

Shetter, R. E., and Muller, M.: Photolysis frequency measurements using actinic flux spectroradiometry during the PEM-Tropics mission: Instrumentation description and some results, Journal of Geophysical Research-Atmospheres, 104, 5647-5661, 10.1029/98jd01381, 1999.

Simpson, W., Carlson, D., Honninger, G., Douglas, T., Sturm, M., Perovich, D., and Platt, U.: First-year sea-ice contact predicts bromine monoxide (BrO) levels at Barrow, Alaska better than potential frost flower contact, Atmospheric Chemistry and Physics, 7, 621-627, 2007.

Spicer, C., Plastridge, R., Foster, K., Finlayson-Pitts, B., Bottenheim, J., Grannas, A., and Shepson, P.: Molecular halogens before and during ozone depletion events in the Arctic at polar sunrise: concentrations and sources, Atmospheric Environment, 36, 2721-2731, 10.1016/S1352-2310(02)00125-5, 2002.

Tuckermann, M., Ackermann, R., Golz, C., LorenzenSchmidt, H., Senne, T., Stutz, J., Trost, B., Unold, W., and Platt, U.: DOAS-observation of halogen radical-catalysed arctic boundary layer ozone destruction during the ARCTOC-campaigns 1995 and 1996 in Ny-Alesund, Spitsbergen, Tellus Series B-Chemical and Physical Meteorology, 49, 533-555, 10.1034/j.1600-0889.49.issue5.9.x, 1997.

CHAPTER 6 CONCLUSIONS

The goal of this dissertation work was to advance the field of Arctic atmospheric chemistry, focusing on the source of atmospheric molecular halogens and the influence of anthropogenic emissions on halogen chemistry. The frequent depletion of ozone from background levels of ~40 ppb to less than 5 ppb during the Arctic springtime has been well documented over the past several decades (Bottenheim et al., 1986;Oltmans et al., 2012). A linkage between these ozone depletion events (ODEs) and halogen chemistry has motivated countless modeling and laboratory studies along with numerous large scale field campaigns to help further understand the unique chemistry occurring in the Arctic (Grannas et al., 2007;Simpson et al., 2007;Pratt et al., 2013;Liao et al., 2012;Liao et al., 2014;Michalowski et al., 2000;Lindberg et al., 2002;Fan and Jacob, 1992;McConnell et al., 1992;Abbatt et al., 2012;Platt and Honninger, 2003;Impey et al., 1997).

Prior to this work Cl_2 and BrCl had only been detected a total of three times in the Arctic ambient air (Liao et al., 2014;Foster et al., 2001;Spicer et al., 2002). In all three cases the source for the molecular halogens was unknown. During this study, for the first time, we observed direct snowpack production of both Cl_2 and BrCl. In Chapter 3 in-snowpack experiments using CIMS conducted in Barrow, Alaska during February, 2014 indicated that the Arctic surface snowpack is able to produce molecular halogens only in the presence of ultraviolet radiation, which suggests a photochemical production

mechanism. This generation was enhanced when the snowpack O_3 concentration was increased, which follows the "bromine explosion" mechanism described in section 3.1. Since the snowpack produces molecular halogens within its interstitial air, it thus has the potential to act as a source for atmospheric molecular halogens. To evaluate this potential, vertical profile measurements were conducted above the tundra surface snowpack (Section 3.2.3). These experiments yielded snowpack flux emission rates ranging from $1.6\pm0.3x10^{7}$ to $1.4\pm0.3x10^{9}$ molecules$\cdot cm^{-2}\cdot s^{-1}$ for both Br_2 and Cl_2. These calculated emission rates imply the snowpack has the quantitative potential to act as a major source of atmospheric molecular halogens. Flux emission rates from the snowpack can be integrated into current Arctic models to evaluate our hypothesis that the snowpack is the main source for atmospheric molecular halogens.

However, our measurements only represent the bottom 100 cm of the Artic boundary layer, where the snowpack can directly influence the molecular halogen ambient concentration. If aerosols produced significant concentrations of molecular halogens, this would be observed from measurements above the influence of snowpack emissions. Future campaigns should focus on ambient measurements above the snowpack at heights which snowpack emissions are insignificant. This would allow for the impact of aerosols as a halogen source to be evaluated. If aerosols were able to release molecular halogens this could explain why air up to several hundred meters have been observed to be depleted in O_3 (Bottenheim et al., 2002)

Along with Cl_2 and BrCl, only one published observation for ambient Arctic ClO existed prior to the study described in Chapter 5 (Tuckermann et al., 1997). ClO was detected using a CIMS instrument during the Bromine, Mercury, and Ozone Experiment

(BROMEX) field campaign which occurred in Barrow, Alaska during the spring of 2012, where daytime concentrations ranged from 3 to 28 ppt, similar to previous modeling estimations and field based observations (Liao et al., 2014;Tuckermann et al., 1997). To further gauge our understanding of Arctic chlorine chemistry we developed a model to simulate the chemistry occurring during the time period of our ClO observations. Our initial simulation using known chemistry yielded ClO concentrations up to 80% less than the observed values. A potential source of error in this model is that Cl_2, which was constrained within the model to observations, is the only source of Cl radicals, although other Cl sources exist. To test this theory an additional source of Cl radicals was added to the model in the form of BrCl. By varying BrCl concentrations (constrained to observed Cl_2), we determined that a BrCl source with a concentration of 6[Cl_2] was needed to create simulated ClO concentrations within the uncertainty of the observed ClO concentrations from the BROMEX field campaign. Several possible photolyzable chlorine sources (HOCl, ClONO2, and $ClNO_2$) exist that have not detected in the Arctic, which could play a role as our missing chlorine atom source. All three can be detected and quantified using current CIMS techniques and should be the focus of future Arctic field campaigns. With correct concentration constraints for all possible Cl atom sources (Cl_2, BrCl, HOCl, $ClONO_2$, and $ClNO_2$), model simulations could be performed to determine if these represent all the sources or if we are still missing any possible sources.

In Chapter 4 we described that it is anticipated that the number of NO_x ($NO+NO_2$) point sources may increase, leading to potential changes in the Arctic halogen cycle (Peters et al., 2011;Corbett et al., 2010). We developed a 0-D model to test the sensitivity of the known halogen chemistry that occurs in the Arctic to elevated

concentrations of NO_x. From our model we found that rising NO_x concentrations lead to ozone depletion rate decreases, with the most profound decreases occurring at the lower NO_x concentration increase (300-500 ppt). We determined that this was due to the suppression of HOBr and BrO production as NO_x concentrations rise, which are needed to continue the bromine cycle and deplete ozone. Instead, the products became, $BrNO_2$ and $BrONO_2$, which are not as effective at depleting ozone. These findings were supported by aircraft measurements of BrO and NO_2, where elevated concentrations of NO_2 correlated with decreased concentrations of BrO. This work highlighted the need to further expand on NO_x-halogen chemistry especially dealing with aqueous phase chemistry. This work could have great importance as the Arctic's atmospheric composition changes in the future, related to NO_x and other pollutants concentrations. It also emphasizes the need to monitor ambient NO_x concentrations when conducting molecular halogen measurements.

From the work presented in this dissertation the influence that the snowpack has on the halogen chemistry occurring in the Arctic boundary layer is quite significant. The snowpack has been shown to act as a dominant source for molecular halogens in the source layer and represents a unique environment where this chemistry occurs. However, there is a large knowledge gap in our understanding of how to properly model the chemistry occurring on snow grain surfaces. Current models treat snow grain surfaces as a quasi-liquid layer (QLL) and uses photolysis and reaction rate coefficients similar to ones measured in dilute solutions. The QLL is hypothesized to be a liquid layer that contains a significant fraction of the reactants present in the snow grain and it's the location of the chemistry. As pointed out by *Domine* et al. this treatment is incorrect as

the snow grain surface is too large to be completely covered by a QLL layer (Domine et al., 2013). They propose that the QLL most likely collects in snow grain boundaries and may have very little impact on the chemistry. In fact they state that a major of the reactions occur on ice surfaces or organic particles located on the ice surfaces.

For snowpack models to properly simulate the real world snowpack significant advances in our understanding of these processes would have to occur, which would be a daunting task. First, further analysis of snow grain properties would have to be performed to confirm the proposals from *Domine* et al. Next, reaction and photolysis rate coefficients would need to be measured on ice surfaces. However, this is quite difficult as sample preparation and analysis are not trivial. Finally, these findings would need to be incorporated into a model that represents a simple snowpack that is extremely well understood.

This dissertation work shows a significant advancement to the field of Arctic halogen chemistry, using both field campaigns and modeling studies. As the atmospheric chemistry of the Arctic changes due to a shift in the composition of the sea ice, atmospheric halogen sources and gas-phase cycle will be impacted.

6.1 References

Abbatt, J. P. D., Thomas, J. L., Abrahamsson, K., Boxe, C., Granfors, A., Jones, A. E., King, M. D., Saiz-Lopez, A., Shepson, P. B., Sodeau, J., Toohey, D. W., Toubin, C., von Glasow, R., Wren, S. N., and Yang, X.: Halogen activation via interactions with environmental ice and snow in the polar lower troposphere and other regions, Atmospheric Chemistry and Physics, 12, 6237-6271, 10.5194/acp-12-6237-2012, 2012.

Bottenheim, J., Fuentes, J., Tarasick, D., and Anlauf, K.: Ozone in the Arctic lower troposphere during winter and spring 2000 (ALERT2000), Atmospheric Environment, 36, 2535-2544, 10.1016/S1352-2310(02)00121-8, 2002.

Bottenheim, J. W., Gallant, A. G., and Brice, K. A.: Measurements of NO_y species and O_3 at 82^o N latitude, Geophysical Research Letters, 13, 113-116, 10.1029/GL013i002p00113, 1986.

Domine, F., Bock, J., Voisin, D., and Donaldson, D. J.: Can We Model Snow Photochemistry? Problems with the Current Approaches, Journal of Physical Chemistry A, 117, 4733-4749, 10.1021/jp3123314, 2013.

Fan, S., and Jacob, D.: Surface Ozone Depletion in Arctic Spring Sustained by Bromine Reactions on Aerosols, Nature, 359, 522-524, 10.1038/359522a0, 1992.

Foster, K., Plastridge, R., Bottenheim, J., Shepson, P., Finlayson-Pitts, B., and Spicer, C.: The role of Br-2 and BrCl in surface ozone destruction at polar sunrise, Science, 291, 471-474, 10.1126/science.291.5503.471, 2001.

Grannas, A. M., Jones, A. E., Dibb, J., Ammann, M., Anastasio, C., Beine, H. J., Bergin, M., Bottenheim, J., Boxe, C. S., Carver, G., Chen, G., Crawford, J. H., Domine, F., Frey, M. M., Guzman, M. I., Heard, D. E., Helmig, D., Hoffmann, M. R., Honrath, R. E., Huey, L. G., Hutterli, M., Jacobi, H. W., Klan, P., Lefer, B., McConnell, J., Plane, J., Sander, R., Savarino, J., Shepson, P. B., Simpson, W. R., Sodeau, J. R., von Glasow, R., Weller, R., Wolff, E. W., and Zhu, T.: An overview of snow photochemistry: evidence, mechanisms and impacts, Atmospheric Chemistry and Physics, 7, 4329-4373, 2007.

Impey, G., Shepson, P., Hastie, D., Barrie, L., and Anlauf, K.: Measurements of photolyzable chlorine and bromine during the Polar sunrise experiment 1995, Journal of Geophysical Research-Atmospheres, 102, 16005-16010, 10.1029/97JD00851, 1997.

Liao, J., Huey, L., Tanner, D., Flocke, F., Orlando, J., Neuman, J., Nowak, J., Weinheimer, A., Hall, S., Smith, J., Fried, A., Staebler, R., Wang, Y., Koo, J., Cantrell, C., Weibring, P., Walega, J., Knapp, D., Shepson, P., and Stephens, C.: Observations of inorganic bromine (HOBr, BrO, and Br-2) speciation at Barrow, Alaska, in spring 2009, Journal of Geophysical Research-Atmospheres, 117, 10.1029/2011JD016641, 2012.

Liao, J., Huey, L., Liu, Z., Tanner, D., Cantrell, C., Orlando, J., Flocke, F., Shepson, P., Weinheimer, A., Hall, S., Ullmann, K., Beine, H., Wang, Y., Ingall, E., Stephens, C., Hornbrook, R., Apel, E., Riemer, D., Fried, A., Mauldin, R., Smith, J., Staebler, R., Neuman, J., and Nowak, J.: High levels of molecular chlorine in the Arctic atmosphere, Nature Geoscience, 7, 91-94, 10.1038/NGEO2046, 2014.

Lindberg, S. E., Brooks, S., Lin, C. J., Scott, K. J., Landis, M. S., Stevens, R. K., Goodsite, M., and Richter, A.: Dynamic oxidation of gaseous mercury in the Arctic troposphere at polar sunrise, Environmental Science & Technology, 36, 1245-1256, 10.1021/es0111941, 2002.

McConnell, J., Henderson, G., Barrie, L., Bottenheim, J., Niki, H., Langford, C., and Templeton, E.: Photochemical Bromine Production Implicated in Arctic Boundary-Layer Ozone Depletion, Nature, 355, 150-152, 10.1038/355150a0, 1992.

Michalowski, B., Francisco, J., Li, S., Barrie, L., Bottenheim, J., and Shepson, P.: A computer model study of multiphase chemistry in the Arctic boundary layer during polar sunrise, Journal of Geophysical Research-Atmospheres, 105, 15131-15145, 10.1029/2000JD900004, 2000.

Oltmans, S. J., Johnson, B. J., and Harris, J. M.: Springtime boundary layer ozone depletion at Barrow, Alaska: Meteorological influence, year-to-year variation, and long-term change, Journal of Geophysical Research-Atmospheres, 117, 18, 10.1029/2011jd016889, 2012.

Platt, U., and Honninger, G.: The role of halogen species in the troposphere, Chemosphere, 52, 325-338, 10.1016/s0045-6535(03)00216-9, 2003.

Pratt, K., Custard, K., Shepson, P., Douglas, T., Pohler, D., General, S., Zielcke, J., Simpson, W., Platt, U., Tanner, D., Huey, L., Carlsen, M., and Stirm, B.: Photochemical production of molecular bromine in Arctic surface snowpacks, Nature Geoscience, 6, 351-356, 10.1038/NGEO1779, 2013.

Simpson, W., von Glasow, R., Riedel, K., Anderson, P., Ariya, P., Bottenheim, J., Burrows, J., Carpenter, L., Friess, U., Goodsite, M., Heard, D., Hutterli, M., Jacobi, H., Kaleschke, L., Neff, B., Plane, J., Platt, U., Richter, A., Roscoe, H., Sander, R., Shepson, P., Sodeau, J., Steffen, A., Wagner, T., and Wolff, E.: Halogens and their role in polar boundary-layer ozone depletion, Atmospheric Chemistry and Physics, 7, 4375-4418, 2007.

Spicer, C., Plastridge, R., Foster, K., Finlayson-Pitts, B., Bottenheim, J., Grannas, A., and Shepson, P.: Molecular halogens before and during ozone depletion events in the Arctic at polar sunrise: concentrations and sources, Atmospheric Environment, 36, 2721-2731, 10.1016/S1352-2310(02)00125-5, 2002.

Tuckermann, M., Ackermann, R., Golz, C., LorenzenSchmidt, H., Senne, T., Stutz, J., Trost, B., Unold, W., and Platt, U.: DOAS-observation of halogen radical-catalysed arctic boundary layer ozone destruction during the ARCTOC-campaigns 1995 and 1996 in Ny-Alesund, Spitsbergen, Tellus Series B-Chemical and Physical Meteorology, 49, 533-555, 10.1034/j.1600-0889.49.issue5.9.x, 1997.

APPENDIX

APPENDIX

Chemical Mechanisms for NO_x Arctic Model

Table A.1 Gas-phase chemical reactions used in the model. All rate constants are calculated for a temperature of 248 K unless otherwise noted and are expressed in units of cm^3 $molecule^{-1}$ s^{-1}.

Reaction	Rate Constant	Reference
$O(^1D) + M \rightarrow O(^3P)$	3.34×10^{-11}	*Ravishankara et al.* [2002]
$O(^3P) + O_2 \rightarrow O_3$	2.12×10^{-14}	*Atkinson et al.* [2004]
$O(^1D) + H_2O \rightarrow 2OH$	2.2×10^{-10}	*Atkinson et al.* [2004]
$OH + O_3 \rightarrow HO_2$	3.84×10^{-14}	*Atkinson et al.* [2004]
$OH + HO_2 \rightarrow H_2O$	1.34×10^{-10}	*Atkinson e t al.* [2004]
$OH + H_2O_2 \rightarrow HO_2 + H_2O$	1.52×10^{-12}	*Atkinson et al.* [2004]
$OH + O(^3P) \rightarrow O_2$	3.74×10^{-11}	*Atkinson et al.* [2004]
$OH + OH \rightarrow H_2O + O(^3P)$	1.74×10^{-12}	*Atkinson et al.* [2004]
$OH + OH \rightarrow H_2O_2$	1.86×10^{-11}	*Atkinson et al.* [2004]
$OH + NO_3 \rightarrow HO_2 + NO_2$	2.0×10^{-11}	*Atkinson et al.* [2004]
$HO_2 + NO_3 \rightarrow HNO_3$	4.0×10^{-12}	*Atkinson et al.* [2004]
$HO_2 + O_3 \rightarrow OH + 2O_2$	1.39×10^{-15}	*Atkinson et al.* [2004]
$HO_2 + HO_2 \rightarrow H_2O_2 + O_2$	2.58×10^{-12}	*Atkinson et al.* [2004]
$NO + OH \rightarrow HONO$	3.49×10^{-11}	*Atkinson et al.* [2004]
$NO + HO_2 \rightarrow NO_2 + OH$	9.59×10^{-12}	*Atkinson et al.* [2004]
$NO + O_3 \rightarrow NO_2$	7.09×10^{-15}	*Sander et al.* [2006]
$NO + NO_3 \rightarrow NO_2 + NO_2$	2.98×10^{-11}	*Sander et al.* [2006]
$NO_2 + OH \rightarrow HNO_3$	1.2×10^{-10}	*Atkinson et al.* [2004]
$NO_2 + HO_2 \leftrightarrow HNO_4$	f: 8.6×10^{-12} r: 1.32×10^{-4}	*Atkinson et al.* [2004]
$NO_2 + O_3 \rightarrow NO_3$	6.15×10^{-18}	*Sander et al.* [2006]
$NO_2 + NO_3 \leftrightarrow N_2O_5$	f: 1.83×10^{-12} r: 3.76×10^{-5}	*Atkinson et al.* [2004]
$NO_2 + CH_3COOO \leftrightarrow PAN$	f: 1.4×10^{-11} r: 3.1×10^{-8}	*Atkinson et al.* [2004]
$NO_3 + NO_3 \rightarrow NO_2 + NO_2$	4.36×10^{-17}	*Sander et al.* [2006]
$N_2O_5 + H_2O \rightarrow HNO_3 + HNO_3$	2.6×10^{-22}	*Atkinson et al.* [2004]
$HONO + OH \rightarrow NO_2 + H_2O$	3.74×10^{-12}	*Sander et al.* [2006]
$HNO_3 + OH \rightarrow NO_3 + H_2O$	1.5×10^{-13}	*Atkinson et al.* [2004]
$HNO_4 + OH \rightarrow NO_2 + H_2O$	6.2×10^{-12}	*Atkinson et al.* [2004]
$CO + OH \rightarrow HO_2 + CO_2$	2.4×10^{-13}	*Atkinson et al.* [2004]
$CH_4 + OH \rightarrow CH_3OO + H_2O$	1.87×10^{-15}	*Sander et al.* [2006]
$C_2H_2 + OH \rightarrow C_2H_2OH$	7.8×10^{-13}	*Atkinson et al.* [2004]
$C_2H_6 + OH \rightarrow C_2H_5OO$	1.18×10^{-13}	*Lurmann et al.* [1986]

$C_2H_4 + OH \rightarrow C_2H_4OH$	1.02×10^{-11}	*hahtin et al.* [2003]
$C_3H_8 + OH \rightarrow nC_3H_7O_2$	1.56×10^{-13}	*Harris and Kerr* [1988]
$C_3H_8 + OH \rightarrow iC_3H_7O_2$	6.64×10^{-13}	*Harris and Kerr* [1988]
$C_3H_6 + OH \rightarrow C_3H_6OH$	3.63×10^{-11}	*Atkinson et al.* [2004]
$C_3H_6O + OH \rightarrow$ Products	2.51×10^{-11}	*Atkinson et al.* [2004]
$nC_3H_7O_2 + NO \rightarrow NO_2 + C_3H_6O + HO_2$	5.4×10^{-11}	*Eberhard et al.* [1996]
$iC_3H_7O_2 + NO \rightarrow NO_2 + CH_3COCH_3 + HO_2$	1.2×10^{-11}	*Eberhard and Howard* [1996]
$nC_4H_{10} + OH \rightarrow nC_4H_9OO$	1.64×10^{-12}	*Donahue et al.* [1998]
$iC_4H_{10} + OH \rightarrow CH_3COCH_3 + CH_3OO$	1.65×10^{-12}	*Donahue et al.* [1998]
$nC_4H_9OO + NO \rightarrow$ n-Butanal $+ NO_2 + HO_2$	5.4×10^{-11}	*Michalowski et al.* [2000]
$nC_4H_9OO + CH_3OO \rightarrow$ n-Butanal $+ HCHO + HO_2 + HO_2$	6.7×10^{-13}	*Michalowski et al.* [2000]
$nC_4H_9OO + CH_3OO \rightarrow$ n-Butanal $+ CH_3OH$	2.3×10^{-13}	*Michalowski et al.* [2000]
$nC_4H_9OO + CH_3OO \rightarrow nC_4H_9OH + HCHO$	2.3×10^{-13}	*Michalowski et al.* [2000]
$CH_3OH + OH \rightarrow CH_3O$	7.09×10^{-13}	*Atkinson et al.* [2004]
n-Butanal + OH → Products	2.0×10^{-11}	*Michalowski et al.* [2000]
$CH_3OO + HO_2 \rightarrow CH_3OOH$	8.82×10^{-12}	*Atkinson et al.* [2004]
$C_2H_5OO + HO_2 \rightarrow C_2H_5OOH$	1.12×10^{-11}	*Atkinson et al.* [2004]
$CH_3COOO + HO_2 \rightarrow CH_3COOOH$	2.54×10^{-11}	*DeMore et al.* [1997]
$C_2H_5OOH + OH \rightarrow C_2H_5OO$	6.0×10^{-12}	*Atkinson et al.* [2004]
$CH_3OO + CH_3OO \rightarrow HCHO + HO_2$	3.64×10^{-13}	*Lurmann et al.* [1986]
$CH_3OOH + OH \rightarrow HCHO + H_2O + OH$	2.54×10^{-12}	*Sander and Crutzen* [1996]
$CH_3OOH + OH \rightarrow CH_3OO + H_2O$	6.01×10^{-12}	*Sander and Crutzen* [1996]
$CH_3OO + HO_2 \rightarrow CH_3OOH$	1.01×10^{-11}	*Atkinson et al.* [2004]
$CH_3OO + NO \rightarrow HCHO + HO_2 + NO_2$	8.76×10^{-12}	*Atkinson et al.* [2004]
$CH_3OO + NO_2 \rightarrow CH_3OONO_2$	9.63×10^{-12}	*DeMore et al.* [1997]
$CH_3OO + nC_3H_7O_2 \rightarrow HCHO + C_3H_6O + HO_2 + HO_2$	6.70×10^{-13}	*Lightfoot et al.* [1992]
$CH_3OO + nC_3H_7O_2 \rightarrow C_3H_6O + CH_3OH$	2.3×10^{-13}	*Lightfoot et al.* [1992]
$CH_3OO + nC_3H_7O_2 \rightarrow HCHO + nC_3H_7OH$	2.3×10^{-13}	*Lightfoot et al.* [1992]
$CH_3OO + iC_3H_7O_2 \rightarrow HCHO + CH_3COCH_3 + HO_2 + HO_2$	1.2×10^{-14}	*Lightfoot et al.* [1992]
$CH_3OO + iC_3H_7O_2 \rightarrow CH_3COCH_3 + CH_3OH$	4.1×10^{-15}	*Lightfoot et al.* [1992]
$CH_3OO + iC_3H_7O_2 \rightarrow HCHO + iC_3H_7OH$	4.1×10^{-15}	*Lightfoot et al.* [1992]
$CH_3OO + C_2H_5OO \rightarrow CH_3CHO + HCHO + HO_2 + HO_2$	2.0×10^{-13}	*Kirchner and Stockwell* [1996]
$CH_3OO + CH_3COOO \rightarrow HCHO + CH_3OO + HO_2$	1.58×10^{-11}	*Kirchner and Stockwell* [1996]
$C_2H_5OO + NO \rightarrow CH_3CHO + HO_2 + NO_2$	8.68×10^{-12}	*Lurmann et al.* [1986]
$C_2H_5OO + NO_2 \rightarrow C_2H_5OONO_2$	8.8×10^{-12}	*Atkinson et al.* [1997]
$C_2H_5OO + HO_2 \rightarrow C_2H_5OOH$	9.23×10^{-12}	*Atkinson et al.* [2004]
$C_2H_5OO + CH_3COOO \rightarrow CH_3CHO + CH_3COO + HO_2$	4.0×10^{-12}	*Michalowski et al.* [2000]
$iC_3H_7O_2 + HO_2 \rightarrow$ iPerox	9.23×10^{-12}	*Michalowski et al.* [2000]
$nC_3H_7O_2 + HO_2 \rightarrow$ nPerox	9.23×10^{-12}	*Michalowski et al.* [2000]
$HCHO + OH \rightarrow HO_2 + CO$	9.3×10^{-12}	*Atkinson et al.* [2004]
$HCHO + HO_2 \rightarrow HOCH_2O_2$	7.53×10^{-14}	*Sander et al.* [2006]
$HCHO + NO_3 \rightarrow HNO_3 + HO_2 + CO$	5.8×10^{-16}	*DeMore et al.* [1997]
$CH_3CHO + OH \rightarrow CH_3COOO + H_2O$	1.98×10^{-11}	*Atkinson et al.* [2004]
$CH_3CHO + NO_3 \rightarrow HNO_3 + CH_3COOO$	1.4×10^{-15}	*DeMore et al.* [1997]
$CH_3COCH_3 + OH \rightarrow H_2O + CH_3COCH_2$	1.37×10^{-13}	*Atkinson et al.* [2004]
$HOCH_2O_2 + NO \rightarrow HCOOH + HO_2 + NO_2$	8.68×10^{-12}	*Lurmann et al.* [1986]
$HOCH_2O_2 + HO_2 \rightarrow HCOOH + H_2O$	2.0×10^{-12}	*Lurmann et al.* [1986]
$HOCH_2O_2 + HOCH_2O_2 \rightarrow HCOOH + HCOOH + HO_2 + HO_2$	1.0×10^{-13}	*Lurmann et al.* [1986]
$HCOOH + OH \rightarrow HO_2 + H_2O + CO_2$	4.0×10^{-13}	*DeMore et al.* [1997]
$CH_3COOO + NO \rightarrow CH_3OO + NO_2 + CO_2$	2.4×10^{-11}	*Atkinson et al.* [2004]
$CH_3COOO + HO_2 \rightarrow CH_3COOH + O_3$	1.87×10^{-11}	*Kirchner and Stockwell* [1996]
$CH_3COOO + CH_3COOO \rightarrow CH_3COO + CH_3COO$	2.5×10^{-11}	*Kirchner and Stockwell* [1996]
$C_2H_5OONO_2 \rightarrow C_2H_5OO + NO_2$	3.2×10^{-3}	*Atkinson et al.* [1997]
$CH_3OONO_2 \rightarrow CH_3OO + NO_2$	3.4×10^{-3}	*Atkinson et al.* [1997]
$Cl_2 + OH \rightarrow HOCl + Cl$	2.85×10^{-14}	*Atkinson et al.* [2004]

$Cl + O_3 \rightarrow ClO$	1.02×10^{-11}	*Atkinson et al.* [2004]
$Cl + H_2 \rightarrow HCl$	3.5×10^{-15}	*Atkinson et al.* [2004]
$Cl + HO_2 \rightarrow HCl$	3.57×10^{-11}	*Sander et al.* [2006]
$Cl + HO_2 \rightarrow ClO + OH$	6.68×10^{-12}	*Sander et al.* [2006]
$Cl + H_2O_2 \rightarrow HCl + HO_2$	2.11×10^{-13}	*Atkinson et al.* [2004]
$Cl + NO_3 \rightarrow ClO + NO_2$	2.4×10^{-11}	*Atkinson et al.* [2004]
$Cl + CH_4 \rightarrow HCl + CH_3OO$	3.99×10^{-14}	*Sander et al.* [2006]
$Cl + C_2H_6 \rightarrow HCl + C_2H_5OO$	5.36×10^{-11}	*Sander et al.* [2006]
$Cl + C_2H_4 \rightarrow HCl + C_2H_5OO$	1.0×10^{-10}	*Atkinson et al.* [2004]
$Cl + MEK \rightarrow HCl$	4.21×10^{-11}	*Atkinson et al.* [2004]
$Cl + C_2H_2 \rightarrow ClC_2CHO$	2.5×10^{-10}	*Atkinson et al.* [2004]
$Cl + C_3H_6 \rightarrow HCl + C_3H_6Cl$	2.7×10^{-10}	*Keil and Shepson* [2006]
$Cl + C_3H_8 \rightarrow HCl + iC_3H_7O_2$	1.65×10^{-10}	*DeMore et al.* [1997]
$Cl + C_3H_8 \rightarrow HCl + nC_3H_7O_2$	1.65×10^{-10}	*DeMore et al.* [1997]
$Cl + C_3H_6O \rightarrow HCl$	1.1×10^{-10}	*Wallington et al.* [1988]
$Cl + iC_4H_{10} \rightarrow HCl + C_4H_9$	1.3×10^{-10}	*Hooshiyar and Niki* [1995]
$Cl + nC_4H_{10} \rightarrow HCl + C_4H_9$	2.15×10^{-10}	*Tyndall et al.* [1997]
Cl + n-Butanal → HCl + Products	1.1×10^{-10}	*Michalowski et al.* [2000]
$Cl + HCHO \rightarrow HCl + HO_2 + CO$	7.18×10^{-11}	*Sander et al.* [2006]
$Cl + CH_3CHO \rightarrow HCl + CH_3COOO$	8.08×10^{-11}	*Atkinson et al.* [2004]
$Cl + CH_3COCH_3 \rightarrow HCl + CH_3COCH_2$	1.39×10^{-12}	*Atkinson et al.* [2004]
$Cl + CH_3OOH \rightarrow CH_3OO + HCl$	2.36×10^{-11}	*Atkinson et al.* [2004]
$Cl + CH_3OOH \rightarrow CH_2OOH + HCl$	3.54×10^{-11}	*Atkinson et al.* [2004]
Cl + CHBr3 → HCl + Br + CBr2O	2.9×10^{-13} (at 298 K)	*Kamboures et al.* [2002]
$Cl + OClO \rightarrow ClO + ClO$	6.35×10^{-11}	*Atkinson et al.* [2004]
$Cl + ClNO_3 \rightarrow Cl_2 + NO_3$	1.12×10^{-11}	*Sander et al.* [2006]
Cl + PAN → HCl + HCHO + NO_3	1.0×10^{-14}	*Tsalkani et al.* [1988]
$Cl + HNO_3 \rightarrow HCl + NO_3$	1.0×10^{-16}	*Wine et al.* [1988]
$Cl + NO_2 \rightarrow ClNO_2$	1.43×10^{-12} (at 298 K)	*Ravishankara et al.* [1988]
Cl + HBr → HCl + Br	4.48×10^{-12}	*Nicovich and Wine* [1990]
$ClO + O(^3P) \rightarrow Cl + O_2$	1.6×10^{-11}	*Atkinson et al.* [2004]
$ClO + OH \rightarrow Cl + HO_2$	2.45×10^{-11}	*Atkinson et al.* [2004]
ClO + OH → HCl	2.37×10^{-13}	*Sander et al.* [2006]
$ClO + HO_2 \rightarrow HOCl$	8.67×10^{-12}	*Atkinson et al.* [2004]
$ClO + CH_3OO \rightarrow Cl + HCHO + HO_2$	2.08×10^{-12}	*Sander et al.* [2006]
$ClO + CH_3COOO \rightarrow Cl + CH_3OO + CO_2$	2.03×10^{-12}	*Michalowski et al.* [2000]
$ClO + NO \rightarrow Cl + NO_2$	2.04×10^{-11}	*Atkinson et al.* [2004]
$ClO + NO_2 \rightarrow ClNO_3$	7.1×10^{-12}	*Atkinson et al.* [2004]
$ClO + ClO \rightarrow Cl_2$	1.64×10^{-15}	*Atkinson et al.* [2004]
ClO + ClO → Cl + Cl	1.54×10^{-15}	*Atkinson et al.* [2004]
ClO + ClO → Cl + OClO	1.40×10^{-15}	*Atkinson et al.* [2004]
OClO + OH → HOCl	1.13×10^{-11}	*Atkinson et al.* [2004]
$OClO + NO \rightarrow ClO + H_2O$	1.51×10^{-13}	*Atkinson et al.* [2004]
$HOCl + OH \rightarrow ClO + H_2O$	4.0×10^{-13}	*Sander et al.* [2006]
$HCl + OH \rightarrow Cl + H_2O$	6.84×10^{-13}	*Atkinson et al.* [2004]
$ClNO_3 + OH \rightarrow HOCl + NO_3$	3.17×10^{-13}	*Atkinson et al.* [2004]
$HOCl + O(^3P) \rightarrow ClO + OH$	1.7×10^{-13}	*Atkinson et al.* [2004]
$Br + O_3 \rightarrow BrO$	6.75×10^{-13}	*Atkinson et al.* [2004]
$Br_2 + OH \rightarrow HOBr$	5.0×10^{-11}	*Atkinson et al.* [2004]
$Br + HO_2 \rightarrow HBr$	1.25×10^{-12}	*Atkinson et al.* [2004]
$Br + C_2H_2 \rightarrow BrCH_2CHO$	3.7×10^{-14}	*Atkinson et al.* [2004]
$Br + C_2H_4 \rightarrow HBr + C_2H_5OO$	1.3×10^{-13}	*Atkinson et al.* [2004]
$Br + C_3H_6 \rightarrow HBr + C_3H_5$	1.60×10^{-12}	*Atkinson et al.* [2004]
$Br + HCHO \rightarrow HBr + CO + HO_2$	6.75×10^{-13}	*Sander et al.* [2006]
$Br + CH_3CHO \rightarrow HBr + CH_3COOO$	2.8×10^{-12}	*Atkinson et al.* [2004]

$Br + C_3H_6O \rightarrow HBr$	9.7×10^{-12}	*Wallington et al.* [1989]
$Br + nButanal \rightarrow HBr$	9.7×10^{-12}	*Michalowski et al.* [2000]
$Br + CH_3OOH \rightarrow HBr + CH_3OO$	4.03×10^{-15}	*Mallard et al.* [1993]
$Br + NO_2 \rightarrow BrNO_2$	6.3×10^{-12}	*Atkinson et al.* [2006]
$Br + NO_2 \leftrightarrow BrONO$	f: 6.3×10^{-12} r: 0.02	*Atkinson et al.* [2006]
		Orlando and Burkholder [2000]
$Br + BrNO_2 \rightarrow Br_2 + NO_2$	5.0×10^{-11}	*Or lando and Burkholder* [2000]
$Br + BrONO \rightarrow Br_2 + NO_2$	1.0×10^{-12}	*Orlando and Burkholder* [2000]
$Br + BrNO_3 \rightarrow Br_2 + NO_3$	4.9×10^{-11}	*Orlando and Tyndall* [1997]
$Br + OClO \rightarrow BrO + ClO$	1.43×10^{-13}	*Atkinson et al.* [2004]
$BrO + O(^3P) \rightarrow Br$	4.8×10^{-11}	*Atkinson et al.* [2004]
$BrO + OH \rightarrow Br + HO_2$	4.93×10^{-11}	*Atkinson et al.* [2004]
$BrO + HO_2 \rightarrow HOBr$	3.38×10^{-11}	*Atkinson et al.* [2004]
$BrO + CH_3OO \rightarrow HOBr + CH_2OO$	4.1×10^{-12}	*Aranda et al.* [1997]
$BrO + CH_3OO \rightarrow Br + HCHO + HO_2$	1.6×10^{-12}	*Aranda et al.* [1997]
$BrO + CH_3COOO \rightarrow Br + CH_3COO$	1.7×10^{-12}	*Michalowski et al.* [2000]
$BrO + C_3H_6O \rightarrow HOBr$	1.5×10^{-14}	*Michalowski et al.* [2000]
$BrO + NO \rightarrow Br + NO_2$	2.48×10^{-11}	*Atkinson et al.* [2004]
$BrO + NO_2 \rightarrow BrNO_3$	1.53×10^{-11}	*Atkinson et al.* [2004]
$BrO + BrO \rightarrow Br + Br$	2.82×10^{-12}	*Sander et al.* [2006]
$BrO + BrO \rightarrow Br_2$	9.3×10^{-13}	*Sander et al.* [2006]
$BrO + HBr \rightarrow HOBr + Br$	2.1×10^{-14}	*Hansen et al.* [1999]
$HBr + OH \rightarrow Br + H_2O$	1.26×10^{-11}	*Sander et al.* [2006]
$CH_3Br + OH \rightarrow H_2O + Br$	1.27×10^{-14}	*Atkinson et al.* [2004]
$CHBr_3 + OH \rightarrow H_2O + Br$	1.2×10^{-13}	*Atkinson et al.* [2004]
$Cl + BrCl \leftrightarrow Br + Cl_2$	f: 1.5×10^{-11} r: 1.1×10^{-15}	*Clyne and Cruse* [1972]
$Cl + Br_2 \leftrightarrow BrCl + Br$	f: 1.2×10^{-10} r: 3.3×10^{-1}	*Clyne and Cruse* [1972]
$BrO + ClO \rightarrow Br + Cl$	7.04×10^{-12}	*Atkinson et al.* [2004]
$BrO + ClO \rightarrow BrCl$	1.15×10^{-12}	*Atkinson et al.* [2004]
$BrO + ClO \rightarrow Br + OClO$	9.06×10^{-12}	*Atkinson et al.* [2004]
$HOBr + OH \rightarrow BrO + H_2O$	5.0×10^{-13}	*Kukui et al.* [1996]
$HOBr + Cl \rightarrow BrCl + OH$	8.0×10^{-11}	*Kukui et al.* [1996]
$HOBr + O(^3P) \rightarrow BrO + OH$	2.12×10^{-11}	*Atkinson et al.* [2004]

Table A.2 Photochemical reactions. J_{max} values for 25 March are shown as an example. J coefficients are expressed in units of s^{-1}.

Reaction	J_{max} **25 March**	**Lifetime**	**Source**
$O_3 + h\nu \rightarrow O_2 + O(^1D)$	3.9×10^{-6}	3.0 days	calculated from OASIS data
$NO_2 + h\nu \rightarrow NO + O(^3P)$	8.6×10^{-3}	1.9 min	calculated from OASIS data
$H_2O_2 + h\nu \rightarrow OH + OH$	3.4×10^{-6}	3.4 days	calculated from OASIS data
$NO_3 + h\nu \rightarrow NO + O_2$	4.5×10^{-2}	22 s	Michalowski et al. [2000]
$N_2O_5 + h\nu \rightarrow NO_2 + NO_3$	1.5×10^{-5}	18 h	calculated from OASIS data
$HONO + h\nu \rightarrow OH + NO$	1.8×10^{-3}	9.2 min	calculated from OASIS data
$HNO_3 + h\nu \rightarrow NO_2 + OH$	1.5×10^{-7}	79 days	calculated from OASIS data
$HNO_4 + h\nu \rightarrow NO_2 + HO_2$	7.3×10^{-7}	16 days	calculated from OASIS data
$HCHO + h\nu \rightarrow HO_2 + HO_2 + CO$	1.5×10^{-5}	19 h	calculated from OASIS data
$HCHO + h\nu \rightarrow CO + H_2$	3.1×10^{-5}	8.8 h	calculated from OASIS data
$CH_3CHO + h\nu \rightarrow CH_3OO + HO_2 + CO$	1.1×10^{-6}	11 days	calculated from OASIS data
$CH_3OOH + h\nu \rightarrow HCHO + HO_2 + OH$	3.2×10^{-6}	3.7 days	calculated from OASIS data
$C3H6O + h\nu \rightarrow HO2 + C2H5OO + CO$	1.4×10^{-6}	8.3 days	calculated from OASIS data
$PAN + h\nu \rightarrow CH_3COOO + NO_2$	1.7×10^{-7}	66 days	calculated from OASIS data
$OClO + h\nu \rightarrow O(^3P) + ClO$	0.12	8.1 s	estimate from *Pöhler et al.* [2010]
$Cl_2 + h\nu \rightarrow Cl + Cl$	2.1×10^{-3}	8.1 min	calculated from OASIS data
$ClO + h\nu \rightarrow Cl + O(^3P)$	2.4×10^{-5}	11 h	calculated from OASIS data
$HOCl + h\nu \rightarrow OH + Cl$	1.4×10^{-4}	2 h	estimate from *Lehrer et al.* [2004]
$ClNO_3 + h\nu \rightarrow Cl + NO_3$	2.9×10^{-5}	9.5 h	calculated from OASIS data
$ClNO_3 + h\nu \rightarrow ClO + NO_2$	3.4×10^{-6}	3.4 days	calculated from OASIS data
$BrNO_3 + h\nu \rightarrow Br + NO_3$	2.1×10^{-4}	1.3 h	calculated from OASIS data
$BrNO_3 + h\nu \rightarrow BrO + NO_2$	1.2×10^{-3}	14.2 min	calculated from OASIS data
$BrO + h\nu \rightarrow Br + O(^3P)$	3.0×10^{-2}	33 s	calculated from OASIS data
$Br_2 + h\nu \rightarrow Br + Br$	4.4×10^{-2}	23 s	calculated from OASIS data
$HOBr + h\nu \rightarrow Br + OH$	2.3×10^{-3}	7.2 min	calculated from OASIS data
$BrNO_2 + h\nu \rightarrow Br + NO_2$	5.7×10^{-3}	2.9 min	estimate from *Scheffler et al.* [1997] & *Landgraf & Crutzen et al.* [1998]
$ClNO_2 + h\nu \rightarrow Cl + NO_2$	4.4×10^{-5}	6.3 h	estimate from *Ganske et al.* [1992]
$BrCl + h\nu \rightarrow Br + Cl$	1.26×10^{-2}	1.3 min	calculated from OASIS data

Table A.3 Mass transfer reactions. All rate constants are expressed in units of s^{-1}.

Reaction	***k* (forward)**	***k* (reverse)**
Particles		
$HCl_{(g)} \rightarrow H^+_{(p)} + Cl^-_{(p)}$	2.58×10^{-3}	
$HBr_{(g)} \rightarrow H^+_{(p)} + Br^-_{(p)}$	1.80×10^{-3}	
$HOCl_{(g)} \rightarrow HOCl_{(p)}$	2.16×10^{-3}	
$HOBr_{(g)} \rightarrow HOBr_{(p)}$	1.26×10^{-3}	
$HOI_{(g)} \rightarrow HOI_{(p)}$	5.42×10^{-4}	
$OH_{(g)} \rightarrow OH_{(p)}$	3.26×10^{-5}	
$O_{3(g)} \leftrightarrow O_{3(p)}$	6.54×10^{-6}	8.76×10^{5}
$Cl_{2(g)} \leftrightarrow Cl_{2(p)}$	2.69×10^{-5}	2.96×10^{7}
$Br_{2(g)} \leftrightarrow Br_{2(p)}$	1.78×10^{-5}	2.97×10^{8}
$BrCl_{(g)} \leftrightarrow BrCl_{(p)}$	6.60×10^{-4}	1.91×10^{10}
$HNO_{3(g)} \rightarrow HNO_{3(p)}$	5.50×10^{-4}	
$N_2O_{5(g)} \rightarrow N_2O_{5(p)}$	1.08×10^{-4}	
$HONO_{(g)} \rightarrow HONO_{(p)}$	1.63×10^{-4}	
$PAN_{(g)} \rightarrow PAN_{(p)}$	2.05×10^{-5}	
$HNO_{4(g)} \rightarrow HNO_{4(p)}$	4.89×10^{-4}	
$ClNO_{2(g)} \rightarrow ClNO_{2(p)}$	1.26×10^{-3}	
$BrNO_{2(g)} \rightarrow BrNO_{2(p)}$	1.26×10^{-3}	
$ClNO_{3(g)} \rightarrow ClNO_{3(p)}$	1.26×10^{-3}	
$BrNO_{3(g)} \rightarrow BrNO_{3(p)}$	1.26×10^{-3}	
Snow		
$HBr_{(g)} \rightarrow H^+_{(s)} + Br^-_{(s)}$	1.67×10^{-5}	
$HCl_{(g)} \rightarrow H^+_{(s)} + Cl^-_{(s)}$	1.67×10^{-5}	
$HOBr_{(g)} \rightarrow HOBr_{(s)}$	1.67×10^{-5}	
$HOCl_{(g)} \rightarrow HOCl_{(s)}$	1.67×10^{-5}	
$OH_{(g)} \rightarrow OH_{(s)}$	1.67×10^{-6}	
$O_{3(g)} \rightarrow O_{3(s)}$	1.67×10^{-6}	
$Cl_{2(g)} \leftrightarrow Cl_{2(s)}$	8.0×10^{-6}	7.71×10^{-2}
$Br_{2(g)} \leftrightarrow Br_{2(s)}$	1.0×10^{-5}	7.71×10^{-2}
$BrCl_{(g)} \leftrightarrow BrCl_{(s)}$	1.25×10^{-5}	7.71×10^{-2}
$HNO_{3(g)} \rightarrow HNO_{3(s)}$	1.67×10^{-5}	
$N_2O_{5(g)} \rightarrow N_2O_{5(s)}$	1.67×10^{-5}	
$HONO_{(g)} \rightarrow HONO_{(s)}$	1.67×10^{-5}	
$PAN_{(g)} \rightarrow PAN_{(s)}$	1.67×10^{-5}	
$HNO_{4(g)} \rightarrow HNO_{4(s)}$	1.67×10^{-5}	
$ClNO_{2(g)} \rightarrow ClNO_{2(s)}$	1.67×10^{-4}	
$BrNO_{2(g)} \rightarrow BrNO_{2(s)}$	1.67×10^{-4}	
$ClNO_{3(g)} \rightarrow ClNO_{3(s)}$	1.67×10^{-4}	
$BrNO_{3(g)} \rightarrow BrNO_{3(s)}$	1.67×10^{-4}	

Table A.4 Aqueous-phase reactions in the model. All aqueous reaction rate constants are converted to units consistent to the gas-phase reactions to be read by the modeling program.

* Third order rate constant, expressed in units of $cm^6 \cdot molecule^{-2} \cdot s^{-1}$
† second order rate constant, expressed in units of $cm^3 \cdot molecule^{-1} \cdot s^{-1}$
‡ first order rate constant, expressed in units of s^{-1}

Reaction	k (actual)	k (particle)	k (snow)	Reference
$Cl^- + HOBr + H^+ \rightarrow BrCl$ *	1.55×10^{-32}	5.17×10^{-21}	9.30×10^{-26}	(Wang et al., 1994)
$Br^- + HOCl + H^+ \rightarrow BrCl$ *	3.59×10^{-36}	1.2×10^{-24}	2.15×10^{-29}	(Sander et al., 1997)
$Br^- + HOBr + H^+ \rightarrow Br_2$ *	4.41×10^{-32}	1.47×10^{-20}	2.64×10^{-25}	(Beckwith et al., 1996)
$Cl^- + HOCl + H^+ \rightarrow Cl_2$ *	6.07×10^{-38}	2.02×10^{-26}	3.63×10^{-31}	(Wang and Margerum, 1994)
$BrCl + Cl^- \rightarrow BrCl_2^-$ †	1×10^{-11}	3.3	5.99×10^{-5}	(Michalowski et al., 2000)
$BrCl_2^- \rightarrow BrCl + Cl^-$ ‡	1.58×10^{9}	1.58×10^{9}	1.58×10^{9}	(Michalowski et al., 2000)
$BrCl + Br^- \rightarrow Br_2Cl^-$ †	1×10^{-11}	3.3	5.99×10^{-5}	(Michalowski et al., 2000)
$Br_2Cl^- \rightarrow BrCl + Br^-$ ‡	3.34×10^{5}	3.34×10^{5}	3.34×10^{5}	(Michalowski et al., 2000, Wang et al., 1994)
$Cl_2 + Br^- \rightarrow BrCl_2^-$ †	1.28×10^{-11}	4.27	7.66×10^{-5}	(Michalowski et al., 2000;Beckwith et al., 1996;Wang et al., 1994)
$BrCl_2^- \rightarrow Cl_2 + Br^-$ ‡	6.94×10^{2}	6.94×10^{2}	6.94×10^{2}	(Michalowski et al., 2000;Wang et al., 1994)
$O_3 + Br^- \rightarrow HOBr$ †	1.35×10^{-20}	4.5×10^{-9}	8.08×10^{-14}	(Michalowski et al., 2000)
$OH + Cl^- \rightarrow HOCl$ †	1.35×10^{-20}	4.5×10^{-9}	8.08×10^{-14}	assumed same as $O_3 + Br^-$
$N_2O_5 + Cl^- \rightarrow ClNO_2$ †	1.66×10^{-12}	5.5×10^{-1}	9.94×10^{-5}	assume diffusion limited
$ClNO_2 + H^+ + Cl^- \rightarrow Cl_2$ †	1.66×10^{-14}	5.5×10^{-3}	9.94×10^{-8}	estimated from (Roberts et al., 2008)
$N_2O_5 + Br^- \rightarrow BrNO_2$ †	1.66×10^{-12}	5.5×10^{-1}	9.94×10^{-5}	assume diffusion limited
$BrNO_2 + H^+ + Br^- \rightarrow Br_2$ †	7.31×10^{-17}	2.44×10^{-5}	4.38×10^{-10}	estimated from (Schweitzer et al., 1998)

Table A.5 Summary of the ambient measurements from OASIS that were used to constrain the model and the instrumental method used. Constrained parameters were input into the model at 10 minute intervals.

Measured Species	Method	Method Reference
O_3 and NO_x	Chemiluminescence	*Ridley et al*. [1992]; *Ryerson et al.* [2000]; *Weinheimer et al*., [1998]
HONO	Long Path Absorption Photometer	*Villena et al.,* [2011]
CO	CO Monitor	
Cl_2 and Br_2	CIMS	*Liao et al*. [2011, 2012]
HCHO	Tunable Diode Laser Absorption Spectroscopy	*Fried et al.*, [2003]; *Lancaster et al.* [2000]
CH_3CHO, CH_3COCH_3, MEK, *n*-C_4H_{10}, *i*-C_4H_{10}	Online GC-MS	*Apel et al.* [2010]
C_2H_2, C_2H_4, C_2H_6, C_3H_8, C_3H_6, *n*-C_4H_{10}, *i*-C_4H_{10}	Canister samples, offline GC-MS	*Russo et al.* [2010]
Photolysis Frequencies	Spectral Actinic Flux Density	*Shetter and Muller et al.* [1999]

References

Apel, E. C., Emmons, L. K., Karl, T., Flocke, F., Hills, A. J., Madronich, S., Lee-Taylor, J., Fried, A., Weibring, P., Walega, J., Richter, D., Tie, X., Mauldin, L., Campos, T., Weinheimer, A., Knapp, D., Sive, B., Kleinman, L., Springston, S., Zaveri, R., Ortega, J., Voss, P., Blake, D., Baker, A., Warneke, C., Welsh-Bon, D., de Gouw, J., Zheng, J., Zhang, R., Rudolph, J., Junkermann, W., and Riemer, D. D.: Chemical evolution of volatile organic compounds in the outflow of the Mexico City Metropolitan area, Atmospheric Chemistry and Physics, 10, 2353-2375, 2010.

Aranda, A., LeBras, G., LaVerdet, G., and Poulet, G.: The BrO+Ch3O2 reaction: Kinetics and role in the atmospheric ozone budget, Geophysical Research Letters, 24, 2745-2748, 10.1029/97gl02686, 1997.

Atkinson, R., Baulch, D. L., Cox, R. A., Crowley, J. N., Hampson, R. F., Hynes, R. G., Jenkin, M. E., Rossi, M. J., and Troe, J.: Evaluated kinetic and photochemical data for atmospheric chemistry: Volume I - gas phase reactions of O-x, HOx, NOx and SOx species, Atmospheric Chemistry and Physics, 4, 1461-1738, 2004.

Beckwith, R. C., Wang, T. X., and Margerum, D. W.: Equilibrium and kinetics of bromine hydrolysis, Inorganic Chemistry, 35, 995-1000, 10.1021/ic950909w, 1996.

Clyne, M. A. A., and Cruse, H. W.: Atomic resonance fluorescence spectrometry for rate constants of rapid bimolecular reactions .1. Reactions O+NO2, Cl+ClNO,Br+CINO, Journal of the Chemical Society-Faraday Transactions Ii, 68, 1281-&, 10.1039/f29726801281, 1972.

DeMore, W. B., Sander, S., Golden, D., Hampson, R., Kurylo, M., Howard, C., Ravishankara, A., Kolb, C., Molina, M., and T, C. I. o.: Jet Propulsion Lab., Pasadena (1997), Chemical kinetics and photochemical data for use in stratospheric modeling, Jet Propulsion Lab., California Inst. of Tech., Pasadena, CA 1997.

Donahue, N. M., Anderson, J. G., and Demerjian, K. L.: New rate constants for ten OH alkane reactions from 300 to 400 K: An assessment of accuracy, Journal of Physical Chemistry A, 102, 3121-3126, 10.1021/jp980532q, 1998.

Eberhard, J., and Howard, C. J.: Temperature-dependent kinetics studies of the reactions of C2H5O2 and n-C3H7O2 radicals with NO, International Journal of Chemical Kinetics, 28, 731-740, 10.1002/(sici)1097-4601(1996)28:10<731::aid-kin3>3.0.co;2-o, 1996.

Eberhard, J., Villalta, P. W., and Howard, C. J.: Reaction of isopropyl peroxy radicals with NO over the temperature range 201-401 K, Journal of Physical Chemistry, 100, 993-997, 10.1021/jp951824j, 1996.

Fried, A., Crawford, J., Olson, J., Walega, J., Potter, W., Wert, B., Jordan, C., Anderson, B., Shetter, R., Lefer, B., Blake, D., Blake, N., Meinardi, S., Heikes, B., O'Sullivan, D.,

Snow, J., Fuelberg, H., Kiley, C. M., Sandholm, S., Tan, D., Sachse, G., Singh, H., Faloona, I., Harward, C. N., and Carmichael, G. R.: Airborne tunable diode laser measurements of formaldehyde during TRACE-P: Distributions and box model comparisons, Journal of Geophysical Research-Atmospheres, 108, 23, 10.1029/2003jd003451, 2003.

Ganske, J. A., Berko, H. N., and Finlaysonpitts, B. J.: Absorption cross-section for gaseous ClNO2 and Cl2 at 298-K - potential organic oxidant source in the marine troposphere, Journal of Geophysical Research-Atmospheres, 97, 7651-7656, 1992.

Hansen, J. C., Li, Y. M., Li, Z. J., and Francisco, J. S.: On the mechanism of the BrO plus HBr reaction, Chemical Physics Letters, 314, 341-346, 10.1016/s0009-2614(99)01093-3, 1999.

Harris, S. J., and Kerr, J. A.: Relative rate measurements of some reactions of hydroxyl radicals with alkanes studied under atmospheric conditions, International Journal of Chemical Kinetics, 20, 939-955, 10.1002/kin.550201203, 1988.

Hooshiyar, P. A., and Niki, H.: Rate constants for the gas-phase reactions of Cl-atoms with C_2-C_8 alkanes at T=296 +/-2K, International Journal of Chemical Kinetics, 27, 1197-1206, 10.1002/kin.550271206, 1995.

Kamboures, M. A., Hansen, J. C., and Francisco, J. S.: A study of the kinetics and mechanisms involved in the atmospheric degradation of bromoform by atomic chlorine, Chemical Physics Letters, 353, 335-344, 10.1016/s0009-2614(01)01439-7, 2002.

Keil, A. D., and Shepson, P. B.: Chlorine and bromine atom ratios in the springtime Arctic troposphere as determined from measurements of halogenated volatile organic compounds, Journal of Geophysical Research-Atmospheres, 111, 11, 10.1029/2006jd007119, 2006.

Kirchner, F., and Stockwell, W. R.: Effect of peroxy radical reactions on the predicted concentrations of ozone, nitrogenous compounds, and radicals, Journal of Geophysical Research-Atmospheres, 101, 21007-21022, 10.1029/96jd01519, 1996.

Kukui, A., Kirchner, U., Benter, T., and Schindler, R. N.: A gaskinetic investigation of HOBr reactions with Cl(P-2), O(P-3) and OH((2)Pi). The reaction of BrCl with OH((2)Pi), Berichte Der Bunsen-Gesellschaft-Physical Chemistry Chemical Physics, 100, 455-461, 1996.

Lancaster, D. G., Fried, A., Wert, B., Henry, B., and Tittel, F. K.: Difference-frequency-based tunable absorption spectrometer for detection of atmospheric formaldehyde, Applied Optics, 39, 4436-4443, 10.1364/ao.39.004436, 2000.

Landgraf, J., and Crutzen, P. J.: An efficient method for online calculations of photolysis and heating rates, Journal of the Atmospheric Sciences, 55, 863-878, 10.1175/1520-0469(1998)055<0863:aemfoc>2.0.co;2, 1998.

Lehrer, E., Honninger, G., and Platt, U.: A one dimensional model study of the mechanism of halogen liberation and vertical transport in the polar troposphere, Atmospheric Chemistry and Physics, 4, 2427-2440, 2004.

Liao, J., Sihler, H., Huey, L., Neuman, J., Tanner, D., Friess, U., Platt, U., Flocke, F., Orlando, J., Shepson, P., Beine, H., Weinheimer, A., Sjostedt, S., Nowak, J., Knapp, D., Staebler, R., Zheng, W., Sander, R., Hall, S., and Ullmann, K.: A comparison of Arctic BrO measurements by chemical ionization mass spectrometry and long path-differential optical absorption spectroscopy, Journal of Geophysical Research-Atmospheres, 116, 10.1029/2010JD014788, 2011.

Liao, J., Huey, L., Tanner, D., Flocke, F., Orlando, J., Neuman, J., Nowak, J., Weinheimer, A., Hall, S., Smith, J., Fried, A., Staebler, R., Wang, Y., Koo, J., Cantrell, C., Weibring, P., Walega, J., Knapp, D., Shepson, P., and Stephens, C.: Observations of inorganic bromine (HOBr, BrO, and Br-2) speciation at Barrow, Alaska, in spring 2009, Journal of Geophysical Research-Atmospheres, 117, 10.1029/2011JD016641, 2012.

Lightfoot, P. D., Cox, R. A., Crowley, J. N., Destriau, M., Hayman, G. D., Jenkin, M. E., Moortgat, G. K., and Zabel, F.: Organic peroxy-radicals - kinetics, spectroscopy and tropospheric chemistry, Atmospheric Environment Part a-General Topics, 26, 1805-1961, 10.1016/0960-1686(92)90423-i, 1992.

Lurmann, F. W., Lloyd, A. C., and Atkinson, R.: A chemical mechanism for use in long-range transport acid deposition computer modeling, Journal of Geophysical Research-Atmospheres, 91, 905-936, 10.1029/JD091iD10p10905, 1986.

Mallard, W. G., Westley, F., Herron, J. T., Hampson, R. F., and Frizzel, D. H.: NIST Chemical Kinetics Database: Version 5.0 National Institute of Standards and Technology, Gaithersburg, MD. , 1993.

Michalowski, B., Francisco, J., Li, S., Barrie, L., Bottenheim, J., and Shepson, P.: A computer model study of multiphase chemistry in the Arctic boundary layer during polar sunrise, Journal of Geophysical Research-Atmospheres, 105, 15131-15145, 10.1029/2000JD900004, 2000.

Nicovich, J. M., and Wine, P. H.: Kinetics of the reactions of O(3P) and Cl(2P) with HBr and Br2, International Journal of Chemical Kinetics, 22, 379-397, 10.1002/kin.550220406, 1990.

Orlando, J. J., and Tyndall, G. S.: Rate coefficients for the thermal decomposition of BrONO2 and the heat of formation of BrONO2, Journal of Physical Chemistry, 100, 19398-19405, 10.1021/jp9620274, 1996.

Orlando, J. J., and Burkholder, J. B.: Identification of BrONO as the major product in the gas-phase reaction of Br with NO2, Journal of Physical Chemistry A, 104, 2048-2053, 10.1021/jp993713g, 2000.

Pohler, D., Vogel, L., Friess, U., and Platt, U.: Observation of halogen species in the Amundsen Gulf, Arctic, by active long-path differential optical absorption spectroscopy, Proceedings of the National Academy of Sciences of the United States of America, 107, 6582-6587, 10.1073/pnas.0912231107, 2010.

Ravishankara, A. R., Smith, G. J., and Davis, D. D.: A kinetics study of the reaction of Cl with NO_2, International Journal of Chemical Kinetics, 20, 811-814, 10.1002/kin.550201005, 1988.

Ravishankara, A. R., Dunlea, E. J., Blitz, M. A., Dillon, T. J., Heard, D. E., Pilling, M. J., Strekowski, R. S., Nicovich, J. M., and Wine, P. H.: Redetermination of the rate coefficient for the reaction of O(D-1) with N-2, Geophysical Research Letters, 29, 4, 10.1029/2002gl014850, 2002.

Ridley, B. A., Grahek, F. E., and Walega, J. G.: A small, high-sensitivity, medium-response ozone detector suitable for measurements from light aircraft, Journal of Atmospheric and Oceanic Technology, 9, 142-148, 10.1175/1520-0426(1992)009<0142:ashsmr>2.0.co;2, 1992.

Roberts, J. M., Osthoff, H. D., Brown, S. S., and Ravishankara, A. R.: N2O5 oxidizes chloride to Cl-2 in acidic atmospheric aerosol, Science, 321, 1059-1059, 10.1126/science.1158777, 2008.

Russo, R. S., Zhou, Y., White, M. L., Mao, H., Talbot, R., and Sive, B. C.: Multi-year (2004-2008) record of nonmethane hydrocarbons and halocarbons in New England: seasonal variations and regional sources, Atmospheric Chemistry and Physics, 10, 4909-4929, 10.5194/acp-10-4909-2010, 2010.

Ryerson, T. B., Williams, E. J., and Fehsenfeld, F. C.: An efficient photolysis system for fast-response NO2 measurements, Journal of Geophysical Research-Atmospheres, 105, 26447-26461, 10.1029/2000jd900389, 2000.

Sander, R., and Crutzen, P. J.: Model study indicating halogen activation and ozone destruction in polluted air masses transported to the sea, Journal of Geophysical Research-Atmospheres, 101, 9121-9138, 10.1029/95jd03793, 1996.

Sander, R., Vogt, R., Harris, G., and Crutzen, P.: Modeling the chemistry ozone, halogen compounds, and hydrocarbons in the arctic troposphere during spring, Tellus Series B-Chemical and Physical Meteorology, 49, 522-532, 10.1034/j.1600-0889.49.issue5.8.x, 1997.

Sander, S. P., Golden, D., Kurylo, M., Moortgat, G., Wine, P., Ravishankara, A., Kolb, C., Molina, M., Finlayson-Pitts, B., and Huie, R.: Chemical kinetics and photochemical data for use in atmospheric studies evaluation number 15 2006.

Scheffler, D., Grothe, H., Willner, H., Frenzel, A., and Zetzsch, C.: Properties of pure nitryl bromide. Thermal behavior, UV/Vs and FTIR spectra, and photoisomerization to trans-BrONO in an argon matrix, Inorganic Chemistry, 36, 335-338, 10.1021/ic9606946, 1997.

Schweitzer, F., Mirabel, P., and George, C.: Multiphase chemistry of N2O5, ClNO2, and BrNO2, Journal of Physical Chemistry A, 102, 3942-3952, 10.1021/jp980748s, 1998.

Shetter, R. E., and Muller, M.: Photolysis frequency measurements using actinic flux spectroradiometry during the PEM-Tropics mission: Instrumentation description and some results, Journal of Geophysical Research-Atmospheres, 104, 5647-5661, 10.1029/98jd01381, 1999.

Tsalkani, N., Mellouki, A., Poulet, G., Toupance, G., and Lebras, G.: Rate constants measurements for the reactions of OH and Cl with peroxyacetyl nitrate at 298 K, Journal of Atmospheric Chemistry, 7, 409-419, 10.1007/bf00058713, 1988.

Tyndall, G. S., Orlando, J. J., Wallington, T. J., Dill, M., and Kaiser, E. W.: Kinetics and mechanisms of the reactions of chlorine atoms with ethane, propane, and n-butane, International Journal of Chemical Kinetics, 29, 43-55, 1997.

Vakhtin, A. B., Murphy, J. E., and Leone, S. R.: Low-temperature kinetics of reactions of OH radical with ethene, propene, and 1-butene, Journal of Physical Chemistry A, 107, 10055-10062, 10.1021/jp030230a, 2003.

Villena, G., Wiesen, P., Cantrell, C., Flocke, F., Fried, A., Hall, S., Hornbrook, R., Knapp, D., Kosciuch, E., Mauldin, R., McGrath, J., Montzka, D., Richter, D., Ullmann, K., Walega, J., Weibring, P., Weinheimer, A., Staebler, R., Liao, J., Huey, L., and Kleffmann, J.: Nitrous acid (HONO) during polar spring in Barrow, Alaska: A net source of OH radicals?, Journal of Geophysical Research-Atmospheres, 116, 10.1029/2011JD016643, 2011.

Wallington, T. J., Skewes, L. M., Siegl, W. O., Wu, C. H., and Japar, S. M.: Gas phase reaction of Cl atoms with a series of oxygenated organic species at 295 K, International Journal of Chemical Kinetics, 20, 867-875, 10.1002/kin.550201105, 1988.

Wallington, T. J., Skewes, L. M., Siegl, W. O., and Japar, S. M.: A relative rate study of the reaction of bromine atoms with a variety of organic compounds at 295 K, International Journal of Chemical Kinetics, 21, 1069-1076, 10.1002/kin.550211108, 1989.

Wang, T. X., Kelley, M. D., Cooper, J. N., Beckwith, R. C., and Margerum, D. W.: Equilibrium, Kinetic, and UV-Spectral Characteristics of Aqueous Bromine Chloride, Bromine, and Chlorine Species, Inorganic Chemistry, 33, 5872-5878, 10.1021/ic00103a040, 1994.

Wang, T. X., and Margerum, D. W.: Kinetics of Reversible Chlorine Hydrolysis: Temperature Dependence and General-Acid/Base-Assisted Mechanisms, Inorganic Chemistry, 33, 1050-1055, 10.1021/ic00084a014, 1994.

Weinheimer, A. J., Montzka, D. D., Campos, T. L., Walega, J. G., Ridley, B. A., Donnelly, S. G., Keim, E. R., Del Negro, L. A., Proffitt, M. H., Margitan, J. J., Boering, K. A., Andrews, A. E., Daube, B. C., Wofsy, S. C., Anderson, B. E., Collins, J. E., Sachse, G. W., Vay, S. A., Elkins, J. W., Wamsley, P. R., Atlas, E. L., Flocke, F., Schauffler, S., Webster, C. R., May, R. D., Loewenstein, M., Podolske, J. R., Bui, T. P., Chan, K. R., Bowen, S. W., Schoeberl, M. R., Lait, L. R., and Newman, P. A.: Comparison between DC-8 and ER-2 species measurements in the tropical middle troposphere: NO, NOy, O-3, CO2, CH4, and N2O, Journal of Geophysical Research-Atmospheres, 103, 22087-22096, 10.1029/98jd01421, 1998.

Wine, P. H., Wells, J. R., and Nicovich, J. M.: Kinetics of the reaction of F(2P) and Cl(2P) with HNO_3, Journal of Physical Chemistry, 92, 2223-2228, 10.1021/j100319a028, 1988.

VITA

VITA

Kyle D. Custard was born in Allegany, NY in December, 1987 to Judith and David Custard. He grew up in rural New York spending his time exploring the outdoors, hunting, and fishing. He worked various jobs throughout his teenage years where he obtained an array of skills along with developing a strong work ethic. He graduated from Allegany-Limestone High School in 2006, and then enrolled in St. John Fisher College where he majored in Chemistry.

During his time at St. John Fisher College he was a member of both the football team and the club ice hockey team. He additionally conducted research under the advisory of Dr. Kimberly Chichester, which fostered his interest in environmental research. He graduated with honors in 2010 with a B.S. in Chemistry as his graduating classes' treasurer. As suggested by his undergraduate advisor he applied to Purdue University for a PhD in analytical chemistry.

There he joined Prof. Paul Shepson's group, as the group's Arctic based research peaked his interest. During his tenure at Purdue he went to the Arctic twice to carry out research. Having the opportunity to perform research in such a difficult environment strengthened his desire to obtain a career that involves the outdoors.

PUBLICATION

(submitted for publication)

The NO_x dependence of bromine chemistry in the Arctic atmospheric boundary layer

Kyle D. Custard[1], Chelsea R. Thompson[1,2], Kerri A. Pratt[1,3], Paul B. Shepson[1,4], Jin Liao[5,6,7], L. Gregory Huey[5], John J. Orlando[8], Andrew J. Weinheimer[8], Eric Apel[8], Samuel R. Hall[8], Frank Flocke[8], Lee Mauldin[8], Rebecca S. Hornbrook[8], Denis Pöhler[9], Stephan General[9], Johannes Zielcke[9], William R. Simpson[10], Ulrich Platt[9], Alan Fried[2], Peter Weibring[2], Barkley C. Sive[11,12], Kirk Ullmann[8],Christopher Cantrell[8], D.J. Knapp[8], D. D. Montzka[8]

1. Department of Chemistry, Purdue University, West Lafayette, IN USA
2. Institute of Arctic and Alpine Research, University of Colorado, Boulder, CO USA
3. Department of Chemistry, University of Michigan, Ann Arbor, MI USA
4. Department of Earth, Atmospheric, and Planetary Sciences & Purdue Climate Change Research Center, Purdue University, West Lafayette, IN USA
5. School of Earth and Atmospheric Sciences, Georgia Institute of Technology, Atlanta, GA USA
6. Cooperative Institute for Research in Environmental Sciences, University of Colorado Boulder, Boulder, CO USA
7. Earth System Research Laboratory, National Oceanic and Atmospheric Administration, Boulder, CO USA
8. National Center for Atmospheric Research, Boulder, CO USA
9. Institute of Environmental Physics, University of Heidelberg, Heidelberg, Germany
10. Geophysical Institute and Department of Chemistry, University of Alaska Fairbanks, Fairbanks, AK USA,
11. Institute for the Study of Earth, Oceans, and Space, University of New Hampshire, Durham, NH USA
12. Now at National Park Service, Air Resources Division, Lakewood, CO USA

Abstract

Arctic boundary layer nitrogen oxides ($NO_x = NO_2 + NO$) are naturally produced in and released from the sunlit snowpack and range between 10 to 100 pptv in the remote background surface layer air. These nitrogen oxides have significant effects on the

partitioning and cycling of reactive radicals such as halogens and HO_x (OH + HO_2). However, little is known about the impacts of local anthropogenic NO_x emission sources on gas-phase halogen chemistry in the Arctic, and this is important because these emissions can induce large variability in ambient NO_x and thus local chemistry. In this study, a zero-dimensional photochemical kinetics model was used to investigate the influence of NO_x on the unique springtime halogen and HO_x chemistry in the Arctic. Trace gas measurements obtained during the 2009 OASIS (Ocean-Atmosphere-Sea Ice-Snowpack) field campaign at Barrow, AK were used to constrain many model inputs. We find that elevated NO_x significantly impedes gas-phase radical chemistry, through the production of a variety of reservoir species, including HNO_3, HO_2NO_2, peroxyacetyl nitrate (PAN), $BrNO_2$, $ClNO_2$ and reductions in BrO and HOBr, with a concomitant, decreased net O_3 loss rate. The effective removal of BrO by anthropogenic NO_x was directly observed from measurements conducted near Prudhoe Bay, AK during the 2012 Bromine, Ozone, and Mercury Experiment (BROMEX). Thus, while changes in snow-covered sea ice attributable to climate change may alter the availability of molecular halogens for ozone and Hg depletion, predicting the impact of climate change on polar atmospheric chemistry is complex and must take into account the simultaneous impact of changes in the distribution and intensity of anthropogenic combustion sources. This is especially true for the Arctic, where NO_x emissions are expected to increase because of increasing oil and gas extraction and shipping activities.

1 Introduction

The episodic depletion of O_3 in the Arctic boundary layer following polar sunrise, referred to as ozone depletion events (ODEs), is attributed to a bromine gas phase reaction scheme, propagated by cycles such as R1-R3 (Simpson et al., 2007;McConnell et al., 1992).

$$Br_2 + h\nu \rightarrow 2Br \qquad \text{R1}$$

$$2Br + 2O_3 \rightarrow 2BrO + 2O_2 \qquad \text{R2}$$

$$BrO + BrO \rightarrow 2Br/Br_2 + O_2 \qquad \text{R3}$$

Ambient measurements at various Arctic sites have revealed maximum BrO mole ratios between 30 to 40 pptv in the springtime (Liao et al., 2012;Pohler et al., 2010). However, modeling studies have shown that heterogeneous chemistry at the surface is needed to facilitate enhanced reactive halogen levels and drive ODEs (Toyota et al., 2014;Thomas et al., 2012;Michalowski et al., 2000), and recent field observations demonstrated that Br_2 is photochemically produced within the surface snowpack (Pratt et al., 2013;Foster et al., 2001). This heterogeneous chemistry mechanism, known as the "bromine explosion", is dependent on reactions involving HO_x (Wennberg, 1999;Tang and McConnell, 1996;Vogt et al., 1996;Fan and Jacob, 1992) to produce hypohalous acids, which then oxidize halide ions at reactive surfaces (Huff and Abbatt, 2002;Abbatt, 1994).

$$BrO + HO_2 \rightarrow HOBr + O_2 \qquad \text{R4}$$

$HOBr \rightarrow HOBr_{(aq)}$ R5

$HOBr_{(aq)} + Br^-_{(aq)} + H^+_{(aq)} \rightarrow Br_{2(aq)} + H_2O$ R6

$Br_{2(aq)} \rightarrow Br_{2(g)}$ R7

Although gas-phase halogen chemistry in the Arctic has now been studied for several decades (Impey et al., 1997;Hausmann and Platt, 1994;Barrie et al., 1988), few studies have examined the effect of atmospheric NO_x on these halogen chemical cycles. Model studies have shown that NO_x can react with halogen radicals through several reactions (as shown in R8 – R12), to produce inorganic halogen nitrates or nitryl halides, which can, in turn, activate further halogen chemistry through heterogeneous reactions (Cao et al., 2014;Toyota et al., 2013;Morin et al., 2012;Thomas et al., 2012;Morin et al., 2007;Evans et al., 2003;Aguzzi and Rossi, 2002;von Glasow et al., 2002;Aguzzi and Rossi, 1999;Thorn et al., 1993), and thereby alter gas phase halogen radical reaction pathways.

$XO + NO_2 \rightarrow XONO_2$ R8

$XO + NO \rightarrow X + NO_2$ R9

$X + NO_2 \rightarrow XNO_2$ R10

$XONO_2 \rightarrow XONO_{2(aq)}$ R11

$XONO_{2(aq)} + H_2O \rightarrow HOX + HNO_3$ R12

Reaction 8 can directly influence the bromine explosion, as lab studies have shown that gas phase $BrONO_2$ can hydrolyze on acidic surfaces to form HOBr, as shown in Reaction 12 (X=Br) (Hanson, 2003;Aguzzi and Rossi, 2002;Hanson et al., 1996). Thus, while reactions involving NO_x can terminate the gas phase radical chain reaction, they can also generate products that contribute to the bromine explosion. Thus, it is not intuitively obvious what impact(s) NO_x ultimately has on halogen chemistry. These halogen reaction pathways are summarized in Figure 1 (Abbatt et al., 2012;Grannas et al., 2007;Simpson et al., 2007). As illustrated in Figure 1, elevated levels of NO_x can impact the halogen cycle through a variety of reactions. However, the sensitivity of the halogen radical chain reaction to NO_x is currently not well understood.

The Arctic boundary layer typically has ambient background levels of NO_x between 10 to 100 pptv resulting from its isolation from major anthropogenic sources, with its primary sources being photochemical production within the snowpack (Villena et al., 2011;Honrath et al., 2002;Ridley et al., 2000), and long range transport of photolyzable species such as organic nitrates (Muthuramu et al., 1994). Arctic field studies have led to observations of NO_x fluxes from sun-lit snow surfaces (Grannas et al., 2007;Ridley and Orlando, 2003;Beine et al., 2002;Honrath et al., 2002;Honrath et al., 1999), and lab studies have demonstrated that frozen solutions of nitrate and nitrite can release NO_x when irradiated with UV light (Dubowski et al., 2002;Dubowski et al., 2001;Honrath et al., 2000).

$$NO_3^- + h\nu \rightarrow NO_2 + O^- \qquad \text{R13}$$

$$NO_2^- + h\nu \rightarrow NO + O^- \qquad \text{R14}$$

With the possibility of increased anthropogenic sources throughout the Arctic, e.g. from coastal development, shipping, and oil and gas exploration, the impacts of increased NO_x are likely to be seen (Peters et al., 2011;Corbett et al., 2010). For this study we investigated the effect of elevated NO_x mole ratios on Arctic halogen radical chemistry, using a zero-dimensional (0-D) photochemical model, constrained by recent observations of a wide variety of relevant precursors and intermediates, during the Ocean-Atmosphere-Sea Ice-Snowpack (OASIS) 2009 campaign conducted at Barrow, AK. To complement the model studies, observational evidence of the impact of NO_x on BrO is shown for aircraft measurements near Prudhoe Bay, AK during the 2012 Bromine, Ozone, and Mercury Experiment (BROMEX).

2 Model Description

A 0-D photochemical model was developed using the modeling software FACSIMILE. The model has been described in detail by Thompson et al. (2014) and is described briefly here. The model includes known Arctic gas-phase chemistry with 189 gas-phase reactions (Table S1) and 28 photolysis reactions (Table S2). The deposition of 19 gas-phase species to aerosols/snow surfaces (Table S3) and 16 aqueous-phase chemical reactions (Table S4) are also included, where the heterogeneous reactions are treated as aqueous reactions. The model is constrained to observations with time varying mole ratios for a list of gas-phase species (Table S5), including halogen radical precursors (Cl_2 and Br_2) and a wide range of volatile organic compounds (C_2H_2, C_2H_4, C_2H_6, C_3H_8, C_3H_6, *n*-C_4H_{10}, *i*-C_4H_{10}, HCHO, CH_3CHO, CH_3OCH_3, and methyl ethyl ketone), as well as

calculated, time varying photolysis rates, from the field study OASIS (Ocean-Atmosphere-Sea Ice- Snowpack) in Barrow, AK. Mole ratios of constrained gas-phase species along with the photolysis rates were called into the model every 10 minutes within the simulation. For this model study, the ten day period from March 24-April 2, 2009 during OASIS 2009 was simulated. During this period, a three-day ozone depletion event (O_3 <5 pbbv) occurred, followed by a full ozone recovery (O_3 >20 pbbv) that was due to vertical mixing (discussed in Section 3.1), and thus, covers a full range of atmospheric and meteorological conditions. It should be noted that the constrained mole ratio for Br_2 on March 30th and 31st in the model is based on the observed diurnal average of March 29th and April 1st. As discussed in Liao et al. (2012) atmospheric observations for Br_2 on March 30th and 31st were not available.

To investigate the role that atmospheric NO_x plays in Arctic halogen chemistry, two different NO_x simulation scenarios were performed. A "Low NO_x" case and a "High NO_x" case were used to create the two different scenarios. This allowed us to isolate a single variable between the two simulations. However, this approach does not consider other chemical species (i.e. VOCs) that could also be elevated along with anthropogenic NO_x. The two diurnal-cycle NO_x profiles were derived from the actual observed NO_x over the time period being simulated, as shown in Figure 2. Representative average polluted (high) and clean (low) NO_x diurnal cycles, which differ by about a factor of 15, were calculated based on observed local NO_x mole ratio data for the period (Figure 2). The clean (low NO_x) and polluted (high NO_x) days during the 10 day (March 24 to April 2) period studied were selected based on the work of Villena et al. (2011), in which

correlations with ambient CO enhancements were used to identify air masses influenced by local emissions (2011). The non-influenced/background days were averaged together to calculate a "low NO_x" diurnal average that ranged between 50 to 100 pptv. These values were in the range of previous observations of background NO_x mole ratios (Villena et al., 2011;Honrath et al., 2002;Ridley et al., 2000). The same was done for the days influenced by local anthropogenic emissions, to create the "high NO_x" diurnal average characterized by NO_x mole ratios from 700 to 1600 pptv. Each diurnal average was fit to a curve to generate temporally smoothed profiles. During the 10 day simulation either the Low NO_x or High NO_x diurnal average was applied to each day of the simulation, to generate the two distinct model scenarios. This allowed us to evaluate the NO_x-dependence of the chemistry, since it was the only parameter altered between the two scenarios.

Molecular halogens respond to changes in the deposition rates and condensed-phase chemistry, the latter of which cannot be well simulated given the current state of knowledge of the snowpack, and physical and chemical processes occurring therein (Domine et al., 2013). Therefore, to ensure proper representation of the gas phase halogen chemistry, the atmospheric molecular halogen (Br_2 and Cl_2) mole ratios were constrained to observations. The observations for these species reflect the impact of NO_x-dependent production of reactive reservoir species, and the impact of their deposition to and chemistry within the snowpack. While the model was constrained to observations for stable species (Table S5), it was used to calculate various radical species' (e.g., BrO and Br) mole ratios given the sources and sinks of these radicals. In

this way, we calculate the effective NO_x-dependence of the radical chemistry and rate of ozone depletion, as discussed below.

3 Results

3.1 Bromine Chain Length

The chain length for a radical chain reaction is the rate of propagation divided by the rate of termination (or initiation). A chain length of < 1 means that most of the radicals terminate after production. Here we calculate the bromine radical chain length (ϕ) for the interconversion of Br and BrO radicals using Equation 1 (Thompson et al., 2014) for the 10 day simulation.

$$\phi = \frac{\begin{pmatrix} 2k[BrO]^2+k[BrO][ClO]+k[BrO][CH_3OO]+k[BrO][OH]+ \\ k[BrO][O(^3P)]+k[BrO][CH_3COOO]+k[BrO][NO]+J[BrO] \end{pmatrix}}{\begin{pmatrix} k[Br][HO_2]+k[Br][C_2H_2]+k[Br][C_2H_4]+k[Br][C_3H_6]+ \\ k[Br][HCHO]+k[Br][NO_2](0.15)+k[Br][CH_3CHO]+ \\ k[Br][C_3H_6O]+k[Br][C_4H_8O]+k[Br][CH_3OOH]+ \\ k[BrO][HO_2]+k[BrO][CH_3OO]+k[BrO][C_3H_6)]+ \\ k[BrO][NO_2] \end{pmatrix}} \qquad (1)$$

Termination reactions include those that form non-radical brominated species (e.g., HBr, HOBr, $BrONO_2$), with photochemical lifetimes substantially longer than that of BrO or Br. It should be noted that although production of certain species represents a termination of the gas phase Br chain reaction (e.g. HOBr and $BrONO_2$), they can also play a crucial role in producing and increasing the Br radicals available for reacting with ozone, either through photolysis or heterogeneous reactions. This emphasizes the complexity of the BrO_x cycle that takes place in the Arctic. In Equation 1 the Br + NO_2

reaction is multiplied by the branching ratio (0.15) for the production of $BrNO_2$ (Orlando and Burkholder, 2000). Orlando and Burkholder (2000) observed that the dominant product for NO_2 reaction with a Br atom is BrONO, and while at lower temperatures isomerization to $BrNO_2$ is possible, the overall yield would still be minor (2000). The production of BrONO is not considered a sink for BrO_x because of its rapid thermal decomposition, photolysis and reaction with Br radicals, regenerating BrO_x (Burkholder and Orlando, 2000;Orlando and Burkholder, 2000). The bromine chain length was only calculated during daylight hours (10:00 to 18:00 AKST) because the bromine radical chain is photochemically initiated via the photolysis of Br_2 (R1). The bromine radical chain length was calculated throughout the entire 10 day simulation for both the low and high NO_x simulations, as shown in Figure 3.

Both the low NO_x and high NO_x simulations show a chain length dependence on ozone mole ratio (Figure 3), with generally higher chain lengths at high O_3, due to reaction R2. When the O_3 mole ratio is >5ppbv, the average low NO_x bromine chain length was 1.72 (±0.70), while the average high NO_x bromine chain length was 1.81 (±0.35). The shorter simulated bromine chain lengths (<1.0) on March 26, 27, 28, and 31 can be explained by the low O_3 mole ratio (<5ppbv). One might hypothesize that the high NO_x simulation would yield a shorter bromine chain length because NO_x acts as a sink for BrO_x. Indeed, the model simulation shows that NO_x, on a percentage basis, is a more dominant sink for BrO_x during the high NO_x simulation compared to the low NO_x simulation (Figure 4). While the Br+NO_2 reaction occurs more frequently (by a factor of 5) during the high NO_x case, the BrO+NO_2 reaction is actually 7% more important as a

sink in the low NO_x simulation. The reaction of HO_2+BrO additionally influences the results of the bromine chain length in that it occurs more frequently, by a factor of 170, during the low NO_x simulation. This is due to the suppression of HO_2 in the high NO_x simulation via Reactions R15 and R16.

$$NO + HO_2 \rightarrow NO_2 + OH \qquad \text{R15}$$

$$OH + NO_2 \rightarrow HNO_3 \qquad \text{R16}$$

One point of interest is the much larger bromine chain length on March 25th, when ozone was partially depleted (<15ppbv), compared to other days with partially depleted ozone (March 30th and April 1st). On this day a very large NO_x plume (~15ppbv) from the town of Barrow was observed compared to the relatively low NO_x conditions observed on March 30th and April 1st. This enhanced bromine chain length can be explained by the fact that we constrain the model to observed Br_2. If the polluted plume also contains HOBr and $BrONO_2$ as important temporary halogen reservoirs, then the flux of Br_2 (e.g. via R6 and R12) from the reactive surfaces would increase, thereby increasing BrO. Spikes were observed for both HOBr and BrO for March 25th (Discussed in Section 3.3), which may indicate such a situation. The rate of reaction R3 is quadratic in BrO mole ratio, and, as discussed by Thompson et al. (2014), and indicated in Equation 1, the observed chain length increases with BrO mole ratio.

3.2 Net O_3 Loss Rate

Although the bromine chain length is relatively unchanged between the two scenarios, high levels of NO_x decrease the rate of net O_3 loss within the model. The net O_3 loss rate was calculated in Equation 2 as the sum of all of the rates of reactions that destroy ozone minus the sum of the rates that produce ozone (Thompson et al., 2014). It should be noted that the reactions in Equation 2 that "produce" ozone are included as offsets for the depleted ozone destruction rate, which includes XO and NO_2 photolysis.

$$\text{Net } O_3 \text{ Loss Rate} = \begin{pmatrix} k[Br][O_3] + k[Cl][O_3] + k[O(^1D)][H_2O] \\ + k[OH][O_3] + k[HO_2][O_3] - k[BrO][NO] \\ - J[BrO] - k[ClO][NO] - J[ClO] \end{pmatrix} \quad (2)$$

Reaction counters were utilized for all the HO_2/RO_2 + NO reactions for both NO_x scenarios to determine the importance of those reactions towards O_3 production. The two different NO_x cases yielded equal numerical values when the counters were summed, indicating NO_x didn't influence these reactions. The calculated net O_3 loss rate for both NO_x scenarios is shown in Figure 5. On average, the net O_3 loss rate is a factor of two times slower for the polluted NO_x simulation compared with the low NO_x simulation. To study this effect further, we calculated the net O_3 destruction rate as a function of NO_x mole ratio by conducting simulations with a wide range of NO_x mole ratios. The various NO_x diurnal cycles were calculated by starting with the low NO_x diurnal profile and step-wise increasing the NO_x by 250 pptv until the diurnal maximum of 2000 pptv was reached. The results, for the period 11:00-13:00 on March 30, are shown in Figure 6. March 30th was selected because it fell into the "clean day" category during OASIS and during a time when ozone was decreasing from 30 to 5 pbbv. As shown in Figure 6, the

net O_3 loss rate decreases steeply, by a factor of 1.5 (from 0.80 to 0.52 ppbv/hr), during the increase of NO_x mole ratios of ~100 – 500 pptv, clearly expressing the strong NO_x-dependence of the chain reaction. We note, however, that this model experiment is directly testing the gas-phase component of this sensitivity on NO_x, and not the NO_x dependence of $BrONO_2$ deposition. However, as discussed later, when NO_x increases, BrO decreases and thus $BrONO_2$ is not sensitive to the NO_x mole ratio. This does not negate the potential importance of $BrONO_2$ during ODEs. Cao et al (2014) found, from a modeling study, that $BrONO_2$ production increased the rate of ozone depletion through the production of HOBr from its hydrolysis (R12) on snow/aerosol surfaces. HOBr is a main component of the bromine explosion and leads to an increased production rate of Br_2 (R5-6). However, regression of the observed [Br_2] vs observed [NO_x] reveals that the highest mole ratios of Br_2 do in fact occur when NO_x is below 300 pptv (Figure S1). This observed Br_2 clearly supports that the O_3 loss rate is minimized when NO_x mole ratios are elevated, as the maximum Br atom production rates will occur at low [NO_x]. The net ozone loss is, of course, also extremely low for days when the observed mole ratios of O_3 were very small (<5pbbv), as the rate of ozone destruction will approach zero as O_3 is nearly completely removed. Based on the results from Figures 5 and 6, the influence that elevated NO_x mole ratios have on decreasing the net ozone loss rate could be a factor in the Arctic as NO_x point sources continue to increase in remote Arctic locations.

The O_3 loss rate for March 30 from 11:00 to 13:00, based on the observations, was approximately 3.4 ppbv/hr. This is much larger than the calculated net O_3 loss rate for

the low NO_x simulation of 0.80 ppbv/hr. The low net O_3 loss rate for the low NO_x simulation could be a result of the constrained model Br_2 mole ratio not being representative of the ambient air in Barrow at that time; as mentioned previously. If we constrained Br_2 to an estimated concentration lower than what was actually present during that time, we would expect a decreased depletion rate. This belief is furthered supported by a comparison of the BrO data for this time period (discussed later). However, this apparent dramatic ozone loss rate could be the observation of an ozone-depleted air mass being transported to the measurement site (Halfacre et al., 2013).

3.3 Model-Simulated Species vs. OASIS 2009 Observations

To further understand both how NO_x decreases the rate of net O_3 loss and affects the bromine chain length, several species that play a crucial role in the bromine cycle were examined. Molecular bromine and its precursors are produced from R6 and R12. The prominent gas-phase recycling reaction is BrO self-reaction (R3) while the formation and subsequent deposition of HOBr and $BrONO_2$ leads to heterogeneous reactions that can form Br_2 (R5-R12). Here we simulated the effect of the low and high NO_x scenarios on BrO, HOBr and $BrONO_2$, and compared the results with the observed mole ratios during OASIS (Figure 7A-C). For the majority of the days, simulated BrO for the low NO_x case is close to that observed during OASIS, as expected since low NO_x conditions were typically observed. However, this is not the case for March 30th and 31st, for which the simulated BrO is lower than what was observed during OASIS. This is likely a result of the fact that atmospheric observations for Br_2 on March 30th and 31st were not available,

as discussed earlier. For those days the constrained Br_2 was a diurnal average of March 29 and April 1st Br_2 observations. The high NO_x simulation results in a highly suppressed BrO mole ratio (Figure 7A), compared to the low NO_x simulation, by more than an order of magnitude throughout the time period. For the high NO_x case, BrO never exceeds 3 pptv, whereas for the low NO_x case, BrO ranges from 2.5 to 25 pptv. For high NO_x days, the BrO mole ratios are low because of reactions R8 and R10, in which BrO and Br radicals are scavenged by NO_x.

HOBr responds in similar fashion to changes in NO_x as does BrO, with the low NO_x simulated HOBr being within ± 5pptv of the OASIS observations while the high NO_x simulated HOBr is much lower. Occasionally the low NO_x simulation HOBr is slightly elevated compared to the observed HOBr (March 26 & 29) because the low NO_x simulation has a greater HO_2 mole ratio compared to the observations.

Figure 7B shows that the high NO_x condition completely suppresses HOBr, and that is what is observed for the high NO_x mole ratios day, March 24th. However, in contrast to the case for BrO and HOBr, $BrONO_2$ is not suppressed by high NO_x mole ratios (Fig. 7C), since while increased NO_x suppresses BrO, the rate of R8 is compensated by the increase in NO_x mole ratios, therefore R8 is largely unchanged. This is shown in Figure 7C as the $BrONO_2$ mole ratio is similar for both the high and low NO_x simulations. Additionally, when the model simulated $BrONO_2$ mole ratio for both NO_x simulations is plotted against the $BrONO_2$ production rate ($k_{BrO+NO2}[BrO][NO_2]$), it affirms that the $BrONO_2$ mole ratios follow $k_{BrO+NO2}[BrO][NO_2]$ (Figure S2).

3.4 BrO_x and NO_x Sinks

It is clear from the discussions above that NO_x influences BrO_x partitioning. The sinks of BrO_x and NO_x were quantified to evaluate their NO_x-dependence by including reaction counters on the relevant reactions in the model that convert BrO_x and NO_x to reservoir species. Over the 10-day simulation period for both low and high NO_x cases, NO_x is a significant sink for BrO_x radicals (>27%), although for the high NO_x case it contributes more than 50% (Figure 4). However, both products of R8 and R10 result in species that can regenerate Br_2. As expected, CH_3CHO plays a major role as a BrO_x sink as well (Shepson et al., 1996), contributing to more than >35% in both simulations. Though anthropogenic emissions are known sources of acetaldehyde, observed CH_3CHO mixing ratios were unaffected by Barrow emissions throughout the 10 day simulation period. Thus it is likely that the snowpack is the dominant CH_3CHO source in this study (Grannas et al., 2002). For NO_x, while reactions with HO_2 are important (~20%), reactions of NO_2 with Br and BrO still represent significant NO_x sinks (~30%). Peroxynitrates result from an important sink pathway of NO_2, e.g. via R17 and R18, below. R17 will be the subject of a separate study.

$$HO_2 + NO_2 \leftrightarrow HO_2NO_2 \qquad \text{R17}$$

$$CH_3O_2 + NO_2 \leftrightarrow CH_3O_2NO_2 \qquad \text{R18}$$

4 BROMEX 2012 Field Observations

To further examine the interactions between NO_x and reactive bromine, NO_2 and BrO were measured within and around a large combustion plume in the coastal Arctic atmosphere. During the spring 2012 Bromine, Ozone, and Mercury Experiment (BROMEX) field campaign in Barrow, Alaska, airborne measurements of BrO and NO_2 column density (from ~700 m to the surface) were conducted using an aircraft-mounted MAX-DOAS (General et al., 2014) in nadir view. The results for the derived BrO and NO_2 differential slant column density (DSCD), the integrated mole ratio along a vertical line, for a section of a flight on March 30 near Prudhoe Bay, AK, are shown in Figure 8. Prudhoe Bay is the largest oil field on the North Slope, located ~330 km southeast of Barrow, AK, and produces significant CO_2, NO_x, and CH_4 (Brooks et al., 1997;Jaffe et al., 1995). Anthropogenic emission plumes can easily be observed from the flight by increased NO_2 column density. This is a good example of the type of point source that is increasing in prevalence in the Arctic (Roiger et al., 2014;Harsem et al., 2011). It can be seen from Figure 8 that an increase in the column density of atmospheric NO_2, corresponding to a plume near Prudhoe Bay, coincided with a decrease in the column density of atmospheric BrO. The BrO mole ratio suppression is further expressed in the Figure 8 insert that shows a plot of BrO vs NO_2 DSCD. This can be explained by R8 and R10 and supports our findings that BrO is suppressed by elevated levels of NO_x (Figure 7A). Thus, while $BrONO_2$ and $BrNO_2$ can be recycled on surfaces to re-emit Br_2, it seems clear that the net effect of high NO_x mole ratios is to slow down the overall halogen chain chemistry, as demonstrated in Figures 8 and S1. It should be noted that in

very large NO_x plumes O_3 can be removed by the reaction of NO with O_3, as shown in Reaction 19, although in day light, a photosteady state will develop from NO_2 photolysis.

$$NO + O_3 \rightarrow NO_2 + O_2 \qquad R19$$

If no ozone is present the BrO_x can repartition from BrO towards Br, via photolysis of BrO. During the March 30, 2012 flight the air mass depleted of BrO also had lower ambient O_3 mole ratios which could explain the BrO depletion.

In Prudhoe Bay, the sources of NO_x are buoyant plumes, located aloft of the surface (smoke stacks), where natural aerosol extinction would be less compared to the surface (Breider et al., 2014). This would limit the availability of surfaces on which $BrONO_2$ could react to re-emit Br_2. However, these NO_x sources also produce aerosols (data not shown)(Peters et al., 2011); if these sources continue to increase in number, a shift in the aerosol extinction could occur, providing increased available aerosol surfaces for reaction of $BrONO_2$.

5 Atmospheric Implications

It is clear that elevated levels of atmospheric NO_x have a significant effect on the atmospheric chemistry that occurs in the Arctic relating to halogen species. With the possibility of more anthropogenic sources appearing in the Arctic as sea ice area continues to decrease, due to gas and oil exploration and increased shipping traffic, a shift in the atmospheric oxidation capacity and chemical pathways could occur. The main springtime atmospheric oxidizers could change from halogens in the surface layer to a greater contribution from OH via O_3 photolysis, via R20, along with a potential decrease in the frequency of ODEs. Further, open water produces convective mixing, bringing O_3

from aloft down to the surface (Moore et al., 2014). However, the climate change impacts on the Arctic atmosphere and associated chemistry are complex. As multiyear ice retreats, the fraction of first year ice is increasing, leading to more saline ice surfaces. However, the findings of Pratt et al. (2013) indicate that the surface snowpack on the sea ice needs to be acidified for halogen activation to occur, and this likely depends on the depth of the snowpack, which is impacted by snowfall rates and timing, as well as the presence of sea ice. It is now known that snowpack depths in the Beaufort and Chukchi seas have been decreasing at a significant rate (Webster et al., 2014). The acidification of the surface snow also depends on long range transport of acidic species, such as SO_2 and HNO_3 (Worthy et al., 1994), which are likely to change. Moreover, increasing latent heat fluxes (Serreze and Barry, 2011) resulting from more open water will increase the OH production rate in the Arctic because of the humidity dependence of ozone photolysis as shown in Reactions 18-20, although a significant increase in humidity would be needed for Reactions 20-22 to have an impact on Arctic OH production.

$$O_3 + h\nu \rightarrow O(^1D) + O_2 \qquad \text{R20}$$

$$O(^1D) + H_2O \rightarrow 2OH \qquad \text{R21}$$

$$O(^1D) + M \rightarrow O(^3P) + M^* \qquad \text{R22}$$

Thus, there are multiple competing variables that influence Arctic atmospheric chemistry, and it is surely the case that we will need to continue to integrate simulations with observations to understand the coupling of physical and chemical processes, as the Arctic continues to warm and undergo change at the surface. Finally, we note that the deposition rates and aqueous phase chemistry for the products from the reaction between atmospheric NO_x and halogen radicals are not well known, and fluxes of molecular

halogens from Arctic surface snow have not been measured to date. Thus further efforts in this area are necessary to gain a greater understanding of these chemical processes to improve models.

Acknowledgements

Financial support was provided by the National Science Foundation Office of Polar Programs (ARC-1107695). K.A. Pratt was supported by a National Science Foundation Postdoctoral Fellowship in Polar Regions Research (ARC-1103423). The author thanks the organizers of the OASIS 2009 field campaign along with all the researchers who contributed to the campaign.

References

Abbatt, J. P. D.: Heterogeneous reaction of HOBr with HBr and HCl on ice surfaces at 228-K, Geophysical Research Letters, 21, 665-668, 10.1029/94gl00775, 1994.

Abbatt, J. P. D., Thomas, J. L., Abrahamsson, K., Boxe, C., Granfors, A., Jones, A. E., King, M. D., Saiz-Lopez, A., Shepson, P. B., Sodeau, J., Toohey, D. W., Toubin, C., von Glasow, R., Wren, S. N., and Yang, X.: Halogen activation via interactions with environmental ice and snow in the polar lower troposphere and other regions, Atmospheric Chemistry and Physics, 12, 6237-6271, 10.5194/acp-12-6237-2012, 2012.

Aguzzi, A., and Rossi, M. J.: The kinetics of the heterogeneous reaction of BrONO2 with solid alkali halides at ambient temperature. A comparison with the interaction of ClONO2 on NaCl and KBr, Physical Chemistry Chemical Physics, 1, 4337-4346, 10.1039/a904611i, 1999.

Aguzzi, A., and Rossi, M. J.: Heterogeneous hydrolysis and reaction of BrONO2 and Br2O on pure ice and ice doped with HBr, Journal of Physical Chemistry A, 106, 5891-5901, 10.1021/jp014383e, 2002.

Barrie, L., Bottenheim, J., Schnell, R., Crutzen, P., and Rasmsssen, R.: Ozone Destruction and Photochemical-Reactions at Polar Sunrise in the Lower Arctic Atmosphere, Nature, 334, 138-141, 10.1038/334138a0, 1988.

Beine, H., Honrath, R., Domine, F., Simpson, W., and Fuentes, J.: NOx during background and ozone depletion periods at Alert: Fluxes above the snow surface, Journal of Geophysical Research-Atmospheres, 107, 10.1029/2002JD002082, 2002.

Breider, T. J., Mickley, L. J., Jacob, D. J., Wang, Q. Q., Fisher, J. A., Chang, R. Y. W., and Alexander, B.: Annual distributions and sources of Arctic aerosol components, aerosol optical depth, and aerosol absorption, Journal of Geophysical Research-Atmospheres, 119, 4107-4124, 2014.

Brooks, S. B., Crawford, T. L., and Oechel, W. C.: Measurement of carbon dioxide emissions plumes from Prudhoe Bay, Alaska oil fields, Journal of Atmospheric Chemistry, 27, 197-207, 10.1023/a:1005890318796, 1997.

Burkholder, J. B., and Orlando, J. J.: UV absorption cross-sections of cis-BrONO, Chemical Physics Letters, 317, 603-608, 10.1016/s0009-2614(99)01412-8, 2000.

Cao, L., Sihler, H., Platt, U., and Gutheil, E.: Numerical analysis of the chemical kinetic mechanisms of ozone depletion and halogen release in the polar troposphere, Atmospheric Chemistry and Physics, 14, 3771-3787, 10.5194/acp-14-3771-2014, 2014.

Corbett, J. J., Lack, D. A., Winebrake, J. J., Harder, S., Silberman, J. A., and Gold, M.: Arctic shipping emissions inventories and future scenarios, Atmospheric Chemistry and Physics, 10, 9689-9704, 10.5194/acp-10-9689-2010, 2010.

Dubowski, Y., Colussi, A. J., and Hoffmann, M. R.: Nitrogen dioxide release in the 302 nm band photolysis of spray-frozen aqueous nitrate solutions. Atmospheric implications, Journal of Physical Chemistry A, 105, 4928-4932, 10.1021/jp0042009, 2001.

Dubowski, Y., Colussi, A. J., Boxe, C., and Hoffmann, M. R.: Monotonic increase of nitrite yields in the photolysis of nitrate in ice and water between 238 and 294 K, Journal of Physical Chemistry A, 106, 6967-6971, 10.1021/jp0142942, 2002.

Evans, M. J., Jacob, D. J., Atlas, E., Cantrell, C. A., Eisele, F., Flocke, F., Fried, A., Mauldin, R. L., Ridley, B. A., Wert, B., Talbot, R., Blake, D., Heikes, B., Snow, J., Walega, J., Weinheimer, A. J., and Dibb, J.: Coupled evolution of BrOx-ClOx-HOx-NOx chemistry during bromine-catalyzed ozone depletion events in the arctic boundary layer, Journal of Geophysical Research-Atmospheres, 108, 12, 10.1029/2002jd002732, 2003.

Fan, S., and Jacob, D.: Surface Ozone Depletion in Arctic Spring Sustained by Bromine Reactions on Aerosols, Nature, 359, 522-524, 10.1038/359522a0, 1992.

Foster, K., Plastridge, R., Bottenheim, J., Shepson, P., Finlayson-Pitts, B., and Spicer, C.: The role of Br-2 and BrCl in surface ozone destruction at polar sunrise, Science, 291, 471-474, 10.1126/science.291.5503.471, 2001.

General, S., Pöhler, D., Sihler, H., Bobrowski, N., Frieß, U., Zielcke, J., Horbanski, M., Shepson, P. B., Stirm, B. H., Simpson, W. R., Weber, K., Fischer, C., and Platt, U.: The Heidelberg Airborne Imaging DOAS Instrument (HAIDI) – a novel Imaging DOAS device for 2-D and 3-D imaging of trace gases and aerosols, Atmos. Meas. Tech. Discuss., 7, 2187-2257, 10.5194/amtd-7-2187-2014, 2014.

Grannas, A., Shepson, P., Guimbaud, C., Sumner, A., Albert, M., Simpson, W., Domine, F., Boudries, H., Bottenheim, J., Beine, H., Honrath, R., and Zhou, X.: A study of photochemical and physical processes affecting carbonyl compounds in the Arctic atmospheric boundary layer, Atmospheric Environment, 36, 2733-2742, 10.1016/S1352-2310(02)00134-6, 2002.

Grannas, A. M., Jones, A. E., Dibb, J., Ammann, M., Anastasio, C., Beine, H. J., Bergin, M., Bottenheim, J., Boxe, C. S., Carver, G., Chen, G., Crawford, J. H., Domine, F., Frey, M. M., Guzman, M. I., Heard, D. E., Helmig, D., Hoffmann, M. R., Honrath, R. E., Huey, L. G., Hutterli, M., Jacobi, H. W., Klan, P., Lefer, B., McConnell, J., Plane, J., Sander, R., Savarino, J., Shepson, P. B., Simpson, W. R., Sodeau, J. R., von Glasow, R., Weller, R., Wolff, E. W., and Zhu, T.: An overview of snow photochemistry: evidence, mechanisms and impacts, Atmospheric Chemistry and Physics, 7, 4329-4373, 2007.

Halfacre, J. W., Knepp, T. N., Shepson, P. B., Stephens, C. R., Pratt, K. A., Li, B., Peterson, P. K., Walsh, S. J., Simpson, W. R., Matrai, P. A., Bottenheim, J. W., Netcheva, S., Perovich, D. K., and Richter, A.: Temporal and spatial characteristics of ozone depletion events from measurements in the Arctic, Atmos. Chem. Phys. Discuss., 13, 30233-30285, 10.5194/acpd-13-30233-2013, 2013.

Hansen, J. C., Li, Y. M., Li, Z. J., and Francisco, J. S.: On the mechanism of the BrO plus HBr reaction, Chemical Physics Letters, 314, 341-346, 10.1016/s0009-2614(99)01093-3, 1999.

Hanson, D., Ravishankara, A., and Lovejoy, E.: Reaction of BrONO2 with H2O on submicron sulfuric acid aerosol and the implications for the lower stratosphere, Journal of Geophysical Research-Atmospheres, 101, 9063-9069, 10.1029/96JD00347, 1996.

Hanson, D.: Reactivity of BrONO2 and HOBr on sulfuric acid solutions at low temperatures, Journal of Geophysical Research-Atmospheres, 108, 10.1029/2002JD002519, 2003.

Harsem, O., Eide, A., and Heen, K.: Factors influencing future oil and gas prospects in the Arctic, Energy Policy, 39, 8037-8045, 10.1016/j.enpol.2011.09.058, 2011.

Hausmann, M., and Platt, U.: Spectroscopic measurement of bromine oxide and ozone in the high arctic during Polar Sunrise Experiment 1992, Journal of Geophysical Research-Atmospheres, 99, 25399-25413, 10.1029/94jd01314, 1994.

Honrath, R. E., Peterson, M. C., Guo, S., Dibb, J. E., Shepson, P. B., and Campbell, B.: Evidence of NOx production within or upon ice particles in the Greenland snowpack, Geophysical Research Letters, 26, 695-698, 10.1029/1999gl900077, 1999.

Honrath, R. E., Guo, S., Peterson, M. C., Dziobak, M. P., Dibb, J. E., and Arsenault, M. A.: Photochemical production of gas phase NOx from ice crystal NO3, Journal of Geophysical Research-Atmospheres, 105, 24183-24190, 10.1029/2000jd900361, 2000.

Honrath, R. E., Lu, Y., Peterson, M. C., Dibb, J. E., Arsenault, M. A., Cullen, N. J., and Steffen, K.: Vertical fluxes of NOx, HONO, and HNO3 above the snowpack at Summit, Greenland, Atmospheric Environment, 36, 2629-2640, 10.1016/s1352-2310(02)00132-2, 2002.

Huff, A. K., and Abbatt, J. P. D.: Kinetics and product yields in the heterogeneous reactions of HOBr with ice surfaces containing NaBr and NaCl, Journal of Physical Chemistry A, 106, 5279-5287, 10.1021/jp014296m, 2002.

Impey, G., Shepson, P., Hastie, D., Barrie, L., and Anlauf, K.: Measurements of photolyzable chlorine and bromine during the Polar sunrise experiment 1995, Journal of Geophysical Research-Atmospheres, 102, 16005-16010, 10.1029/97JD00851, 1997.

Jaffe, D. A., Honrath, R. E., Furness, D., Conway, T. J., Dlugokencky, E., and Steele, L. P.: A determination of the CH_4, NO_x, and CO_2 emissions from the Prudhoe Bay, Alaska oil development, Journal of Atmospheric Chemistry, 20, 213-227, 10.1007/bf00694494, 1995.

Liao, J., Huey, L., Tanner, D., Flocke, F., Orlando, J., Neuman, J., Nowak, J., Weinheimer, A., Hall, S., Smith, J., Fried, A., Staebler, R., Wang, Y., Koo, J., Cantrell, C., Weibring, P., Walega, J., Knapp, D., Shepson, P., and Stephens, C.: Observations of inorganic bromine (HOBr, BrO, and Br-2) speciation at Barrow, Alaska, in spring 2009, Journal of Geophysical Research-Atmospheres, 117, 10.1029/2011JD016641, 2012.

McConnell, J., Henderson, G., Barrie, L., Bottenheim, J., Niki, H., Langford, C., and Templeton, E.: Photochemical Bromine Production Implicated in Arctic Boundary-Layer Ozone Depletion, Nature, 355, 150-152, 10.1038/355150a0, 1992.

Michalowski, B., Francisco, J., Li, S., Barrie, L., Bottenheim, J., and Shepson, P.: A computer model study of multiphase chemistry in the Arctic boundary layer during polar sunrise, Journal of Geophysical Research-Atmospheres, 105, 15131-15145, 10.1029/2000JD900004, 2000.

Moore, C. W., Obrist, D., Steffen, A., Staebler, R. M., Douglas, T. A., Richter, A., and Nghiem, S. V.: Convective forcing of mercury and ozone in the Arctic boundary layer induced by leads in sea ice, Nature, 506, 81-84, 10.1038/nature12924, 2014.

Morin, S., Savarino, J., Bekki, S., Gong, S., and Bottenheim, J. W.: Signature of Arctic surface ozone depletion events in the isotope anomaly (Delta O-17) of atmospheric nitrate, Atmospheric Chemistry and Physics, 7, 1451-1469, 2007.

Morin, S., Erbland, J., Savarino, J., Domine, F., Bock, J., Friess, U., Jacobi, H. W., Sihler, H., and Martins, J. M. F.: An isotopic view on the connection between photolytic emissions of NOx from the Arctic snowpack and its oxidation by reactive halogens, Journal of Geophysical Research-Atmospheres, 117, 15, 10.1029/2011jd016618, 2012.

Muthuramu, K., Shepson, P. B., Bottenheim, J. W., Jobson, B. T., Niki, H., and Anlauf, K. G.: Relationships Between Organic Nitrates and Surface Ozone Destruction During Polar Sunrise Experiment 1992, Journal of Geophysical Research-Atmospheres, 99, 25369-25378, 10.1029/94jd01309, 1994.

Orlando, J. J., and Tyndall, G. S.: Rate coefficients for the thermal decomposition of BrONO2 and the heat of formation of BrONO2, Journal of Physical Chemistry, 100, 19398-19405, 10.1021/jp9620274, 1996.

Orlando, J. J., and Burkholder, J. B.: Identification of BrONO as the major product in the gas-phase reaction of Br with NO2, Journal of Physical Chemistry A, 104, 2048-2053, 10.1021/jp993713g, 2000.

Peters, G. P., Nilssen, T. B., Lindholt, L., Eide, M. S., Glomsrod, S., Eide, L. I., and Fuglestvedt, J. S.: Future emissions from shipping and petroleum activities in the Arctic, Atmospheric Chemistry and Physics, 11, 5305-5320, 10.5194/acp-11-5305-2011, 2011.

Pohler, D., Vogel, L., Friess, U., and Platt, U.: Observation of halogen species in the Amundsen Gulf, Arctic, by active long-path differential optical absorption spectroscopy, Proceedings of the National Academy of Sciences of the United States of America, 107, 6582-6587, 10.1073/pnas.0912231107, 2010.

Pratt, K., Custard, K., Shepson, P., Douglas, T., Pohler, D., General, S., Zielcke, J., Simpson, W., Platt, U., Tanner, D., Huey, L., Carlsen, M., and Stirm, B.: Photochemical production of molecular bromine in Arctic surface snowpacks, Nature Geoscience, 6, 351-356, 10.1038/NGEO1779, 2013.

Ridley, B., Walega, J., Montzka, D., Grahek, F., Atlas, E., Flocke, F., Stroud, V., Deary, J., Gallant, A., Boudries, H., Bottenheim, J., Anlauf, K., Worthy, D., Sumner, A., Splawn, B., and Shepson, P.: Is the Arctic surface layer a source and sink of NOx in winter/spring?, Journal of Atmospheric Chemistry, 36, 1-22, 10.1023/A:1006301029874, 2000.

Ridley, B. A., Grahek, F. E., and Walega, J. G.: A small, high-sensitivity, medium-response ozone detector suitable for measurements from light aircraft, Journal of Atmospheric and Oceanic Technology, 9, 142-148, 10.1175/1520-0426(1992)009<0142:ashsmr>2.0.co;2, 1992.

Ridley, B. A., and Orlando, J. J.: Active nitrogen in surface ozone depletion events at alert during spring 1998, Journal of Atmospheric Chemistry, 44, 1-22, 10.1023/a:1022188822920, 2003.

Roiger, A., Thomas, J. L., Schlager, H., Law, K. S., Kim, J., Schäfler, A., Weinzierl, B., Dahlkötter, F., Krisch, I., Marelle, L., Minikin, A., Raut, J. C., Reiter, A., Rose, M., Scheibe, M., Stock, P., Baumann, R., Bouarar, I., Clerbaux, C., George, M., Onishi, T., and Flemming, J.: “Quantifying emerging local anthropogenic emissions in the Arctic region: the ACCESS aircraft campaign experiment”, Bulletin of the American Meteorological Society, 10.1175/BAMS-D-13-00169.1, 2014.

Serreze, M. C., and Barry, R. G.: Processes and impacts of Arctic amplification: A research synthesis, Global and Planetary Change, 77, 85-96, 10.1016/j.gloplacha.2011.03.004, 2011.

Shepson, P. B., Sirju, A. P., Hopper, J. F., Barrie, L. A., Young, V., Niki, H., and Dryfhout, H.: Sources and sinks of carbonyl compounds in the arctic ocean boundary layer: Polar ice floe experiment, Journal of Geophysical Research-Atmospheres, 101, 21081-21089, 10.1029/96jd02032, 1996.

Simpson, W., von Glasow, R., Riedel, K., Anderson, P., Ariya, P., Bottenheim, J., Burrows, J., Carpenter, L., Friess, U., Goodsite, M., Heard, D., Hutterli, M., Jacobi, H., Kaleschke, L., Neff, B., Plane, J., Platt, U., Richter, A., Roscoe, H., Sander, R., Shepson, P., Sodeau, J., Steffen, A., Wagner, T., and Wolff, E.: Halogens and their role in polar boundary-layer ozone depletion, Atmospheric Chemistry and Physics, 7, 4375-4418, 2007.

Steffen, A., Bottenheim, J., Cole, A., Douglas, T., Ebinghaus, R., Friess, U., Netcheva, S., Nghiem, S., Sihler, H., and Staebler, R.: Atmospheric mercury over sea ice during the OASIS-2009 campaign, Atmospheric Chemistry and Physics, 13, 7007-7021, 10.5194/acp-13-7007-2013, 2013.

Tang, T., and McConnell, J.: Autocatalytic release of bromine from Arctic snow pack during polar sunrise, Geophysical Research Letters, 23, 2633-2636, 10.1029/96GL02572, 1996.

Thomas, J., Dibb, J., Huey, L., Liao, J., Tanner, D., Lefer, B., von Glasow, R., and Stutz, J.: Modeling chemistry in and above snow at Summit, Greenland - Part 2: Impact of snowpack chemistry on the oxidation capacity of the boundary layer, Atmospheric Chemistry and Physics, 12, 6537-6554, 10.5194/acp-12-6537-2012, 2012.

Thompson, C., Shepson, P., Liao, J., Huey, G., Apel, E., Cantrell, C., Flocke, F., Fried, A., Hall, S., Hornbrook, R., Knapp, D. J., Mauldin III, R., Montzka, D., Sive, B., Ullman, K., Weibring, P., and Weinheimer, A.: Interactions of bromine, chlorine, and iodine photochemistry during ozone depletions in Barrow, Alaska, Atmospheric Chemistry and Physics, *Submitted*, 2014.

Thorn, R. P., Daykin, E. P., and Wine, P. H.: Kinetics of the BrO+NO2 association reaction. Temperature and pressure dependence in the falloff regime, International Journal of Chemical Kinetics, 25, 521-537, 10.1002/kin.550250703, 1993.

Toyota, K., Dastoor, A. P., and Ryzhkov, A.: Air-snowpack exchange of bromine, ozone and mercury in the springtime Arctic simulated by the 1-D model PHANTAS – Part 2: Mercury and its speciation, Atmos. Chem. Phys. Discuss., 13, 22151-22220, 10.5194/acpd-13-22151-2013, 2013.

Toyota, K., McConnell, J. C., Staebler, R. M., and Dastoor, A. P.: Air-snowpack exchange of bromine, ozone and mercury in the springtime Arctic simulated by the 1-D model PHANTAS - Part 1: In-snow bromine activation and its impact on ozone, Atmospheric Chemistry and Physics, 14, 4101-4133, 10.5194/acp-14-4101-2014, 2014.

Villena, G., Wiesen, P., Cantrell, C., Flocke, F., Fried, A., Hall, S., Hornbrook, R., Knapp, D., Kosciuch, E., Mauldin, R., McGrath, J., Montzka, D., Richter, D., Ullmann, K., Walega, J., Weibring, P., Weinheimer, A., Staebler, R., Liao, J., Huey, L., and Kleffmann, J.: Nitrous acid (HONO) during polar spring in Barrow, Alaska: A net source

of OH radicals?, Journal of Geophysical Research-Atmospheres, 116, 10.1029/2011JD016643, 2011.

Vogt, R., Crutzen, P., and Sander, R.: A mechanism for halogen release from sea-salt aerosol in the remote marine boundary layer, Nature, 383, 327-330, 10.1038/383327a0, 1996.

von Glasow, R., Sander, R., Bott, A., and Crutzen, P.: Modeling halogen chemistry in the marine boundary layer - 1. Cloud-free MBL, Journal of Geophysical Research-Atmospheres, 107, 10.1029/2001JD000942, 2002.

Webster, M. A., Rigor, I. G., Nghiem, S. V., Kurtz, N. T., Farrell, S. L., Perovich, D. K., and Sturm, M.: Interdecadal changes in snow depth on Arctic sea ice, Journal of Geophysical Research-Oceans, 119, 5395-5406, 10.1002/2014jc009985, 2014.

Wennberg, P.: Atmospheric chemistry - Bromine explosion, Nature, 397, 299-+, 10.1038/16805, 1999.

Worthy, D. E. J., Trivett, N. B. A., Hopper, J. F., Bottenheim, J. W., and Levin, I.: Analysis of long-range transport events at Alert, Northwest Territories, during the Polar Sunrise Experiment, Journal of Geophysical Research-Atmospheres, 99, 25329-25344, 10.1029/94jd01209, 1994.

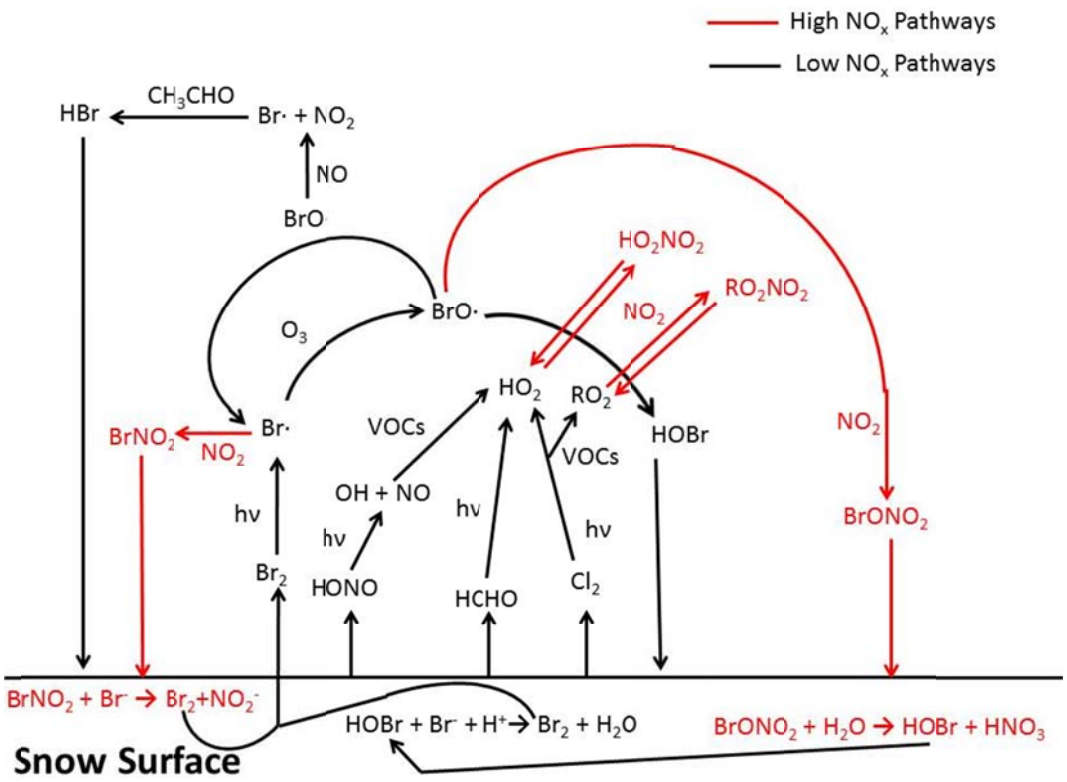

Figure 1. Halogen cycle in the Arctic boundary layer with (red trace) and without (black trace) the influence of anthropogenic NO_x (Abbatt et al., 2012;Simpson et al., 2007;Grannas et al., 2007).

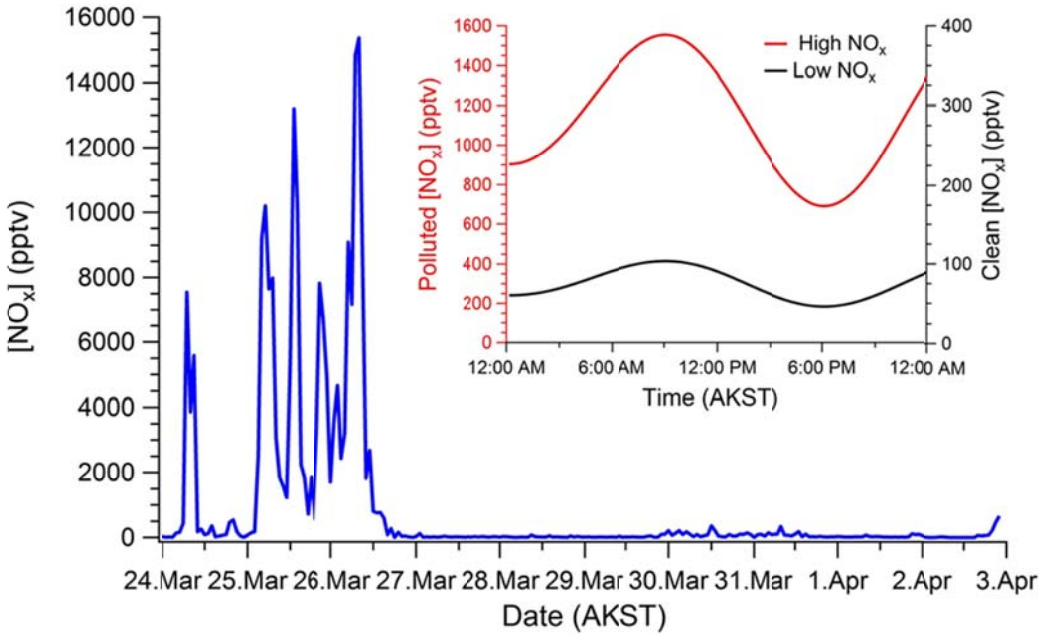

Figure 2. Observed (blue) NO_x mole ratios for the 10-day OASIS period in Barrow, AK, as well as model scenario diurnal NO_x mole ratios for low (black) and high (red) cases.

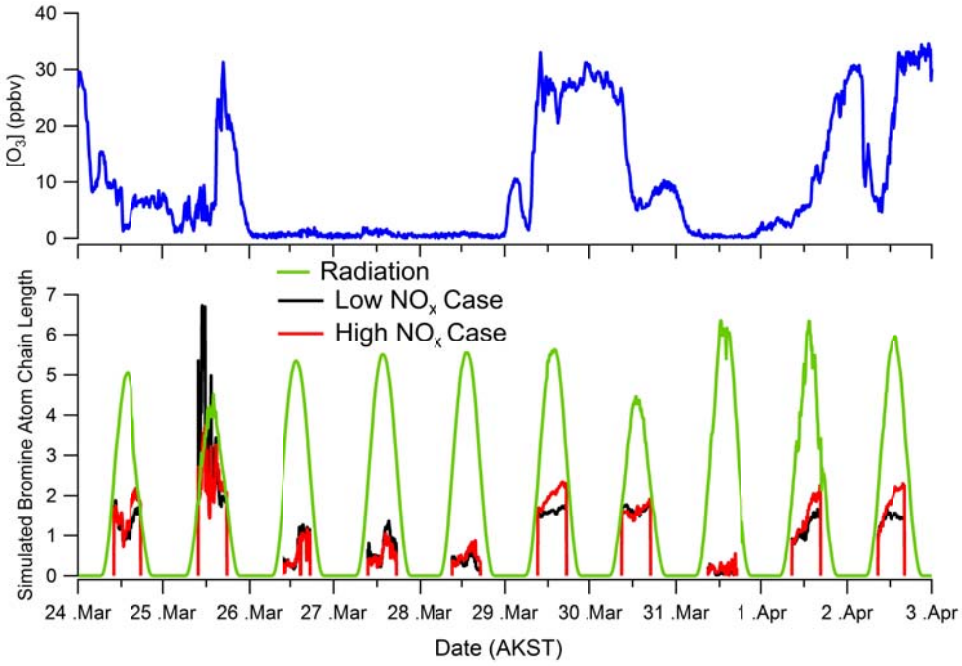

Figure 3. Calculated bromine chain length for the low NO_x simulation and the high NO_x simulation along with observed O_3 and radiation.

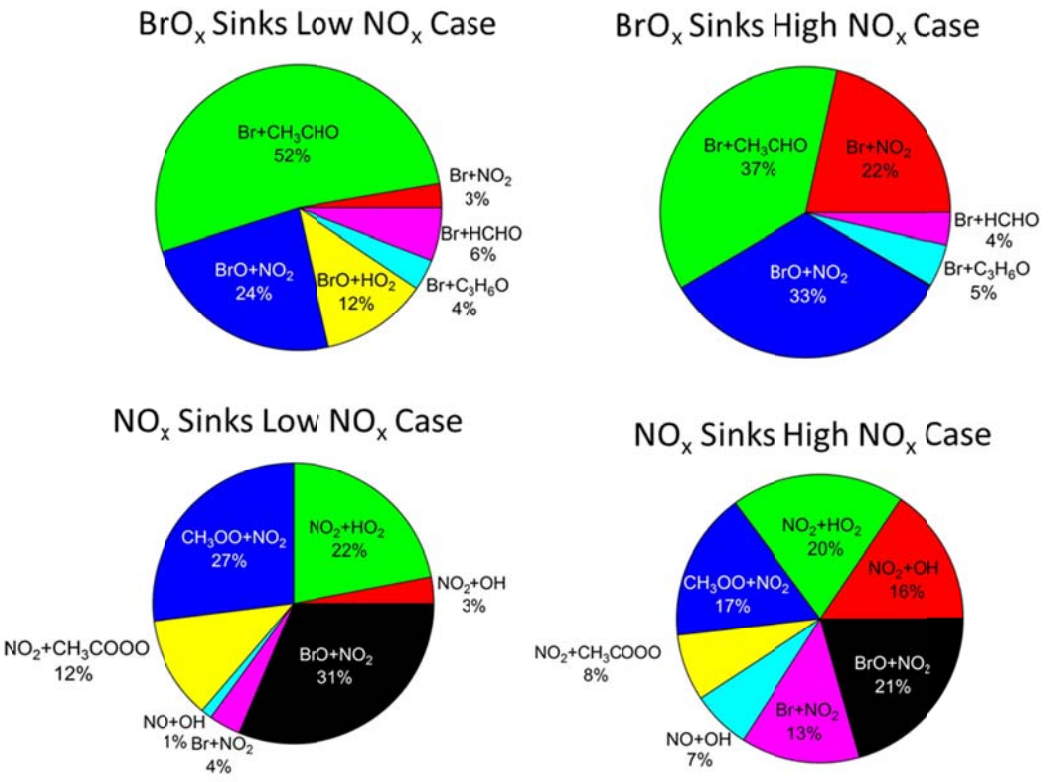

Figure 4. Fractional contributions of BrO_x and NO_x sink reactions from the low and high NO_x simulation cases.

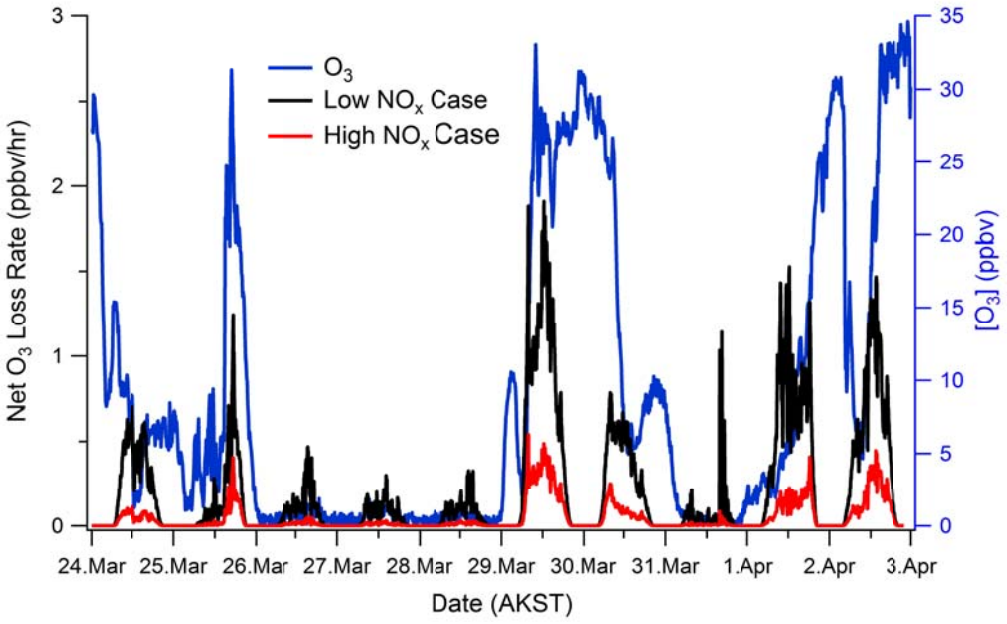

Figure 5. Calculated net O_3 loss rate for the low NO_x and high NO_x simulations, along with the observed O_3 mole ratios.

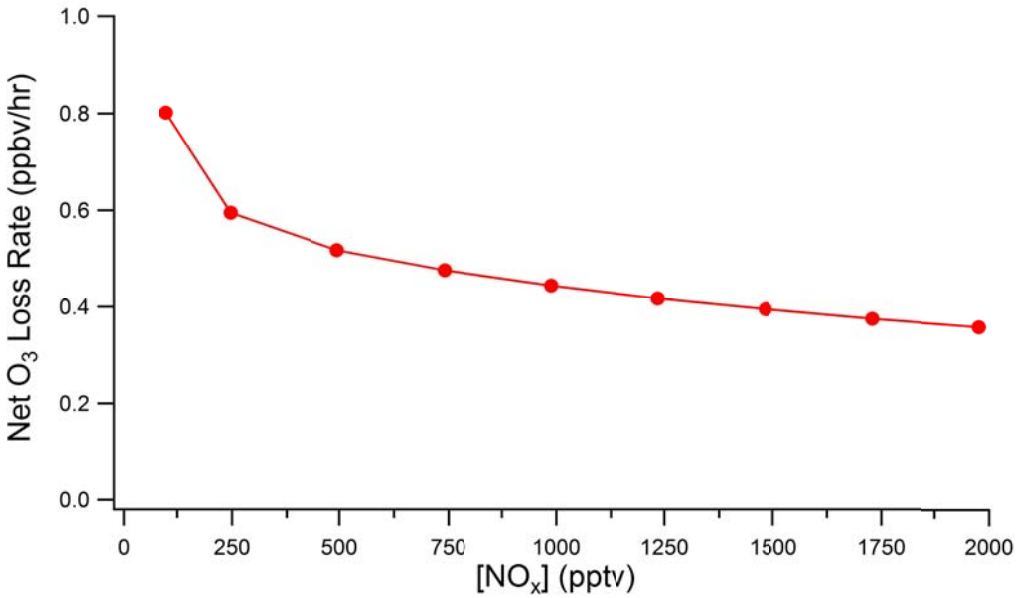

Figure 6. Net O_3 loss rate as a function of the NO_x mole ratio, for March 30th mid-day (11:00 to 13:00 AKST) conditions.

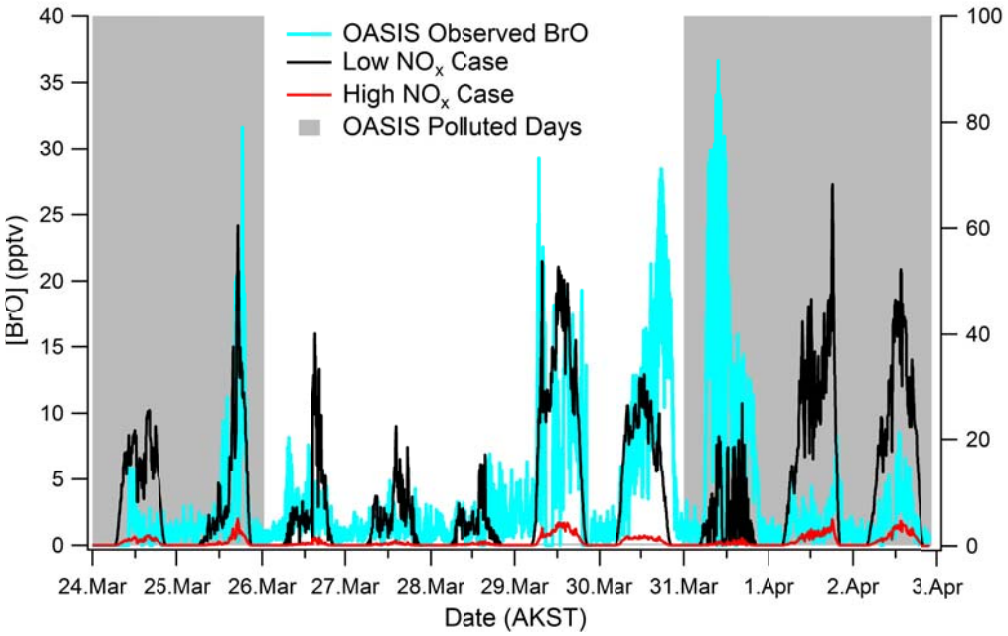

Figure 7A. Simulated BrO mole ratio (low NO_x & high NO_x cases) and the observations during the study period.

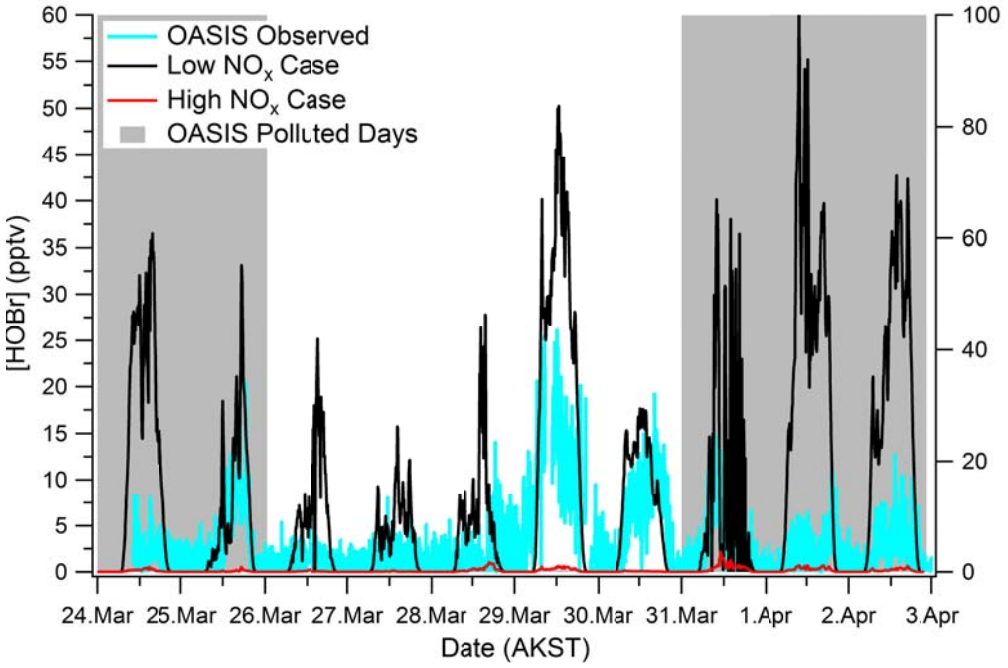

Figure 7B. HOBr levels from the model simulations (low NO_x & high NO_x cases) and the observations during the simulation dates.

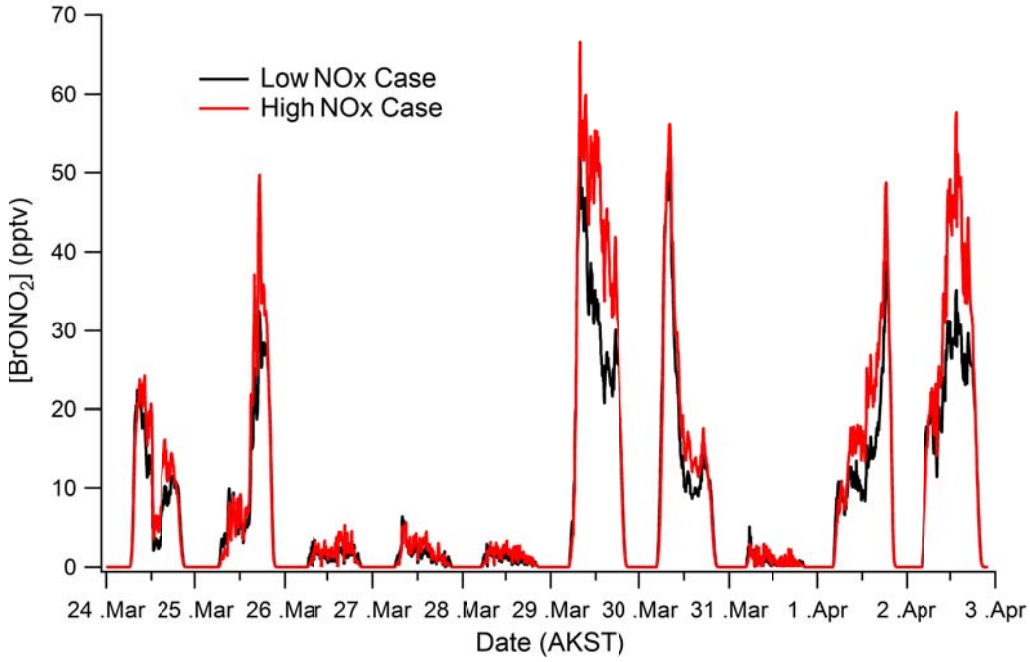

Figure 7C. $BrONO_2$ mole ratio from the two simulation cases.

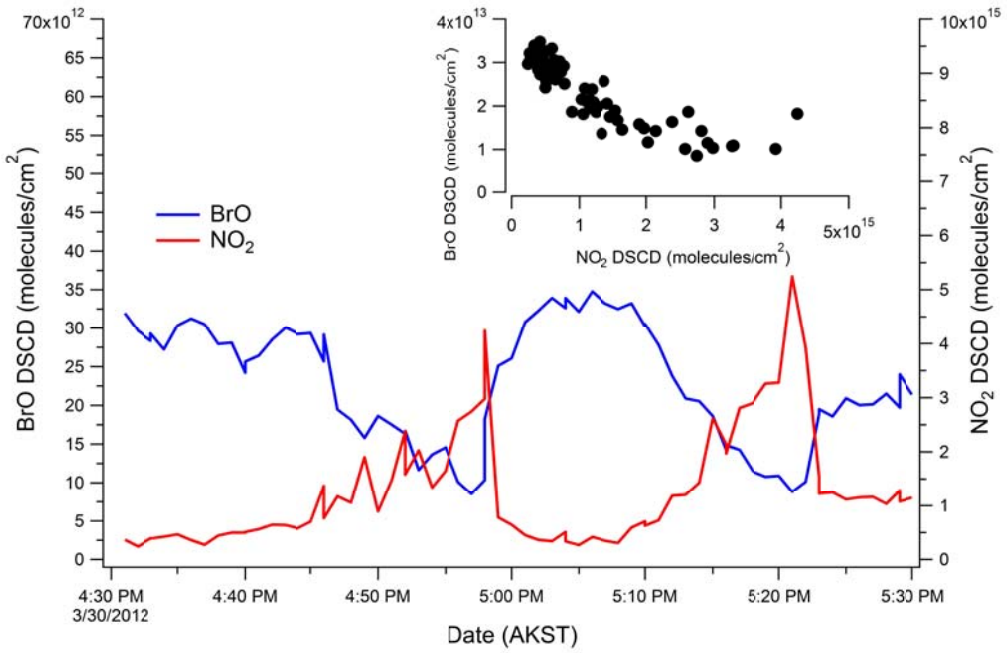

Figure 8. BrO and NO_2 measured mole ratios via MAX-DOAS during the BROMEX field campaign, near Prudhoe Bay (70°N,149°W), AK at 700m above the surface on March 30, 2012. The insert of the NO_2 versus BrO shows the anti-correlation between the two species.